

NOTES

B1293

(2)

CONF 810512

MASTER  
Proceedings of the Workshop

EBT STABILITY

May 13-14, 1981  
Oak Ridge, Tennessee

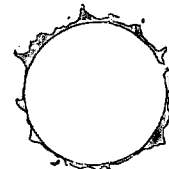
Sponsored by

OAK RIDGE NATIONAL LABORATORY

FUSION ENERGY DIVISION

Oak Ridge, Tennessee 37830

ornl



## PREFACE

Oak Ridge, Tennessee was the site of the May 13-14, 1981, EBT Stability Theory Workshop. It was attended by more than 80 participants, including essentially all of the physicists who have worked and/or are presently working on stability (theory and/or experiment) relevant to the EBT configuration.

The workshop organizing committee members were:

- N. A. Uckan, Chairman, Oak Ridge National Laboratory
- C. L. Hedrick, Chairman, Oak Ridge National Laboratory
- D. E. Baldwin, Lawrence Livermore National Laboratory
- H. L. Berk, University of Texas at Austin
- H. Grad, Courant Institute, New York University
- N. A. Krall, JAYCOR
- D. A. Spong, Oak Ridge National Laboratory

The purpose of the workshop was to provide a forum for (1) discussion and review of the status of the EBT stability theory not often aired at more academic conferences and (2) assessment of the various models used as well as the importance of modes predicted from these models on the operating regimes of past, present, and future experiments.

The first part of the workshop was devoted to presentations of 15 papers describing the status and various aspects (theory and/or experiment) of the EBT stability. The second part of the workshop was devoted to enthusiastic open-session discussions of (1) critical evaluations of existing models and (2) the influence of predicted beta limits on reactor performance.

These proceedings include (1) workshop summaries prepared by the session chairmen (N. A. Uckan, D. E. Baldwin, H. L. Berk, H. Grad, C. L. Hedrick, N. A. Krall, and D. A. Spong) and (2) full-length manuscripts that were submitted to the workshop and presented at the following workshop sessions: Overview (3 papers); Experimental Observations (2 papers); Ring-Core Coupling, Low Frequency Modes (4 papers); High Frequency Modes (2 papers); Equilibrium and Computational Formalism of Stability (3 papers); and Reactor Implications (1 paper). An Author Index, the Attendance List, and the Agenda conclude the proceedings.

(Because of the camera-ready publication, the variations in style and format were inevitable.)

The workshop was sponsored by the Fusion Energy Division (FED) Oak Ridge National Laboratory (ORNL) and could not have been successful without the efforts of many dedicated individuals — the Workshop Organizing Committee, Session Chairmen, Authors, participants, and last but not least, the workshop secretaries.

The chairman wishes to acknowledge a special appreciation to four delightful coworkers: Caila Cox, the workshop secretary, who handled a myriad of details prior to, during, and after the workshop in an efficient, complete, and professional manner; DeLena Akers, her secretary, who handled all aspects of the abstracts and preliminary program along with the preparation of many of the drafts and/or incomplete manuscripts submitted by some of the authors while simultaneously performing her ORNL work in exemplary fashion; Susan Stockbridge, who handled all of the art work and designed the covers of the abstract booklet (distributed during the workshop) and these proceedings; and Ethel Cagle, who coordinated the assembly of the papers. Thanks are also due to the staff of the FED Reports Office, the editors, and graphic artists who handled much of the workshop paperwork.

Nermin A. Uckan  
Oak Ridge, Tennessee  
June 1981

## CONTENTS

1.	SUMMARY OF THE WORKSHOP — N. A. Uckan, D. E. Baldwin, H. L. Berk, C. L. Hedrick, H. Grad, N. A. Krall, and D. A. Spong .....	1
2.	OVERVIEW .....	12
	RUDIMENTARY THEORIES OF THE STABILITY OF MICROWAVE HEATED PLASMAS — G. E. Guest .....	15
	REVIEW OF RECENT EBT COUPLED RING-CORE STABILITY THEORY — D. A. Spong .....	33
	BRIEF SURVEY OF EXPERIMENTAL INVESTIGATION OF INSTABILITIES IN MICROWAVE HEATED PLASMAS — N. A. Uckan and G. R. Haste .....	63
3.	EXPERIMENTAL OBSERVATIONS .....	73
	FLUCTUATION MEASUREMENTS IN EBT — L. Bighel, G. R. Haste, and A. Komori .....	75
	HOT-ELECTRON RING STABILITY AT THE UNIVERSITY OF TENNESSEE — I. Alexeff and M. Saylor .....	83
4.	RING-CORE COUPLING, LOW FREQUENCY MODES .....	95
	EIGENMODE STABILITY ANALYSIS FOR A BUMPY TORUS — J. W. Van Dam, H. L. Berk, M. N. Rosenbluth, and D. A. Spong .....	97
	NUMERICAL SOLUTIONS OF THE EBT RADIAL EIGENMODE PROBLEM — D. A. Spong, J. W. Van Dam, H. L. Berk, and M. N. Rosenbluth .....	115
	STABILITY OF HOT ELECTRON PLASMA IN THE ELMO BUMPY TORUS — K. T. Tsang and C. Z. Cheng .....	141
	ANALYTICAL THEORY OF INTERCHANGE AND COMPRESIONAL ALFVÉN INSTABILITIES IN EBT — C. Z. Cheng and K. T. Tsang ...	161
5.	HIGH FREQUENCY MODES .....	179
	MICROINSTABILITY OF THE EBT BOUNDARY — N. T. Gladd, N. A. Krall, S. Hamasaki, and J. L. Sperling .....	181
	ELECTRON CYCLOTRON RESONANT HEATED ELECTRON DISTRIBUTION FUNCTIONS — Y. Matsuda, W. M. Nevins, and R. H. Cohen .....	211
6.	EQUILIBRIA AND CALCULATIONAL FORMALISM OF STABILITY .....	227
	NUMERICAL ANALYSIS OF EQUILIBRIUM AND STABILITY IN BUMPY CYLINDER — H. Sanuki, T. Onigo, S. Ishiguro, and T. Kamimura .....	229
	KINETIC STABILITY ANALYSES IN A BUMPY CYLINDER — R. R. Dominguez and H. L. Berk .....	249
	BALLOONING STABILITY IN TOROIDAL DEVICES — Shoichi Yoshikawa .....	265

7. REACTOR IMPLICATIONS .....	279
EFFECT OF BETA LIMITS ON REACTOR PERFORMANCE	
IN EBT — N. A. Uckan, D. A. Spong, and D. B. Nelson .....	281
AUTHOR INDEX .....	297
ATTENDANCE LIST .....	299
AGENDA .....	305

## 1. INTRODUCTION

The first workshop on the ELMO Bumpy Torus (EBT) stability theory was held at Oak Ridge, Tennessee, May 13-14, 1981. It was attended by about 80 participants, including essentially all of the physicists who have worked and/or are presently working on stability (theory and/or experiment) relevant to the EBT configuration in one way or the other.

The organizing committee members who arranged the workshop were: C. L. Hedrick and N. A. Uckan (Chairmen), D. E. Baldwin, H. L. Berk, H. Grad, N. A. Krall, and D. A. Spong.

The purpose of the workshop was to provide a forum for (1) discussion and review of the status of the EBT stability theory not often aired at more academic conferences and (2) assessment of the various models used as well as the importance of modes predicted from these models on the operating regimes of past, present, and future experiments.

The first part of the workshop was devoted to presentations of 15 papers describing the status and various aspects (theory and/or experiment) of the EBT stability. The second part of the workshop was devoted to enthusiastic open-session discussions of (1) critical evaluation of existing models and (2) influence of  $\beta$  limits on reactor performance.

The proceedings containing the summary of the workshop and the full-length papers presented will be published by the Oak Ridge National Laboratory [EBT Stability Theory, Proceedings of the Workshop, CONF-810512, Oak Ridge, Tennessee (1981)]. It is convenient to review the workshop under subject headings chosen for the sessions.

## 2. OVERVIEW (Chairmen: N. A. Krall and N. A. Uckan)

There is perhaps more background information on EBT stability, both theoretical and experimental, than most of us realize; thus, the workshop began with an overview session that described a good bit of this background. Theoretical reviews were given by Guest and Spong. A brief survey of experimental investigations was presented by Haste.

The EBT has several features that make the theoretical treatment of its stability difficult and quite different from other confinement devices. This is due largely to the presence of high- $\beta$ , hot electron rings that modify the magnetic field to produce a local magnetic well in each mirror sector. Stability problems often fall into two general categories, macrostability and microstability. However, in EBT these distinctions are somewhat complicated by the requirement of kinetic treatment for traditional macroscopic modes (interchanges, for example) because the requirements for MHD (large scale length, long time scale, slow drift velocity, etc.) are not satisfied by the hot electron rings. This also results in a given class of modes being called different names by different authors in the literature, and the clarification of mode name definitions was one of the lengthy and fruitful discussions in the open forum(!). Nevertheless, there are macrostability properties that influence  $\beta$  limits, stable operating regimes, acceptable geometries, etc., and there are microinstability properties, that influence boundary layer behavior, radial transport, ambipolar potentials, possible impurity transport and heating, etc. Both of these aspects of stability were treated in the workshop.

There is a large body of stability work relevant to EBT, including studies based on mirror machines, Z-pinch,  $\theta$ -pinch, and general high- $\beta$ , hot electron, and strong curvature studies, in addition to studies specific to EBT. The general form of these results is to determine the limits of density ( $\omega_p/\omega_c$ ), beta ( $\beta$ ), anisotropy ( $T_\perp/T_\parallel$ ), etc.; theories in increasing layers of complexity have attempted to derive these limits.

Instabilities considered by the early MHD work, reviewed by Guest, include anisotropy driven modes and loss cone modes, which predict a stable window of density, centered around  $\omega_{pe} \approx \omega_{ce}$ , surrounded by instability at both much lower and much higher densities. Another instability of this type is the Whistler, which limits the anisotropy  $T_\perp/T_\parallel$  of the ring plasma. The most annoying instability in early MHD work was the ring interchange mode, which in simple model predicted instability even at  $\beta \rightarrow 0$  for global modes and at higher  $\beta$  for ballooning modes, which is contrary to the experimentally observed stability. Later work has provided an explanation for ring stability in that the inclusion of a cold plasma background stabilized the global ring interchange, and the high

precessional drift frequency of the hot electrons  $\omega_{dh}$  (which is comparable to ion cyclotron frequency  $\omega_{ci}$ ) permitted stabilization of ballooning modes. Conventional fluid or guiding center theories were inadequate because the kinetic effects were expected to be important due, for example, to the observation that the hot electron diamagnetic drift was comparable or greater than the thermal speed of the background plasma and larger than characteristic frequencies for typical MHD of interest. Further, the ring width was not a great deal larger than few hot electron and cold plasma ion gyroradii, and the perpendicular wave length of the flute modes can be comparable for relatively low poloidal mode numbers.

During the past several years, EBT stability calculations have evolved with respect to treatment of ring-core plasma coupling effects. Some effects, reviewed by Spong, of treating the multispecies problems and of including kinetic effects were that (1) the core is unstable against interchange instability at low ring  $\beta$  (bad curvature), and rings stabilize the toroidal core if ring pressure is high enough to create a local magnetic well (e.g.,  $\beta_{ring} \lesssim 2\Delta/\langle R_c \rangle$ , where  $\Delta$  and  $\langle R_c \rangle$  are the characteristic ring scale length and average magnetic radius of curvature, respectively), (2) ring stability requires a finite level of core density (e.g.,  $n_{cold}/n_{hot} > \text{some number}$ ), (3) core plasma becomes interchange unstable if core  $\beta$  is larger than a few  $\Delta/R_c$ , (4) high  $m$  modes (where  $m$  is the poloidal mode number) are dominated by kinetic effects, (5) core density is limited by compressional Alfvén waves, and (6) ring density is limited by ring interchange instability at high ring  $\beta$ .

On the experimental side, there is a wealth of observations of fluctuations on devices related to EBT. These devices include simple and minimum-B mirrors, canted mirrors, and toroidal geometries. A brief survey of results from these experiments, presented by Haste, indicated that fluctuations from very low frequencies ( $\lesssim 100$  kHz) to frequencies in the few GHz range are observed, with peaks that can be related to theoretical prediction. For example, fluctuations are observed in the plasma core, which disappear when the ring  $\beta$  reaches a value consistent with theoretical predictions of average min-B stability. Anisotropy driven modes of hot electrons were also observed, however, they were stabilized by the addition of upper off resonance heating. Theoretically, the stabilizing effect of upper off resonant heating was shown to be due

to the reduction in temperature anisotropy of the hot electrons and the relativistic broadening of the particle cyclotron spectrum. It would be far too sanguine to imply that all or most of these observed fluctuations correlate with theory. The diagnostics of most of these experiments would not be sufficient to demonstrate such correlation even if it existed. The details of this overview, contained in three papers by Guest, Spong, and Haste of this workshop, provided the framework for the ongoing research, which was the business of the workshop.

### 3. EXPERIMENTAL OBSERVATIONS (Chairmen: W. B. Ard and H. Grad)

Nearly twenty years of experimental investigations of instabilities exist in hot electron plasmas; much of it was surveyed in the overview session and much of it was compiled in the EBT Ring Physics Proceedings [1]. In this session two specific papers were presented by the Oak Ridge group (Bighel et al.) on fluctuation measurements in EBT and by Alexeff on a small scale hot electron ring experiment.

The study of plasma fluctuations could play an important role in understanding EBT transport as well as stability. Fluctuations in EBT have been measured with several techniques, including rf measurements with loop antennas, movable Langmuir probes, and visible light sensors. As described by Bighel, several features of the fluctuations have been observed: (1) they are predominantly low frequencies ( $<200$  kHz), (2) the C-T-M mode hierarchy can be correlated with the fluctuation activity where the fluctuation amplitude decreases at the C-T transition with the formation of hot electron rings and increases near T-M transition, (3) high frequency fluctuations, especially in the T-mode, are generally found outside the rings, and (4) enhanced fluctuations near the T-M transition may have some correlation with the increased high energy ion-tail densities and deep potential wells [2].

In a small magnetic mirror experiment, a hollow ring has been formed by electron cyclotron heating ( $\sim 2.8$  GHz) in close proximity to the wall. Alexeff pointed out that the ring was stable and the ring stability was not due to "line tying;" however, moving the ring from the wall caused instability. It was pointed out that there was not enough cold plasma to stabilize the ring.

#### 4. RING-CORE COUPLING, LOW FREQUENCY MODES

(Chairmen: D. E. Baldwin and C. L. Hedrick)

The theory of Van Dam and Lee, developed two years ago and presented at the Ring Physics Workshop [1], which limited the core plasma  $\beta$ -value that could be MHD stabilized by a hot electron ring, had profound implications for the EBT reactor concept. It also has an important bearing on certain elements of the tandem mirror thermal barrier concept. That theory (which was an extension of the theory by Nelson) concluded that the plasma, or toroidal core,  $\beta$ -value was limited by a value proportional to the ratio of ring thickness to the vacuum magnetic field radius of curvature ( $\beta \sim \Delta/R_c$ ). Thus, an important EBT reactor design concept, that the rings could be made thin to minimize ring power losses, appeared to necessitate low plasma  $\beta$  values.

Although in arriving at this result a number of simplifications and approximations were made, which led to some ambiguity in the interpretation, the qualitative validity of the result has by now been generally accepted, and much of the ambiguity has been removed in the past year. Attention has shifted to detailed calculations of beta-limits, including effects of proper line averaging, radial mode structure, hot electron distribution function, and general sensitivity to the several physics parameters entering the theory. This has uncovered other modes of instability, as described in the papers of this session, but the original Van Dam-Lee limitation appeared to be the most important.

Interest in this problem for tandem mirror application relates to the implications for the low frequency behavior of the hot, anisotropic electrons now seen as necessary in versions of thermal barriers, viz., those formed by sloshing ions such as in TMX upgrade and MFTF-B. Roughly speaking, the Van Dam-Lee result shows that for plasma  $\beta$  below the critical value, the hot electrons are rigid in the sense of not participating in the low frequency modes. For plasma  $\beta$  above the critical value, the hot electrons behave as a MHD fluid. Correspondingly, the hot electron pressure should not or should, respectively, be included in MHD stability analyses. The desirability of doing so will depend on whether the hot electrons are in a well of bad or good curvature. Again,

determination of the critical  $\beta$  value and its dependence on parameters is important for assessing design options.

The four papers of this session were given by two sets of authors, each separately presenting analytic and numerical results.

The papers by Van Dam et al. and Spong et al. extend the original slab calculations to shortwave length modes (1 to B) in general geometry, giving a local condition with appropriate line averages. These results confirm the result that  $\beta$  values and curvatures are to be measured at the location of the hot electron ring rather than the field line average of the curvature as had been assumed in the early interpretations of slab models. Since the curvature in a bumpy cylinder changes sign, the local value is larger than the average value; hence, the newer  $\beta$  limits can be significantly larger. The authors then map the EBT problems to a related Z-pinch configuration in order to examine radial mode structure in a model cylindrical geometry. They find modifications to the local results; however, the quantitative implications for the original EBT configuration are not clear. In particular, a new region of instability, when  $\omega_{ci} \approx \omega_{dh}$ , should be strongly influenced by the axial nonuniformity of mod-B in real geometry.

Cheng and Tsang, in two separate papers, examined a wider parameter survey of the original theory (following the formulation of Nelson), including finite hot electron drift speeds and a variation of the hot electron distribution function. They found sensitivity to these effects, and they calculated different shaped, and perhaps wider,  $\beta$  (core) versus  $\beta$  (hot electron) windows of stability.

##### 5. HIGH FREQUENCY MODES (Chairmen: H. L. Berk and D. A. Spong)

The paper by Gladd et al. was a discussion of microinstabilities of the core plasma in the steep gradient region and of the hot electron rings. It was pointed out that in the edge region, where gradients are the steepest, anomalous transport could be present due to instabilities, such as the lower hybrid drift mode and the drift cyclotron instability. These could alter the fraction of a cold-to-hot plasma density, which is an important factor in the stability of the ring-core system. A local and

it was concluded that the presence of the diamagnetic well produced by the hot electrons could lower the growth rate for this mode.

The Whistler instability of the hot electrons was also examined to determine if it persisted at relativistic temperatures (because earlier work indicated relativistic stabilization of Whistlers). This mode is driven by the extreme temperature anisotropy of the ring and could result in an enhanced energy drain on the ring electrons above classical values. A localized dispersion relation was solved for the mode, assuming a model hot electron distribution function that is not necessarily characteristic of the EBT ring, but it may well represent tandem mirror, including relativistic effects. Although relativistic effects were stabilizing, growth rates remain finite at relativistic temperatures for sufficiently large anisotropy ( $T_{\perp}/T_{\parallel} > 10$ ).

In a paper by Nevins et al. preliminary numerical results were discussed of a bounce-averaged, Fokker-Planck code that solves for the energetic electron tail formed by electron cyclotron heating at the second harmonic. The distribution functions were non-Maxwellian and indicated that at high energies, the frictional drag from Coulomb collisions was less than that from rf collisions. Estimates of these critical energies were made both with fundamental and second harmonic heating. The calculations were based on a nonrelativistic model with the distribution function going to zero at the speed of light. There was discussion about what effect properly including relativistic corrections would have on the results, and it was difficult to make any projections. Although the study was focused primarily on mirror-confined electrons, it was felt that a bounce-averaged Fokker-Planck code would be very useful in studying the electron distributions in EBT as well as for analyzing both the stability and power balance of the hot electron rings.

## 6. EQUILIBRIA AND CALCULATIONAL FORMALISM OF STABILITY

(Chairmen: H. Grad and N. A. Krall)

This session featured work on equilibria and stability, particularly the approach to equilibrium and a variational-like technique for stability analysis.

In treating the approach to equilibria, Sanuki and co-workers of Nagoya presented a numerical solution of the nonlinear time evolution of double, adiabatic (anisotropic) macroscopic equations in a bumpy cylinder configuration. Artificial viscosity ( $\mu \nabla^2 v$ ) and damping ( $\nu v$ ) allow an approach to static equilibrium. These time-dependent equations are not used for stability study, but the resulting equilibria are examined for stability by an assortment of currently available theoretical criteria (interchange, Van Dam, etc.). The ring and core are fully interactive with regard to equilibrium and the approach to equilibrium. The stability interaction (ring with core) depends on what is built into the package used to calculate stability. It was pointed out that the  $\beta$  estimates, which were lower than predicted earlier, should be considered as tentative.

In contrast to the standard approaches of normal mode analysis of the Vlasov-Maxwell equations to predict stability, a variational-like technique was discussed, which could eventually combine some of the complexities of EBT geometry, along with kinetic effects. In this light, a fully kinetic formulation was presented by Dominguez and Berk, applicable to the core-ring stability interaction in a bumpy cylinder configuration. The work is preliminary, involving an ingenious reduction of the complicated coupled Maxwell-Vlasov system to a form that should involve less numerical work than other techniques to approximate global eigenfunctions and their related eigenvalues. The simplification is obtained despite the non-self-adjoint character of the system and not (as is claimed) by a reduction to self-adjoint. Numerical results are not yet available.

In an attempt to derive a generalized, marginal stability condition of ballooning instabilities in toroidal geometries (tokamaks, multipoles, stellarators, EBTs, etc.), Yoshikawa pointed out that the EBT geometry is very simple in that it is a closed field line device, and stability analysis should reduce to one obtained from  $\oint dl/B$ .

## 7. REACTOR IMPLICATIONS AND OPEN-SESSION DISCUSSIONS

(Panel: N. A. Uckan, D. E. Baldwin, H. L. Berk, C. L. Hedrick,  
H. Grad, G. E. Guest, and N. A. Krall)

In order to provide a focus for open-session discussions and point out the difficulties involved in interpretation of results from the present theories, the paper by Uckan considered the influence of core  $\beta$  limits on EBT reactor performance and discussed the uncertainties involved in the extrapolation.

In the present experiments the plasma core  $\beta$  is limited to  $\beta_{\text{core}} \lesssim 0.5\%$  because of transport and heating (small size as well) rather than stability, whereas  $\beta_{\text{ring}} \sim 10\text{--}40\%$  is routinely attained, and the stabilization of a low  $\beta_{\text{core}}$  plasma by the hot electron has been amply demonstrated. Experimental confirmation of high  $\beta_{\text{core}}$  predictions are not possible at the present. However, the next planned device, the EBT Proof-of-Principle (EBT-P), is expected to have  $\beta_{\text{core}}$  values on the order of a few percent and should be able to test some of the predictions discussed at the workshop.

At present, EBT stability calculations have indicated the existence of three modes that can limit the core  $\beta$ , core density, and ring density; these are the core interchange (Van Dam and Lee), the compressional Alfvén, and the hot electron interchange modes. Although the most limiting modes depend on which models and/or assumptions are used, all of the analyses indicate that a stable finite  $\beta$  operating regime does exist. However, estimates on the core  $\beta$  limit range from a few percent to 10–20% for reasonable but different parameters within the same model. Some of the parameters that enter into these  $\beta$  limits ( $\Delta/R_c$ ,  $n_{\text{cold}}/n_{\text{hot}}$ ,  $T_{\text{hot}}/T_i$ ,  $\omega_{\text{dh}}/\omega_{\text{ci}}$ ,  $\omega_{\text{dh}}/kV_A$ ,  $\beta_{\text{ring}}$ , etc.) change significantly in going from present-day experiments to reactor-like devices. Results from a parametric study that include boundaries of the operating regime for an EBT reactor indicated that the overall reactor  $Q_{\text{Electric}}$  value range from as low as 2–5 to  $\sim 50$  depending on the uncertainties, mostly in ring scale lengths ( $\Delta$ ) and limiting core  $\beta$ . It was pointed out that providing stability against the hot electron interchange mode will require a certain minimum value of  $\omega_{\text{dh}}/\omega_{\text{ci}}$ , which requires large  $T_{\text{hot}}$  or small  $\Delta$ . Of course, there is a trade-off between the hotter electrons, which cause large radiation losses, and smaller  $\Delta$ , which lowers ring volume and core  $\beta$ .

The rest of the discussions in the open session were centered on the following: (1) detailed understanding of the models used, (2) validity of the approximations made, (3) applicability of the results obtained, and (4) clarification of the definitions used. It is difficult to draw any conclusions from these discussions. It should be pointed out that in the absence of experimental data, theoretical analyses have been undertaken to establish the limits of core  $\beta$ . These analyses require simplification of the physics (although considerable progress has been made in numerical and analytical treatment of the ring and core coupling), since the full problem involves a multispecies, kinetic, and finite gyroradius effects in 3-D geometry. However, these simplified models give a qualitative picture of EBT stability and are a valuable guide for experiments, not only because of the possibility of finding optimization paths but because of the interesting conjecture that deoptimization might permit experimental verification of theory at modest  $\beta$  values. It is also fair to say that at the present time, the theory is in a state of flux. There is agreement on general features, but details and the quantitative predictions will require perhaps another year's work.

#### REFERENCES

- [1] UCKAN, N. A., ed., EBT Ring Physics, Proceedings of the Workshop, CONF-791228, Oak Ridge, Tennessee (1980).
- [2] UCKAN, N. A., ed., Ambipolar Potential Formation and Control in Bumpy Tori and Mirrors, Proceedings of the Workshop, CONF-810511, Oak Ridge, Tennessee (to be published), and Summary of the Workshop to be published in Nucl. Fusion.

#### ACKNOWLEDGMENT

This workshop was sponsored by the Fusion Energy Division, Oak Ridge National Laboratory, supported by the Office of Fusion Energy, U.S. Department of Energy, under contract W-7504-eng-26 with the Union Carbide Corporation.

RUDIMENTARY THEORIES OF THE STABILITY OF  
MICROWAVE-HEATED PLASMAS

G. E. Guest

Applied Microwave Plasma Concepts  
Encinitas, California 92024

The ELMO Bumpy Torus poses several difficult problems in the theory of plasma stability whose resolution affects important practical issues such as the extent of stable operating regimes, limits of the maximum stable core-plasma pressure, and so on. The difficulties arise largely because of the importance of both microscopic and macroscopic properties of the system, such as kinetic effects, multiple-species effects, and specific aspects of the magnetic configuration. Limitations in readily available theoretical techniques have led to the evolution of a patchwork of theoretical predictions for idealized models of EBT, with incomplete and generally qualitative or indirect empirical confirmation.

Here we review briefly the main results from early theoretical studies of two obvious sources of plasma instability; viz., anisotropic distributions of particle velocities and locally unfavorable curvature in the magnetic lines of force. We identify three distinct components of the underlying theoretical models and assess the degree of realism or completeness achieved in each: the basic equilibrium model; the set of field equations and polarizations assumed; and the plasma constitutive relations used.

RUDIMENTARY THEORIES OF THE STABILITY OF  
MICROWAVE-HEATED PLASMAS

G.E. Guest

AMPC

1. INTRODUCTION

The theory of plasma stability has played an important role in the evolution of the ELMO Bumpy Torus concept, starting with the fundamental assumption that the ELMO rings could stabilize low-frequency modes in a bumpy torus, and continuing to the present efforts to predict the value of core plasma pressure at which that stabilization might break down. Indeed, many of the relevant theories date to the earlier days of fusion research when various notions of "line-tying" were invoked to explain the empirical stability of mirror-confined, hot-electron plasmas, the forerunners of the ELMO rings. Despite this long history, the stability theory for EBT remains an unsatisfactory patch work of idealized models and specific modes, with relatively little experimental validation.

The difficulties in achieving greater scope and predictive capability in EBT stability theory arise largely from the simultaneous importance of both microscopic and macroscopic properties of the EBT plasma configuration. This is particularly true with respect to curvature-driven instabilities such as interchange and ballooning modes. Ideal, single-fluid models of these instabilities generally predict the ELMO ring plasmas to be unstable, whereas the experiments generally exhibit a stable plasma, provided the ambient gas pressure is above a critical value. This striking disparity between theoretical predictions and empirical fact has spawned roughly two decades of theoretical effort to develop models that described more accurately the basic experimental observations. These models were usually based on more microscopic descriptions of the plasma response than in the fluid pictures, in order to include in the model a number of physical phenomena expected to contribute to the observed stabilization of "flutes": the

response of cold electrons, particularly in plasmas of finite axial extent; the finite gyroradius of plasma ions and the finite radial dimension of the plasma; the broad distribution in energy of hot electrons in ECH plasmas, and so on. In order to describe these phenomena theoretically, it was necessary to use greatly simplified models of the plasma equilibrium; so that, although many stabilizing tendencies were found, the predictive quality of the theory became questionable.

This possible loss of predictive capability is, again, most likely in regard to the curvature-driven modes. For example, in the case of "ballooning" modes, the essential physics thought to govern the onset of instability is the competition between growth of the wave in a region of unfavorable curvature and damping of that same wave in regions of favorable curvature. As long as the local growth rate is less than the rate at which the (shear Alfvén) waves can communicate between the two regions, the plasma is expected to remain stable. Since the local growth rate increases with beta, while the Alfvén speed decreases with beta, the local growth rate will exceed the effective damping rate above some critical value of beta.

In the more microscopic description of the finite-beta plasma, it has not yet been possible to include this stabilizing coupling to the shear Alfvén waves. The current theoretical models are forced to treat slab models without regions of favorable curvature, and generally investigate only the compressional Alfvén waves in the flute limit ( $k_{\parallel} = 0$ ) in which they are decoupled from the shear Alfvén waves. This unsatisfactory theoretical situation is the object of a very intensive effort at the present time.

Fortunately, the simplified models are more likely to provide a reliable description of the very high frequency, velocity-space instabilities that can also be important to the EBT concept. We therefore wish to provide a brief review of some of the anticipated modes for ECH plasmas in general and EBT plasmas in particular. For a more complete discussion, the reader is urged to see Ref. 1 and other works cited there.

## 2. QUALITATIVE FEATURES OF MICROSCOPIC MODES IN ECH PLASMAS

It is a fundamental property of electron cyclotron heating to produce a plasma with two distinct groups of electrons, one of which is very energetic and generally anisotropic in velocity space, while the other is much lower in temperature and more nearly isotropic. Since the plasma ions are heated only indirectly by ECH, they are also generally isotropic and low in energy. In such a plasma, the propagation of waves at frequencies near the electron gyrofrequency is determined mainly by the colder, isotropic electron group. Whether these waves will grow or decay is determined largely by their ability to extract the excess free energy of the hot-electron group. In anticipation of modes with wavelengths comparable to electron gyroradii (and thus much smaller than the dimensions of the plasmas), we will use infinite, homogeneous, uniform magnetic field strength models of the plasma equilibrium. We can then describe the plasma dynamics with the Vlasov equation, and adopt some limiting case of Maxwell's equations to describe the fluctuating fields of the waves. Because

$$\frac{\omega_{pe}^2}{c^2 k^2} = \frac{\omega_{pe}^2}{\Omega_e^2} \cdot \frac{v_e^2}{c^2} \cdot \frac{\Omega_e^2}{k^2 v_e^2} \lesssim 1$$

for plasma parameters and waves typical of ECH situations, we shall consider electrostatic and electromagnetic modes separately [2], starting with the electrostatic modes.

The essential results of the dispersion relation for electrostatic modes near the electron gyrofrequency are shown in Figure 1. Normal modes of the plasma must satisfy the cold-electron dispersion relation shown there, while the growth or damping is determined by the real part of the longitudinal conductivity. This is simply because the work done by the field of the wave is

QUALITATIVE FEATURES OF MICROSCOPIC MODES  
IN ECH PLASMAS

WAVE PROPAGATION DETERMINED MAINLY BY "COLD" ELECTRONS:

$$\gamma \cong \frac{\omega_{pe,c}^2}{\omega^2} \frac{k_{\parallel}^2}{k^2} + \frac{\omega_{pe,c}^2}{\omega^2 - \Omega_e^2} \frac{k_{\perp}^2}{k^2}$$

WAVE GROWTH OR DAMPING DETERMINED BY "HOT" ELECTRONS  
THROUGH NEGATIVE DISSIPATION

$$\frac{\text{Re } \sigma_{\ell}}{\omega \epsilon_0} = 2\sqrt{\pi} \frac{\omega_{pe,h}^2}{k^2 \alpha_{\parallel}^2} \frac{\Omega_e}{k_{\parallel} \alpha_{\parallel}} \sum_{n=-\infty}^{\infty} \exp \left[ - \left( \frac{\omega - n\Omega_e}{k_{\parallel} \alpha_{\parallel}} \right)^2 \right]$$

$$\times \left[ \left( \frac{\omega}{\Omega_e} - n \right) C_n(\lambda) + \frac{\alpha_{\parallel}^2}{\alpha_{\perp}^2} n D_n(\lambda) \right]$$

$$f_0(v_{\parallel}, v_{\perp}) = \frac{g_0(v_{\perp})}{\sqrt{\pi} \alpha_{\parallel}} \exp \left( - \frac{v_{\parallel}^2}{\alpha_{\parallel}^2} \right)$$

$$C_n(\lambda) \equiv 2\pi \int_0^{\infty} v_{\perp} dv_{\perp} J_n^2 \left( \frac{k_{\perp} v_{\perp}}{\Omega} \right) g_0(v_{\perp})$$

$$D_n(\lambda) \equiv \left( - \frac{\alpha_{\perp}^2}{2} \right) 2\pi \int_0^{\infty} v_{\perp} dv_{\perp} J_n^2 \left( \frac{k_{\perp} v_{\perp}}{\Omega} \right) \frac{1}{v_{\perp}} \frac{dg_0}{dv_{\perp}}$$

$$\lambda \equiv k_{\perp}^2 \alpha_{\perp}^2 / 2\Omega^2$$

Figure 1

$$\begin{aligned} \langle \vec{E} \cdot \vec{j} \rangle &= \frac{1}{2} \operatorname{Re}(\vec{E}^* \cdot \vec{g} \cdot \vec{E}) \\ &= \frac{1}{2} |\vec{E}|^2 \operatorname{Re} \sigma_{\ell} \quad . \end{aligned}$$

If  $\sigma_{\ell} > 0$ , the wave does net work on the plasma, and the wave will damp if its characteristic energy is positive. If  $\sigma_{\ell} < 0$ , the plasma does net work on the wave, and a positive-energy wave will grow. Since all waves satisfying the cold-electron dispersion relation are positive-energy waves, we shall only be concerned here with identifying the conditions necessary for  $\sigma_{\ell} < 0$ , i.e. conditions for negative dissipation. The sign of  $\sigma_{\ell}$  is determined by the weighted moments of the distribution function,  $C_n$  and  $D_n$ . These have been discussed extensively in Ref. 3, and illustrative examples are shown in Figure 2 and 3.

We first consider waves propagating nearly perpendicular to the magnetic field so that  $k_{\parallel}$  is small in the sense that

$$H \equiv k_{\parallel} \alpha_{\parallel} / \Omega_e \ll 1 \quad .$$

Here,  $\alpha_{\parallel}$  is the parallel thermal speed of the hot-electron group and  $\Omega_e$  is the electron gyrofrequency. In this limit, the contributions to  $\sigma_{\ell}$  from the infinite series of gyroresonances are well separated and can be adequately approximated by the two harmonics bracketing a given frequency, as shown in Figure 4.

If the temperature anisotropy is extreme,  $T_{\parallel} \ll T_{\perp}$  (or  $T \ll 1$  in the language of Figure 4),  $\sigma_{\ell}$  can become negative if

$$(\omega/\Omega - N)C_n < 0 \quad ,$$

and

$$|NTD_n| < |(\omega/\Omega - N)C_n| \quad .$$

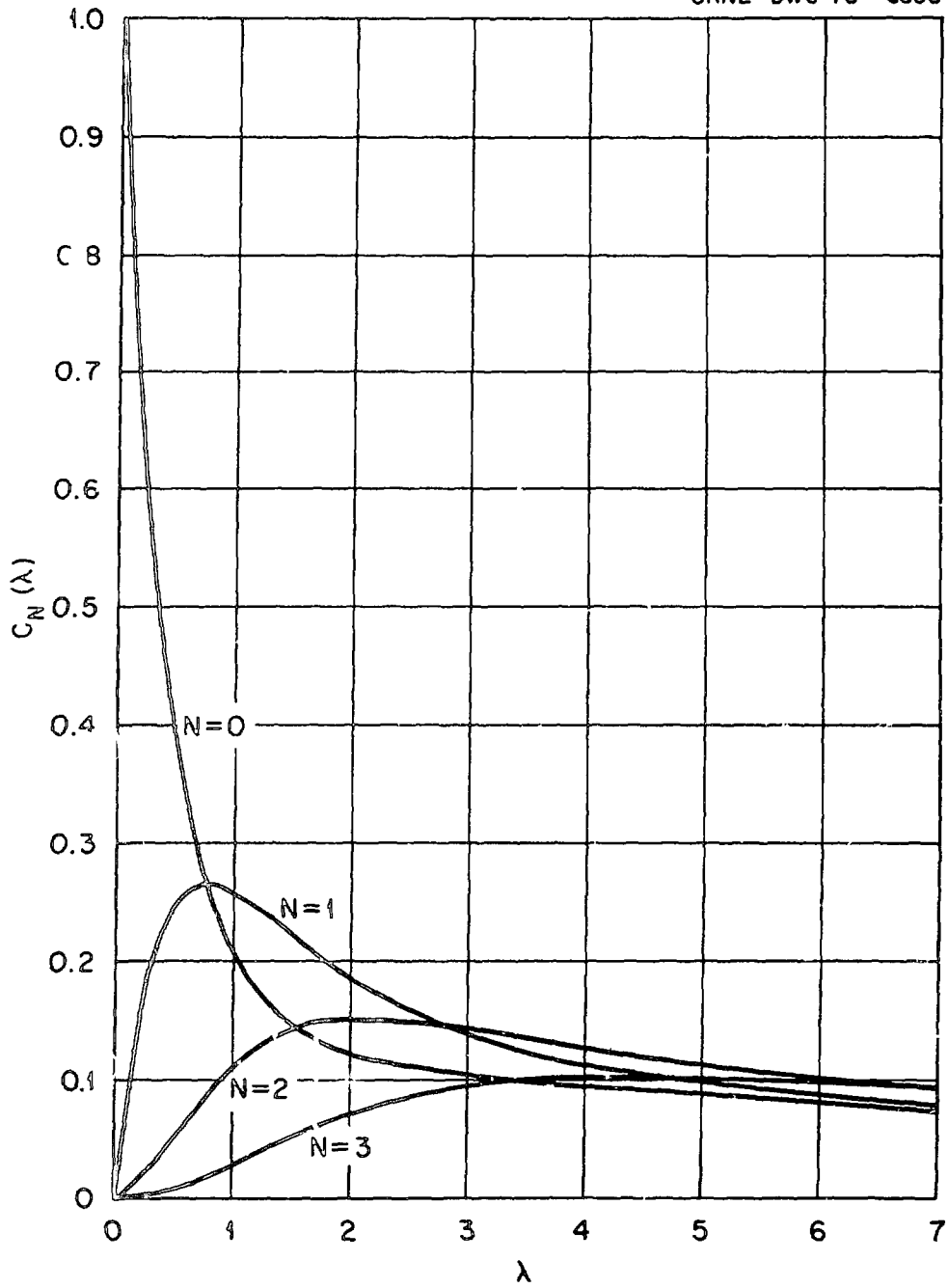


Figure 2

ORNL-DWG 70-6349

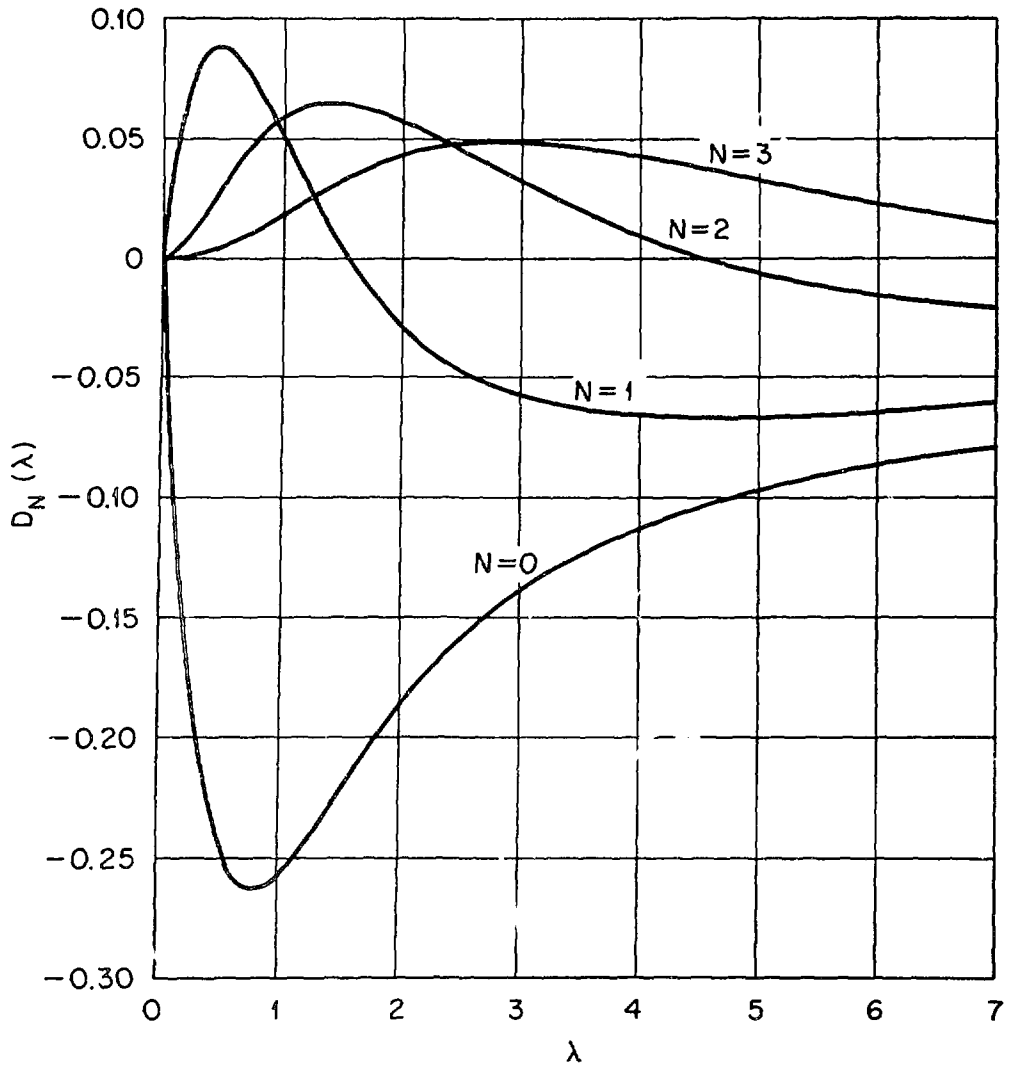


Figure 3

PROPERTIES OF MODES WITH LONG PARALLEL WAVELENGTHS

$$\text{IF } H \equiv k_{\parallel} \alpha_{\parallel} / \Omega_e \ll 1$$

$$\frac{\text{Re } \sigma_{\ell}}{\omega \epsilon_r} \sim 2\sqrt{\pi} \frac{\omega_{ph,e}^2}{k^2 \alpha_{\parallel}^2} \frac{1}{H} \left\{ \exp\left[-\left(\frac{1}{2} + \eta\right)^2\right] \times \left[ \left(\frac{1}{2} + \eta\right) C_N + N T D_N \right] \right. \\ \left. + \exp\left[-\left(-\frac{1}{2} + \eta\right)^2\right] \times \left[ \left(-\frac{1}{2} + \eta\right) C_{N+1} + (N+1) T D_{N+1} \right] \right\}$$

$$\eta \equiv \frac{\omega}{\Omega} - N - \frac{1}{2}$$

$$\tau \equiv \tau_{\parallel} / \tau_{\perp}$$

Figure 4

In Figure 5, we show frequencies near the first gyroharmonic and wavelengths for which  $\text{Re}\sigma_{\ell} < 0$ , using the temperature anisotropy,  $T$ , as a parameter and fixing  $\lambda = 0.69$  to maximize  $C_1$ . Strong negative dissipation is thus possible if

- (i)  $\omega/\Omega \geq 0.5$
- (ii)  $k_{\parallel}\alpha_{\parallel} \sim \Omega - \omega \leq \Omega/2$
- (iii)  $k_{\perp}\alpha_{\perp}/\Omega \geq 1$  .

The conditions under which normal modes of the appropriate frequency and wavelength will exist are determined from the cold-electron dispersion relation

$$\frac{\omega_{pe}^2}{\Omega^2} \geq \frac{3}{4} \frac{1 + 8\lambda T}{3 - 8\lambda T} .$$

Even if the hot-electron distribution is as nearly isotropic as permitted by collisionless confinement in a magnetic mirror ( $T \rightarrow 1$ ), negative dissipation is still possible if

$$\text{NTD}_n < 0 ,$$

and

$$|(\omega/\Omega - N)C_n| < |\text{NTD}_n| .$$

For modes near the first gyroharmonic, and specializing to the illustrative distribution function for which  $D_n$  has been shown here, negative dissipation is possible if

- (i)  $\omega/\Omega - 1 \leq 0.67 T$
- (ii)  $k_{\parallel}\alpha_{\parallel} \approx \omega - \Omega$
- (iii)  $k_{\perp}\alpha_{\perp}/\Omega \geq 1$  .

The appropriate normal modes are upper hybrid waves:

ORNL-DWG 70-6348

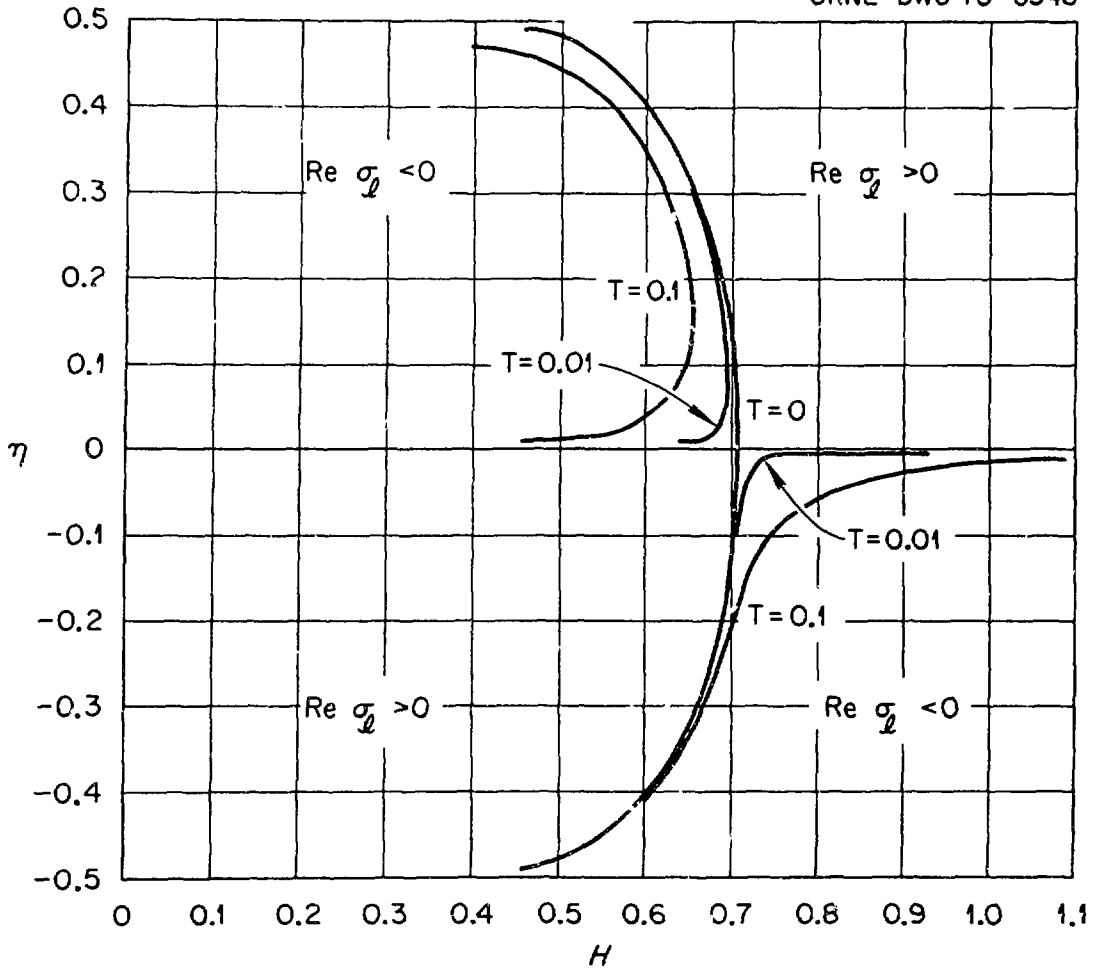


Figure 5

$$\omega/\Omega \cong \omega_{uh}/\Omega \cong \sqrt{1 + \omega_{pc}^2/\Omega^2}$$

$$\cong 1 + 0.67 T$$

or

$$\frac{\omega_{pc}^2}{\Omega^2} \leq 1.34 T + 0.45 T^2$$

The characteristics of these two distinct classes of modes can be summarized on a Brillouin plot, as in Figure 6. The solid lines show the normal modes, while the dashed lines indicate conditions for strong growth. Note especially that anisotropy-driven modes can occur if the density exceeds a threshold value,

$$\frac{\omega_{pc}^2}{\Omega^2} > \frac{1}{4} \quad \text{for anisotropy-driven growth,}$$

while the loss-cone modes can occur if the density is less than a critical value,

$$\frac{\omega_{pc}^2}{\Omega^2} \leq 1.34 T + 0.45 T^2 \quad \text{for loss-cone driven growth.}$$

There is thus a stable intermediate range of cold-electron densities, as shown in Figure 7.

On Figure 7, we also show a curve obtained by numerical solution of the dispersion relation for an artificial case in which all electrons are hot. The general conclusions are not altered, indicating a rather weak dependence on temperature of the normal mode dispersion relation. In fact, the character of these modes has been analyzed in great detail and the interested reader is referred to Ref. 1 for additional detail.

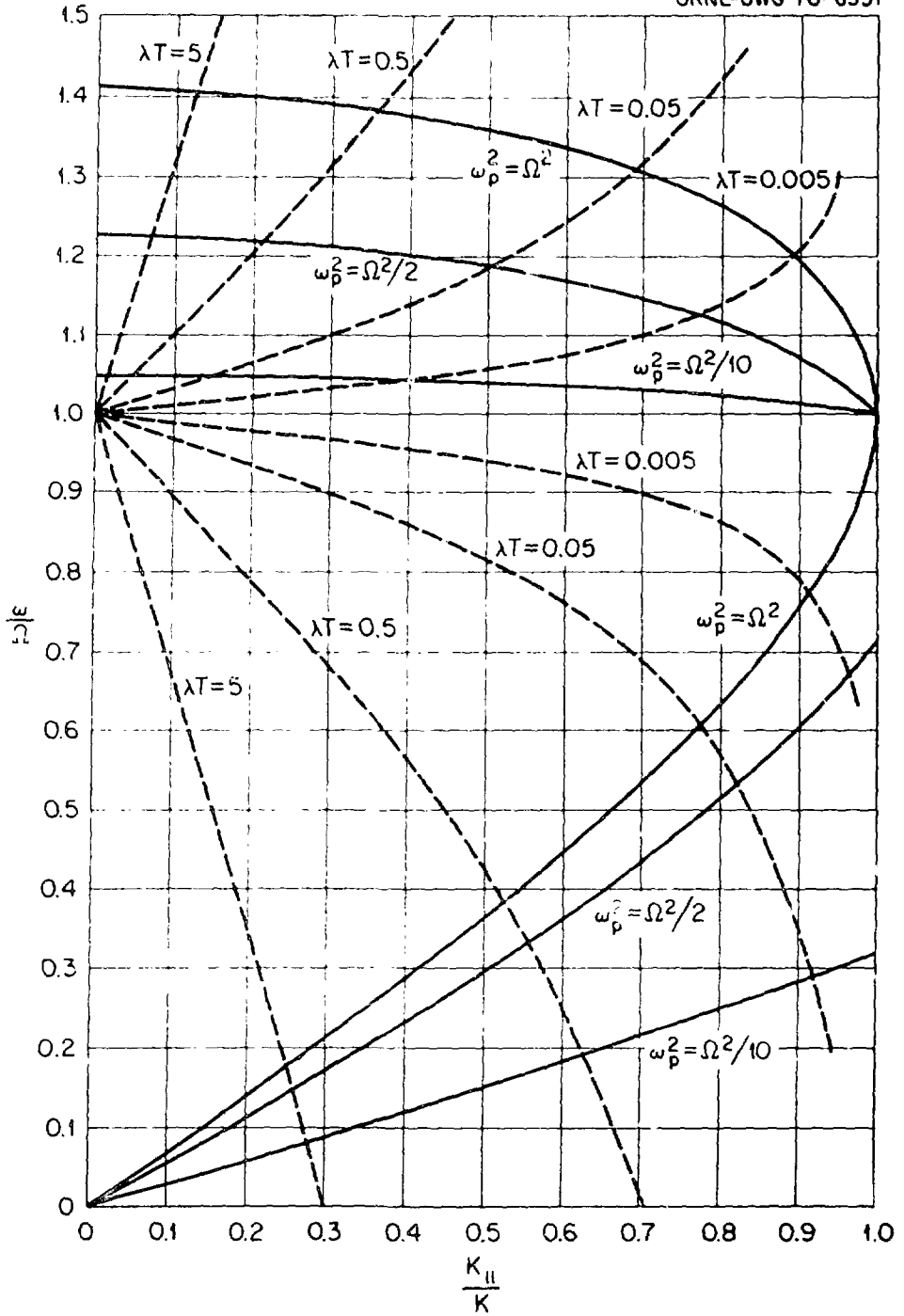


Figure 6

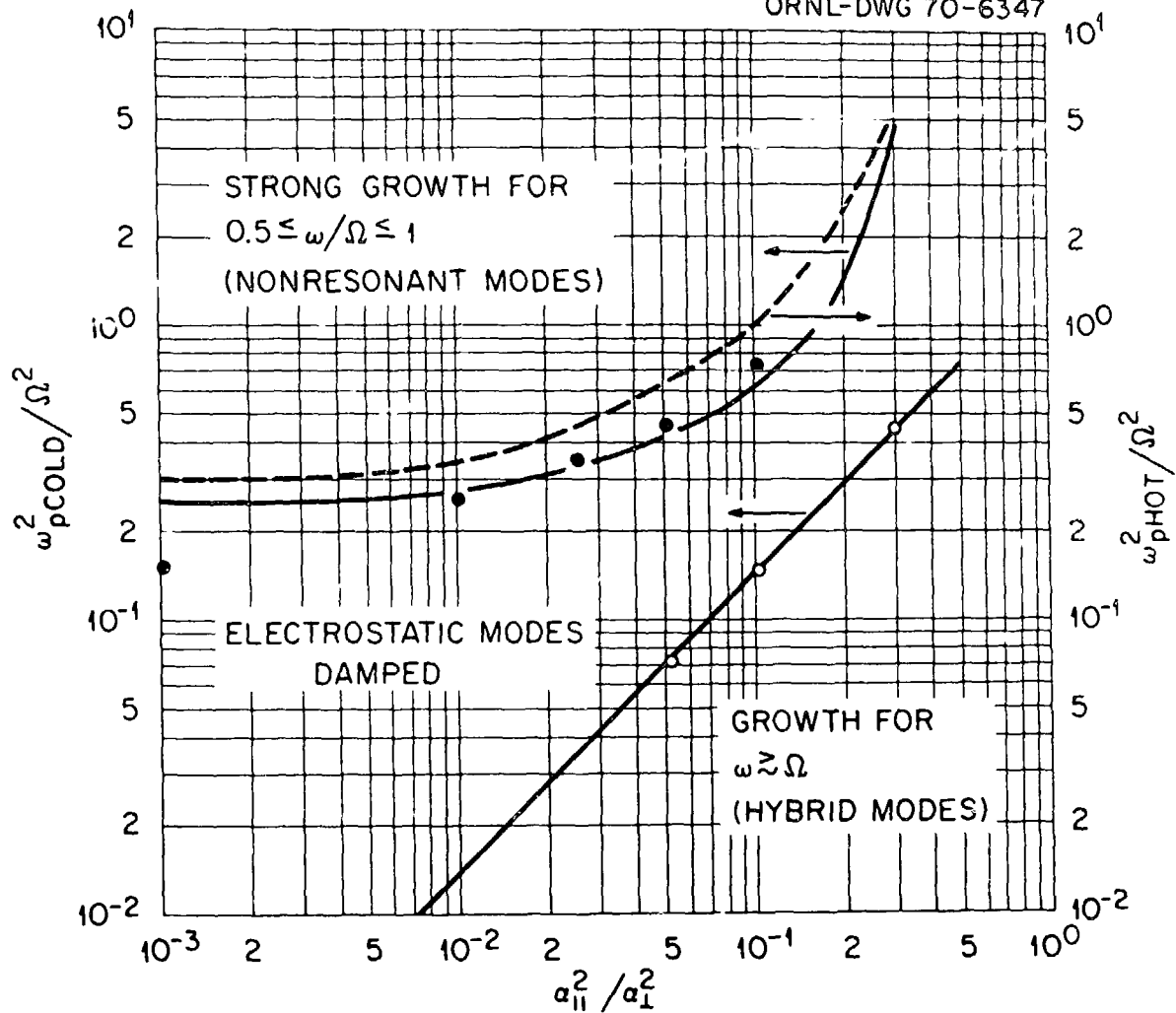


Figure 7

Unstable electromagnetic waves propagating in the whistler mode are known to occur in ECH plasmas [4] if the pressure is sufficiently anisotropic. Here, we shall only cite a few key criteria. In particular, the growth changes from absolute to convective if [5]

$$T_{\parallel}/T_{\perp} \geq \left(\frac{2}{3}\right)^{3/2} \left(\frac{\omega p_{\perp}}{\Omega_c}\right) = (8\beta_{\perp}/27)^{1/2} \quad ,$$

and growth ceases if [6]

$$T_{\parallel}/T_{\perp} \geq (\beta_{\perp}/2)^{1/2} \quad .$$

The unstable whistler modes are also stabilized by the relativistic spread in electron mass in hot-electron ECH plasmas. Stability criteria have been obtained only for specific distributions.

To this point, we have used the temperature anisotropy simply as a parameter, without any regard for its relation to other system parameters. However, electron cyclotron heating permits some useful conclusions regarding this contribution to the hot-electron free energy, since heated electrons tend to be confined within the resonant surface:

$$B = B_{\mu} = 2\pi f_{\mu} m/e \quad .$$

Here,  $B_{\mu}$  is the magnetic field strength at which the electron gyrofrequency equals the applied microwave frequency. Since heated electrons turn within that surface, the individual electrons satisfy

$$\frac{E}{\mu} < B_{\mu} \quad .$$

On the mid-plane, where  $B = B_0$ , the electrons lie in a region of velocity space given by

$$\frac{v_{\parallel}^2}{v_1^2} \lesssim \frac{B_{\mu}}{B_0} - 1 \quad .$$

Thus it is reasonable to suppose that

$$T \equiv \frac{T_{\parallel}}{T_1} \lesssim \frac{B_{\mu}}{B_0} - 1 \quad .$$

If the magnetic field strength and microwave frequency are such that  $B_{\mu} > B_0$ ,  $T$  will be small and instabilities may occur. If, on the other hand,  $B_{\mu}/B_0$  exceeds a certain critical value, the anisotropy may be moderate enough to circumvent some of these modes. Moreover, as the plasma beta increases,  $B_{\mu}/B_0$  will increase, roughly as

$$\frac{B_{\mu}}{B_0} \sim \left( \frac{B_{\mu}}{B_0} \right)_{\text{vac}} \frac{1}{\sqrt{1 - \beta}} \quad ,$$

and the anisotropy will diminish still further.

We conclude this material with a brief summary in Figure 8 and 9.

#### REFERENCES

- [1] GUEST, G.E. and SIGMAR, D.J., Nucl. Fusion 11, 151 (1971).
- [2] CALLEN, J.D. and GUEST, G.E., Nucl. Fusion 13, 87 (1973).
- [3] GUEST, G.E. and DORY, R.A., Physics Fluids 8, 1853 (1965).
- [4] IKEGAMI, H., et al., "Characteristics of Microinstabilities in a Hot Electron Plasma," Plasma Physics and Controlled Nuclear Fusion Research (Proc. Conf. Novosibirsk, 1968) 2, 423 (1969), IAEA, Vienna.
- [5] HEDRICK, C.L., ORNL Thermonuclear Division Annual Progress Report (1971).
- [6] BERS, A. and ROBERTSON, E.A., MIT Quarterly Progress Report No. 79, 111 (1965).

## SUMMARY

## 1.0 MICROSCOPIC MODES

## 1.1 Temperature Anisotropy

$$0.5 \leq \omega/\Omega_e \leq 1$$

$$\omega_{pe,c}^2/\Omega_e^2 \geq 1/4$$

$$T_{\parallel}/T_{\perp} \leq 1/6$$

## 1.2 Loss Cone/Anisotropy

$$\omega/\Omega_e \geq 1$$

$$\omega_{pe,c}^2/\Omega_e^2 \leq 1.34 T_{\parallel}/T_{\perp} + 0.45 T_{\parallel}^2/T_{\perp}^2$$

## 1.3 Whistlers

$$T_{\parallel}/T_{\perp} \lesssim (\beta_{\perp}/2)^{1/2}$$

Figure 8

## SUMMARY (Continued)

## 2.0 MACROSCOPIC MODES

## 2.1 Mirror Instabilities

$$\beta \left( \frac{T_{\perp}}{T_{\parallel}} - 1 \right) < 1 \quad \text{for stability}$$

But,

$$\frac{T_{\parallel}}{T_{\perp}} \lesssim R_{\mu} - 1 \sim \frac{R_{\mu 0}}{(1 - \beta)^{1/2}} - 1$$

Therefore,

$$R_{\mu 0} \gtrsim 1.2 \quad \text{for stability}$$

## 2.2 Curvature Driven Instabilities

## 2.2.1 Fluid Models (Bumpy Cylinder)

- o realistic geometry, arbitrary beta, non-local
- o generally unstable: interchange at low beta  
ballooning at high beta
- o models lack

FLR stabilization

cold-plasma stabilization

other kinetic effects

## 2.2.2 Microscopic Models (cf Don Spong)

Figure 9

REVIEW OF RECENT EBT COUPLED  
RING-CORE STABILITY THEORY\*

D. A. Spong  
Oak Ridge National Laboratory  
Oak Ridge, Tennessee

During the past several years Elmo Bumpy Torus (EBT) stability calculations have evolved with respect to treatment of ring-core plasma coupling effects. This evolution began with recognition of the important role of ring compressibility and paramagnetic effects on core beta limits. Since then, models have continued to increase in sophistication, including ring-core frequency coupling, velocity space and hot electron distribution function effects, and radially dependent models. Some of these features have resulted in wide variations in predicted plasma performance limitations. A number of the models will be reviewed and assumptions to which they are particularly sensitive will be discussed.

---

\*Research sponsored by the Office of Fusion Energy, U.S. Department of Energy, under contract W-7405-eng-26 with the Union Carbide Corporation.

## I. Introduction

Elmo Bumpy Torus (EBT) stability theory has become an area of increasing interest recently due to the recognition of a number of novel nonmagnetohydrodynamic effects associated with a hot electron annulus and its coupling to the core plasma. Such effects are of importance both in understanding the various operating regimes of the present device and in extrapolating to future larger devices.

The earlier calculations of EBT stability tended to decouple the ring and core plasmas and treat them as separate components for simplicity. Ring stability calculations<sup>1-3</sup> generally assumed cold, pressureless core plasmas, whereas core stability calculations often used rigid noninteracting ring models.<sup>4-5</sup> Ring-core coupling effects were first included in slab models<sup>6-7</sup> which treated the ring as an interacting charge and current element but which did not retain the full frequency coupling between ring and core due to the assumption that their temperatures were widely separated. Such calculations indicated the importance of ring compressibility and paramagnetic effects on the core beta limits. That is, the magnetic well and resulting maximum in  $\oint d\ell/B$  can only stabilize interchanges up to some maximum core beta at which the ring and core begin to interact. More recent calculations<sup>8-14</sup> have included the ring-core coupling in greater detail. This has resulted in the appearance of a new mode involving interaction between the compressional Alfvén wave of the core plasma and the free energy of the hot electron component, which leads to an upper limit on the core density. In addition, the core interchange<sup>6-7</sup> and hot electron interchange<sup>1-3</sup> modes still remain. These set upper

limits on the core beta and lower limits on the core density, respectively.

In this review, the development of EBT coupled ring-core stability work will be traced over the past several years, beginning with the early slab models<sup>6-7</sup> and going through some of the recent nonlocal models which treat the radial dependence of the modes.

## II. Vlasov-Maxwell Slab Model

The first detailed treatments<sup>6-7</sup> of ring-core coupling in EBT were made in simplified slab geometry in order to isolate the coupling and kinetic effects from the geometry. The analysis is normally localized to the outside half of the annulus where magnetic field gradients are fully reversed. This is related to the fact that only in this region can substantial core pressure gradients be stably supported. In the normal magnetic gradient region (i.e.,  $B' < 0$ ), a finite pressure gradient can stably exist up to a certain value. However, this is not usually the limiting region for overall stability; rather, the outside region is. The slab models continue to be investigated as they provide a useful framework in which qualitative effects of various changes in the model may be investigated.

The slab geometry is displayed in Fig. 1. It normally consists of a wave propagating in the y direction, an artificial gravity in the -x direction, a magnetic field in the z direction, magnetic field and density gradients in the x direction, and a guiding center drift in the y direction. The B field is modeled as

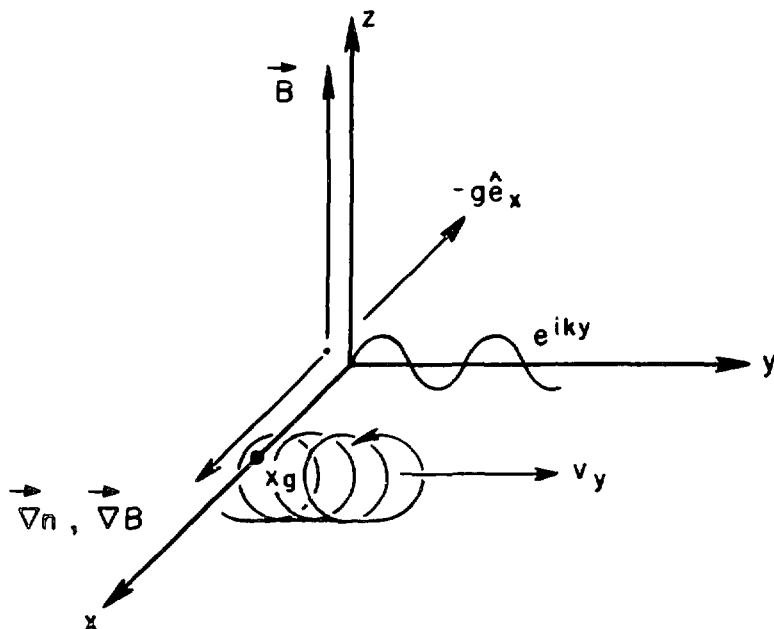


Fig. 1. Directions of gradients, B field, artificial gravity, drift velocity, and wave propagation in Vlasov-Maxwell model.

$$\vec{B} = B_0(1 + \epsilon x)\hat{e}_z \quad (1)$$

In this geometry the constants of the motion are:  $H$ , the total energy;  $x_g$ , the guiding center position; and  $v_{\parallel}$ , the velocity component along the magnetic field line. An equilibrium distribution of the following form may then be chosen:

$$f_0(H, x_g) = N_0(\alpha/\pi)^{-3} e^{-(v^2 + 2gx)/\alpha^2} (1 + \epsilon' x_g) \quad (2)$$

Taking moments of this distribution and using charge neutrality (Poisson's equation), the momentum balance equation, and Ampere's law, the parameters  $\epsilon$  and  $\epsilon'$  are obtained as

$$\begin{aligned} \epsilon' &= \frac{1}{L_n} + \frac{2}{R_c} \\ \epsilon &= -\frac{\beta}{2} \left( \frac{1}{L_n} + \frac{2}{R_c} \right) \end{aligned} \quad (3)$$

For the configuration shown in Fig. 1, the single particle orbits are

$$\begin{aligned} \dot{x} &= v_{\perp} \sin \chi \\ \dot{y} &= -v_{\perp} \cos \chi + v_D \end{aligned} \quad (4)$$

where

$$v_D = \frac{v_{\perp}^2 \epsilon}{2\Omega} + \frac{kT}{2\Omega R_c}$$

The perturbed distribution is then obtained by solving the linearized Vlasov equation. For the model under consideration, the perturbed electromagnetic fields may be described by the electrostatic potential  $\phi$  and the vector potential  $A_x$ . In this case the kinetic equation may be written as

$$\frac{\partial f_1}{\partial t} = q \frac{\partial f_0}{\partial H} \frac{\partial \phi}{\partial t} + \frac{iq\omega}{m} D(\phi - v_x A_x) \quad (5)$$

where

$$D = m \frac{\partial f_0}{\partial H} + \frac{k}{\omega\Omega} \frac{\partial f_0}{\partial x_g}$$

The perturbed distribution is then obtained, using standard orbit integration techniques, as

$$f_1 = -\frac{qNf_B}{kT} (1 + \epsilon' x_g) \left\{ \phi \left[ 1 - (\omega - \omega_*) \sum_{n,m} \frac{J_m J_n e^{i(m-n)\theta}}{kv_d - \omega - m\Omega_c} \right. \right. \\ \left. \left. + i v_{\perp} A_x (\omega - \omega_*) \sum_{n,m} \frac{J'_m J_n e^{i(m-n)\theta}}{kv_d - \omega - m\Omega_c} \right] \right\} \quad (6)$$

From this the perturbed charge and current may be obtained as

$$\rho = -\frac{\omega_p^2}{\alpha^2} \phi \left[ 1 + (\omega - \omega_*) \int d^2 v f_B \sum \frac{J_m^2}{kv_d - \omega - m\Omega_c} \right]$$

$$-\frac{i\omega_p^2}{\alpha^2} A_x(\omega - \omega_*) \int d^2v f_B \Sigma \frac{v_{\perp} J_m J_m'}{kv_d - \omega - m\Omega_c} \quad (7)$$

$$j_x = \frac{i\omega_p^2}{\alpha^2} \phi(\omega - \omega_*) \int d^2v f_B \Sigma \frac{v_{\perp} J_m J_m'}{kv_d - \omega - m\Omega_c}$$

$$-\frac{\omega_p^2}{\alpha^2} A_x(\omega - \omega_*) \int d^2v f_B \Sigma \frac{v_{\perp}^2 J_m'^2}{kv_d - \omega - m\Omega_c} \quad (8)$$

Combining Eq. (7) and (8) with Maxwell's equations one obtains the following dispersion relation:

$$D_{es} D_{em} + CT^2 = 0 \quad (9)$$

$$D_{es} = \frac{\omega_p^2}{k^2 \alpha^2} \left[ 1 + (\omega - \omega_*) \int d^2v f_B \Sigma \frac{J_m^2}{kv_d - \omega - m\Omega_c} \right]$$

$$D_{em} = 1 + \frac{\omega_p^2}{k^2 c^2 \alpha^2} (\omega - \omega_*) \int d^2v f_B \Sigma \frac{v_{\perp}^2 J_m'^2}{kv_d - \omega - m\Omega_c}$$

$$CT = \frac{\omega_p^2}{c^2 k^2 \alpha^2} (\omega - \omega_*) \int d^2v f_B \Sigma \frac{v_{\perp} J_m J_m'}{kv_d - \omega - m\Omega_c}$$

where

$$d^2v = 2\pi v_{\perp} dv_{\perp} dv_{\parallel}$$

We shall now discuss several of the approximations that have been made in solving the above dispersion relation in recent years and their relationship to each other.

### A. NVL Approximation

In work by Nelson<sup>7</sup> and Van Dam and Lee<sup>6</sup> (referred to here as NVL) Eq. (9) is reduced to a quadratic equation in  $\omega$  by assuming  $\omega_{\ast i}, \omega_{di} \ll \omega \ll \omega_{\ast H}, \omega_{dH}, \Omega_{ci}$ , where the  $i$  subscripts refer to the ions and the  $H$  subscripts refer to the hot electrons. The resulting dispersion relation is

$$A\omega^2 + b\omega + C = 0 \quad (10)$$

where

$$A = \frac{1}{2} k^2 \rho_1^2 + \delta^2 \frac{\beta_i}{2} D_{em}^{-1} \left( \frac{C_2 \omega_{\ast H}}{\omega_{dH}} - 1 \right)^2$$

$$B = \frac{\delta}{2} \left[ \omega_{\ast i} - \omega_{di} + \beta_i D_{em}^{-1} (\omega_{\ast i} - \omega_{di} - \omega_{Bi}) \times \left( \frac{C_2 \omega_{\ast H}}{\omega_{dH}} - 1 \right) \right]$$

$$C = (\omega_{\ast i} - \omega_{di}) \omega_{di} + \frac{1}{2} \beta_i D_{em}^{-1} (\omega_{\ast i} - \omega_{di} - \omega_{Bi})^2$$

$$D_{em} = 1 + \beta_i + \frac{1}{2} C_3 \beta_h \frac{\omega_{\ast H}}{\omega_{dH}}$$

Two models for the hot electron distribution were considered in this work, a delta function<sup>1-2</sup> and a Maxwellian.<sup>7</sup> In the case of the delta function, the constants  $C_1$ ,  $C_2$ , and  $C_3$  are all equal to unity. For the Maxwellian, they may be expressed in terms of exponential integrals:

$$C_1 = \frac{e^{-\omega_{\ast H}}}{\omega_{\ast H} - \omega_{dH}} \left[ 1 + \frac{\omega_{\ast H}}{\omega_{dH}} F(a) \right]$$

$$C_2 = \frac{\omega_{dH}}{\omega_{BH}} [1 - aF(a)] \quad (11)$$

$$C_3 = \frac{\omega_{dH}}{\omega_{BH}} [1 + a - a^2F(a)]$$

where

$$F(a) = e^{-a} \text{Ei}(a)$$

$$a = - \frac{\omega_{gH}}{\omega_{BH}}$$

The resulting stability boundaries, obtained by requiring  $B^2 - 4AC > 0$ , are plotted in Fig. 2 for the delta function and in Fig. 3 for a Maxwellian. These show that the  $\beta_H$  threshold for stabilization of flute modes in the core is similar to that obtained from some of the earlier noninteracting ring models; i.e.,

$$\beta_i + \beta_H > \frac{4\Delta/R_C}{1 + 2\Delta/R_C} = 15-20\% \quad (12)$$

where

$\Delta$  = ring half width

$R_C$  = radius of curvature

However, the upper limit on  $\beta_c$  is now in the 20-30% range for a delta function and in the 10-15% range for the Maxwellian. For the delta function this is given approximately by:

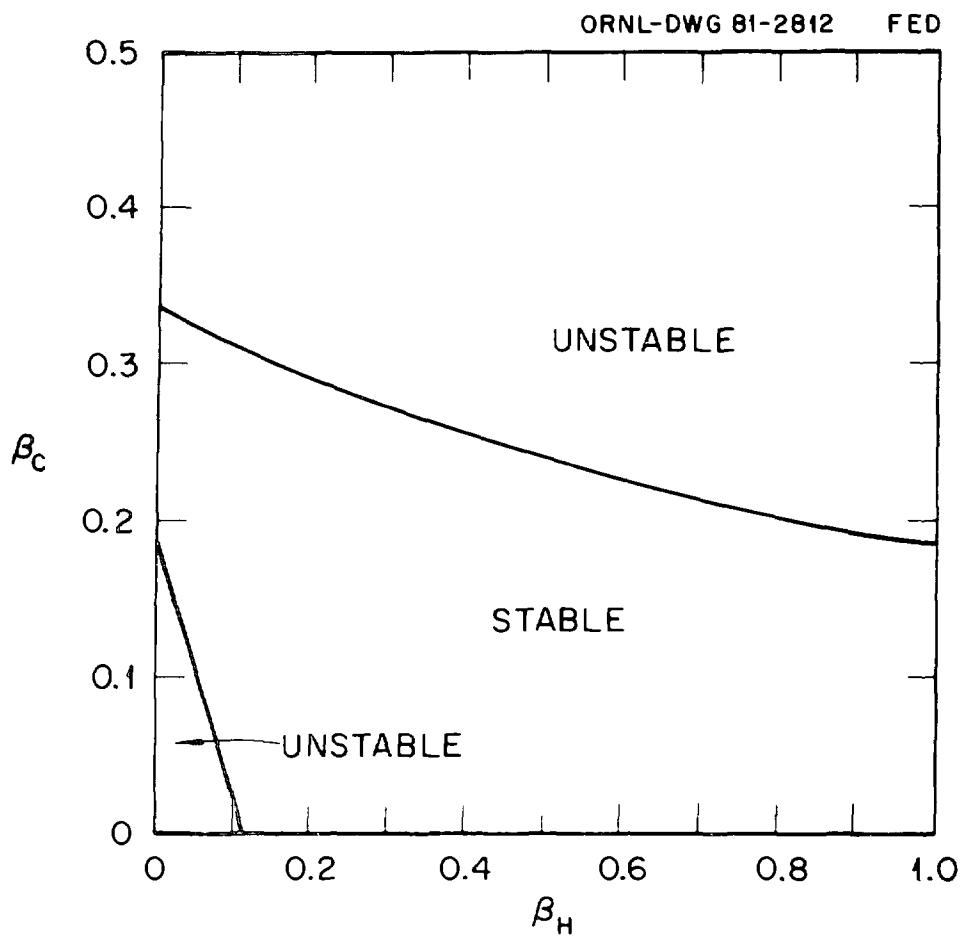


Fig. 2. Stability boundaries as predicted by Eq. (10) for a delta function hot electron distribution with  $n_H/n_c = 0.05$ ,  $ka_f = 0.1$ , and  $\Delta/R_c = 0.05$ .

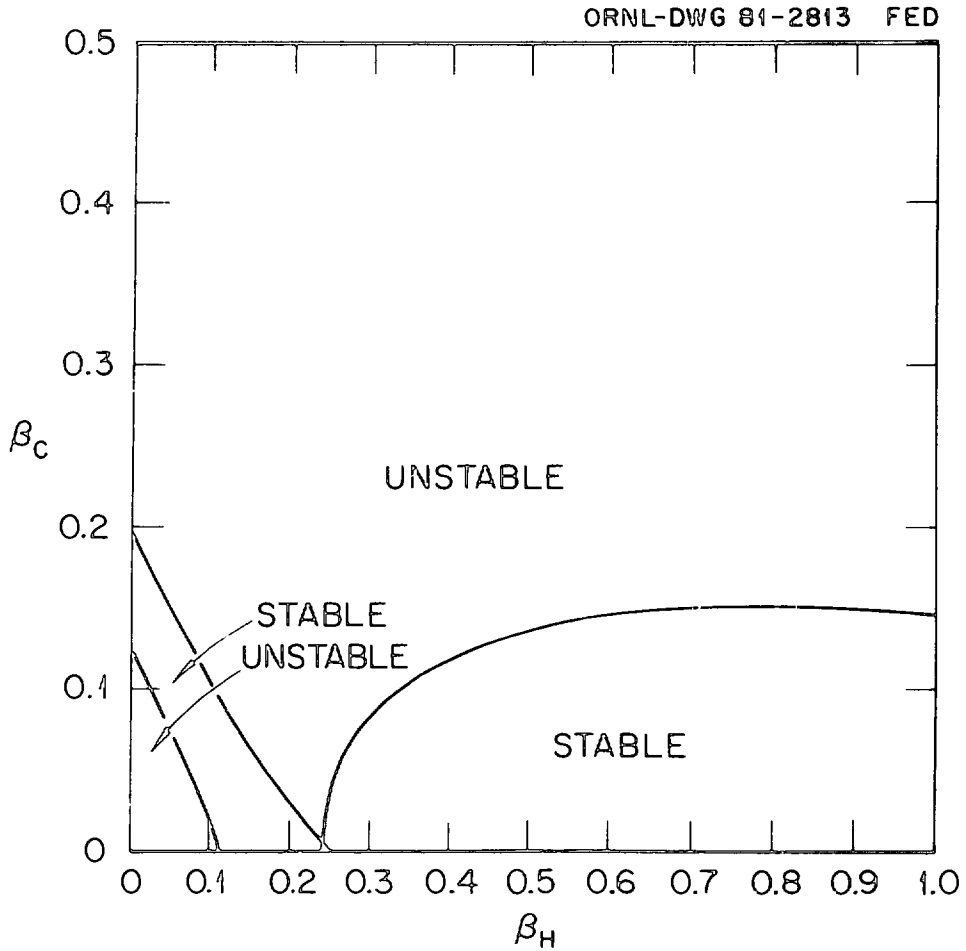


Fig. 3. Stability boundaries as predicted by Eq. (10) for a Maxwellian hot electron distribution with  $n_H/n_C = 0.05$ ,  $ka_1 = 0.1$ , and  $\Delta/R_C = 0.05$ .

$$\beta_c < \frac{4\Delta/R_c}{1 + \beta_H} \quad (13)$$

whereas for the Maxwellian it is

$$\beta_c < \frac{2\Delta/R_c}{1 + 6\Delta/R_c} \quad (14)$$

In applying the above results, there is some ambiguity over what value to use for the magnetic field-line radius of curvature  $R_c$ . Energy principle calculations, which will be mentioned latter, have indicated that the curvature at the rings, rather than the field line averaged curvature, is the appropriate value to take.

The upper limits of  $\beta_{\text{core}}$  given by Eqs. (13) and (14) are related to the ineffectiveness of the self-dug well of the hot electrons in stabilizing perturbations in the core plasma. At very low  $\beta_c$  the well stabilizes the core plasma by reversing the ion drift velocity to the opposite direction from the ion diamagnetic drift. As  $\beta_c$  is raised, the ion drifts begin to be influenced<sup>14</sup> by  $\delta B_z$  such that the drift reversal which is stabilizing at low  $\beta_c$  can no longer be attained. As a result, the plasma response to the perturbation changes phase and the well is ineffective. In terms of Eq. (10),  $D_{\text{em}}$  becomes very small due to a near cancellation of terms near the stability boundary, and the magnetic field perturbation  $\delta B_z$  is greatly enhanced. This effect depends on the presence of the hot electrons and can also be viewed as an enhancement in their compressibility<sup>1</sup> since  $\tilde{p}_{1H}$  scales directly as  $\delta B_z$ .

### B. Inclusion of Ring-Core Frequency Coupling

As mentioned earlier, the NVL approximation is based upon the ordering  $\omega_{*i}, \omega_{Di} \ll \omega \ll \omega_{*H}, \omega_{dH}, \Omega_{ci}$ . From the results of this calculation, it would be expected that a breakdown of this ordering should occur near the stability boundaries. For example, at the boundary in the lower left-hand corners of Figs. 2 and 3 (i.e., where the hot electron beta is just sufficient to produce a well and stabilize the core interchange mode),  $\omega_{dH}$  and  $\omega_{di}$  pass through zero and reverse direction. Thus, the assumption that  $\omega_{di} \ll \omega \ll \omega_{dH}$  is inadequate in this region. Also, near the upper limit on  $\beta_{core}$ , the frequency  $\omega$  becomes large and is comparable to the hot electron drift and diamagnetic frequencies. These considerations motivated a more accurate treatment of the frequency dependence in the slab model dispersion relation.

A dispersion relation which retains  $\omega$  relative to the hot electron drift and diamagnetic frequencies is given below:

$$D_{es}D_{em} + CT^2 = 0 \quad (15)$$

where

$$D_{es} = \sum_s \frac{n_s}{n_i} \frac{T_i}{T_s} \left\{ 1 - \frac{\omega - \omega_{*s}}{\omega_{BS}} \left[ F(x_s) + \frac{k^2 \rho_s^2}{2} (1 - x_s F(x_s)) \right] \right\}$$

$$D_{em} = 1 - \sum_s \frac{\beta_s (\omega - \omega_{*s})}{2\omega_{BS}} [1 + x_s - x_s^2 F(x_s)]$$

$$CT = \sqrt{\frac{\beta_i}{2}} \sum_s \sigma_s \frac{n_s}{n_i} \frac{\omega - \omega_{*s}}{\omega_{BS}} [1 - x_s F(x_s)]$$

$$F(x_s) = e^{-x_s} \text{Ei}(x_s)$$

$$x_s = \frac{\omega - \omega_{gs}}{\omega_{BS}}$$

$$\omega_{BS} = \frac{k\alpha_s^2 \epsilon}{2\Omega_s}$$

$$\omega_{gs} = \frac{k\alpha_s^2}{\Omega_s R_c}$$

$$\omega_{*s} = \frac{k\alpha_s^2}{2\Omega_s \Delta} \left(1 + 2 \frac{\Delta}{R_c}\right)$$

$\sum_s$  = sum over species  $s$

$n_s, T_s$  = density and temperature of species  $s$

$\Delta, R_c$  = ring half-width and B field radius of curvature

$$\alpha_s^2 = 2T_s/m_s$$

The stability boundaries for this dispersion relation may be examined by plotting the zeros of Eq. (15) for  $\omega$  real and looking for points where two roots coalesce into a single root. An example of this is given in Fig. 4 where zeros of Eq. (15) are plotted for  $T_e = T_i$ ,  $T_H/T_i = 500$  and  $1000$ ,  $ka_i = 0.1$ ,  $n_H/n_c = 0.001$ ,  $\beta_H = 0.5$ , and  $\Delta/R_c = 0.05$  along with the zeros of the quadratic dispersion relation of Eq. (10) for a Maxwellian hot electron distribution. As may be seen, the instability boundaries of Eq. (15) are somewhat lower than those of Eq. (10). Also, there is now a scaling with  $T_H/T_i$  present when  $\omega$ ,  $\omega_{dH}$ , and  $\omega_{*H}$  are retained as being of similar order. It may be seen

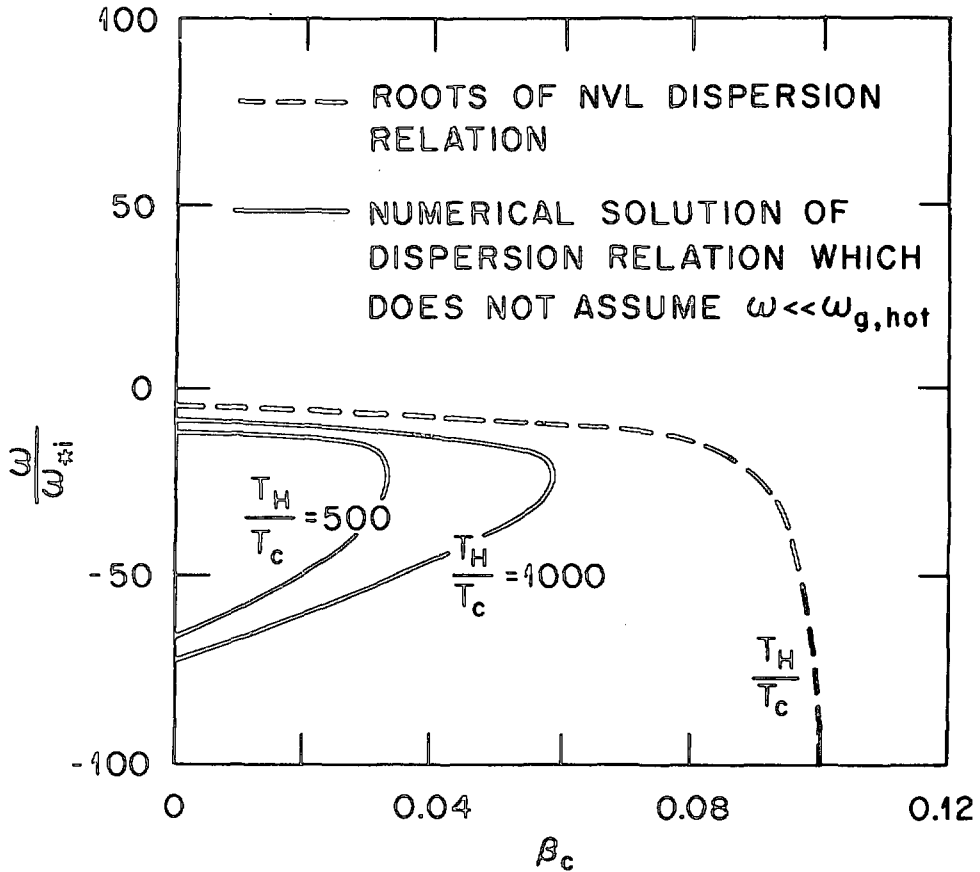


Fig. 4. Roots of dispersion relation (15) vs  $\beta_c$  for  $T_H/T_c = 500, 1000$  as compared with the roots of Eq. (10). Here,  $ka_1 = 0.1$ ,  $n_H/n_c = 0.001$ ,  $\beta_H = 0.5$ , and  $\Delta/r_c = 0.05$ .

from this figure that the  $\beta_c$  limit is related to a coupling between the core interchange mode (the upper half of the solid curves) and the hot electron drift frequency ( $\omega_{gH}/\omega_{*i} \approx -90$ , i.e., the lower half of the solid curves).

This observation of coupling between two disparate frequencies then motivated the inclusion of additional physics in the model, namely the ion cyclotron harmonics and the core Alfvén wave.<sup>8-9</sup> Such terms can be of importance in EBT since the hot electron drift frequency in the present device is on the same order of or larger than the ion cyclotron frequency.<sup>15</sup> Including these effects then results in the following modifications to the dispersion relation given in Eq. (15).

$$D'_{es} = D_{es} + \frac{k^2 \rho_1^2}{2} \frac{(\omega - \omega_{*i})(\omega - \omega_{gi})}{(\omega - \omega_{gi})^2 - \Omega_{ci}^2} \quad (16)$$

$$D'_{em} = D_{em} + \frac{\beta_i}{k^2 \rho_1^2} \frac{(\omega - \omega_{*i})(\omega - \omega_{gi})}{(\omega - \omega_{gi})^2 - \Omega_{ci}^2} \quad (17)$$

$$CT' = CT + \sqrt{\frac{\beta_i}{2}} \frac{(\omega - \omega_{*i})(\omega - \omega_{gi})}{(\omega - \omega_{gi})^2 - \Omega_{ci}^2} \quad (18)$$

where  $D_{es}$ ,  $D_{em}$ , and  $CT$  are given in Eq. (15). This dispersion relation then incorporates the first ion cyclotron harmonic. Higher harmonics have been included,<sup>9</sup> but generally the first is sufficient to accurately describe the resulting modes. In Fig. 5, the zeros of this dispersion relation have been plotted against the core beta for several values of the parameter  $Q = kv_{dh}/\Omega_{ci}$ . This parameter controls the importance of the ion cyclotron terms. That is, for  $Q \ll 1$ ,  $\Omega_{ci}$  is

effectively infinite in comparison to  $\omega$ , and one returns to the approximation given in Eq. (15); however, when  $Q \approx 1$ , Eq. (15) is no longer adequate and  $\omega$  is comparable to  $\Omega_{ci}$ . As may be seen from Fig. 5, for small  $Q$  the results of Fig. 4 are recovered. However, as  $Q$  is raised a new type of frequency coupling enters in, resulting in a higher frequency mode which goes unstable at lower values of  $\beta_c$  than the NVL mode. This mode has generally come to be known as the compressional Alfvén wave mode and is related to a coupling between the hot electron drift frequency and the core Alfvén wave, as may be seen from the figure.

This instability results in an upper limit on the warm core density and was first recognized within the past year.<sup>8-9,11-12</sup> The original estimates<sup>8-9,11</sup> of the density limit from this mode were quite low (i.e.,  $\beta_{core} \lesssim 10^{-4}$  to  $10^{-3}$ ) and, in some cases, less than that obtained in the present experiment. This led initially to speculation that the Alfvén mode could possibly be a cause for the T-M transition. However, subsequent work<sup>11,13-14</sup> resulted in significantly higher values for the density limit which were well above the achieved densities in the existing device. A number of factors are responsible for this change and will be mentioned briefly here. For one thing, the earlier estimates generally used the lowest azimuthal wave number ( $m = 1$ ) which would fit in the machine since this resulted in the most limiting density. However, the localized theory should only be expected to be valid when the radial wavelength is small compared with the azimuthal (the direction the small way around the torus) wavelength. Since the earlier localized theories took the radial wavelength large compared to the annulus half width ( $k_r \approx 0$ ), they are

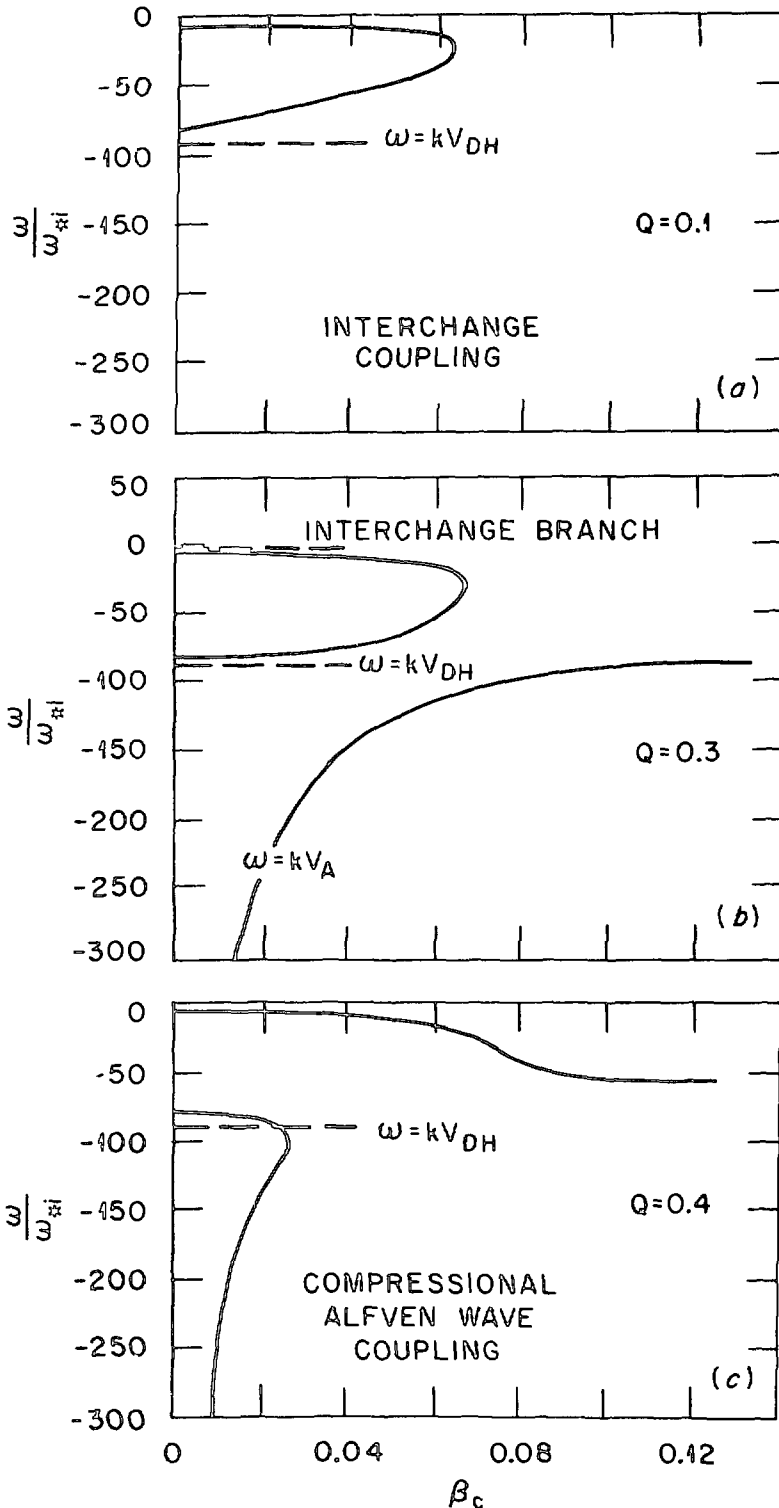


Fig. 5. Roots of dispersion relation (16)-(18) vs  $\beta_c$  as  $Q = kv_{dH}/\Omega_{ci}$  is raised. For low values of  $Q$  the hot electron free energy couples with the core interchange whereas for higher values it couples with the core compressional Alfvén wave. Here,  $ka_1 = 0.1$ ,  $n_H/n_c = 0.001$ ,  $\beta_H = 0.3$ ,  $\Delta/R_c = 0.05$ , and  $T_H/T_c = 1000$ .

not really applicable to low  $m$  modes. Another problem with the original estimates is that they assumed the ratio of the hot electron to core density was quite small. Later calculations<sup>11</sup> have allowed this ratio to be finite and have maintained a self-consistent relation between it and the other free parameters:  $\beta_{\text{core}}$ ,  $\beta_{\text{hot}}$ , and  $T_{\text{hot}}/T_{\text{core}}$ . Also, recent calculations<sup>12-13</sup> have included finite values for the radial wave number. This can enter in through factors of  $(k_{\perp}/k_y)^2$ , which scales as the aspect ratio of the ring squared,  $(a_p/\Delta)^2$ . This is a large factor ( $\approx 100$ ) and significantly increases the limiting density. Such calculations will be discussed in more detail in Sect. IV. Finally, a number of detailed refinements have been made in the calculations involving such things as: retaining the full two-dimensional energy and pitch angle dependence of the hot electron drift frequency<sup>11</sup> [in Eqs. (15)-(18) only the energy dependence is included], using both the delta function and the Maxwellian and anisotropic Maxwellian distribution functions<sup>11</sup> for the hot electrons, and taking into account<sup>14</sup> the shift from particle position to guiding center position in evaluating the perturbed distribution  $f_1$ . The importance of the latter effect was first pointed out in Ref. 5 for the hot electron interchange mode and is generally important for high frequency modes when inhomogeneities are present. Sensitivity of the results to the form of the hot electron distribution function was investigated in Ref. 11 where both delta function and Maxwellian models were used. It was found that coupling between the hot electron drift frequency and the core Alfvén wave was not present when a delta function hot electron distribution was used; however, with the

Maxwellian this coupling again entered in for sufficiently high  $\beta_{\text{hot}}$  (i.e.,  $\beta_{\text{hot}} \geq 0.15$ ).

In addition to the Alfvén compressional mode, most of the more recent calculations mentioned above<sup>11-14</sup> also find lower limits on the ratio of  $n_c/n_H$  due to the hot electron interchange mode. The different models presently predict a range of results which will not be reviewed in detail here, except to point out that this mode is presently expected to be responsible for the T-M transition.

In conclusion, the Vlasov slab models generally predict a finite operating window with the upper limit in  $\beta_{\text{core}}$  due to either the Alfvén mode or the NVL mode and with the lower limit due to the hot electron interchange. This lower limit is relatively easy to satisfy by providing sufficient  $n_{\text{core}}/n_{\text{hot}}$ . Estimates of the upper limit depend on the model used, and there is presently some controversy as to whether this is ultimately determined by the Alfvén mode or the NVL mode. The scaling of the NVL mode boundary was given in Eqs. (13)-(14). Some specific estimates of the Alfvén mode boundary will be given in Sect. IV, and others are contained in the references quoted earlier.

### III. Generalized Kinetic Energy Principles

Paralleling the development of the Vlasov-Maxwell slab models, work was underway on generalized kinetic energy principles which could be applied to the hot electron rings in EBT.<sup>12-13,16-17</sup> These calculations also indicated the existence of a compressional Alfvén

instability arising from similar terms in the energy principle, which resulted in the mirror instability.

These calculations differ from previous work on energy principles for guiding center, anisotropic plasmas<sup>18-21</sup> in that the magnetic lines of force are not assumed to be frozen in the plasma. This assumption is not applicable to the energetic electron rings in EBT where energies can be in the 100-500 keV range. The earlier energy principles<sup>18-21</sup> may generally be derived from the condition that the single particle magnetic moment ( $\mu = mv_{\perp}^2/2B$ ) and longitudinal invariant ( $J \sim \oint dl v_{\parallel}$ ) be conserved during the period of a fluctuation.<sup>17</sup> In the generalized energy principle  $\mu$ ,  $J$ , and the magnetic flux invariant ( $\Phi = \oint \vec{B} \cdot d\vec{\xi}$ ) are assumed conserved by the perturbation.<sup>17</sup> This avoids the assumption that the plasma is tied to the magnetic field lines. The drift orbits are free to leave magnetic lines provided the magnetic flux they enclose is conserved. This will be satisfied if the frequency of the fluctuation is low compared to the drift frequency of the hot electrons. Such an approximation is appropriate for the core interchange modes but not necessarily for the compressional Alfvén mode or the hot electron interchange.

Application of the generalized energy principle to EBT geometry is discussed in detail in Refs. 12, 16, and 17. A few of the results given there will be mentioned here. First, the interchange mode is found to be stabilized if the following inequality is satisfied.

$$-p_c' \oint \frac{dl}{B^3} + 2 \oint \frac{dl}{B} k + \frac{\oint \frac{dl}{B^3} \left( \frac{2p_c}{B^2} \right) \oint \frac{dl}{B} \left( 2k - \left[ \frac{(p_H + p_c)'}{B^2} \right] \right)}{\oint \frac{dl}{B^3}} < 0 \quad (19)$$

Here  $k = \vec{\kappa} \cdot \vec{\nabla}\psi$ ,  $\vec{\kappa}$  is the field-line curvature,  $p_c$  and  $p_H$  are the core and hot electron pressures, and prime denotes derivatives with respect to  $\psi$ . Equation (19) has not been evaluated using computed EBT equilibria yet; however, a local approximation to this equation indicates  $\beta_c < 15\%$ ,<sup>22</sup> which is in reasonable agreement with the earlier slab models.<sup>6-7</sup> Evaluation of Eq. (19) also provides insight as to the value of the magnetic field-line radius of curvature  $R_c$ , which should be used in the local models.<sup>22</sup> This indicates that the radius of curvature at the ring location (near the midplane) is the appropriate value rather than a field-line-averaged curvature. The generalized energy principle further provides a stability condition for the lower  $\beta_{hot}$  threshold to reverse the magnetic drifts and stabilize the core at low  $\beta_c$ :<sup>17</sup>

$$\beta_{hot} > \frac{4 \oint \frac{d\ell}{B} k}{(B^2 \oint \frac{d\ell}{B^3})(p'_H/p_H)} \quad (20)$$

This again is in rough agreement with slab model results.<sup>6-7</sup>

Unfortunately, the generalized kinetic energy principle is not adequate to treat high frequency modes where  $\omega > \omega_{d,hot}$  due to the use of the flux invariant. Also, it has been shown<sup>2,3</sup> recently that it only provides a necessary condition for stability in the case of equal temperature Maxwellian ions and electrons, which is not the case in EBT. It indicates the presence of a purely magnetic mode (i.e., the compressional Alfvén mirror mode) precisely when Eq. (19) is satisfied.<sup>17</sup> It would therefore predict no stability window since the

Alfvén mode would be unstable when the core interchange is stable and the core interchange would be unstable when the Alfvén mode is stable. This lack of stability is a result of the fact that the Alfvén mode occurs at a higher frequency than Eq. (19) is valid for. A longitudinally dependent normal mode analysis of this instability has been given in Ref. 17 which indicates that a frequency shift is introduced by retaining terms of order  $\omega/\omega_d$ . The resulting stability condition given there<sup>17</sup> (for the isotropic case)

$$N_1 M_1 (p_H')^3 \oint \frac{d\ell}{B^7} |\vec{\nabla}\alpha|^2 \oint \frac{d\ell}{B} \left( 2k - \frac{p_C'}{B^2} \right) < N_H'^2 \left( \oint \frac{d\ell}{B} \right)^2 \quad (21)$$

indicates that there is a finite window where both the core interchange [Eq. (19)] and the Alfvén mode [Eq. (21)] will be stabilized.

To summarize this section, the generalized kinetic energy principle provides a useful means for taking into account the variation of quantities along the field line without actually solving the longitudinal problem. Its applicability is limited to low frequency modes such as the core interchange for which it is in approximate agreement with slab models. For higher frequency modes, such as the compressional Alfvén instability, it must be supplemented by a suitably field-line-averaged normal mode analysis.

#### IV. Radially Dependent Normal Mode Analysis

The radial structure of eigenmodes in EBT has become of interest since both modes which are localized within the annulus (Alfvén mode, hot electron interchange) and modes extending into the core plasma (core interchange) have been predicted to be unstable. The localized models cannot yield any information on how such modes connect to the inner core and outer surface plasma regions. Several radially resolved calculations have recently been attempted.<sup>10,13</sup> They are generally based on using either the Vlasov or drift kinetic equations for the hot species, coupled with fluid-like equations for the core plasma.

For example, in Ref. 13 the momentum balance equation with ion inertial effects is used:

$$\rho \frac{d\vec{v}}{dt} = \vec{j} \times \vec{B} - \nabla \cdot \underline{\underline{P}} \quad (22)$$

This is augmented by the drift kinetic equation for the hot electron pressure tensor:  $\underline{\underline{P}} = p_{\parallel} \underline{\underline{bb}} + p_{\perp} (\underline{\underline{I}} - \underline{\underline{bb}})$  where

$$\begin{pmatrix} p_{\parallel} \\ p_{\perp} \end{pmatrix} = \int \frac{dH d\mu B}{|p_{\parallel}|} \begin{pmatrix} p_{\parallel}^2 \\ \mu B \end{pmatrix} F(r, H, \mu) \quad (23)$$

and  $F$  is described by

$$\frac{\partial F}{\partial t} + \left( v_{\parallel} \underline{\underline{b}} + \frac{\vec{E} \times \vec{B}}{B^2} + \vec{v}_d \right) \cdot \vec{\nabla} F + \left( \vec{E} \cdot \vec{v}_d + \mu \frac{\partial B}{\partial t} \right) \frac{\partial F}{\partial \epsilon} = 0$$

Now if the  $\theta$  component of Eq. (22) and the result obtained from operating on Eq. (22) with  $\vec{B} \cdot \vec{\nabla}_x$  are combined and if a transformation is made from a bumpy cylinder to a z pinch geometry, a purely radial eigenmode equation results:

$$\begin{aligned} & \frac{1}{r} \frac{d}{dr} \left[ \left( \frac{\alpha r B^2 T}{\alpha - T} \right) \frac{\partial \xi_r}{\partial r} \right] + \xi_r \left\{ \rho \omega^2 \left( \frac{\alpha}{\alpha - T} \right) \right. \\ & - \rho \lambda \left( \frac{T}{\alpha - T} \right) - \frac{1}{r} \frac{\partial}{\partial r} (p_{\parallel} + p_{\perp}) - \frac{B^2 R}{r^2} \\ & \left. - \left( \frac{2\alpha B^2 S}{r} \right) \left( \frac{k\omega}{\Omega} \right) \frac{1}{\alpha - T} - \frac{(SB/r)^2}{\alpha - T} \right. \\ & \left. - \frac{1}{r} \frac{\partial}{\partial r} \left[ \left( \frac{\alpha r B^2}{\alpha - T} \right) \left( \frac{S}{r} + \frac{k\omega T}{\Omega} \right) \right] \right\} = 0 \end{aligned} \quad (24)$$

Here,  $\lambda = \omega^2 \Omega_{ci}^2 / (\Omega_{ci}^2 - \omega^2)$ ,  $\alpha = \lambda / k^2 V_A^2$ , and  $\xi_r = i(\vec{E} \times \vec{B})_r / \omega B^2$ ; T, S, and R are kinetic integrals, the details of which are given elsewhere in these proceedings.<sup>24</sup> Equation (24) has been solved both locally, by using a WKB approach, and nonlocally, using numerical shooting methods. The stability criteria which result from the localized, short wavelength approximation are as follows:

$$\frac{v_A^2}{v_{k\perp}^2} > \frac{4 \left( \frac{k_{\theta}^2}{k_{\perp}^2} \right) \left( \frac{R_c}{\Delta_g} \right)}{\left( 1 - \frac{k_{\theta}^2}{k_{\perp}^2} \left| \frac{v_{k\perp}}{\omega_{ci} \Delta} \right| \right)^2} \quad (25)$$

(compressional Alfvén mode)

$$\frac{V_A^2}{V_{k\perp}^2} < \frac{k_{\perp}^2 \Delta_B R_C}{4 \left[ 1 + \left( \frac{v_{k\perp} k_{\theta}^2}{\omega_{ci} \Delta k_{\perp}^2} \right) \right]} \quad (26)$$

(hot electron interchange mode)

where  $V_{k\perp}$  is the hot electron curvature drift velocity and  $\Delta_B$  is the magnetic field gradient scale length in the ring. These have been obtained from a cubic dispersion relation by considering small and large  $V_A$  limits, respectively. When the results from this dispersion relation are compared with instability boundaries obtained from numerical solutions of Eq. (24), the agreement is reasonable (within a factor of 3-4) for the cases which have been considered. For further details on this calculation, see Ref. 24.

Agreement between numerical shooting solutions and local approximations was also obtained in Ref. 10. Here, the continuity equation was solved in conjunction with the Vlasov equation and Maxwell's equations over the outer half of the hot electron ring region.

In addition to the short radial wavelength modes localized to the annulus region, which are considered above, preliminary estimates have been made of stability boundaries for longer radial wavelength global modes.<sup>22</sup> Dispersion relations for such modes have been obtained by integrating the radial differential Eq. (24) over the annulus region

and by assuming the eigenfunction  $\xi_r$  does not vary appreciably over the width of the annulus. Such modes have been predicted<sup>22</sup> to be potentially more dangerous (i.e., occurring at lower density) than the short wavelength modes. They generally are of a resonant nature and depend on the hot electron curvature drift  $\omega_k$  being close to the ion cyclotron frequency  $\omega_{ci}$ . The present thinking is that the longitudinal variation in B is likely to have an important effect on these modes since it will tend to smooth out this resonance. Such effects have not been included yet in these models. Current estimates of density limits from such modes are below those observed experimentally.

#### V. Conclusion

To conclude, a number of different models have been applied to the EBT stability problem in recent years. These include the Vlasov-Maxwell slab models, generalized kinetic energy principles, and various types of radially dependent calculations (fluid drift kinetic, fluid Vlasov). Although these models differ in various details, which have been discussed here, they agree qualitatively that a triangular-shaped stability window exists for EBT. On the left-hand side the window is bounded by the hot electron stabilization of the core interchange mode, requiring a threshold  $\beta_{hot}$  of 15-20%. The upper side of the window is bounded by the compressional Alfvén mode and the core interchange (or NVL) mode. Which of these two modes is the most limiting is not presently agreed upon and depends on the parameters and model used. Finally, the lower part of the window is related to the

hot electron interchange mode which requires some minimum core density for stabilization.

Elmo Bumpy Torus stability theory is incomplete in a number of areas, some of which have been mentioned earlier. First of all, the sensitivity of the models to various forms of the hot electron distribution function requires further work. If the results are sensitive to  $f_{0H}$ , it would then be of interest to understand what characteristics of the distribution are of particular importance. Next, the coupling to the shear Alfvén wave ( $k_{\parallel} \neq 0$ ) has not been investigated in any detail yet.

Related to this, it would be desirable to examine in more detail the effects of longitudinal dependence of equilibrium quantities. Preliminary estimates of this have been made from the energy principle analysis. Next, the present radially dependent calculations generally assume  $k_{\perp}\rho_H, k_{\perp}\rho_i \ll 1$ . Since this is only very marginally satisfied in the existing experiment, it will be necessary at some point to include finite Larmor radius corrections. As the radially dependent calculations become more developed, it will be of interest to examine the coupling between the cold outer surface plasma region (usually unstable) and the inner core plasma. Finally, over the longer term, multidimensional models which simultaneously take into account the radial and the longitudinal dependences will be necessary.

## REFERENCES

- <sup>1</sup>J. W. Van Dam, Y. C. Lee, EBT Ring Physics, Proceedings of the Workshop, Oak Ridge, 1979, Oak Ridge National Laboratory (1980) 471.
- <sup>2</sup>D. B. Nelson, Phys. Fluids 23 (1980) 1850.
- <sup>3</sup>N. A. Krall, Phys. Fluids 9 (1966) 820.
- <sup>4</sup>H. L. Berk, Phys. Fluids 19 (1976) 1255.
- <sup>5</sup>R. R. Dominquez, H. L. Berk, Phys. Fluids 21 (1978) 827.
- <sup>6</sup>D. B. Nelson, C. L. Hedrick, Nucl. Fusion 19 (1979) 283.
- <sup>7</sup>H. Sanuki, M. Fujiwara, Nagoya University Research Report IPPJ-426 (December, 1979).
- <sup>8</sup>A. M. El Nadi, Oak Ridge National Laboratory, private communication.
- <sup>9</sup>D. A. Spong, A. M. El Nadi, Bull. Am. Phys. Soc. 25 (1980) Abstract 6U14.
- <sup>10</sup>A. M. El Nadi, K. T. Tsang, Annual Controlled Fusion Theory Conference, Austin, Texas, April 8-10, 1981, Abstract 1B3.
- <sup>11</sup>K. T. Tsang, C. Z. Cheng, Annual Controlled Fusion Theory Conference, Austin, Texas, April 8-10, 1981, Abstract 3B24.
- <sup>12</sup>J. W. Van Dam, Y. C. Lee, M. N. Rosenbluth, Bull. Am. Phys. Soc. 25 (1980) Abstract 6U16.
- <sup>13</sup>J. W. Van Dam, H. L. Berk, M. N. Rosenbluth, D. A. Spong, Annual Controlled Fusion Theory Conference, Austin, Texas, April 8-10, 1981, Abstract 3B33.
- <sup>14</sup>A. M. El Nadi, Oak Ridge National Laboratory, private communication.
- <sup>15</sup>G. E. Guest, C. L. Hedrick, D. B. Nelson, Phys. Fluids 18, (1975) 871.
- <sup>16</sup>J. W. Van Dam, Y. C. Lee, M. N. Rosenbluth, 1980 Sherwood Meeting Theoretical Aspects of Controlled Thermonuclear Research, Tucson, Arizona, April 23-25, 1980, Abstract 3A4.
- <sup>17</sup>J. W. Van Dam, M. N. Rosenbluth, Y. C. Lee, University of Texas Report IFSR #12, (March 1981).

- <sup>18</sup>M. D. Kruskal, C. R. Oberman, *Phys. Fluids* 1 (1958) 275.
- <sup>19</sup>M. N. Rosenbluth, N. Rostoker, *Phys. Fluids* 2 (1959) 23.
- <sup>20</sup>J. B. Taylor, R. J. Hastie, *Phys. Fluids* 8 (1965) 232.
- <sup>21</sup>H. Grad, *Phys. Fluids* 9 (1966) 225.
- <sup>22</sup>J. W. Van Dam, H. L. Berk, M. N. Rosenbluth, D. A. Spong, "Radially Dependent Stability Theory for EBT," paper presented at the EBT Stability Workshop, Oak Ridge, Tennessee, May 13-14, 1981. May 13-14, 1981, Oak Ridge, Tennessee.
- <sup>23</sup>T. M. Antonsen, Jr., B. Lane, J. J. Ramos, "Variational Principle for Low Frequency Stability of Collisionless Plasmas," Massachusetts Institute of Technology Report PRR-80/15 (July 1980).
- <sup>24</sup>D. A. Spong, J. W. Van Dam, H. L. Berk, M. N. Rosenbluth, "Numerical Solutions of the EBT Radial Eigenmode Problem," paper presented at the EBT Stability Workshop, Oak Ridge, Tennessee, May 13-14, 1981.

BRIEF SURVEY OF EXPERIMENTAL INVESTIGATION OF  
INSTABILITIES IN MICROWAVE-HEATED PLASMAS\*

N. A. Uckan and G. R. Haste  
Oak Ridge National Laboratory  
Oak Ridge, Tennessee 37830

ABSTRACT

Nearly two decades of experimental investigations exist on instabilities in hot electron plasmas in open (simple and minimum-B mirrors) and closed (bumpy tori, EBT and NBT) geometries. A brief review is given for some, but not all, of the results from these experiments. Also discussed is the observed behavior of the plasma in C-T and T-M transitions in EBT.

---

\*Research sponsored by the Office of Fusion Energy, U.S. Department of Energy, under contract W-7405-eng-26 with the Union Carbide Corporation.

## DISCUSSIONS

There is a wealth of observations of fluctuations on devices related to the ELMO Bumpy Torus (EBT). These devices include simple and minimum-B mirrors, canted mirrors, and toroidal geometries. The hot electron plasmas in these experiments are created by electron cyclotron heating (ECH). Results from these experiments indicate that the observed frequency spectrum of the fluctuations range from very low frequencies ( $\sim 100$  kHz) to frequencies in the GHz range. In most cases, these fluctuations can be correlated to theoretical predictions; however, some of those correlations are qualitative rather than quantitative because of the limitations of the diagnostics and the theory.

Tables I and II summarize the observed modes in various experiments. A partial listing of references is provided at the end for detailed information. The following is a brief summary from these observations.

## ELMO and Canted Mirror [1]

Three microwave heating sources (10.6, 35.0, and 55.0 GHz) were available for use in various combinations of fundamental resonance and off-resonant heating. Low frequency ( $\sim 74$ -kHz) stable oscillations were observed with end-loss detectors at low pressure and low cold plasma density. These flute-like modes were thought to be electrostatic in character and, therefore, susceptible to cold plasma stabilization. Anisotropy driven modes of hot electrons were also observed. With only resonant heating, although low power experiments exhibited narrow band instabilities near the half harmonic of the ECH frequency, high power experiments displayed broad-bands because of the excitation of the cavity modes. However, upper off-resonant heating (UORF) suppresses this instability, and perhaps others, by reducing the hot electron anisotropy (by heating throughout the volume) and by relativistic effects.

Table I. Instabilities in hot electron plasmas (low frequency)

Frequency	Identification	Device	Remarks
74 kHz	Flute-like	ELMO	Observed with end-loss detectors Stable oscillation
150 kHz	Flutes	IMP	Affected by feedback to circum- ferential electrode. Not stabilized
3-30 MHz	Hot electron flutes	PTF	Loss of hot electrons across magnetic field lines. High m mode numbers (4-10) stabilized by cold plasma
150 MHz	Lower hybrid (?) Beam-plasma (?)	INTEREM	Observed at collector of electron beam along the axis.
$n f_{ci}$	DCLC Two component (?) Hot electron instability (?)	PHOENIX	$\sim 10$ W (average) at 33 GHz stabilized $n = 3$ , "sort-of" $n = 2$ ; dc stabilized $n = 1$
$f_{ci}$		ALICE	10 W ECH decreased repetition rate, but increased amplitude of $f_{ci}$ . Density increases $\sim 25\%$

Table II. Instabilities in hot electron plasmas (high frequency)

Frequency	Identification	Device	Remarks
$n \times 2.1$ GHz ( $\sim 1/3 f_{ce}$ )	Whistler	TPM	Could be triggered ES or EM Axial loss of hot electrons Anisotropy driven
$3/4 f_{ce}$ ( $\sim 4$ GHz)	Whistler	Bille-en-Tête	$\theta$ -pinch, $T_e \sim 6-8$ keV, $p_{\parallel}/p_{\perp} \sim 10\%$ 20% reduction in 2 $\mu$ s of $p_{\perp}$ Anisotropy driven
8.6-8.8 GHz	Whistler	INTEREM	$f > f_{co}(1-T_{\parallel}/T_{\perp})$ , narrow band at threshold. Originates on edge of minimum-B volume. All axial current arrives in bursts. Limits confinement. Stabilized by UORH
9.5 GHz	Double distribution	INTEREM	Originates on axis Stabilized by UORH
11 GHz	Upper hybrid	INTEREM	Stabilized by UORH
5.1-5.3 GHz	Timofeev (one-half harmonic)	ELMO	Axial loss of electrons Stabilized by UORH
5.3 GHz ( $\sim 1/2 f_{ce}$ )	Mirror mode	PTF	Triggering of instability depends on B (as B lowered limiting beta increased)

## PTF [2]

Two types of instabilities were observed. One of the modes was identified as a flute mode driven by hot electron  $\nabla B$  drifts, which caused loss of energetic hot electrons across magnetic field lines. The oscillation frequency was  $\sim 3$ -30 MHz ( $\sim 10$  MHz appeared to be most prevalent), and flutes with  $m > 1$  were dominant ( $4 < m < 10$ ). This mode was stabilized by increasing the cold plasma density. The second mode, which was high frequency ( $\sim \frac{1}{2}\omega_{ce} \sim 5.3$  GHz; with 10.6-GHz as the ECH source), was driven by beta and identified as mirror mode (loss of equilibrium). This instability, which dumped the hot electrons out along the field lines, depended on an external magnetic field value, which indicated that the instability was associated with velocity space anisotropy.

## INTEREM [3]

The INTEREM device used 10.6-GHz resonant power in combination with 35 GHz. With 10.6 GHz alone, high frequency instabilities ( $\omega \sim \omega_{ce}$ ) associated with velocity space anisotropy were observed. The observed frequency spectrum indicated three modes: (1) 8.6-8.8 GHz results from Whistler instability, (2) 9.5 GHz from the double distribution mode, and (3) the band at  $\sim 10$ -11 GHz, corresponding to the frequency expected from upper hybrid or negative mass. These modes were suppressed by UORH (at 35 GHz). Also, oscillations at  $\sim 150$  MHz, possibly due to beam-plasma interactions were observed.

## TPM [4]

Additional hot electron plasma was produced by a microwave pulse ( $\sim 200$  ms) at 6.4 GHz, which permitted external triggering of microinstabilities. Strong electromagnetic instabilities at one-third harmonic ( $\sim 2.1$  GHz) were observed. The instability was characterized by the sudden loss of hot electrons, but not of cold electrons. This instability was triggered by either pulsed microwave power (electromagnetic triggering) or the extraction of cold electrons (electrostatic triggering). Associated with the extraction technique, a flute-like low frequency instability was also detected.

## EBT [6]

Experimental results from EBT indicated many similarities in the behavior of hot electron plasma (hot electron rings) to simple mirror results. However, many of the instabilities observed in mirrors are not present in the bumpy torus experiments. For example, the half-harmonic microwave emission common in ELMO is not present. In EBT, the toroidal core plasma fluctuations are mainly low frequency ( $\sim 100$  kHz) with high frequencies restricted to the region outside the ring (surface plasma). By forming a magnetic well of sufficient depth, the rings provide stabilization for the core plasma. Experimentally, stabilization is evidenced by a reduction of the fluctuation amplitude coincident with the formation of rings with sufficient beta (C-T transition). The experimental value of critical ring beta at which this transition occurs is consistent with the theoretical predictions of average min-B stability. Figure 1 shows the range of beta values at the C-T transition for various power levels in EBT-I. Near the T-M transition, enhanced fluctuations are observed. Experimental and theoretical investigations of the T-M transition are in a relatively early stage of development.

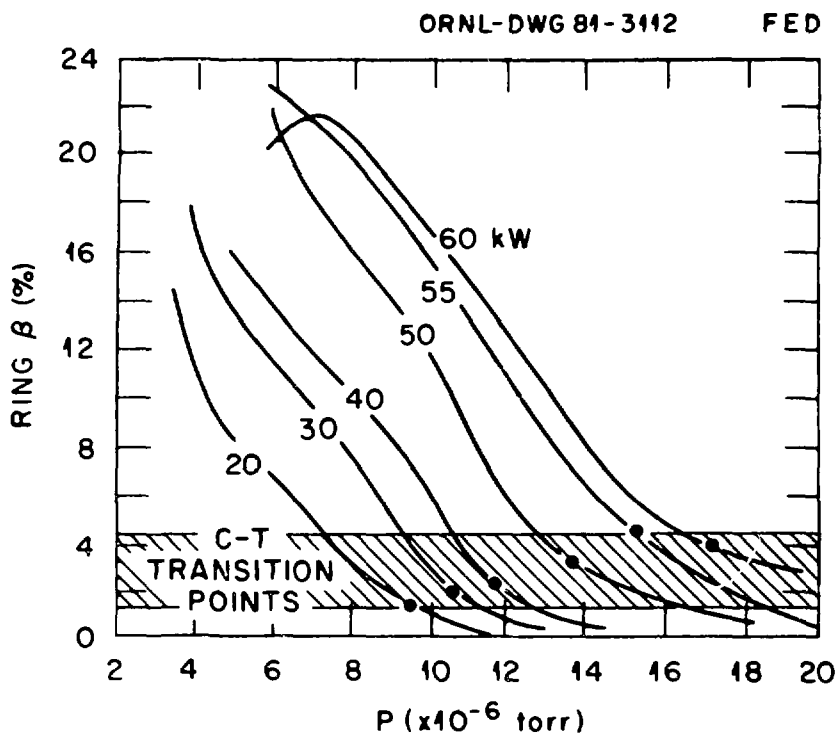


Figure 1. The experimental values of beta at the C-T transition fall in the range of a few per cent.

## REFERENCES (Partial Listing)

## 1. ELMO and CANTED MIRROR

R. A. Dandl et al., *Proc. Int. Conf. Plasma Physics and Controlled Nuclear Fusion Research* Vol. II, p. 435 (1969).

R. A. Dandl et al., *Nucl. Fusion* 11, 411 (1971).

R. A. Dandl et al. *Nucl. Fusion* 13, 693 (1973).

R. A. Dandl et al., *Proc. Int. Conf. Plasma Physics and Controlled Nuclear Fusion Research* Vol. II, p. 607 (1972).

R. A. Dandl et al., in *EBT Ring Physics: Proc. Workshop*, N. A. Uckan, ed., Oak Ridge National Laboratory CONF-791228 p. 31 (1980).

Thermonuclear Division Semi-Annual Progress Reports, Oak Ridge National Laboratory ORNL-4150 (April 1967) and ORNL-4688 (December 1970).

## 2. PTF

W. B. Ard et al., *Phys. Fluids* 9, 1498 (1966).

W. B. Ard and R. A. Dandl, *Proc. 6th Int. Conf. Ionization Phenomena in Gases*, Vol. 4, 75 (1963).

R. A. Dandl et al., *Nucl. Fusion* 4, 344 (1964).

E. H. Christi, Ph.D Thesis, Tulane University (1966).

W. B. Ard, in *EBT Ring Physics: Proc. Workshop*, N. A. Uckan, ed., Oak Ridge National Laboratory CONF-791228, 499 (1980).

## 3. IMP and INTEREM

G. R. Haste, in *Feedback and Control of Plasma*, ed., T. K. Chu and W. W. Hendel, American Institute of Physics, New York, 1970.

W. B. Ard et al., *Proc. Int. Conf. Plasma Physics and Controlled Nuclear Fusion Research* Vol. II, p. 619 (1972).

Thermonuclear Division Semi-Annual Progress Reports, Oak Ridge National Laboratory ORNL-4401 (December 1968), ORNL-4545 (December 1969), and ORNL-4688 (December 1970).

## 4. TPM

H. Ikegami et al., *Phys. Fluids* 111061 (1968).

H. Ikegami, et al., *Proc. Int. Conf. Plasma Physics and Controlled Nuclear Fusion Research* Vol. II, 423 (1969).

H. Ikegami, *EBT Ring Physics: Proc. Workshop*, ed., N. A. Uckan, Oak Ridge National Laboratory CONF-791228, 59 (1980).

## 5. ALICE, PHOENIX, and BILLE-EN-TÊTE

*Proc. Int. Conf. Plasma Physics and Controlled Nuclear Fusion Research* Vol. II (1969). (See p. 253 Alice, p. 267 Phoenix, and p. 347 Bille-en-Tête).

## 6. EBT

N. A. Uckan, ed., *EBT Ring Physics, Proc. Workshop*, Oak Ridge National Laboratory CONF-791228 (1980).

R. A. Dandl et al., *Proc. Int. Conf. Plasma Physics and Controlled Nuclear Fusion Research* Vol. II, 365 (1979); Vol. II, 145 (1977).

R. A. Dandl et al., Oak Ridge National Laboratory Report ORNL-TM-4941 (1975); ORNL/TM-6457 (1978).

N. A. Uckan et al., "Physics of Hot Electron Rings in EBT: Theory and Experiment," paper presented at International Conf. Plasma Physics and Controlled Nuclear Fusion Research Brussels, 1980.

D. B. Nelson and C. L. Hedrick, *Nucl. Fusion* 19, 283 (1979).

G. E. Guest, C. L. Hedrick, and D. B. Nelson, Oak Ridge National Laboratory Report ORNL-TM-4077 (1972).

A. Komori, Oak Ridge National Laboratory Report ORNL/TM-7530 (1981).

### **3. EXPERIMENTAL OBSERVATIONS**

*W. B. Ard and H. Grad, Session Chairmen*

## FLUCTUATION MEASUREMENTS IN EBT

L. Bighel, G. Haste, A. Komori  
 Oak Ridge National Laboratory  
 Oak Ridge, Tennessee 37830

Fluctuation studies in EBT have been aimed at questions of plasma stability and transport. The stability aspects associated with fluctuations in EBT-I have been investigated with probes and with light detectors. The EBT-S environment is not suitable to the use of probes, except near the wall. Laser-microwave scattering techniques are being investigated for spatially resolved fluctuation measurements in EBT-S. A large effort is currently aimed at correlating the fluctuation behavior with the ambipolar potential and the hot ion component in the plasma. There is also considerable interest in studying fluctuation phenomena associated with ICRH experiments in EBT.

Figures 1, 2 and 3 show the fluctuation amplitude, spectrum, and spatial distribution respectively as a function of background pressure. The quantity  $I$  is the photodetector current output. Figure 4 shows the spatial distribution of the fluctuation amplitude as a function of frequency. It is seen that the core fluctuations are mainly low frequency with the high frequencies restricted to the region outside the rings. This observation is further verified with Langmuir probes as shown in Fig. 5.

These observations generally indicate that:

- (1) The C-T-M hierarchy is clearly correlated with plasma fluctuation activity.
- (2) Most of the fluctuation energy is at low frequencies ( $<100$  kHz)
- (3) High frequencies appear at low pressures and high microwave power, and are generally found outside the rings.
- (4) Enhanced fluctuations near the T-M transition correlate with increased ion-tail densities and deep potential wells.

There is a considerable diagnostic effort currently aimed at studying fluctuation phenomena in the EBT plasma. Figure 6 shows schematically the CW FIR laser scattering system.

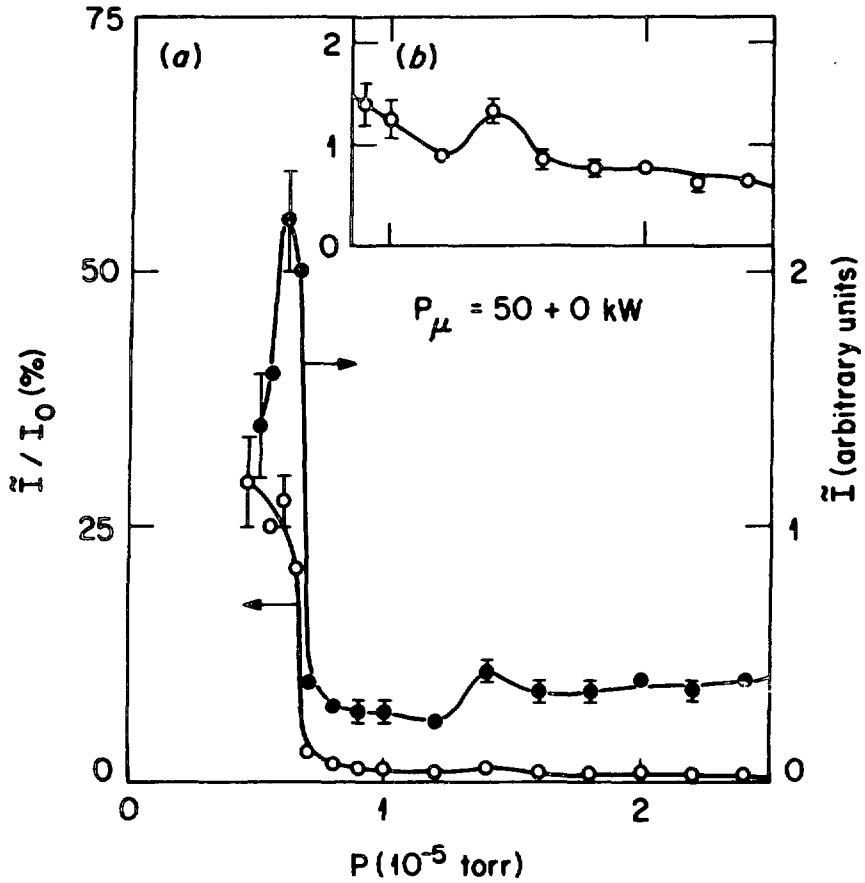


Figure 1. (a) Fluctuation of  $I$  and normalized fluctuation level  $\tilde{I}/I_0$  as a function of neutral pressure. (b)  $\tilde{I}/I_0$  in the regime of high neutral pressure; the vertical scale is different from that of (a).

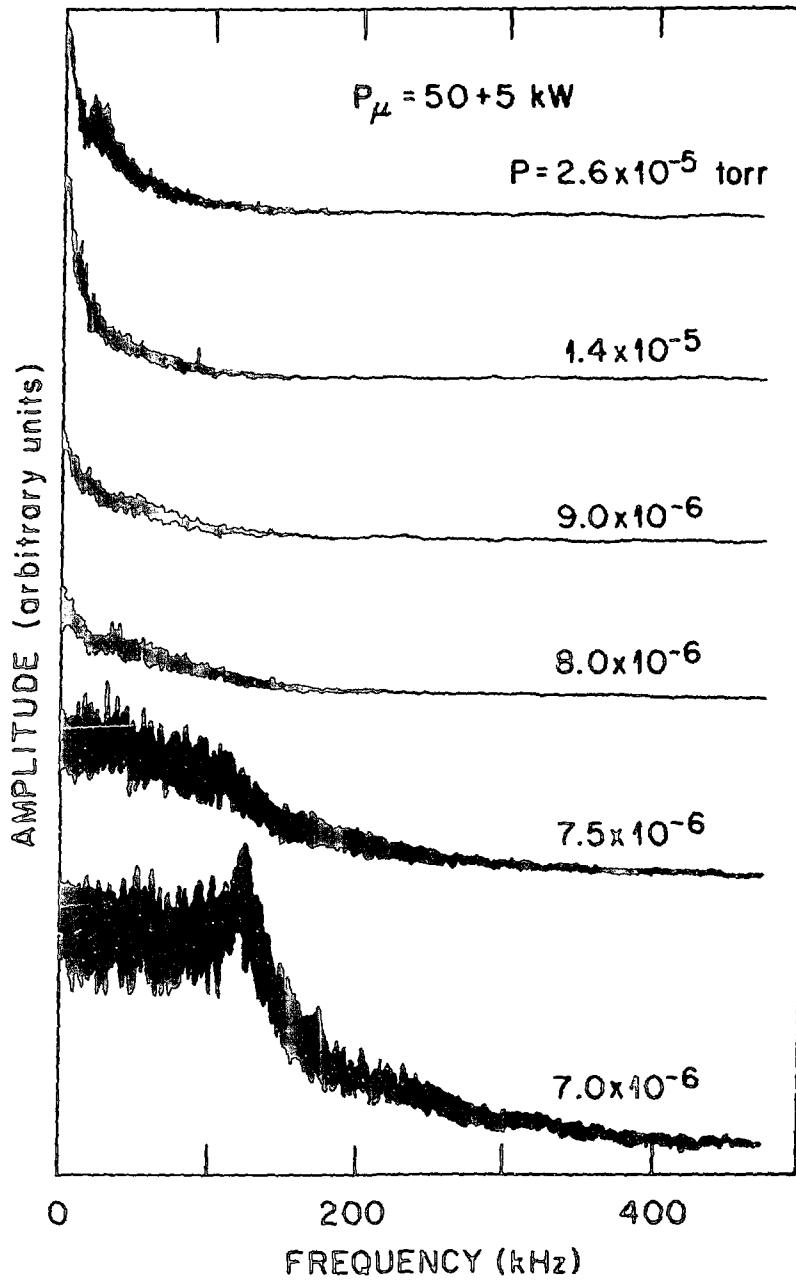


Figure 2. Frequency spectra of  $\tilde{I}$  as a function of neutral pressure.

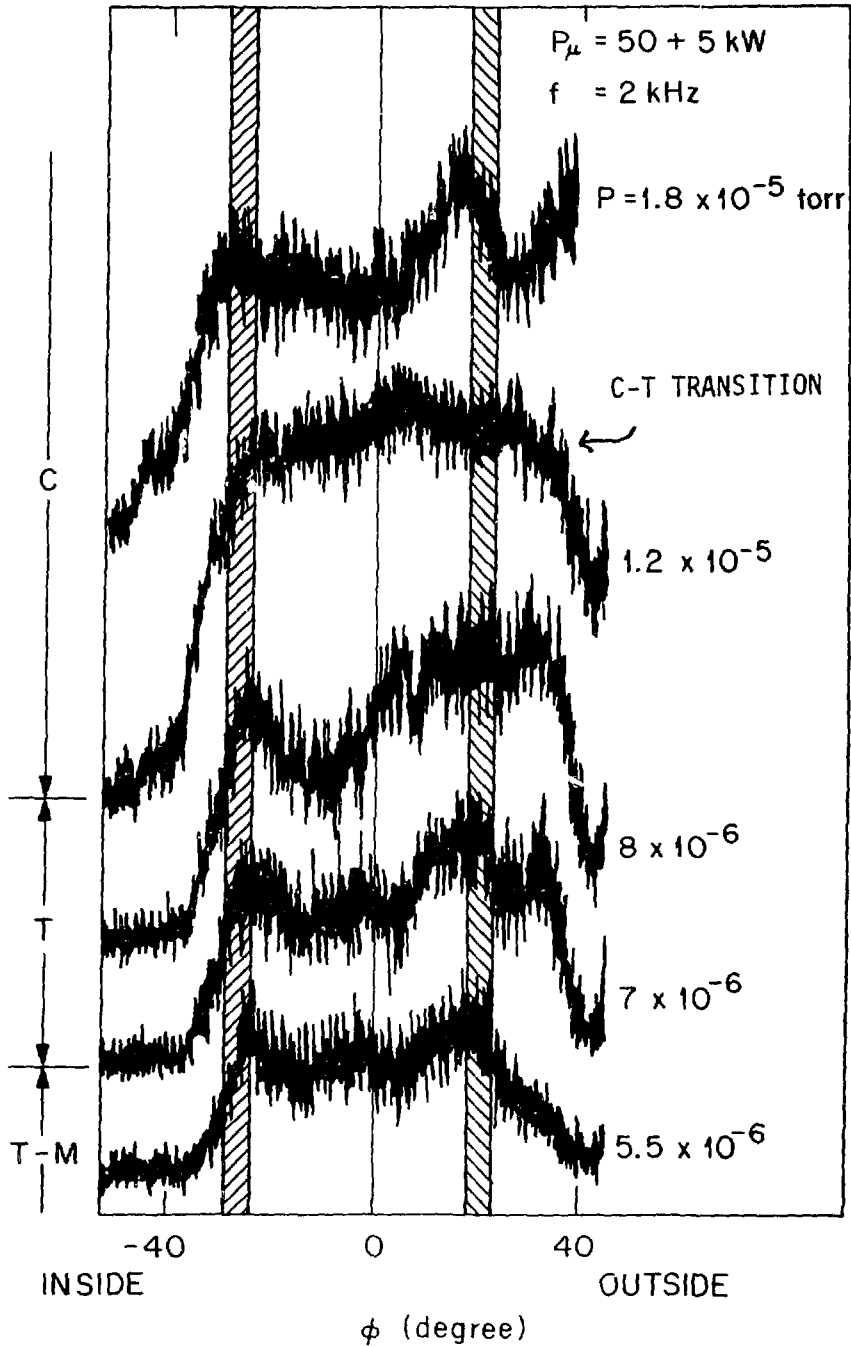


Figure 3. Spatial distribution of  $\tilde{I}$  for 2-kHz fluctuations. Hatches represent locations of hot electron annuli on the equatorial plane.

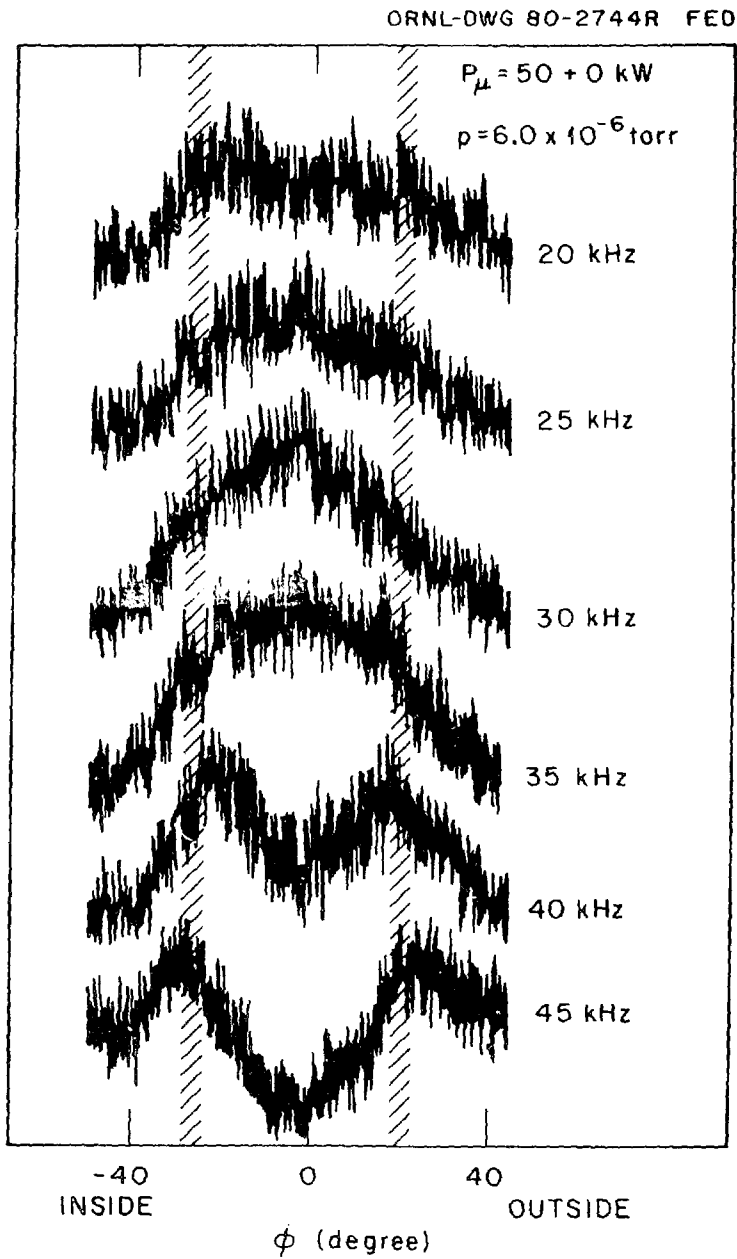


Figure 4. Spatial distribution of  $\bar{I}$  for a fixed neutral pressure as a function of frequency.

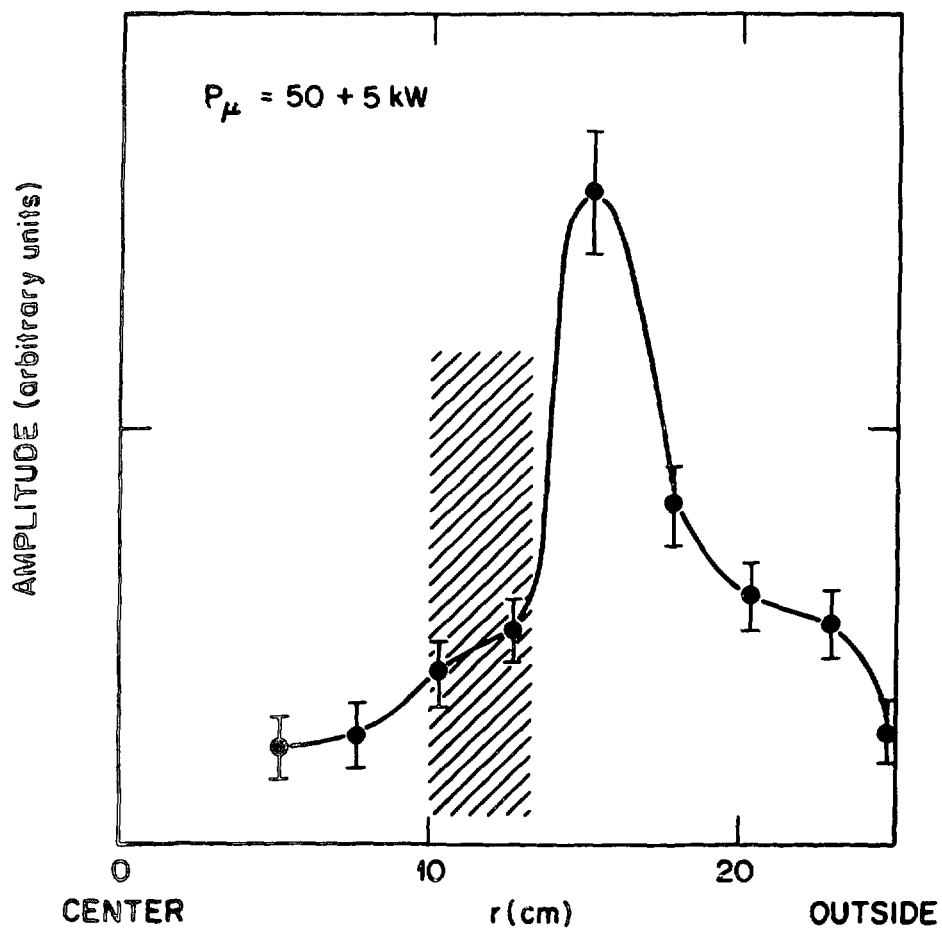


Figure 5. Spatial distribution of the fluctuation amplitude at 150-kHz obtained with a Langmuir probe in the midplane ( $P_0 = 6 \times 10^{-6}$  torr).

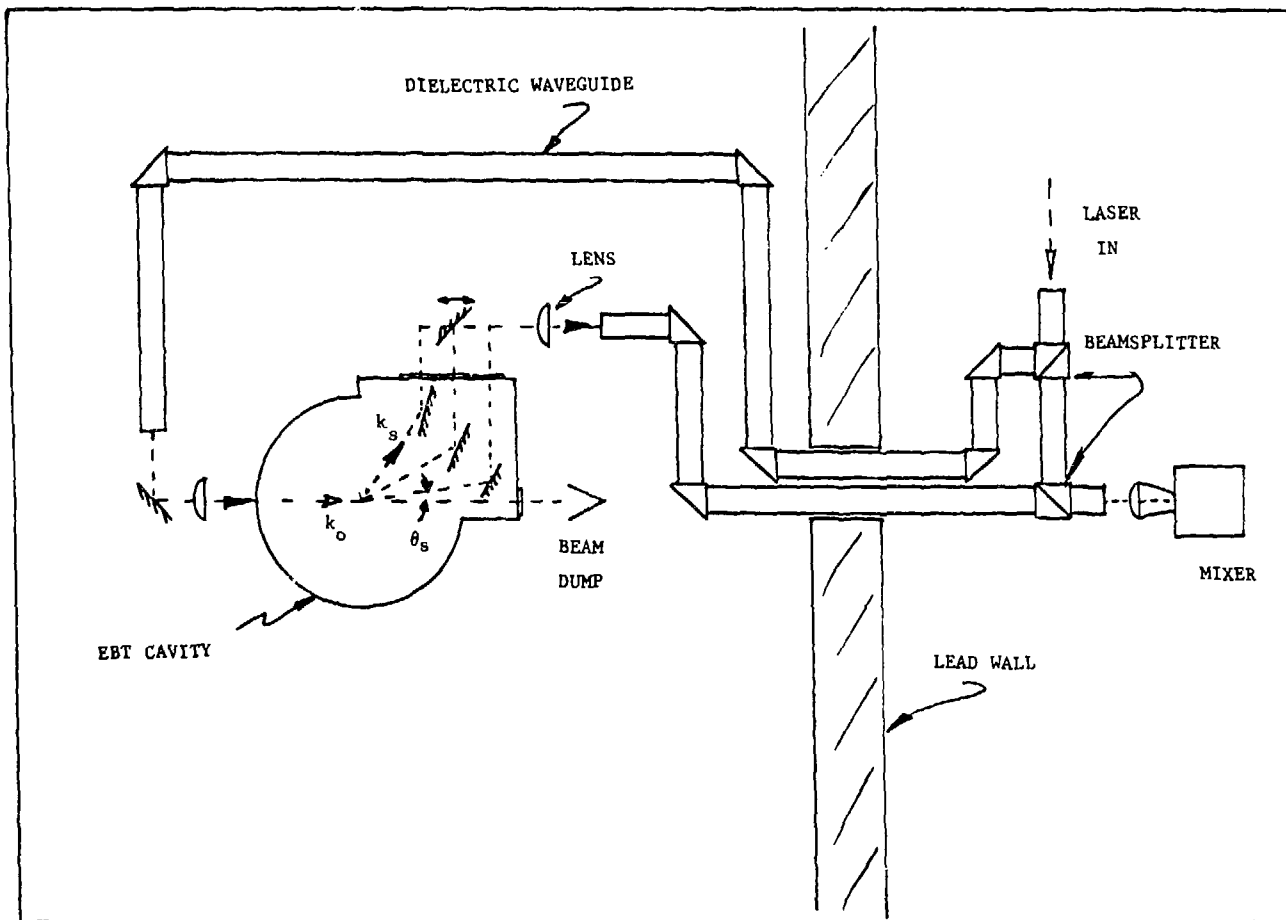


Figure 6. FIR laser scattering system for fluctuation measurements on EBT-S.

82

Hot-Electron Ring Stability  
 at The University of Tennessee  
 Igor Alexeff  
 The University of Tennessee  
 and  
 Marshall Saylor  
 The University of Kentucky

We supply a model that is sufficient to explain the observed stability of the hot-electron ring at The University of Tennessee. We have created a hot-electron ring with the following approximate parameters;  $T_e \hat{=} 10^5$  electron-volts,  $n_e \hat{=} 10^{11} - 10^{12} \text{ cm}^{-3}$ ,  $T \hat{=} 1/30$  second. The plasma was created by 10 cm electron cyclotron resonance in a magnetic mirror with  $B \hat{=} 1$  kilogauss at the ring position.

We observe that the plasma forms a hollow ring in close proximity to the copper wall. Moving the ring away from the copper wall causes instability, plasma loss, or simply prevents the ring from forming. The ring was moved from the wall by magnetic compression or by a metal or a ceramic limiter. The stability was not due to current flow along B-lines, or "line tying", because the ring was stable both at low pressure ( $\hat{=} 10^{-7}$  torr gauge), and with nonconducting glass end walls.

We explain the stability quantitatively by the following model. We note that the ring is not homogeneous, but appears to have a precessing azimuthal structure. As a limit, we approximate the ring first as a precessing sector, then as a precessing rigid magnetic dipole. This dipole is repelled from the wall and stabilized by an image magnetic dipole in the wall. Quantitatively we compute that the ring is 1 cm from the wall, as is observed, and that moving it 2 cm from the wall results in instability. This distance appears as the 4th root of an equation, and is remarkably invariant to the parameters of the ring.

Our main intellectual step was in demonstrating that the power required to maintain the image dipole in the wall was small enough not to limit the confinement time of the ring. This was done by using the MHD equations to find E and B in the copper wall, and then by evaluating Poynting's vector at the plasma - metal interface.

\*Supported in part by NSF grant ENG-78-03400

Workshop on EBT Stability Theory, May 13-14, 1981, Oak Ridge, Tennessee

The basic objective of this calculation is to explain how the hot-electron ring in the Mirror-Machine experiment at the University of Tennessee is stabilized by a metal wall.

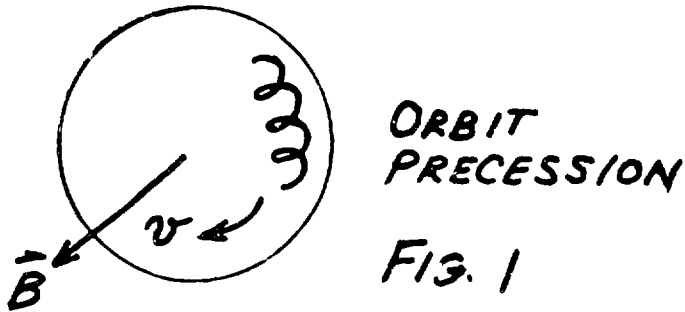
The first part of this calculation explains how such a ring may be stabilized; the second part explains how the power losses are not abnormally high, and the third part puts limits on the amount of material that may be confined.

The experiment works as follows. A microwave source at  $\lambda = 10$  cm heats plasma electrons confined in a magnetic mirror. The electrons are heated to  $T_e = 10^5$  electron - volts, or  $10^9$  °K. The electrons form a hollow, precessing shell near the metal wall. The observed confinement time is about 1/30 second. Moving the electrons away from the wall by moving the magnetic field, or by placing a ceramic scraper in the system results in a rapid plasma loss, or inhibits the formation of the ring, respectively. The conclusion is that the ring is stabilized radially, by the presence of the conducting wall. This is the observation that we now must explain.

Two features are present when hot electrons are confined in a magnetic mirror.

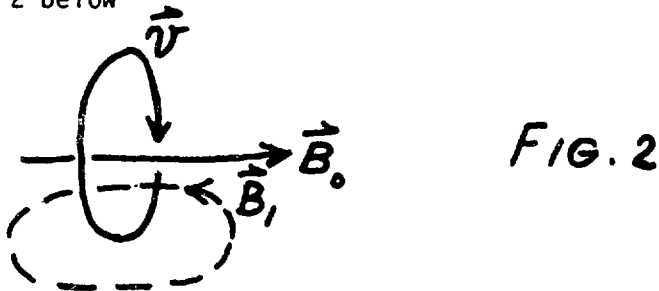
1. The electrons precess.
2. The electrons are diamagnetic.

The electrons precess in a magnetic mirror because the magnetic field decreases with radius. Thus, the portion of an electron orbit in the outer region experiences a lower field than the portion in the inner region, and the electron precesses, as shown in FIG. 1.



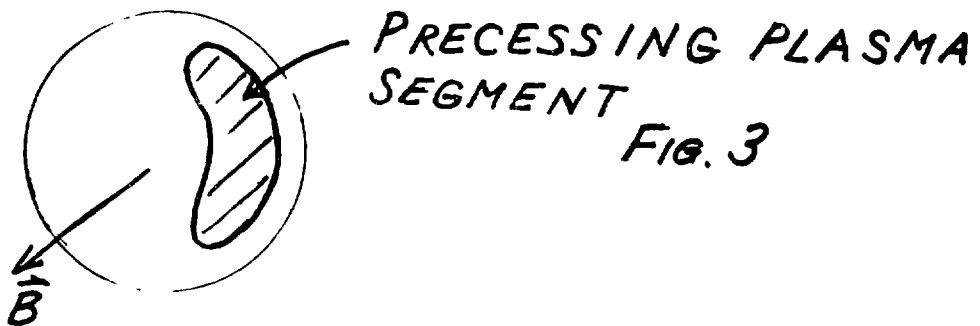
Consider a positive charge for example.  $\vec{F} = e\vec{v} \times \vec{B}$ . The precession is shown above.

The electron is diamagnetic. This means that an electron or ion acts as a magnetic dipole oriented against the magnetic field. This feature is shown in FIG. 2 below

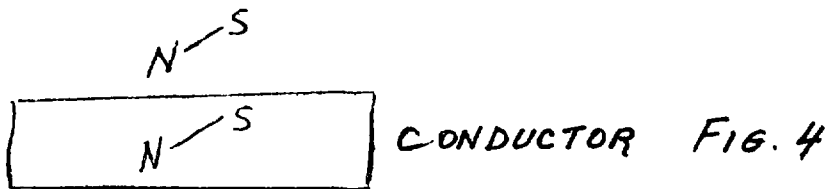


Consider a charge above. A positive charge in orbit generates a magnetic field inside its orbit that opposes the initial magnetic field, and outside its orbit that aids the initial magnetic field. In general, inside a hot plasma in a mirror, the magnetic field is reduced, meaning that the plasma is diamagnetic ( $\mu < \mu_0$ ).

A third feature that seems to be present in our device is that the plasma seems to form a clump rather than a ring. The precession frequency is about  $10^6 \text{ Hz}$ . This feature is needed for stabilization. See FIG. 3 below.



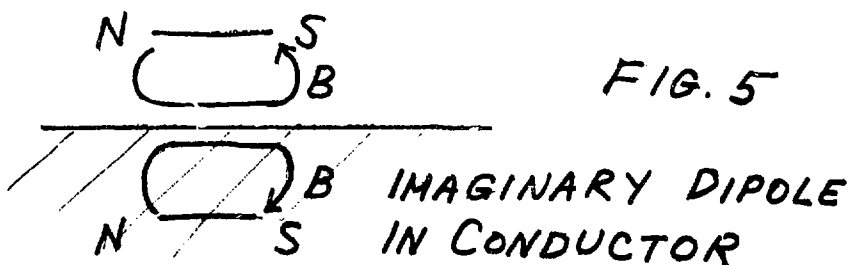
In view of the above, let us represent the plasma as a precessing magnetic dipole, and show that it is kept off the wall. Consider a linear model as an example. See FIG. 4 below.



If the dipole precesses rapidly, the magnetic field cannot penetrate the conductor. One way of computing this is in terms of the skin depth  $Z_0$ .

$$Z_0 = \sqrt{\frac{2}{\sigma \mu_0 \omega}}$$

Another way is using the method of images. A way of keeping a magnetic dipole's field from penetrating the surface is by having a second, imaginary dipole of equal strength inside the conductor. See FIG. 5 below. This formalism allows us to compute the restoring force on the dipole!



My major objection to the above formalism is that we have to drag a magnetic field through a conducting medium, and this involves losses. I needed a method of computing the energy losses, and this is where MHD comes in.

For simplicity, consider a magnetic field propagating over the surface of a conducting medium. Let  $\vec{B} = \hat{j}B_0 e^{i(kx - \omega t)}$  (complex notation). Inside the medium, the relevant equation is  $\nabla^2 \vec{B} = \sigma \mu_0 \frac{\partial \vec{B}}{\partial t}$ . To fit this equation, we need something fitting inside the medium, plus fitting the boundary conditions. A solution is given by

$$\vec{B} = \hat{j}B_0 e^{i(k_x x + k_z z - \omega t)}$$

Putting this into the above equation, we get the following differential equation,

$$(ik_x)^2 + (ik_z)^2 = \sigma \mu_0 (-i\omega),$$

$$-k_x^2 - k_z^2 = -i\omega \sigma \mu_0,$$

The above equation MUST fit, because it fits both the differential equation, and the boundary conditions. It has two limits of interest. 1st,  $\omega \rightarrow 0$ . In this case,  $k_x^2 + k_z^2 = 0$ . or  $\pm i k_x = k_z$ . Hence,

$$\vec{B} = \hat{j}B_0 e^{i(k_x s \pm ik_z z - \omega t)},$$

or the spatial dependence is  $e^{ik_x x - k_z z}$ . Thus, the dependence is sinusoidal in x- space, and decays exponentially in Z- space. This is the D.C. response.

The second limit is if  $\omega \rightarrow \infty$ , so that  $k_z^2 = i\omega \sigma \mu_0$ . Here

$$k_z = \pm \left( \frac{1}{\sqrt{2}} \omega \sigma \mu_0 + \frac{1}{\sqrt{2}} \omega \sigma \mu_0 \right)$$

Having obtained the expression for the magnetic field in the medium, we can compute the energy flux through the surface of the medium. Power flow is given by  $\vec{W} = \vec{E} \times \vec{H} = \frac{\vec{E} \times \vec{B}}{\mu_0}$ . On the average, where  $E$  and  $B$  are peak values,

$$\langle \vec{W} \rangle = \frac{1}{2} \frac{E_0 \times B_0}{\mu_0}.$$

$$\text{Now } \vec{B} = \hat{j} B_0 e^{i(k_x x + k_z z - \omega t)} = \hat{j} B_0 e^{i(k_z z - \omega t)}$$

$$\nabla \times \vec{E} = - \frac{\partial \vec{B}}{\partial t}$$

Assume  $\vec{E}$  has the same form as  $\vec{B}$ , except for a phase shift and direction

$$\vec{E} = \hat{i} E_0 e^{i(k_z z - \omega t)}$$

$$\nabla \times \vec{E} = \begin{vmatrix} \hat{i} & \frac{\partial}{\partial x} & E_x \\ \hat{j} & \frac{\partial}{\partial y} & E_y \\ \hat{h} & \frac{\partial}{\partial z} & E_z \end{vmatrix}$$

no current flow = 0

$$= \hat{i} \frac{\partial}{\partial z} E_y = - \hat{i} \frac{\partial}{\partial z} E_y$$

$$\nabla \times \vec{E} = - \hat{i} \frac{\partial}{\partial z} E_y = - \hat{i} E_0 (ik_z) e^{i(k_z z - \omega t)}$$

$$- \frac{\partial \vec{B}}{\partial t} = - i\omega \hat{j} B_0 e^{i(k_z z - \omega t)}$$

$$\text{So } E_0 = \frac{\omega}{k} B_0$$

$$\text{And } \langle \vec{w} \rangle = \frac{1}{2} \frac{B_0^2}{\mu_0} \left( \frac{\omega}{k} \right)$$

NOTE that  $k$  is a complex number and only the value of  $\frac{\omega}{k}$  that is real contributes!

$$\frac{\omega}{k_r + i k_i} = \frac{\omega(k_r - i k_i)}{k_r^2 + k_i^2} = \frac{\omega}{2k_r} \text{ since } k_r = k_i/$$

$$\text{Thus } \langle \bar{W} \rangle = \frac{1}{4} \frac{B_0^2}{\mu_0} \left( \frac{\omega}{k_r} \right)$$

The + value of  $\langle W \rangle$  means that the power is moving in the + - Z direction - INTO the metal.

Our final equation for power flow into the metal is as follows

$$\begin{aligned} \langle \bar{W} \rangle &= \frac{1}{4} \frac{B_0^2}{\mu_0} \left( \sqrt{\frac{\omega}{\sigma \mu_0}} \right) \\ &= \frac{1}{4} \frac{B_0^2}{\mu_0} \sqrt{\frac{2\omega}{\sigma \mu_0}} \\ &= \frac{1}{2\sqrt{2}} B_0^2 \sqrt{\frac{\omega}{\sigma}} \frac{1}{\mu_0^{3/2}} \end{aligned}$$

Let us now estimate the power loss for a typical case.

$$\nu = 10^6 \text{ Hz} \rightarrow 2\pi \times 10^6 \text{ radian/sec}$$

$$B_0 = 0.1 \text{ tesla (max-B field in problem)}$$

$$\sigma = 10^8 \text{ mHo/meter}$$

$$\mu_0 = 10^{-6} \text{ henry/meter}$$

$$\langle \bar{W} \rangle = \frac{1}{2\sqrt{2}} (0.1)^2 \sqrt{\frac{2 \times \pi \times 10^6}{10^8}} \frac{1}{(10^{-6})^{3/2}} = 8.86 \times 10^5 \text{ watts/m}^2$$

Next, consider the energy stored in a cubic meter of plasma.

$$\text{Work} = nKT = 10^{18} \times 1.38 \times 10^{-23} \times 10^9 = 1.38 \times 10^{+4} \text{ Joule}$$

$$\tau = \frac{\text{Work}}{\text{Power}} = \frac{1.38 \times 10^4}{0.86 \times 10^5} = 1.56 \times 10^{-2} \text{ second.}$$

This number is remarkably close to our value of 30 msec ( $3.3 \times 10^{-2}$  second), considering that  $B_0 \approx 0.1$  tesla is an upper limit. Thus, the power loss through the metal surface is tolerable, which is the question posed at the start of this section of this investigation.

Next, we consider the relative forces between magnetic dipoles as shown in FIG. 6.

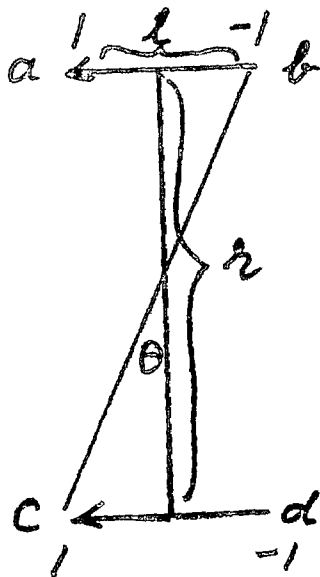


FIG. 6

The repulsion between b and d is

$$F_r = \frac{bd}{4\pi\epsilon_0 r^2} \quad (\text{An electrostatic analogy is used})$$

The attraction between b and c is

$$\begin{aligned} F_a &= \frac{bc}{4\pi\epsilon_0 (r^2 + \ell^2)} \cos \theta \\ &= \frac{bc}{4\pi\epsilon_0} \frac{1}{(r^2 + \ell^2)} \frac{r}{(r^2 + \ell^2)^{1/2}} \\ &= \frac{bc}{4\pi\epsilon_0} \frac{r}{(r^2 + \ell^2)^{3/2}} \end{aligned}$$

The difference is (for all 4 units)

$$\begin{aligned} F_r &= 2 \left( \frac{q^2}{4\pi\epsilon_0 r^2} - \frac{q^2}{4\pi\epsilon_0 r^2} \frac{1}{(1 + (\frac{\ell}{r})^2)^{3/2}} \right) \\ &= 2 \frac{q^2}{4\pi\epsilon_0 r^2} \left( 1 - \frac{1}{(1 + (\frac{\ell}{r})^2)^{3/2}} \right) \\ (1 + (\frac{\ell}{r})^2)^{-3/2} &= 1 - \frac{3}{2} (\frac{\ell}{r})^2 \text{ -----} \\ &= 2 \frac{q^2 \ell^2}{4\pi\epsilon_0 r^2} \left( + \frac{3}{2} (\frac{\ell}{r})^2 + \text{-----} \right) \\ &= 2 \frac{q^2}{4\pi\epsilon_0 r^4} \frac{3}{2} \\ &= 3 \frac{q^2 \ell^2}{4\pi\epsilon_0 r^4} \end{aligned}$$

Hence, the repulsive force is the product of the dipole moments,  $q\ell$ , and varies as the inverse 4th power.

NEXT, we compute the destabilizing effect of the magnetic mirror. We represent the magnetic mirror as a uniform magnetic field, plus a magnetic dipole. The field of a magnetic dipole can be represented as follows.

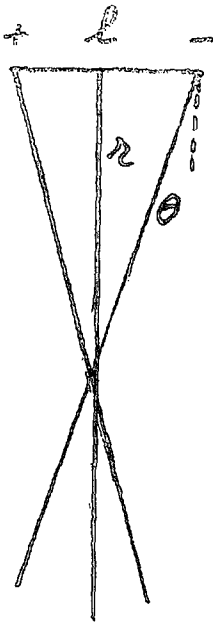


FIG. 7

$$E_- = - \frac{q^1}{4\pi\epsilon_0 r^2} \sin(\theta_-)$$

$$E_+ = + \frac{q^1}{4\pi\epsilon_0 r^2} \sin(\theta_+)$$

$$E = 2 \frac{q^1}{4\pi\epsilon_0 r^2} \theta$$

$$= 2 \frac{q^1 \ell}{4\pi\epsilon_0 r^3}$$

At our radius we represent  $B$  as  $B_0 + B_s$ . The value of  $B_s$  is determined by the magnetic field gradient.  $\frac{\partial B}{\partial r} \frac{1}{B} = 2 \frac{q^1 \ell}{4\pi\epsilon_0} (-3r^{-4}) \frac{1}{B_0} = \text{add} = \text{measured gradient}$ .

We now can find an effective dipole moment

$$q^1 \ell^1 = \frac{4\pi\epsilon_0}{2} \left(-\frac{r^4}{3}\right) B_0 \left(\frac{\partial B}{\partial r} \frac{1}{B}\right)$$

↑  
measured

Now, the repulsion of the plasma dipole from the center can be computed.

$$F_r = 3 \frac{q\ell}{4\pi\epsilon_0 r^4} \times \frac{4\pi\epsilon_0}{2} \left(-\frac{r^4}{3}\right) B_0 \left(\frac{\partial B}{\partial r} \frac{1}{B}\right)$$

$$= - q\ell B_0 \left(\frac{\partial B}{\partial r} \frac{1}{B}\right)$$

The wall restoring force is (noting that the wall - dipole spacing  $S = \frac{r}{2}$ )

$$3 \frac{q^2 \ell^2}{4\pi\epsilon_0 (2S)^2}$$

For stability, we get

$$- q\ell B_0 \left( \frac{\partial B}{\partial r} \frac{1}{B} \right) \leq 3 \frac{q^2 \ell^2}{4\pi\epsilon_0 (2S)^4}$$

measured

Minus

$$- B_0 \left( \frac{\partial B}{\partial r} \frac{1}{B} \right) \leq 3 \frac{q\ell}{4\pi\epsilon_0 (2S)^4}$$

We must evaluate the magnetic analogy of a dipole,  $\frac{q\ell}{4\pi\epsilon_0}$ , but one thing is clear - STABILITY INCREASES with dipole moment.

The equation obviously fails when  $S$  becomes comparable with the skin depth.

Computation of dipole moment.

$$\frac{q\ell}{4\pi\epsilon_0} = B_0 a^2 \ell \frac{nKT}{B_0^2 / 2\mu_0} = 0.1 \text{ tesla} \times (.01\text{cm})^2 \times 0.1\text{cm} \times 0.1 = 10^{-7} \quad (\beta = 0.1)$$

$$- B_0 \left( \frac{\partial B}{\partial r} \frac{1}{B} \right) = - 0.1$$

+ +

$$0.1 \text{ tesla}^{-1} \text{ meter}^{-1}$$

PUT INTO INEQUALITY

$$-0.1 < 3 \frac{10^{-7}}{(2S)^4}$$

$$(2S)^4 < 3 \times 10^{-6}$$

$$S \approx 2\text{cm.}$$

## **4. RING-CORE COUPLING, LOW FREQUENCY MODES**

*D. E. Baldwin and C. L. Hedrick, Session Chairmen*

## Eigenmode Stability Analysis for a Bumpy Torus

J. W. Van Dam, H. L. Berk, M. N. Rosenbluth  
Institute for Fusion Studies, University of Texas, Austin, TX 78712

and

D. A. Spong  
Fusion Energy Division, Oak Ridge National Laboratory  
Oak Ridge, TN 37830

### Abstract

The analysis of eigenmodes in a bumpy torus yields several stability boundaries that indicate the existence of a parameter regime for generally stable operation consistent with current experiments. However, there are a relatively narrow band of parameters where instability persists.

## I. Introduction

The bumpy torus has several features that make the theoretical treatment of its linear stability quite different from that of other confinement devices. In particular, its plasma contains an extremely energetic high-beta electron population, which creates a deep diamagnetic well in each mirror sector. Conventional fluid or guiding center theories are inadequate because the magnetic drift frequency of the hot electrons is comparable to the ion cyclotron frequency and larger than characteristic frequencies for typical magnetohydrodynamic fluctuations of interest. Furthermore, the plasma ion and the energetic electron gyroradii are comparable, and the diamagnetic well has a half width of several gyroradii, which suggests that the radial mode structure and finite Larmor radius effects are important.

The stability investigations reported in this work have their roots in several previous findings: (1) a hot electron plasma can be stabilized with respect to interchange if there is enough cold ion plasma present;<sup>1,2</sup> (2) the hot electron rings in the bumpy torus device stabilize the toroidal core plasma against interchange if the ring pressure is high enough;<sup>3</sup> and (3) the core plasma becomes interchange unstable if its pressure exceeds a certain threshold.<sup>4,5</sup> The last observation led to some concern about whether the bumpy torus would be a viable reactor and hence underscored the significance of linear stability theory for this device. Subsequent studies extended the linear stability theory to include non-local geometrical effects<sup>6</sup> and high frequency mode coupling.<sup>7,8</sup>

In the present work, we consider the axial eigenmode equation and we point out the importance of considering the radial eigenmode problem. The major results is that we obtain various stability boundaries that generally indicate the existence of a parameter regime for stable bumpy torus operation which is consistent with current experiments. However, over a relatively narrow wavenumber band instability still persists in the otherwise stable regime.

In order to appreciate the significance of this result, we will first describe the somewhat pessimistic stability predictions that were obtained from an energy principle analysis. Then, in Sec. III, the development of normal mode equations for a bumpy cylinder is sketched. Axial and radial eigenmodes are separately discussed in Secs. IV and V, respectively.

## II. Kinetic Energy Principle Approach

A useful way to approach the problem of linear stability has often been through the use of an energy principle, since this makes quite clear the physical mechanism for possible instabilities. However, usual fluid or guiding center theories are not adequate, since the plasma in a bumpy torus contains an extremely energetic electron population. Due to their large cross-field magnetic drift, these electrons cannot be considered to be "frozen in" with the magnetic field in the usual fluid sense.

A new kinetic energy principle<sup>6</sup> has been developed, which accounts for this interesting non-fluid feature by using single-particle adiabatic invariants to describe the behavior of the hot electrons. These invariants are the magnetic moment  $\mu = Mv_{\perp}^2/2B$ , the longitudinal action  $J_{\parallel} = \oint v_{\parallel} d\ell$ , and the magnetic flux through the particle precessional drift orbit. Although developed for the bumpy torus, this new energy principle is of more general interest since it provides a rare application of the third adiabatic invariant. It has also been used to study linear stability in the tandem mirror<sup>9</sup> and tokamak<sup>10</sup> devices.

In a bumpy torus, this energy principle has been used to examine low frequency fluctuations whose frequency is larger than the diamagnetic frequencies and the magnetic drift frequencies (evaluated at typical energies) of the ions and electrons in the toroidal core plasma, but smaller than the diamagnetic and magnetic drift frequencies of the energetic electrons.

Application of the Schwartz inequality to this energy principle shows that a new, purely magnetic mode will be unstable in a bumpy torus at low values of the core plasma pressure given by

$$-\frac{\partial p_c}{\partial \psi} < - \frac{\oint \frac{dl}{B} k \frac{\partial}{\partial \psi} (p_{\parallel h} + p_{\perp h})}{\oint \frac{dl}{B^3} \frac{\partial p_{\perp h}}{\partial \psi}} \quad (1)$$

Here,  $p_c$  is the core pressure, assumed to be isotropic;  $dl$  is the arc length increment along a line of force;  $p_{\parallel h}$ ,  $p_{\perp h}$  are the anisotropic hot electron pressure components;  $\psi$  is the magnetic flux, used as the "radial" coordinate; and  $k = (\hat{b} \cdot \nabla \hat{b}) \cdot \nabla \psi / |\nabla \psi|^2$  is the field line curvature in the  $\hat{\psi}$  direction, normalized by  $|\nabla \psi| = rB$ . In obtaining Eq. (1), we have assumed azimuthal symmetry and considered  $m \gg 1$  modes, with  $m$  the azimuthal mode number.

The criterion of Eq. (1) may be more easily understood if we use a local approximation (i.e.,  $|\nabla \psi| k \rightarrow -R_c^{-1}$ , where  $R_c$  is a measure of the mirror field curvature, and  $|\nabla \psi| (\partial p / \partial \psi) \rightarrow -p/\Delta$ , with the scale length  $\Delta$  taken to be the same for the ring and core pressures) to rewrite it as a core plasma beta limit ( $\beta_c = 2p_c/B^2$ ):

$$\beta_{\text{core}} < 2 \left( \frac{\Delta}{R_c} \right) \left( 1 + \frac{p_{\parallel h}}{p_{\perp h}} \right) \quad (2)$$

If we use  $\Delta/R_c \cong 0.05$  (although this experimental ratio is not well known), we obtain the threshold core beta value to be about 10% for a fairly anisotropic ring. Note, however, that this threshold for the core beta is approximately half the ring beta threshold for  $\oint dl/B$  stability due to a rigid ring, i.e., half of the ring beta value that is usually associated with the operational C-T transition.

For core pressures  $p_c$  above the limit specified in Eq. (1), the magnetic mode is stable. However, the new energy principle, minimized with respect to the magnetic field perturbation, shows that the low frequency interchange mode can then be unstable.

This apparent dilemma is resolved by noticing that the new energy principle is sufficient, but not necessary, for stability. Necessity has been demonstrated only for high- $m$  modes in a plasma of equal temperature Maxwellian ions and electrons, which is not the case in bumpy torus experiments. Thus, the actual determination of stability will require a normal mode analysis, which is presented in the following sections.

Nonetheless, the energy principle approach does serve to indicate (a) the existence of a new potentially dangerous magnetic mode, similar to the well-known mirror instability (i.e., compressional Alfvén mode) although driven not by extreme anisotropy but by the negative compressibility of the paramagnetic hot electrons, and (b) the existence of an upper limit on the core plasma pressure for interchange stability. The latter was previously pointed out from a local slab-geometry dispersion relation<sup>4,5</sup> and is thus confirmed by the non-local energy principle analysis.

### III. Normal Mode Equations for an Axisymmetric Bumpy System

The bumpy torus is a large aspect ratio device.<sup>3</sup> Not only is the major radius much larger than either the plasma radius or the inner radius of the mirror coils, but also the curvature of the local mirror field is much larger than the toroidal curvature. Thus, it is reasonable to assume azimuthal symmetry and reduce the investigation of stability to a two-dimensional problem, viz., that of a bumpy cylinder. For such a system, we choose the orthogonal curvilinear coordinates  $\psi$ ,  $\theta$ , and  $X$ , where  $\psi$  is the magnetic flux function,  $\theta$  is the azimuthal angle, and  $X$  is the coordinate

along the equilibrium magnetic field, which is represented as  $\underline{B}_0 = \underline{\nabla}\psi \times \underline{\nabla}\theta = 1/r (\underline{\nabla}\psi \times \hat{\underline{\theta}})$ . Let  $\mathcal{J} = [(\underline{\nabla}\psi \times \underline{\nabla}\theta) \cdot \underline{\nabla}\chi]^{-1} = (B_0 |\underline{\nabla}\chi|)^{-1}$  be the Jacobian for this coordinate system.

Our basic equation of motion will be taken to be that for momentum transfer:

$$\rho \frac{d\underline{v}}{dt} = \underline{J} \times \underline{B} - \underline{\nabla} \cdot \underline{P} \quad . \quad (3)$$

This is the exact first velocity moment of the Vlasov equation. No electric field appears in Eq. (3) as long as we assume charge neutrality. The mass density  $\rho \approx N_i M_i$  in Eq. (3) is mostly that of ions; also,  $\underline{v}$  is the fluid velocity,  $\underline{J} = \underline{\nabla} \times \underline{B}$  the total current, and  $\underline{P}$  the total stress tensor. In this study, we will neglect Larmor radius effects. Then the pressure has the diagonal form  $\underline{P} = p_{\parallel} \hat{\underline{b}} \hat{\underline{b}} + p_{\perp} (\underline{I} - \hat{\underline{b}} \hat{\underline{b}})$ , with  $\hat{\underline{b}} = \underline{B}_0 / B_0$  the unit vector along the equilibrium field. The pressures  $p_{\parallel, \perp}$  are to be obtained from a guiding center distribution function  $f(\underline{x}, \epsilon, \mu, t)$ , which obeys the drift kinetic equation:

$$\frac{\partial f}{\partial t} + \left( v_{\parallel} \hat{\underline{b}} + \underline{v}_d + \frac{c \underline{E} \times \underline{B}}{B^2} \right) \cdot \underline{\nabla} f + \left( q E_{\parallel} v_{\parallel} + q \underline{E} \cdot \underline{v}_d + \mu \frac{\partial B}{\partial t} \right) \frac{\partial f}{\partial \epsilon} = 0 \quad . \quad (4)$$

This drift kinetic equation is derived by averaging the Vlasov equation over the rapid gyromotion, in the small Larmor radius limit. The spatial gradient  $\underline{\nabla} f$  in Eq. (4) is taken with the velocity space variables  $\mu = M v_{\perp}^2 / 2B$  and  $\epsilon = 1/2 M v_{\parallel}^2 + \mu B$  held fixed. Also,  $\underline{E}$  is the electric field and  $\underline{v}_d = (c/qB) \hat{\underline{b}} \times (M v_{\perp}^2 \hat{\underline{b}} - \underline{\nabla} \hat{\underline{b}} + \mu \underline{\nabla} B)$  the curvature and gradient-B magnetic drifts.

When we take  $E_{\parallel} = 0$  and neglect the longitudinal motion (i.e., the coupling to drift waves), the momentum equation (3) yields two scalar

equations. One is its azimuthal component:

$$\rho_i \dot{\underline{v}}_{\perp i} \cdot \underline{\nabla}\theta = - \underline{\nabla}\theta \cdot \left[ \underline{\nabla} \left( \frac{1}{2} B^2 + p_{\perp} \right) - \underline{B} \cdot \underline{\nabla} (\sigma \underline{B}) \right] , \quad (5)$$

where  $\dot{\underline{v}}_{\perp i} = d\underline{v}_{\perp i}/dt$  and  $\sigma = 1 + (p_{\perp} - p_{\parallel})/B^2$ . As the other scalar equation, instead of the  $\underline{\nabla}\psi$  component, we will use the parallel component of the curl of Eq. (3). After linearization, it may be seen that this operation conveniently annihilates information about the Alfvén mode already contained in the azimuthal equation, (5). Taking  $\underline{B} \cdot \underline{\nabla} \times$  of Eq. (3) yields

$$\begin{aligned} \underline{\nabla} \cdot (\underline{B} \times \rho \dot{\underline{v}}) + B^2 \underline{B} \cdot \underline{\nabla} \left( \frac{\sigma \underline{j} \cdot \underline{B}}{B^2} \right) - (\underline{B} \times \hat{\underline{b}} \cdot \underline{\nabla} \hat{\underline{b}}) \cdot \underline{\nabla} \left( \frac{1}{2} B^2 - p_{\parallel} \right) \\ + \rho \dot{\underline{v}} \cdot (\hat{\underline{b}} \times \underline{\nabla} B) = 0 \quad . \end{aligned} \quad (6)$$

The next step is to linearize Eqs. (5) and (6), using  $\underline{B} = \underline{B}_0 + \tilde{\underline{B}}$  and  $\underline{\xi} = \tilde{\underline{\xi}}_1$ , with tildes indicating perturbed quantities. We will not consider ambipolar effects associated with an equilibrium electrostatic potential. Also, once having linearized the equations, we will drop the nought subscript on equilibrium quantities. Perturbed quantities are taken to vary as  $\exp(im\theta - i\omega t)$ . The magnetic field perturbation may be written as  $\tilde{\underline{B}} = \underline{\nabla} \times (\underline{\xi} \times \underline{B}_0)$ , where  $\underline{\xi}(\underline{x}) = i(\tilde{\underline{\xi}} \times \hat{\underline{b}})/\omega B$  is the displacement of a field line. In particular, it is useful to define the two contravariant components of the displacement,  $X = \underline{\xi} \cdot \underline{\nabla}\psi$  and  $Y = \underline{\xi} \cdot \underline{\nabla}\theta$ , in terms of which the longitudinal perturbed field can be written as  $\tilde{B}_{\parallel}/B = -imY - \partial X/\partial\psi$ .

The linearized azimuthal momentum equation is

$$-i\omega \rho \dot{\underline{v}} \cdot \underline{\nabla}\theta = - im |\underline{\nabla}\theta|^2 (B\tilde{B}_{\parallel} + \tilde{p}_{\perp}) + |\underline{\nabla}\theta|^2 \underline{B} \cdot \underline{\nabla} \left( \frac{\sigma}{|\underline{\nabla}\theta|^2} \underline{B} \cdot \underline{\nabla} Y \right) \quad . \quad (7)$$

Linearizing the parallel current equation, (6), is slightly more complicated.

It helps to note that  $\tilde{\underline{B}} \cdot \underline{\nabla}\psi = \underline{B} \cdot \underline{\nabla} X$  and  $\tilde{\underline{B}} \cdot \underline{\nabla}\theta = \underline{B} \cdot \underline{\nabla} Y$  and that, for an

axisymmetric system,  $\underline{j} \cdot \underline{\nabla}\psi = 0 = j_{\parallel}$  and  $\underline{j} \cdot \underline{\nabla}\theta = - (B^2 g)' / g = B^2 (B' / B - k)$  where a prime means  $\partial/\partial\psi$ . We obtain the following linearized form:

$$\begin{aligned} \frac{1}{B} \left[ \frac{\partial}{\partial\psi} (B \tilde{p}_{\parallel} + \tilde{p}_{\perp}) \right]' - i \omega \rho \left( \frac{\tilde{v} \cdot \underline{\nabla}\psi}{|\underline{\nabla}\psi|^2} \right) - \underline{B} \cdot \underline{\nabla} \left( \frac{\sigma}{|\underline{\nabla}\psi|^2} \underline{B} \cdot \underline{\nabla}x \right) + k (\tilde{p}_{\parallel} - B \tilde{B}_{\parallel}) \\ + \frac{i}{m} \frac{\underline{B} \cdot \underline{\nabla}Y}{|\underline{\nabla}\theta|^2} \left\{ \underline{b} \cdot \underline{\nabla} \left[ B \sigma' + B \sigma \left( \frac{2B'}{B} - k \right) \right] - k \left( \underline{b} \cdot \underline{\nabla}B - \frac{1}{B} \underline{b} \cdot \underline{\nabla}p_{\parallel} \right) \right. \\ \left. - \sigma \underline{b} \cdot \underline{\nabla}B' + \frac{\sigma B'}{B} \underline{b} \cdot \underline{\nabla}B = 0 \right\}. \quad (8) \end{aligned}$$

Eqs. (7) and (8) must be supplemented by the solution of the linearized drift kinetic equation for the hot electrons:

$$\tilde{f}_h(\psi, \epsilon, \mu) = - \chi \frac{\partial f_h}{\partial \psi} - \left[ \frac{\omega \frac{\partial f_h}{\partial \epsilon} + m \frac{\partial f_h}{\partial \psi}}{\omega - \frac{m}{q} \langle \mu B' + v_{\parallel}^2 k \rangle} \right] \langle \mu \tilde{B}_{\parallel} + (v_{\parallel}^2 k + \mu B') x \rangle. \quad (9)$$

We have taken the hot electrons to be trapped and rapidly bouncing in the magnetic mirror of each bumpy sector, so that field quantities must be bounce averaged using  $\langle \dots \rangle = [\oint dl (\dots) / v_{\parallel}] / [\oint dl / v_{\parallel}]$ . The two pressure components are calculated from  $\{\tilde{p}_{\parallel}, \tilde{p}_{\perp}\} = \int d\epsilon d\mu B v_{\parallel}^{-1} \tilde{f} \{ M v_{\parallel}^2, \mu B \} + \tilde{B}_{\parallel} \left\{ \frac{\partial p_{\parallel}}{\partial B}, \frac{\partial p_{\perp}}{\partial B} \right\}$ . The equilibrium pressure  $p_c$  for the core plasma ions and electrons is much smaller than that for the ring and is assumed to be isotropic. To calculate the perturbed pressure  $\tilde{p}_c$ , we may use either a fluid theory or a distribution function approach.

Finally, since the ion beta is small, it is sufficient to use the cold plasma response and include only ion  $\mathbf{E} \times \mathbf{B}$  and polarization drifts in the inertia term:

$$\tilde{v}_i = \left( \frac{\omega_{ci}^2}{\omega_{ci}^2 - \omega^2} \right) \left( \frac{1}{B} \right) \left[ \tilde{\mathbf{E}} \times \underline{b} + i \frac{\omega}{\omega_{ci}} \tilde{\mathbf{E}}_{\perp} \right]. \quad (10)$$

where  $\omega_{ci} = eB/M_i c$  is the ion gyrofrequency. All other kinetic effects enter through the perturbed pressures. Eq. (10) can be decomposed into two components:

$$-i\omega \tilde{\mathbf{v}} \cdot \nabla \psi = -\lambda \left[ X + \left( \frac{i\omega B}{\omega_{ci} |\nabla \theta|^2} \right) Y \right], \quad (11)$$

$$-i\omega \tilde{\mathbf{v}} \cdot \nabla \theta = -\lambda \left[ Y - \left( \frac{i\omega B}{\omega_{ci} |\nabla \psi|^2} \right) X \right], \quad (12)$$

with  $\lambda = \omega^2 \omega_{ci}^2 / (\omega_{ci}^2 - \omega^2)$ .

Eqs. (11) and (12), together with (7), (8), and (9), constitute the linear system of equations whose stability is to be investigated.

#### IV. Axial Eigenmodes

The equations for the full two-dimensional bumpy cylinder problem are fairly complicated. We are, however, able to make some progress on the basis of two assumptions. First, we argue that the magnetic field line bending term in Eq. (8) should be eliminated if we wish to consider the most unstable types of perturbations possible. Thus, we assume that  $X$  is predominantly flute-like. Second, we assume that the diamagnetic well is sufficiently strong so that the field curvature term is small in the equilibrium condition, i.e.,  $B^{-1}(\partial B/\partial \psi) \approx -B^{-2}(\partial p_1/\partial \psi) \gg k$ . In other words, if we define a gradient- $B$  scale length  $\Delta_B$  and a curvature scale length  $R_c$ , we have  $\Delta_B \approx 2A/\beta_{1h}$  (since  $\beta_{1h} \gg \beta_c$ ) and  $\Delta_B/R_c < 1$ . For the ratio  $\Delta_B/R_c$  to be a respectable expansion parameter requires a large ring pressure:  $\beta_{1h} > 20\%$  at least. For such high beta rings, we then find that the lowest-order solution of Eq. (7) for the perturbed magnetic field is  $\tilde{\mathbf{B}}_\perp = c(\psi) \partial \mathbf{B} / \partial \psi$ . Here,  $\tilde{\mathbf{B}}_\perp$  is the Lagrangian perturbed parallel magnetic field, measured in a reference frame moving with the lines of force and hence related to the Eulerian perturbation  $\tilde{\mathbf{B}}_\parallel$  by  $\tilde{\mathbf{B}}_\perp = \tilde{\mathbf{B}}_\parallel + X \mathbf{B}'$ .

We now multiply the two normal mode equations, (7) and (8), by the lowest-order solutions for  $\tilde{B}_1$  and  $\chi$ , respectively, and integrate over all space. This procedure removes the dominant terms and leaves two consistency conditions which specify the higher order behavior of the  $\psi$ -displacement and the longitudinal perturbed magnetic field.

To illustrate this procedure, let us specifically consider modes with  $m \gg 1$  so that the analysis can be performed on individual field lines. This corresponds to looking only at the axial eigenmodes, with no consideration for the transverse structure.

In particular, if we set  $\chi = 0$  in Eq. (7), we obtain a line-averaged dispersion relation for the modified compressional Alfvén mode:

$$\omega^2 \oint \frac{d\ell}{B} \left( \frac{\rho B'^2}{m^2 B^2 |\nabla\theta|^2} \right) - \frac{\omega}{m} \oint d\ell \frac{\partial}{\partial\psi} \left( \frac{N_h}{B} \right) - \oint \frac{d\ell}{B} \left[ k B B' \left( 1 - \frac{p_{\parallel h}'}{B B'} \right) - B B' \left( \frac{p_c}{B} \right)' + \frac{\sigma}{m^2 |\nabla\theta|^2} \left( \underline{B} \cdot \underline{\nabla} \frac{B'}{B} \right)^2 \right] = 0 \quad (13)$$

Here,  $N_h = \int d\epsilon d\mu B v_{\parallel}^{-1} f_h$  is the equilibrium ring density. Consider the frequency-independent term in Eq. (13). If the sign of the term in brackets is negative, the dispersion relation can be unstable. With negligible pressure  $k = B'/B$ , and the sign of the term is positive and the balance of the first and third terms give the usual Alfvén wave. However, with sufficiently large hot electron pressure,  $kB'/B$  becomes negative and the sign of the third term is negative when  $p_c$  is sufficiently small and  $m$  sufficiently large. This then gives the modified mirror instability that was pointed out in the energy principle analysis described in Sec. II. However, this mode can be stabilized by the frequency shift due to the term linear in  $\omega$  if

$$4N_i M_i \oint \frac{d\ell}{B^5} |\nabla\psi|^2 B'^2 \oint \frac{d\ell}{B} \left[ k(p_{\parallel h} + p_{\perp h})' - \frac{p_c' p_{\perp h}'}{B^2} \right] < \left[ \oint d\ell \left( \frac{N_h}{B} \right)' \right]^2, \quad (14)$$

where we assumed  $p_c \ll p_{\perp h}$  and  $|kB/B'| \ll 1$ . The term linear in  $\omega$  in Eq. (13) represents non-adiabatic behavior of the hot electrons; that is,  $\omega$  is not small compared to the magnetic drift frequency, and the hot electrons do not respond instantaneously to changes in the magnetic flux through their drift orbits. The significance of Eq. (14) is that the modified mirror mode and the interchange mode can both be stable at low core pressures, when the ion cyclotron frequency is treated as large. This suggests that in this limit there is a parameter regime for stable bumpy torus operation.

If we solve Eq. (7) for  $C(\psi) = \tilde{B}_1(\partial B/\partial \psi)^{-1}$  in terms of  $X = X(\psi)$  and use the result (with  $\omega$  set equal to zero) in Eq. (8), we obtain a dispersion relation in the high  $m$  limit for the low-frequency flute interchange mode

$$\rho_i \omega^2 \oint \frac{d\ell}{B^3} + p_c' \oint \frac{d\ell}{B} \left( k + \frac{B'}{B} \right) - \frac{\left[ \oint \frac{d\ell}{B^3} p_c' p_{\perp h}' \right]^2}{\left[ \oint \frac{d\ell}{B^3} p_c' p_{\perp h}' - \oint \frac{d\ell}{B} k (p_{\parallel h} + p_{\perp h}') \right]} = 0 \quad (15)$$

This yields the same upper limit, (1), on the core pressure for interchange stability as was obtained from the energy principle treatment.

## V. Radial Eigenmodes

That the radial mode structure should be important in a bumpy torus is suggested by the following rough plausibility argument. The azimuthal mode number should not actually be infinite, as in the axial analysis of the previous section, because of the presence of finite Larmor radius effects. Also, bumpy torus stability is mainly determined by what happens within the ring region, which is somewhat narrow. Thus, if we suppose a mode could be localized within this region, we may estimate its radial wavenumber to be  $k_r \approx \pi/\Delta$ . Comparing this with the azimuthal wavenumber  $k_\theta = m/a$ , where

$a \approx (5-10)\Delta$  is the radial ring location, we see that the mode is dominated by its radial variation even for sizeable mode numbers ( $m < 15-30$ , approximately).

We can isolate the exact radial problem by considering the bumpless limit, i.e., no equilibrium variation along the magnetic field lines.

However, because the magnetic field curvature is important [cf. the beta limit of Eq. (1)], we prefer that it enter naturally and not through an artificial gravity. The simplest model of a bumpless, axisymmetric device with natural curvature is the z-pinch. We will adopt this model in order to pursue the purely radial problem.

The geometry for the z-pinch model is cylindrical, with coordinates  $(r, \phi, z)$ . The system is periodic in the z-direction with length  $2\pi L$ . The magnetic field lines  $\underline{B}_0 = B(r)\hat{\phi}$  lie on nested concentric cylindrical shells, which we associate with the flux (or mod-B) surfaces. Also, the coordinates  $r, \phi,$  and  $z$  correspond to the flux coordinate  $\psi$ , the longitudinal coordinate  $x$ , and the azimuthal angle  $\theta$ , respectively, of a bumpy system. Finally, the hot electron pressure is localized radially about a radius  $r_0$ , whose value we choose so as to be equal to the effective radius of curvature,  $R_c$ , of a bumpy system. Since there is no equilibrium variation along  $\underline{B}$ , we will consider the case of flute modes.

The general geometry theory of Sec. III can be readily transformed to the z-pinch geometry by means of the relationships  $\underline{\nabla}\psi = \hat{r}BL$ ,  $\underline{\nabla}\theta = -\hat{z}/L$ ,  $\underline{\nabla}x = \hat{\phi}/r$ ,  $\mathcal{A} = r/B$ ,  $\chi = LB\xi_r$ ,  $\partial/\partial\psi = (LB)^{-1} \partial/\partial r$ , and  $k = -(LBr)^{-1}$ . The result is that we can combine Eqs. (7) and (8) to obtain the following radial eigenmode equation:

$$\frac{1}{r} \frac{d}{dr} \left[ \frac{\alpha r B^2 \tau}{\alpha - \tau} \left( \frac{d\xi_r}{dr} \right) \right] + \xi_r \left\{ \rho \omega^2 \left( \frac{\alpha}{\alpha - \tau} \right) - \rho \lambda \left( \frac{\tau}{\alpha - \tau} \right) - \frac{1}{R} \frac{d}{dr} (p_{\parallel} + p_{\perp}) - \frac{B^2 R}{r^2} \right. \\ \left. - \left( \frac{2\alpha B^2 S}{r} \right) \left( \frac{k_z \omega}{\Omega} \right) \left( \frac{1}{\alpha - \tau} \right) - \frac{(BS/r)^2}{\alpha - \tau} - \frac{1}{r} \frac{\partial}{\partial r} \left[ \frac{\alpha r B^2}{\alpha - \tau} \left( \frac{S}{r} + \frac{k_z \omega \tau}{\Omega} \right) \right] \right\} = 0 \quad (16)$$

In Eq. (16), we have used the notation  $\alpha = \lambda/k_z^2 v_A^2$ , where  $k_z = m/L$  corresponds to the azimuthal wavenumber of a bumpy system,  $v_A = B^2/\sqrt{\rho_i}$  is the Alfvén speed, and  $\lambda = \omega^2 \omega_{ci}^2 / (\omega_{ci}^2 - \omega^2)$  was introduced earlier, with  $\omega_{ci}$  the ion gyrofrequency. Also, we have defined three kinetic integrals:

$$T = 1 + \frac{1}{B} \frac{\partial P_{\perp}}{\partial B} - \int \frac{d\epsilon d\mu B}{v_{\parallel} \Omega} \left[ \omega \frac{\partial f}{\partial \epsilon} + \left( \frac{ck_z}{qB} \right) \frac{\partial f}{\partial r} \right] \mu^2, \quad (17)$$

$$S = \sigma + \int \frac{d\epsilon d\mu B}{v_{\parallel} \Omega} \left[ \omega \frac{\partial f}{\partial \epsilon} + \left( \frac{ck_z}{qB} \right) \frac{\partial f}{\partial r} \right] \frac{\mu v_{\parallel}^2}{B}, \quad (18)$$

$$R = \sigma - \int \frac{d\epsilon d\mu B}{v_{\parallel} \Omega} \left[ \omega \frac{\partial f}{\partial \epsilon} + \left( \frac{ck_z}{qB} \right) \frac{\partial f}{\partial r} \right] \frac{v_{\parallel}^4}{B^2}, \quad (19)$$

where

$$\Omega = \omega - \frac{k_z}{q} \left( \frac{\mu}{B} \frac{dB}{dr} - v_{\parallel}^2/r \right),$$

the velocity integrals are understood to include a sum over species.

These kinetic integrals have been evaluated in two ways.

One is to use the  $\Delta_B/R_C \ll 1$  approximation discussed earlier, for which we find

$$T \sim -\frac{\Delta_B}{R_C} \left[ 1 \left( -\frac{dp_{\parallel h}/dr}{B \frac{dB/dr}} \right) - \frac{\omega}{\omega_B} + \left( \beta_c - \frac{dp_c/dr}{B \frac{dB/dr}} \right) \right], \quad (20)$$

for example. The integrals  $S$  and  $R$  can be evaluated similarly. The quantity

$$\omega_B = ck_z \left( \frac{dB}{dr} \right)^2 / qB^2 \frac{d}{dr} \left( \frac{N_h}{B} \right)$$

is then a characteristic grad-B drift frequency for the hot electrons.

Another approach is to use a delta-function distribution for the hot

electrons:  $f_h = (p_{\perp h}/\mu_0 B^2) \delta(\mu - \mu_0) \delta(v_{\parallel})$ , in the extreme anisotropic limit, normalized to yield the equilibrium transverse pressure. With this approach, one obtains

$$T = \frac{\omega(1 + \beta_{\perp}) - \omega_{cv\perp} \left(1 + r \frac{d}{dr} (p_c/B^2)\right)}{\omega - \omega_{DB}} \quad (21)$$

where

$$\omega_{DB} = \frac{k\mu}{eB} \frac{dB}{dr}, \quad \omega_{cv} = -\frac{k\mu}{er}$$

and so forth.

Numerical solutions of the differential equation (16) are reported in the companion paper by Spong<sup>11</sup> and in forthcoming publications. By means of analytical considerations, however, it is possible to glean certain information about the radial modes.

Two general categories of modes emerge when we analyze the radial equation (16). The first category is that of modes with radial wavelength larger than the annulus width. To treat this type, we integrate Eq. (16) across the ring layer, the mode being nearly constant over the annulus region and then connecting to an evanescent solution outside. One such mode arises from a denominator singularity and is described by  $\omega^2 \omega_{ci}^2 (\omega_{ci}^2 - \omega^2)^{-1} = (k_z v_A)^2 T(\omega)$ . This is similar to the electromagnetic mirror mode discussed earlier, although it experiences strong gyrofrequency effects. This mode is stabilized when  $(k_z v_A)^2 (\Delta_B/R_C) > \omega_{ci}^2$ , but it leads to a rather serious instability when the gyrofrequency  $\omega_{ci}$  and the hot electron characteristic curvature drift frequency,  $\omega_{cv\perp}$  are close in value, which occurs in current bumpy torus experiments.

Another such long wavelength mode is the interchange mode driven by the gradient of the core pressure only. This is again seen to be stable for  $\beta_c < 2(\Delta R_c)$  and unstable above.

The second category is that of short wavelength modes. For these, we may use a WKB approach and replace the radial derivative on the perturbation by an effective wavenumber  $k_r$ , where it is assumed that  $k_r \Delta > 1$ . In fact, for a linear density gradient, Eq. (16) can be approximately solved in terms of Bessel functions, from which we estimate  $k_r \approx 2n/\Delta$  ( $n = 1, 2, 3, \dots$ ) for the modes that can fit within the ring layer. The WKB procedure yields a fourth-order dispersion relation in the frequency if we use the small  $\Delta_B/R_c$  expression for the kinetic integral  $T$  (fifth order if we use the  $\delta$ -function expression). The explicit form of the dispersion relation is given in Ref. 11. One of the modes is low frequency and corresponds to the core plasma interchange. As before, it imposes an upper limit on the core pressure for interchange stability. Specifically, it is unstable if

$$\beta_c \left( \frac{R_c}{2\Delta} \right) > 1 - \frac{(k_\perp r_h)^2/4}{\Delta_B/R_c} > 0 \quad . \quad (22)$$

Eq. (22) includes the effect of finite Larmor radius,  $r_h$ , for the hot electrons.

The other modes described by the local dispersion relation are higher frequency. These modes are manifestations of the mirror-like instability and the hot electron interchange. We find that the stability condition for the former mode is given by

$$\frac{\omega_{pi}^2}{\omega_{ci}^2} < \frac{c^2 \Delta_B k_\perp^2}{4 v_{cvi}^2 R_c k_z^2} \left( 1 - \alpha \frac{v_{cvi} k^2}{\omega_{ci} \Delta k_\perp^2} \right)^2 \quad (23)$$

where  $\alpha = 1 - R_c \rho_c / \Delta B^2$  and  $k_I^2 = k_z^2 + k_r^2$ . This mode limits the density of the background plasma. For sufficiently large  $\omega_{ci}$ , this density limit is quite tolerable for EBT operation. However, when

$$\frac{v_{cvi}}{\omega_{ci} \Delta} \frac{k_z^2}{k_I^2} \sim 1,$$

the background density threshold dips to zero. This condition for instability is readily met in current experiment and thus there is an apparent contradiction with experimental observation and this theory. However, a more careful evaluation of the eigenmode is needed in this parameter regime. In addition finite electron Larmor radius effects are stabilizing when  $(k_I r_h)^2 > \Delta B_0 / R_c$ .

The condition for stabilizing the hot electron interchange mode is found to be,

$$\frac{\omega_{pi}^2}{\omega_{ci}^2} > \frac{2c^2}{\alpha^2 v_{cvi}^2} \frac{\left( 1 + \alpha \frac{v_{cvi} k_z^2}{\omega_{ci} \Delta k_I^2} \beta_h \right)}{k_I^2 R_c \Delta} \quad (24)$$

For  $\omega_{ci}$  sufficiently large we see that Eqs. (23) and (24) tend to have a stability window of operation if  $\rho_c R_c / \Delta < 1$ . However, for finite  $\omega_{ci}$ , the stability window disappears for special values of  $k_z^2 / k_I^2$ . The accompanying article exhibits various stability plots for parameters associated with typical operation of EBT-S/P devices.

## VI. Summary

A new kinetic energy principle that was developed to study low frequency modes in bumpy tori is pessimistic, since it predicts a new mirror-type instability below the core pressure threshold for interchange stability. However, the energy principle approach does not include several effects, e.g., hot electron non-adiabatic behavior, that are important for stability and is not strictly necessary for stability.

Linearized equations for normal modes in an axisymmetric configuration were developed. Small Larmor radius effects can be included. This two-dimensional problem was decomposed into two one-dimensional problems first by considering only the axial mode structure in the high  $m$  limit and then by studying radial effects exactly in the z-pinch model.

An analysis of the radial eigenmode equations indicates the existence of a parameter regime for stable bumpy torus operation if certain resonance regions in parameter space are ignored. The present-day EBT-I/S devices typically operate within this stability window, and scaling up to the proposed EBT-P device appears possible.

We still find conditions where instability persists. For example, the long-radial-wavelength denominator mirror-type mode seems to pose stability difficulties when its frequency, which is approximately the hot electron curvature drift (evaluated at a characteristic transverse temperature), is near the ion cyclotron frequency in value. Likewise, the WKB mirror-like mode has stability difficulties if  $v_{CVI} k_z^2 / \omega_{ci} \Delta k_{\perp}^2 \approx 1$ . However, our theory probably needs to account for the axial variation of the magnetic field in order to handle this point properly. We are also working on incorporating full Larmor radius effects.

### Acknowledgments

Informative discussions with C. L. Hedrick and other members of the Oak Ridge National Laboratory EBT Theory and Experimental Groups are gratefully acknowledged. We also had valuable suggestions from Y. C. Lee, who initially pointed out the important stability condition of Eq. (14), and conversations with A. M. El-Nadi.

This research was supported by the U. S. Department of Energy under Contract No. DE-FG-80-ET-53088 with the University of Texas and under Contract No. W-7405-ENG 26 with the Union Carbide Corporation.

### References

1. N. A. Krall, *Phys. Fluids* 9, 820 (1966).
2. R. R. Dominguez and H. L. Berk, *Phys. Fluids* 21, 827 (1978).
3. D. B. Nelson and C. L. Hedrick, *Nucl. Fusion* 19, 283 (1979).
4. J. W. Van Dam and Y. C. Lee, in EBT Ring Physics (Proc. of the Workshop, Oak Ridge, Dec. 1979), Oak Ridge National Laboratory CONF-791228 (1980), p. 471.
5. D. B. Nelson, *Phys. Fluids* 23, 1850 (1980).
6. J. W. Van Dam, M. N. Rosenbluth, and Y. C. Lee, submitted to *Phys. Fluids*.
7. D. A. Spong and A. M. El-Nadi, *Bull. Am. Phys. Soc.* 25, 964 (1980).
8. H. L. Berk, M. N. Rosenbluth, J. W. Van Dam, in Proc. of U.S.-Japan Workshop on "The Theory of Non-Axisymmetric Confinement Systems," Dec. 1980, Institute for Fusion Studies Report, University of Texas, Austin.
9. M. N. Rosenbluth, to be published in *Phys. Rev. Lett.*
10. T. M. Antonsen, B. Lane, and J. J. Ramos, submitted to *Phys. Fluids*.
11. D. A. Spong, H. L. Berk, J. W. Van Dam, and M. N. Rosenbluth, in this Proceedings.

NUMERICAL SOLUTIONS OF THE EBT  
RADIAL EIGENMODE PROBLEM\*

D. A. Spong  
Oak Ridge National Laboratory  
Oak Ridge, Tennessee 37830

J. W. Van Dam, H. L. Berk, M. N. Rosenbluth  
Institute for Fusion Studies  
University of Texas  
Austin, Texas 78712

ABSTRACT

The radial structure of eigenmodes in EBT is of interest since both modes which are localized within the annulus and modes which extend into the core plasma have been predicted to be unstable within appropriate parameter regimes. Radially resolved calculations have been done for a z-pinch model which corresponds to a bumpless, azimuthally symmetric version of EBT. A shooting method is employed which solves two-point boundary value problems on the inside and outside of the ring and which matches derivatives at the center. Comparison of these results with those of a localized dispersion relation will be discussed.

---

\*Research sponsored by the Office of Fusion Energy, U.S. Department of Energy, under contract W-7405-eng-26 with the Union Carbide Corporation.

## I. Introduction

Recent calculations have indicated the important role of ring-core coupling effects on EBT stability. Since the hot electron rings are radially localized to regions of the electron cyclotron resonances, it is of interest to examine how modes which are driven by the presence of both hot and cold plasma components connect to the inner core plasma and outer surface plasma regions. To address such questions, a radially resolved eigenmode calculation is required. Eventually, more multidimensional models may be necessary to treat the variations of quantities along the field lines as well; however, it is desirable at this point to consider radial and axial variations separately. The formulation of such a radial problem in a  $\pi$ -pinch geometry (which allows a decoupling of the radial and axial problems) was discussed in the previous talk.<sup>1</sup> In the present paper, we shall discuss methods and results of numerical solutions of the resulting radial eigenmode problem and their comparison with localized solutions.

## II. Basic Equations

Using the momentum balance equation for core plasma and hot electron ring components, supplemented by the drift kinetic equation for perturbed ring pressures, the following radial eigenmode equation has been derived:

$$-\frac{v_A^2}{rB^2} \frac{d}{dr} \left[ \frac{\lambda r B^2 T}{v_A^2 (T - \alpha)} \frac{\partial \xi}{\partial r} \right] - \xi \left\{ \frac{\omega^2 \lambda}{v_A^2 (T - \alpha)} - k^2 \lambda \frac{T}{T - \alpha} \right\}$$

$$\begin{aligned}
& - \frac{2\lambda k\omega_S}{r\Omega(T - \alpha)} - \frac{v_A^2}{B^2 r} \frac{\partial}{\partial r} \left[ \frac{\lambda B^2 r}{v_A^2(T - \alpha)} \left( \frac{S}{r} + \frac{k\omega T}{\Omega} \right) \right] \\
& + k^2 v_A^2 \left[ \frac{1}{rB^2} \frac{d}{dr} (p_{\parallel} + p_{\perp}) + \frac{R}{r^2} - \frac{S^2}{r^2(T - \alpha)} \right] \Big\} = 0
\end{aligned} \tag{1}$$

where  $k$  = azimuthal wave number

$$\lambda = \frac{\omega^2 \Omega^2}{\Omega^2 - \omega^2}$$

$$\Omega = \omega_{ci}$$

$$\alpha = \frac{\lambda}{k^2 v_A^2}$$

$$\xi = \frac{i(\mathbf{E} \times \mathbf{B})}{\omega B^2}$$

In deriving this equation, a transformation from a bumpy cylinder to a z-pinch geometry has been made and variations of quantities along field lines have been neglected. The quantities  $T$ ,  $S$ , and  $R$  are kinetic integrals given by:

$$T = \tau - \int \frac{B d\mu d\epsilon}{v_{\parallel}} \frac{(\omega \frac{\partial f}{\partial \epsilon} + m \frac{\partial f}{\partial \psi})}{\omega - \omega_d} \mu^2 \tag{2}$$

$$S = \sigma + \frac{1}{B} \int \frac{B d\mu d\epsilon}{v_{\parallel}} \frac{(\omega \frac{\partial f}{\partial \epsilon} + m \frac{\partial f}{\partial \psi})}{\omega v - \omega_d} \mu v_{\parallel}^2 \tag{3}$$

$$R = \sigma - \frac{1}{B^2} \int \frac{B d\mu d\epsilon}{v_{\parallel}} \frac{(\omega \frac{\partial f}{\partial \epsilon} + m \frac{\partial f}{\partial \psi})}{\omega - \omega_d} v_{\parallel}^4 \tag{4}$$

where

$$\tau = 1 + \frac{1}{B} \frac{\partial p_{\perp}}{\partial B}$$

$$\sigma = 1 + \frac{p_{\perp} - p_{\parallel}}{B^2}$$

$$\omega_d = k \left( \mu \frac{dB}{dr} - \frac{v_{\parallel}^2}{R_c} \right)$$

A number of different models and approximations have been used in evaluating these integrals. For most of the calculations discussed in this paper, the hot electron thin annulus limit has been taken. This assumes that the ring electrons are sufficiently hot that  $\omega \ll \omega_{DB}$ ,  $\omega_{*H}$  and  $\Delta_B/R_c \ll 1$  where  $\Delta_B$  is the magnetic field gradient scale length in the ring region,  $R_c$  is the magnetic field line radius of curvature, and  $\omega_{DB}$  and  $\omega_{*H}$  are the hot electron gradient B drift and diamagnetic drift frequencies, respectively. In this limit the above integrals are not dependent on the details of the distribution function and may be written as follows:

$$T \approx - \frac{\Delta_B}{R_c} \left( 1 - \frac{dp_{\parallel,H}/dr}{BdB/dr} \right) - \frac{\omega}{\omega_{DB}} + \beta_{\perp c} - \frac{dp_{\perp c}/dr}{BdB/dr} \quad (5)$$

$$S \approx 1 - \frac{dp_{\parallel,H}/dr}{BdB/dr} - \frac{1}{2} \beta_{\parallel c} \quad (6)$$

$$R \approx 1 + \frac{1}{2} (\beta_{\perp H} - \beta_{\parallel H} + \beta_{\perp c} + 2\beta_{\parallel c}) \quad (7)$$

Since  $\Delta_B/R_c$  is of  $O(1/4$  to  $1/3)$  in EBT experiments and  $\omega$  is not necessarily small compared to  $\omega_{dH}$  for some of the high frequency modes of interest, the kinetic integrals have also been evaluated for models of the hot electron distribution function where it is not necessary to make these approximations. One such model is a delta function in  $\mu$  and  $v_{\parallel}$ :

$$f_{\text{Hot}} = \frac{P_1}{\mu_0 B^2} \delta(\mu - \mu_0) \delta(v_{\parallel}) \quad (8)$$

In this case, the integrals are:

$$T = \frac{\omega(1 + \beta) - \omega_{K1} [1 - (R_c/\Delta)(P_c/B^2)(1 + 2\Delta/\Delta_B)]}{\omega - \omega_{DB}} \quad (9)$$

$$S = 1 + O(\beta_c) \quad (10)$$

$$R = \sigma = 1 + \frac{1}{2}\beta_H + O(\beta_c) \quad (11)$$

where

$$\omega_{K1} = \frac{(\gamma^2 - 1)c^2 k_{\theta}}{2\gamma R_c \omega_{ce}}$$

$$\Delta = -\left(\frac{1}{P_c} \frac{dP_c}{dr}\right)^{-1}$$

It is also relatively simple to evaluate these integrals for the case of Maxwellian times a delta function in  $v_{\parallel}$ . In this case they may be

expressed in terms of exponential integrals. As mentioned above, the results given in this paper are based on the approximations of T, S, R given in Eqs. (5)-(7). Work is presently underway to use better approximations for these integrals.

### III. Localized Model

Before discussing the radially dependent calculations, results of a calculation localized to the ring region will be mentioned. The radially dependent calculations will then be compared against certain of these results.

A local dispersion relation may be obtained from Eq. (1) by assuming the existence of an evanescent eigenmode, localized to the annulus region:

$$\xi(r) = \begin{cases} \cos(Qr') & \text{inside the layer} \\ \exp(-kr') & \text{outside the layer} \end{cases} \quad (12)$$

where  $r' = r - r_0$ .

Neglecting gradients which act on equilibrium quantities, the radial differential equation becomes

$$Q^2 + k^2 = \frac{(T - \alpha)}{\lambda T} \left\{ \frac{\omega^2 \lambda}{v_A^2 (T - \alpha)} - \frac{2\lambda k \omega s}{r \Omega (T - \alpha)} \right\} + \frac{k^2 v_A^2}{R_c} \left[ \frac{1}{B^2} \frac{d}{dr} (p_{\parallel} + p_{\perp}) + \frac{R}{R_c} - \frac{S^2}{R_c (T - \alpha)} \right] \quad (13)$$

Expanding this equation and collecting terms results in a cubic if we assume  $\beta_c \ll \Delta/R_c$  (we shall investigate stability for a background beta below the Lee-Van Dam limit where near term experiments operate).

$$\frac{v_{DB}^2}{v_A^2} \left( 1 + \frac{v_A^2}{|\Omega \Delta v_{DB}|} \right) t^3 - \left( \frac{k_{\perp}^2}{k_{\theta}^2} + \left| \frac{v_{DB} \Delta_B}{\Omega \Delta R_c} \right| \right) t^2 + \frac{k_{\perp}^2 \Delta_B}{k_{\theta}^2 R_c} t + \frac{v_A^2}{k_{\theta}^2 v_{DB}^2 R_c \Delta_B} = 0 \quad (14)$$

where  $t = \omega/kv_{DB}$ .

The expansion parameters for the validity of Eq. (14) are:  $\Delta_B/R_c$ ,  $\beta_c R_c/\Delta$ ,  $\beta_H \ll 1$ .

To analyze Eq. (14) for stability, first neglect the last term (valid procedure if  $v_A$  is sufficiently small) and we obtain a dispersion relation for the compressional Alfvén mode for which the marginal stability condition is found to be:

$$\frac{v_A^2}{v_{cv}^2} > \frac{4 \left( \frac{k_{\theta}}{k_{\perp}} \right)^2 \frac{R_c}{\Delta_B}}{\left( 1 - \frac{k_{\theta}^2}{k_{\perp}^2} \left| \frac{v_{cv}}{\omega_{ci} \Delta} \right| \right)} \quad (15)$$

where  $v_{cv} = v_{DB} \Delta_B / R_c$ .

If we assume  $v_A$  is sufficiently large, then the first term in Eq. (14) may be neglected and the resulting quadratic equation yields the marginal stability condition for the hot electron interchange mode:

$$\frac{V_A^2}{V_{CV}^2} < \frac{k_{\perp}^2 \Delta R_C}{2\beta_H \left(1 + \left| \frac{V_{CV}}{\omega_{ci} \Delta} \right| \frac{k_{\theta}^2}{k_{\perp}^2} \right)} \quad (16)$$

A stability window then exists if we can satisfy the condition,

$$\frac{k_{\perp}^2 R_C \Delta}{2\beta_H \left(1 + \left| \frac{V_{CV}}{\Delta \omega_{ci}} \right| \frac{k_{\theta}^2}{k_{\perp}^2} \right)} > \frac{V_A^2}{V_{CV}^2} > \frac{4 \frac{R_C}{\Delta B} \frac{k_{\theta}^2}{k_{\perp}^2}}{\left(1 - \frac{k_{\theta}^2}{k_{\perp}^2} \left| \frac{V_{CV}}{\omega_{ci} \Delta} \right| \right)^2} \quad (17)$$

If  $V_{CV}/\omega_{ci} \Delta \ll 1$ , a stability window can be readily found. However, if  $V_{CV}/\omega_{ci} \Delta > 1$ , one can find values of  $k_{\theta}/k_{\perp}$  where there is no stability window. In current experiments  $V_{CV}/\omega_{ci} \Delta \approx 5-10$ , hence there appears to be disagreement with the experimentally observed stable operation. The window disappears for a relatively narrow parameter range, and more careful calculations with more realistic geometry are needed to restore a theoretical stability window. In addition to these analytic estimates of the stability boundaries, numerical solutions of the cubic Eq. (14) have also been performed. Typical results of such calculations are indicated in Figs. 1 and 2 where stability boundaries in  $n_{CORE}/n_{HOT}$  vs  $\beta_{hot}$  are plotted for mode numbers  $m = 1, 2, 3, 4$  for EBT-S and EBT-P. There is a substantially wider window of stability present at high  $m$  numbers for EBT-P than for EBT-S due to the larger values of  $R_C$  and the magnetic field.

## EBT-S STABILITY BOUNDARIES

ORNL-DWG 81-3145 FED

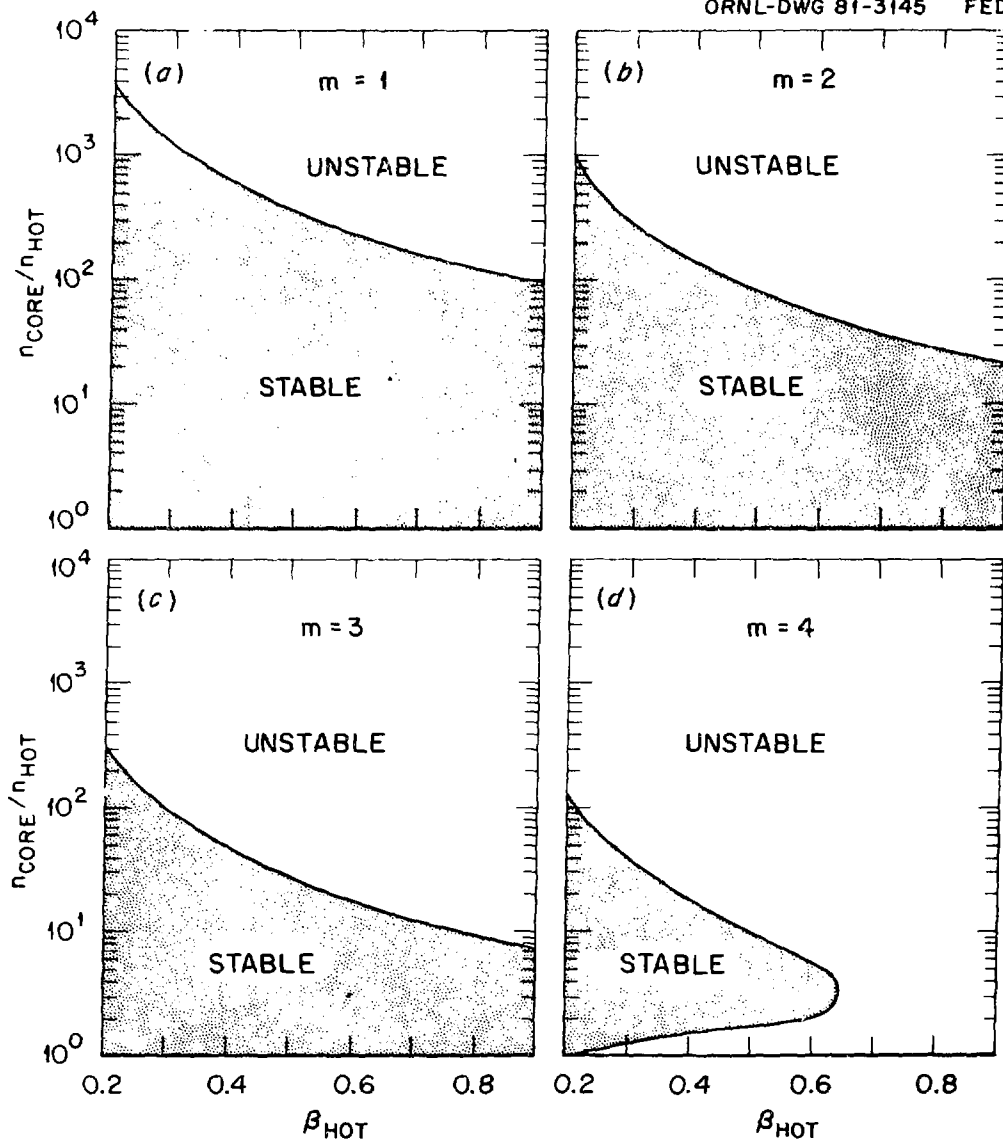


Fig. 1 EBT-S stability boundaries as predicted by the cubic equation (14) for  $m = 1, 2, 3, 4$  ( $B_{\text{ring}} = 4.5$  kG, plasma radius = 10 cm, ring width = 1 cm, radius of curvature = 20 cm,  $\beta_{\text{core}} = 0.005$ ,  $E_{\text{ring}} = 500$  keV,  $k_T = 2/\Delta$ ).

## EBT-P STABILITY BOUNDARIES

ORNL-DWG 81-3146 FED

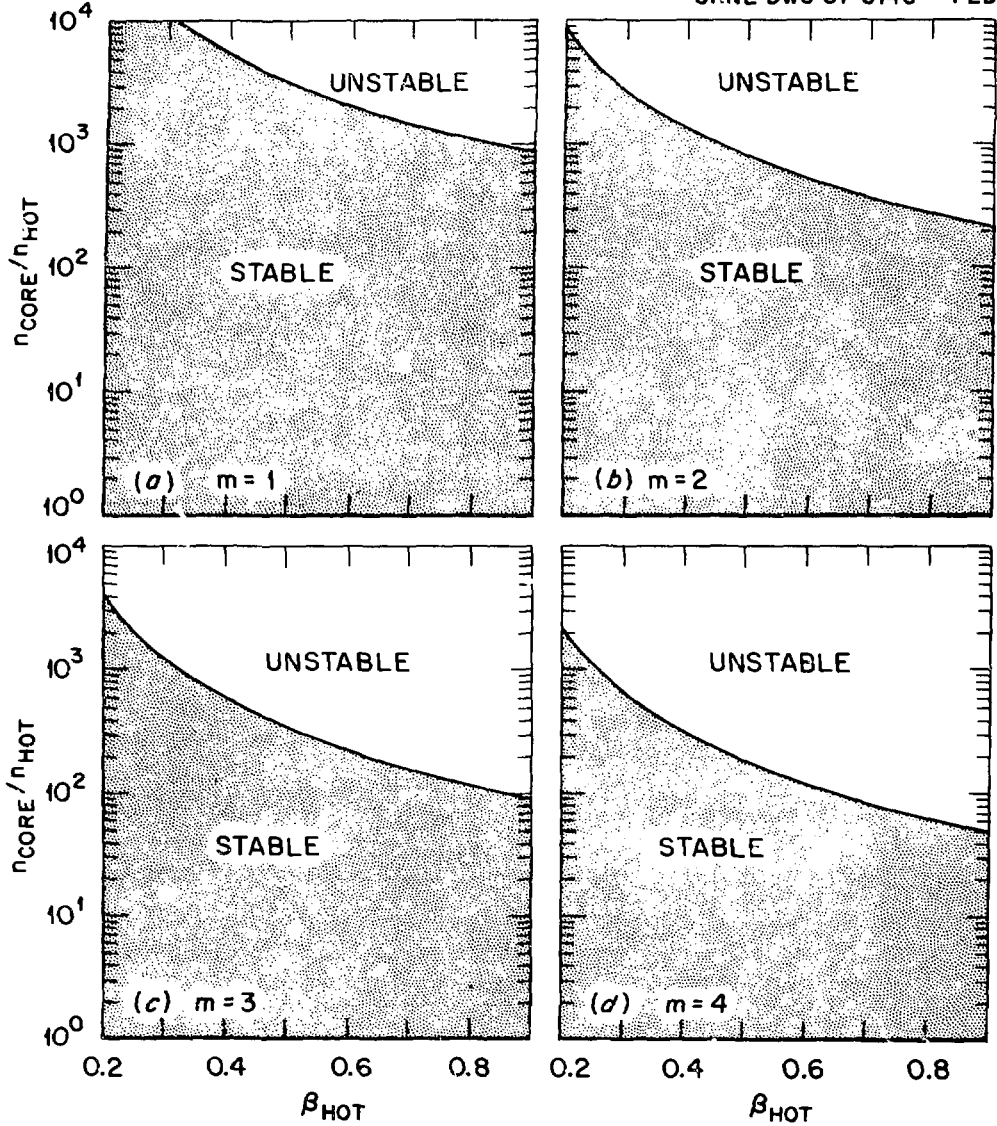


Fig. 2 EBT-P stability boundaries as predicted by the cubic equation (14) for  $m = 1, 2, 3, 4$  ( $B_{\text{ring}} = 11$  kG, plasma radius = 18 cm, ring width = 1.5 cm, radius of curvature = 26 cm,  $\beta_{\text{core}} = 0.2$ ,  $E_{\text{ring}} = 1$  MeV  $k_{\text{T}} = 2/\Delta$ ).

#### IV. Radially Dependent Calculations

In addition to the localized solutions of the radial eigenmode equation (1), numerical solutions have also been obtained which take into account the radial structure. In obtaining these results, assumptions have been made concerning the plasma and hot electron equilibrium profiles. These will be described below along with the numerical method used in solving the equations. Such calculations are still in a somewhat preliminary phase, as various plasma and hot electron models are under consideration, and those mentioned here may not turn out to be the most appropriate.

The core plasma density and temperature are expected to be relatively constant in the core region (within the hot electron ring) and drop off through the ring region. It is likely the maximum core gradients are localized to the outside of the ring (where magnetic field gradients are reversed); otherwise, the inside half of the ring could become unstable for core gradients above a certain level. Two typical sets of core density, temperature, and pressure profiles which exhibit these features are

$$\begin{aligned}
 n_c &= n_{co} \sqrt{\frac{1 - \tanh(x - a)}{2}} \\
 T_c &= T_{co} \sqrt{\frac{1 - \tanh(x - a)}{2}} \\
 p_c &= p_{co} \frac{1 - \tanh(x - a)}{2}
 \end{aligned} \tag{18}$$

(Profile I)

where 
$$x = \frac{r - r_0}{\Delta}$$

$r_0$  = annulus central radius

$\Delta$  = annulus half width

$a$  = a variable parameter usually taken to be 1

and

$$n_c = n_{co} \begin{cases} 1 & x < 0 \\ e^{-x^2} & x > 0 \end{cases}$$

$$T_c = \frac{n_c}{n_{co}} T_{co} \quad (19)$$

$$p_c = p_{co} \begin{cases} 1 & x < 0 \\ e^{-2x^2} & x > 0 \end{cases}$$

(Profile II)

In the following, results will be given for each of the above core plasma profile models. Both pressure profiles are plotted in Fig. 3(a). With the profile I model the core pressure extends somewhat outside the ring region whereas, with the profile II model the core pressure decays more rapidly outside the edge of the ring.

The ring density and temperature are localized on the outer edge of the core plasma, centered about a minor radius  $r = r_0$ . A Gaussian profile is typically assumed for the hot electron density and temperature as given below:

$$n_H = n_{H0} e^{-x^2}$$

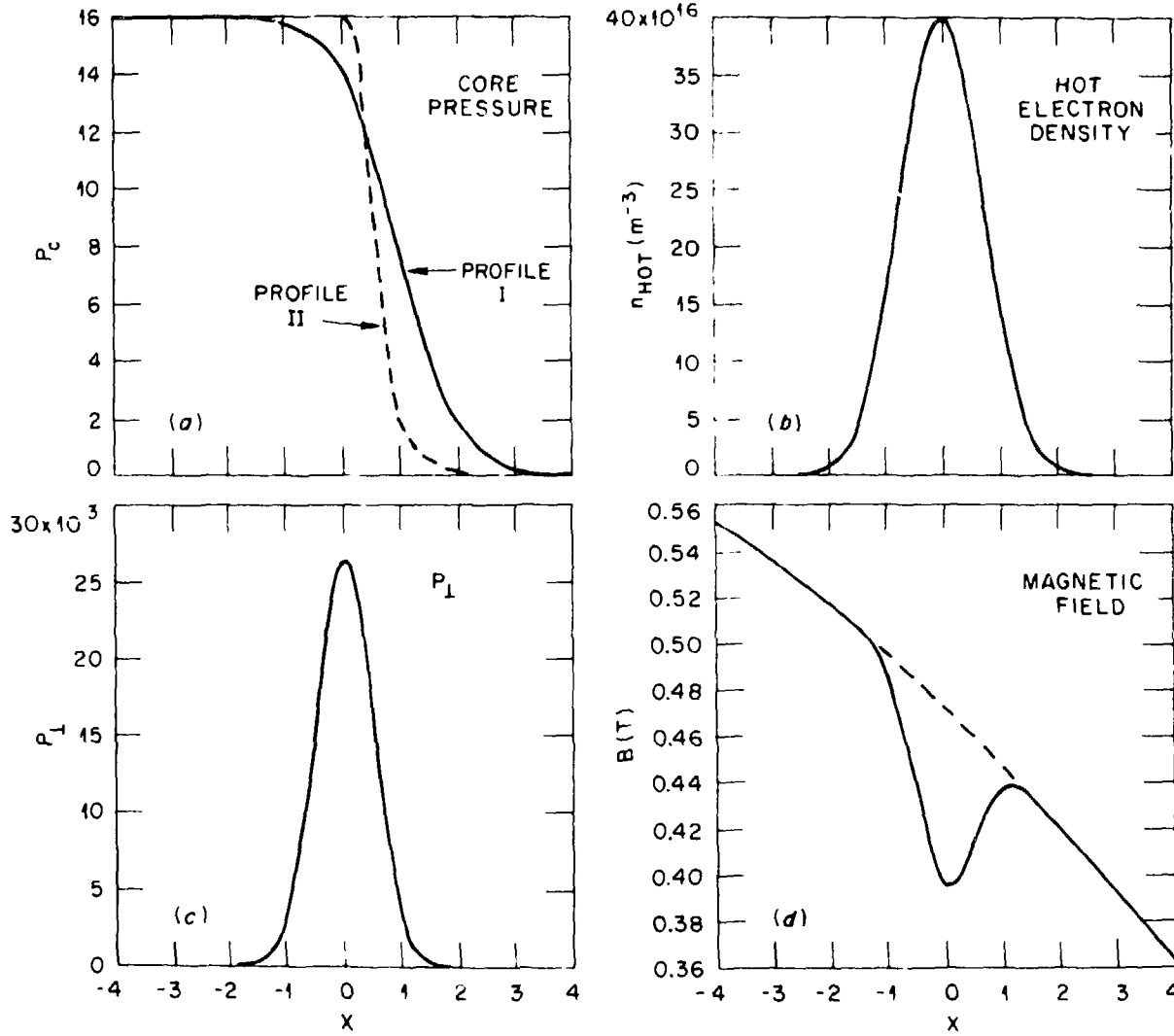


Fig. 3 Plasma pressure, hot electron density, hot electron pressure  $p_{\perp}$ , and magnetic field profile as a function of  $x = (r - r_0)/\Delta$ .

$$T_H = T_{HO} e^{-x^2} \quad (20)$$

$$P_H = P_{HO} e^{-2x^2}$$

Profiles of the hot electron density and temperature are shown in Figs. 3(b) and 3(c).

Since the stability properties of EBT are strongly influenced by the existence of a finite  $\beta$  depression of the magnetic field, it is important to use a self-consistent magnetic field equilibrium in these calculations. An approximate model has been employed here which assumes that the scale length for the variation of the field in the annulus region is separated from that for the variation in the vacuum field (i.e.,  $\Delta_B/R_C \ll 1$ ).

The finite beta magnetic field equilibrium is described by the momentum balance equation and Ampere's Law:

$$\vec{\nabla} \cdot \vec{P} = \vec{J} \times \vec{B}$$

$$\mu_0 \vec{J} = \vec{\nabla} \times \vec{B} \quad (21)$$

Combining these equations and taking the component perpendicular to the field lines results in

$$\vec{\nabla}_\perp \left( p_\perp + \frac{B^2}{2\mu_0} \right) = \left( p_\perp - p_\parallel + \frac{B^2}{\mu_0} \right) \vec{K} \quad (22)$$

where  $\vec{K} = (\hat{b} \cdot \vec{\nabla}) \hat{b} = \text{curvature}$ . If  $\Delta_B$  (finite beta gradient B scale length) is assumed to be small compared to  $R_C$  (the radius of curvature of the vacuum magnetic field), then the above equation reduces to

$$p_{\perp} + \frac{B^2}{2\mu_0} = \frac{B_{vac}^2}{2\mu_0} \quad (23)$$

where  $B_{vac}$  = vacuum magnetic field. For the present calculations  $B_{vac}$  has been taken as the vacuum magnetic field in a bumpy cylinder (such as given in Ref. 4, for example). Using this in Eq. (23) results in a B field profile such as plotted in Fig. 3(d). Here, the dashed line indicates the vacuum magnetic field and the solid line indicates the self-consistent finite beta field. More exact equilibrium models for the z-pinch model are under development and will be implemented into the code in the near future.

The numerical solution procedure used for solving Eq. (1) is based on the SUPORT<sup>5</sup> code. This solves linear two-point boundary value problems and uses the method of superposition coupled with orthonormalization of the basis solutions to the homogeneous equation when linear dependence threatens. It employs a variable-step integration scheme.

Equation (1) may be written in the form

$$\frac{1}{r} \frac{d}{dr} \left( rP \frac{d\xi}{dr} \right) - Q\xi = 0 \quad (24)$$

In order to use the SUPORT code, this is broken up into two coupled first-order equations:

$$\frac{dy_1}{dr} = (rP)^{-1} cy_2$$

(25)

$$\frac{dy_2}{dr} = rQy_1$$

where  $y_1 = \xi$  and  $y_2 = P \frac{d\xi}{dr}$ . This system of equations is then solved as two separate two-point boundary value problems on the intervals  $r_{\min} - r_0$  and  $r_0 - r_{\max}$ . The boundary conditions are

$$y_1(r_{\min}) = y_1(r_{\max}) = 0$$

and

$$y_1(r_0) = 1$$

The SUPORT code then returns values for the derivatives of  $y_1$  at  $r = r_0$ , and these are matched at the center of the hot electron ring:

$$D(\omega) = \left. \frac{dy_1}{dr} \right|_{r=r_0^+} - \left. \frac{dy_1}{dr} \right|_{r=r_0^-} = 0 \quad (26)$$

This condition determines the eigenvalue  $\omega$  which is normally solved for by using a Newton's method.

Some typical results of this calculation are shown in Figs. 4 and 5. Here, eigenfunctions are plotted vs radial position for profile model I (Fig. 4) and profile model II (Fig. 5). The plasma and ring parameters are indicated on the figures. As may be seen, both eigenfunctions are characterized by two nodes — one near the center of the ring and one somewhat outside the ring. The dip in the eigenfunction outside the ring region is expected to be related to the

RADIAL EIGENMODE (REAL PART)

$$T_{\text{HOT}} = 500 \text{ keV}, N_{\text{HOT}} = 4 \times 10^{17} \text{ m}^{-3}$$

$$N_{\text{CORE}} = 1 \times 10^{18} \text{ m}^{-3}, \text{RING WIDTH} = 0.01 \text{ m}$$

$$R_0 = 0.1 \text{ m}, B_0 = 0.6 \text{ T}, T_{\perp} / T_{\parallel} = 2$$

$$T_{\text{CORE}} = 100 \text{ eV}, \text{MODE No.} = 2, \omega / \omega_{\text{CI}} = 11.7, \\ 4.15 \times 10^{-7}$$

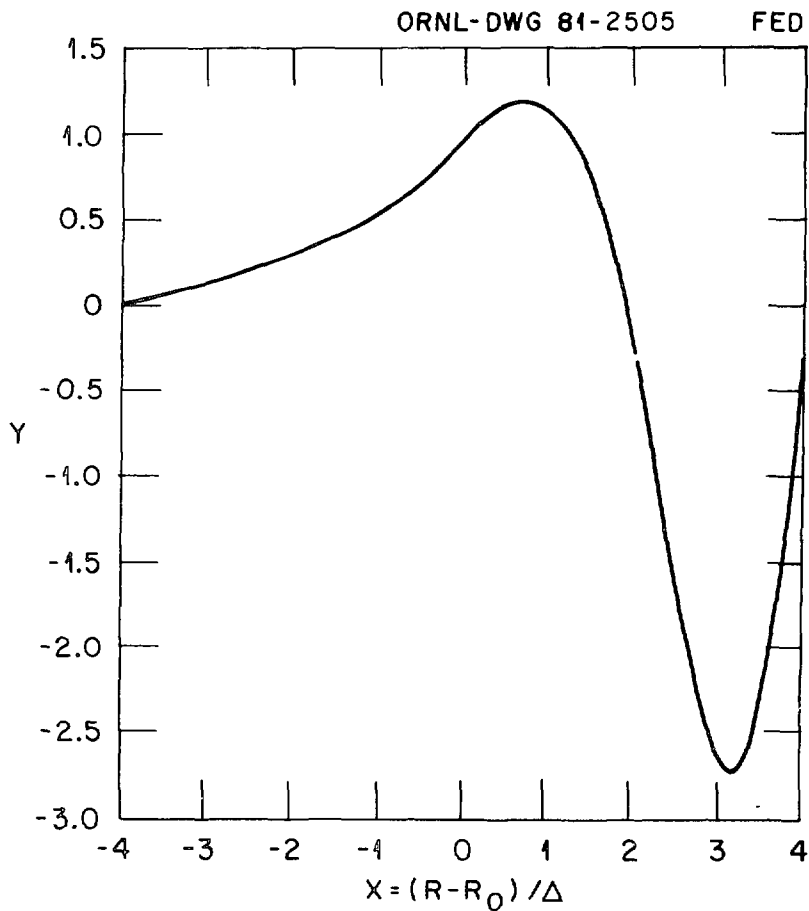


Fig. 4 Radial eigenmode as a function of  $x$  for profile I model.

## RADIAL EIGENMODE (REAL PART)

$$T_{\text{HOT}} = 500 \text{ keV}, N_{\text{HOT}} = 4 \times 10^{17} \text{ m}^{-3}$$

$$N_{\text{CORE}} = 4 \times 10^{18} \text{ m}^{-3}, \text{RING WIDTH} = 0.01 \text{ m}$$

$$R_0 = 0.4 \text{ m}, B_0 = 0.6 \text{ T}, T_{\perp} / T_{\parallel} = 5$$

$$T_{\text{CORE}} = 400 \text{ eV}, \text{MODE No.} = 2, \omega / \omega_{\text{CI}} = 9.5, \\ -3.22 \times 10^{-6}$$

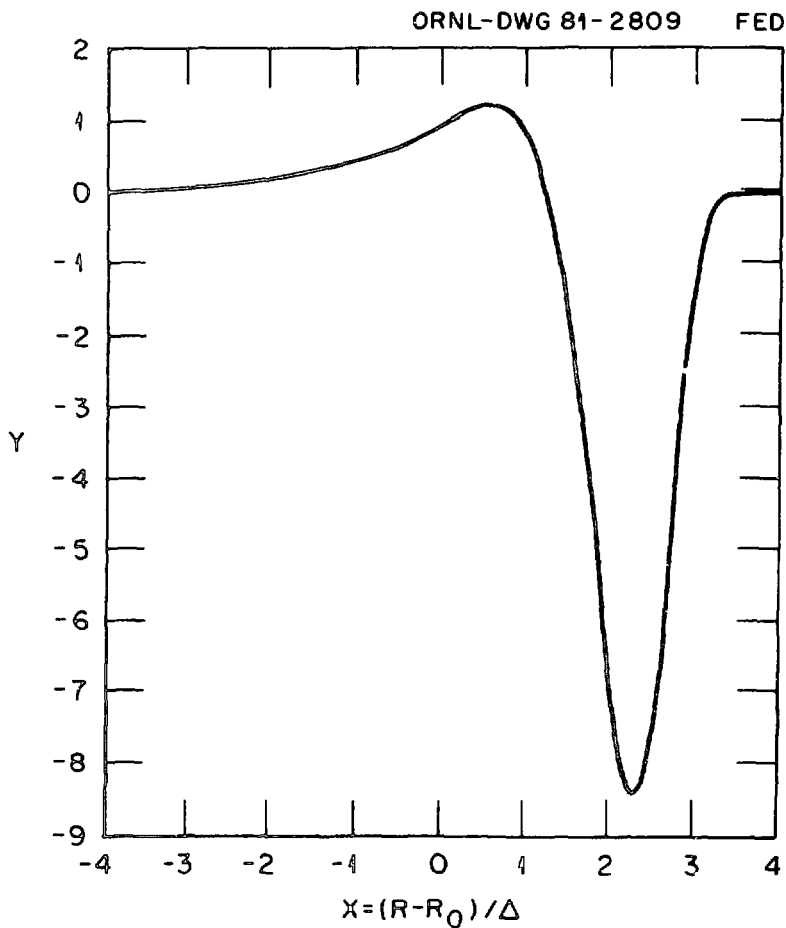


Fig. 5 Radial eigenmode as a function of  $x$  for profile II model.

fact that  $d(\ln n_c)/dr$  is finite outside the ring region for the profile models used here, even though  $n_c$  and  $dn_c/dr$  are both going separately to zero. This portion of the eigenfunction is not expected to be related to the coupled ring-core stability properties and work is presently underway to determine if it remains with profiles which have  $d(\ln n_c)/dr = 0$  outside the annulus region. The inner peak in the eigenfunction is located in the region where both annulus and core densities and temperatures are still finite and is close to the position where the maximum derivative in the core and ring pressures occur. The form of this peak is qualitatively what one would expect from analytic solutions of Eq. (1) using simplified (i.e., linear or constant) dependences in the plasma and ring profiles. As may be seen, the eigenfunction in Fig. 5 using the profile II model is somewhat better localized than that in Fig. 4 due to the steeper falloff on the outside of the core plasma parameters and the fact that these parameters have no gradients within  $r = r_0$ .

Stability boundaries have been studied using the radially dependent code by starting out at stable roots (i.e., as in Figs. 4 and 5) and varying an appropriate parameter, such as core density until the imaginary part of  $\omega$  begins to be significant. Such results are illustrated in Figs. 6, 7, and 8 where localized results [obtained from solving Eq. (14)] are compared with the nonlocal results for azimuthal mode numbers  $m = 1, 2, 3, 4$ , respectively. The localized theory used here would not be expected to be exactly comparable to the nonlocal calculation since it has not been evaluated at the position of the inside peak in the eigenfunction. In general, the nonlocal boundaries are more pessimistic than those of the localized theory.

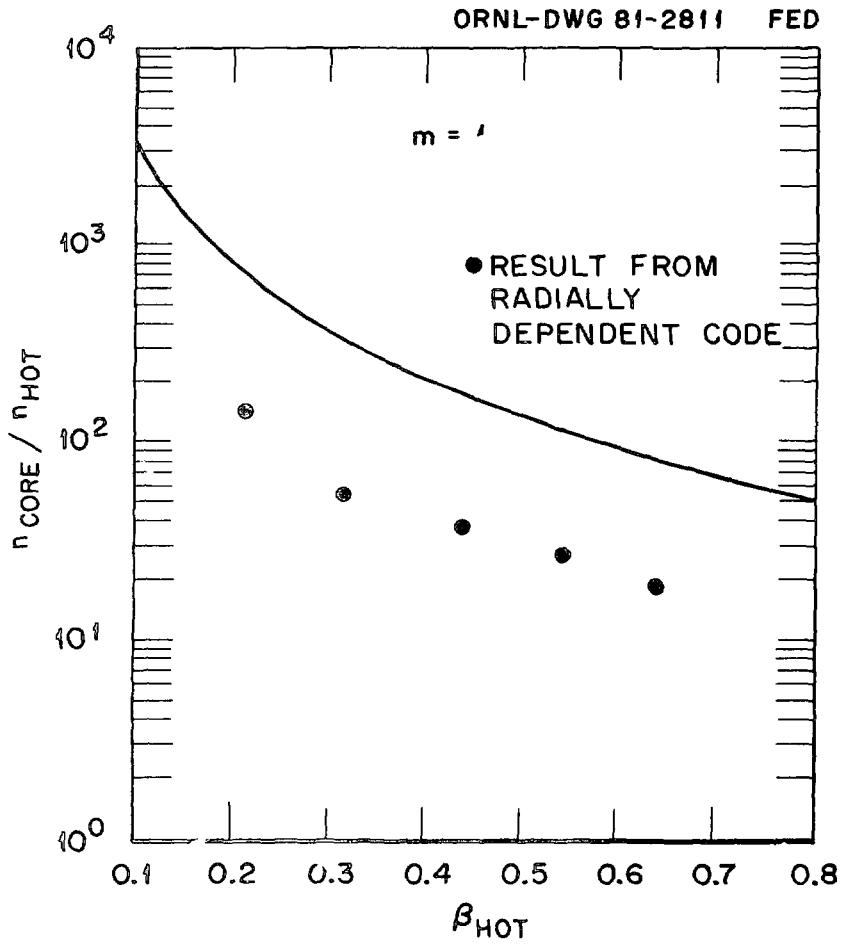


Fig. 6 Comparison of local and nonlocal stability boundaries for  $m = 1$ .

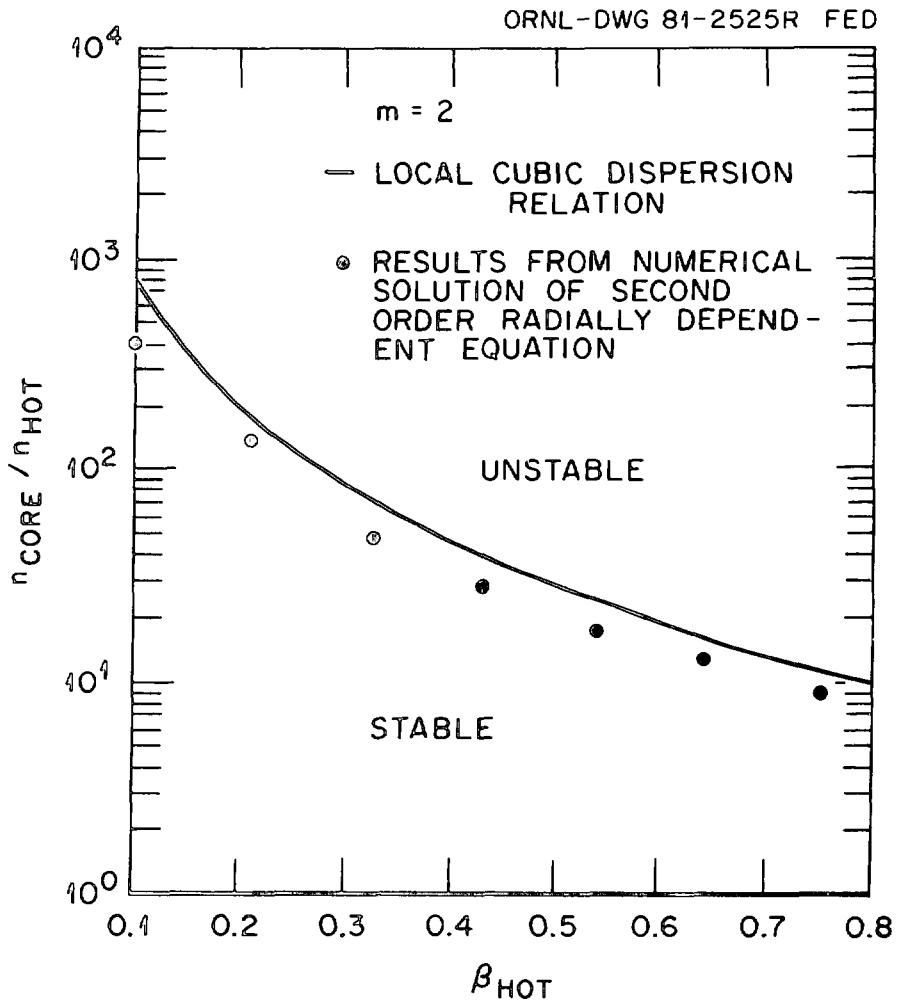


Fig. 7 Comparison of local and nonlocal stability boundaries for  $m = 2$ .

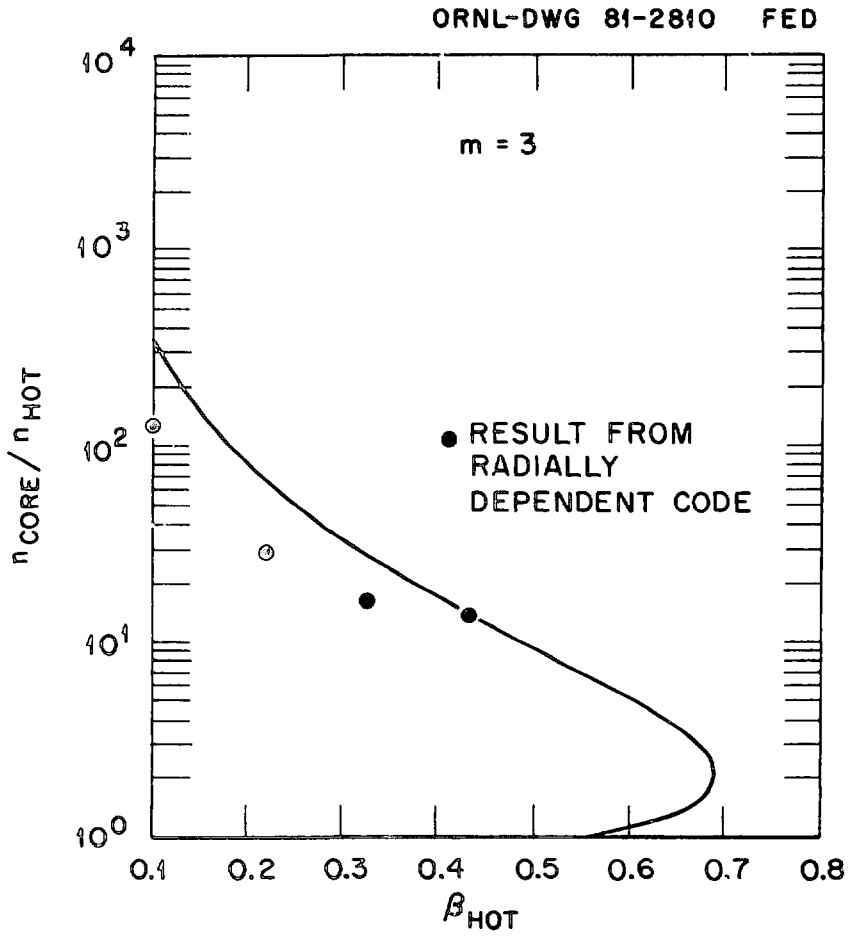


Fig. 8 Comparison of local and nonlocal stability boundaries for  $m = 3$ .

The results are within a factor of 3-5 of each other with the closest agreement being for  $m = 2$ . The points indicated here are for the upper density limit due to the compressional Alfvén wave-hot electron interaction. They are all obtained using the profile I model for the core plasma. The code has been used to check a few points on the lower density limit due to the hot electron interchange mode; the profile II model has also been used. These again indicate qualitative agreement with the localized theory, but more work needs to be done in this area. Also, the calculations presented here use the  $\Delta_B/R_C \ll 1$  approximation in evaluating the kinetic integrals [see Eqs. (5)-(7)]. Work is underway to incorporate more exact evaluations of these integrals into the code using the delta-function model of the hot electrons [Eqs. (9)-(10)] and, eventually, a Maxwellian.

## V. Conclusions

Results have been presented from both local and nonlocal EBT stability models which are based upon a radial eigenmode equation. The core plasma is considered as being cold with ion inertial effects included while the hot electron plasma is treated using the drift kinetic equation.

The local and nonlocal results show qualitatively similar trends for the upper stability boundary (related to coupling between the core Alfvén wave and the hot electrons) over the range of parameters which have been considered. As mentioned earlier, a wider range of parameters, profile shapes, and models for the hot electron distribution function are under examination. In addition, it will eventually be of interest to incorporate finite Larmor radius effects

into such calculations. This will lead to higher order differential equations, but these may be solved using similar techniques to those outlined here.

## ACKNOWLEDGMENTS

The authors would like to gratefully acknowledge assistance from John Whitson of the Computer Sciences Division at Oak Ridge National Laboratory in the use of the SUPORT code and the Newton's root solver.

The work of D. A. Spong was supported by the U.S. Department of Energy under Contract W-7405-eng 26 with the Union Carbide Corporation. The work of J. W. Van Dam, H. L. Berk, and M. N. Rosenbluth was supported by the U. S. Department of Energy under Contract No. DE-FG-80-ET-53088 with the University of Texas.

## REFERENCES

<sup>1</sup>J. W. Van Dam, H. L. Berk, M. N. Rosenbluth, and D. A. Spong, "Radially-Dependent Stability Theory for EBT," paper presented at the EBT Stability Workshop, May 13-14, 1981, Oak Ridge, Tennessee.

<sup>2</sup>N. A. Krall, *Phys. Fluids* 9, 820 (1966).

<sup>3</sup>R. R. Dominguez and H. L. Berk, *Phys. Fluids* 21, 827 (1978).

<sup>4</sup>A. I. Morozov and L. S. Solov'ev, in *Reviews of Plasma Physics*, Vol. 2, ed. by M. A. Leontovich, Consultants Bureau, New York (1966).

<sup>5</sup>M. R. Scott and H. A. Watts, *SIAM J. Numerical Anal.* 14, 40 (1977).

STABILITY OF HOT ELECTRON PLASMA IN THE ELMO BUMPY TORUS<sup>\*</sup>

K. T. Tsang  
Fusion Energy Division  
Oak Ridge National Laboratory  
Oak Ridge, Tennessee 37830

and

C. Z. Cheng  
Princeton Plasma Physics Laboratory  
Princeton, New Jersey 08540

## ABSTRACT

The stability of a hot electron plasma in the ELMO Bumpy Torus is investigated using two different models. In the first model, where the hot electron distribution function is assumed to be a delta function in the perpendicular velocity, we find a new stability boundary in addition to those discussed by Nelson and by Van Dam and Lee. In the second model, where the hot electron distribution function is assumed to be a Maxwellian in the perpendicular velocity, we find stability boundaries significantly different from those of the first model. Coupling of the Nelson-Van Dam-Lee mode to the compressional Alfvén mode is now possible. This leads to a higher permissible core plasma beta value for stable operation.

---

<sup>\*</sup>Research sponsored by the Office of Fusion Energy, U.S. Department of Energy, under contract W-7405-eng-26 with the Union Carbide Corporation.

## 1. INTRODUCTION

The beta limitation of a magnetic confinement system is a crucial problem in determining its economic merits as a fusion reactor. In the ELMO Bumpy Torus (EBT) this limitation is determined by the stability property of the hot electron plasma. An early study by Nelson and Hedrick [1] treating the hot electron annulus as a rigid noninteracting current ring by a modified magnetohydrodynamic (MHD) approach predicted a stable equilibrium for a beta value of the core plasma roughly proportional to and comparable to that of the hot electron annulus, which is on the order of 50%. This optimistic prediction placed the EBT far ahead of the tokamak in the race of attaining a high beta value. Later, Nelson and Van Dam and Lee [2-3] included the hot electron annulus in the stability analysis using a Vlasov approach. They found a stability boundary roughly given by  $\beta_i \leq 4\epsilon/(1 + \beta_h)$ , where  $\beta_i$  and  $\beta_h$  are the beta values for the core ions and hot electrons, respectively, and  $\epsilon$  is the ratio of the density scale length to the radius of curvature. This change of the stability boundary is attributed to the enhanced compressibility of the plasma when the hot electrons are included.

Both calculations mentioned above investigated the stability of low frequency ( $\omega \ll \Omega_i$ , where  $\omega$  is the mode frequency and  $\Omega_i$  is the ion cyclotron frequency) flute-interchange modes. However, the diamagnetic drift and the magnetic gradient and curvature drift frequencies of the hot electrons, which are the source of the instability, are greater than or comparable to the ion cyclotron frequency for typical parameters in EBT. Therefore, a more realistic determination of the stability boundaries should include the consideration of higher frequency modes ( $\omega \sim \Omega_i$ ).

In fact, Dominguez and Berk [4] included the high frequency ( $\omega \sim \Omega_i$ ) flute interchange in their analysis and found these modes may exist with  $\omega \gg \Omega_i$ . However, it is not clear how their result related to those of Nelson and of Van Dam and Lee [2-3].

In this work, we extend the work of Refs [2-3] to include modes with  $\omega \sim \Omega_i$ . By removing unnecessary assumptions and using different models for the equilibrium hot electron distribution function, we find the stability boundaries can be significantly different.

Using a delta function in perpendicular velocity  $v_{\perp}$  for the hot electron distribution function, we find our result qualitatively agrees with that of Refs [2-3]. However, a new stability boundary not realized by them is also discovered. The reason for this is that the  $\omega/\omega_{dh}$  (where  $\omega_{dh}$  is the magnetic drift frequency of the hot electron) expansion made by them is not valid because one of the stability boundaries is roughly given by  $\omega_{dh} \approx 0$ . With this additional stability boundary, the Nelson and Van Dam and Lee result is basically valid and consistent with the model they used (in that the frequency of the mode considered is smaller than  $\Omega_i$  and there is no coupling of the low frequency mode with high frequency modes).

However, when a Maxwellian in  $v_{\perp}$  (instead of a delta function) is used for the hot electron distribution function, the situation is completely changed. Coupling of the flute interchange ( $\omega < \Omega_i$ ) to the high frequency compressional Alfvén wave ( $\omega \sim \Omega_i$ ) is possible when the hot electron beta  $\beta_h$  is sufficiently large. This is because the contribution of  $\beta_h$  to the electromagnetic part of the dispersion relation is weighted by a larger factor. Similar coupling has also been noticed by

El-Nadi [5] although he used a delta function distribution for the hot electrons and a slightly different dispersion equation derived from fluid equations. As a result of this coupling, the stability boundaries are greatly changed. The boundary roughly given by  $\beta_i \lesssim 4\epsilon/(1 + \beta_h)$  discovered by Nelson and Van Dam and Lee is now roughly given by  $\beta_i \propto \beta_h$ . This change in the scaling of critical  $\beta_i$  may permit a higher core beta operation of EBT than that predicted by the Nelson and Van Dam and Lee theory.

## 2. DISPERSION RELATION

Our model is similar to that employed in Refs [2-3]: i.e., slab geometry with density and magnetic field gradients in the x direction and an equilibrium magnetic field  $\vec{B} = B(x)\hat{z}$ . The plasma is composed of three species: core ions, core electrons, and hot electrons. The temperature of each species is constant in space. We are interested in waves with a zero parallel wave number  $k_{\parallel} = 0$  and a long perpendicular wavelength  $k_{\perp} \rho_i \ll 1$ , where  $\rho_i$  is the gyroradius of the core ion. We restrict ourselves to local analysis and set  $k_x = 0$ .

Under these assumptions, the perturbed electromagnetic field is completely specified by the electrostatic potential  $\phi$  and the x component of the vector potential  $A_x$ . Employing standard orbit integration techniques to solve the Vlasov equation for the perturbed distribution function and relating the relevant perturbed quantities by Maxwell equations, we obtain the dispersion relation for this problem. The detail of the derivation is similar to that presented in Ref. [2], and we present only the result here. We assume also  $\omega_{pi}/\Omega_i \gg 1$  and  $\omega/c k \ll 1$ , where  $\omega_{pi}$  is the ion plasma frequency and c is the speed of light. These two conditions are well satisfied in experiments for the modes we have considered. The dispersion relation can then be simplified to the form

$$D_1 D_2 - \frac{\delta_i D_3^2}{2} = 0 \quad (1)$$

where

$$D_1 = \frac{\omega_{di}(\omega_{di} - \omega_{*i})(1 + \tau)}{(\omega - \omega_{di})(\omega - \omega_{de})} + \frac{\omega - \omega_{*i}}{\omega - \omega_{di}} \frac{\Omega_i^2 b}{(\omega - \omega_{di})^2 - \Omega_i^2}$$

$$+ \frac{\omega_{*e} - \omega_{de}}{\omega - \omega_{de}} \frac{\delta}{\tau} + (1 + C_1) \frac{\delta}{\tau_h}$$

$$D_2 = 1 + \beta_i \frac{\omega - \omega_{*i}}{\omega - \omega_{di}} \left\{ 1 + \frac{(\omega - \omega_{di})^2}{2b[(\omega - \omega_{di})^2 - \Omega_i^2]} \right\} + \beta_e \frac{\omega - \omega_{*e}}{\omega - \omega_{de}} + \beta_h C_2$$

and

$$D_3 = \frac{\omega - \omega_{*i}}{\omega - \omega_{di}} \frac{\Omega_i^2}{(\omega - \omega_{di})^2 - \Omega_i^2} + \frac{\omega - \omega_{*e}}{\omega - \omega_{de}} (1 - \delta) + C_3 \delta$$

In Eq. (1),  $\delta = N_h/N_i$  is the density ratio of the hot electron to the core ion,  $\tau = T_e/T_i$  is the temperature ratio of the core electron to the core ion,  $\tau_h = T_h/T_i$  is the temperature ratio of the hot electron to the core ion,  $b = (k_y \rho_i)^2 = T_i m_i (k_y c/eB)^2$ ,  $\beta_s = 8\pi N_s T_s / B^2$ ,  $\omega_{*s} = \lambda_s k_y \rho_i (T_s/T_i) \times (\rho_i/L_s)\Omega_i$ ,  $\omega_{ds} = \omega_{Bs} + \omega_{cs}$ ,  $\omega_{Bs} = \lambda_s k_y \rho_i (T_s/T_i) (\rho_i/L_B)\Omega_i$ ,  $\omega_{cs} = \lambda_s k_y \rho_i (T_s/T_i) (\rho_i/L_c)\Omega_i$ ,  $L_s^{-1} = \partial \ln N_s / \partial x$ ,  $L_B^{-1} = \partial \ln B / \partial x$ ,  $L_c^{-1} = \vec{B} \cdot \vec{\nabla} \vec{B} \cdot \hat{x} / B^2$  is the radius of curvature of the magnetic field,  $s$  is the subscript referring to the three species,  $\lambda_s = 1$  for the core ion, and  $\lambda_s = -1$  for the core/hot electron.

The equilibrium density scale lengths are related by the neutrality condition

$$\frac{1}{L_i} = \frac{1 - \delta}{L_e} + \frac{\delta}{L_h} \quad (2)$$

From the equilibrium MHD force balance equation, we have also

$$\frac{1}{L_B} = \frac{1}{L_c} - \frac{1}{2} \left( \frac{\beta_i}{L_i} + \frac{\beta_e}{L_e} + \frac{\beta_h}{L_h} \right) \quad (3)$$

Using Eqs (2) and (3), we can eliminate two out of the five scale lengths. Furthermore, we restrict ourselves to the outer region of the hot electron annulus because it is most unstable and assume  $L_i = L_h$  as in Refs [2-3]. Therefore, we choose  $L_i$  and  $\varepsilon = L_i/L_c$  as independent parameters to specify the gradients.

For isotropic Maxwellian hot electrons, the constants  $C_1$ ,  $C_2$ , and  $C_3$  are given by

$$C_1 = \frac{2}{\pi^{1/2}} (\omega - \omega_{*h}) \int \frac{x \, dx \, dy}{\omega'} \exp(-x^2 - y^2) \quad (4a)$$

$$C_2 = \frac{1}{\pi^{1/2}} (\omega - \omega_{*h}) \int \frac{x^5 \, dx \, dy}{\omega'} \exp(-x^2 - y^2) \quad (4b)$$

and

$$C_3 = \frac{2}{\pi^{1/2}} (\omega - \omega_{*h}) \int \frac{x^3 \, dx \, dy}{\omega'} \exp(-x^2 - y^2) \quad (4c)$$

where  $\omega' = \omega - (\omega_{Bh} x^2/2 + \omega_{ch} y^2)$ .

If a delta function distribution in  $v_i^2$  is used for the hot electron, then

$$C_1 = 2C_2 = C_3 = \frac{(\omega - \omega_{*h})}{(\omega - \omega_{dh})} \quad (5)$$

With  $C_1$ ,  $C_2$ , and  $C_3$  given by Eq. (5), Eq. (1) reduces to the same dispersion relation as in Ref. [2] in the appropriate limit. The main difference between the dispersion relation given by Eqs (1) and (5) here and that of Nelson is that in Ref. [2] the limit  $\omega \ll \omega_{*h}$ ,  $\omega_{dh}$  was explicitly used so that  $C_1 = 2C_2 = C_3 = \omega_{*h}/\omega_{dh}$ . Because of this, the temperature ratio  $\tau_h$  does not appear in the dispersion relation in Ref. [2], so that the density ratio  $\delta$  is a free parameter. Motivated by the facts that  $\omega_{dh} \propto \omega_{di}$  and that the electrostatic interchange dispersion relation  $D_1 = 0$  roughly gives a stability boundary  $\omega_{di} \cong 0$  when  $\delta \ll 1$ , we retain  $\omega$  compared with  $\omega_{dh}$  as in Eq. (5). Now,  $\delta$  is no longer a free parameter and relates to other parameters by

$$\delta = \frac{\beta_h}{\tau_h \beta_i} \quad (6)$$

We choose to employ  $\beta_h$ ,  $\beta_i$ , and  $\tau_h$  as independent parameters because they are directly measurable in experiments. We show in the next section that this difference leads to a new stability boundary not contained in the Nelson and Van Dam and Lee theory.

## 3. NUMERICAL RESULT

Although the dispersion relation given by Eqs (1) and (5) is an algebraic equation, it is sufficiently intractable to warrant numerical investigation. We first solve Eqs (1) and (5) for real  $\omega$  for each set of the parameters:  $\beta_i$ ,  $\beta_h$ ,  $k_y \rho_i$ ,  $\tau$ ,  $\tau_h$ ,  $\rho_i/L_i$ , and  $\epsilon$ .

In Fig. 1, we show a plot of  $\omega/\Omega_i$  vs  $\beta_i$  for different values of  $\beta_h$  and for  $k_y \rho_i = 0.1$ ,  $\tau = 1$ ,  $\tau_h = 1000$ ,  $\rho_i/L_i = -0.04$ , and  $\epsilon = 1/40$ . On each of these curves,  $\omega$  is a function of  $\beta_i$ . Since the dispersion relation is a real algebraic equation, an instability would appear when two real roots merge to a double root or  $\partial\beta_i/\partial\omega = 0$ . For example, the curve for  $\beta_h = 5\%$  shows that the plasma is unstable for  $\beta_i \geq 3.7\%$  or  $\beta_i \leq 2.5\%$  and is stable in between.

In Fig. 2, we summarize the stability information provided by Fig. 1 in the curve labeled  $\tau_h = 1000$ . For scaling purposes, the curve with  $\tau_h = 2000$  is also shown in Fig. 2. The plasma is stable within a closed area in the  $\beta_i$ - $\beta_h$  space and unstable outside. The stability boundary is similar to that of the Nelson and Van Dam and Lee theory except that the stable region is closed below by a new boundary not contained in the previous theory. However, Fig. 2 also shows that as  $\tau_h$  increases, the stable region approaches that given by the Nelson and Van Dam and Lee theory. This is consistent with the discussion in the previous section about the approximation involved in the Nelson and Van Dam and Lee theory.

This new lower stability boundary in  $\beta_i$  is related to the close contours in the  $\omega$ - $\beta_i$  plane shown in Fig. 1. It is obvious from Eq. (6) that  $\delta$  increases as  $\beta_i$  decreases for fixed  $\beta_h$  and  $\tau_h$ . In the Nelson and

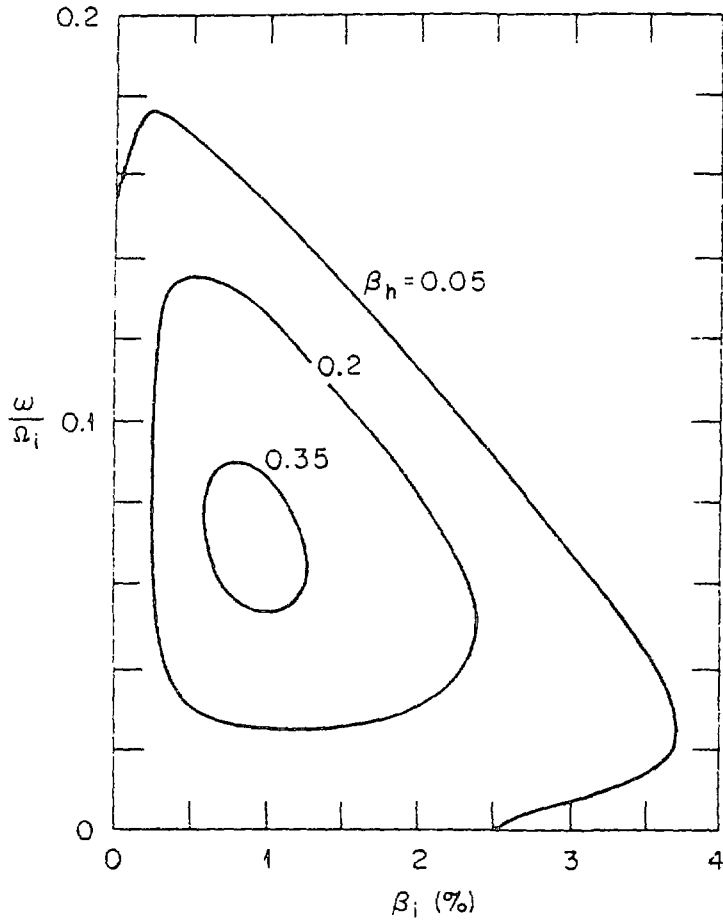


FIG. 1. Low frequency mode solution of the dispersion relation given by Eqs (1) and (5), delta function model, for  $k_y \rho_i = 0.1$ ,  $\tau = 1$ ,  $\tau_h = 1000$ ,  $\rho_i/L_i = -0.04$ , and  $\epsilon = 1/40$ .

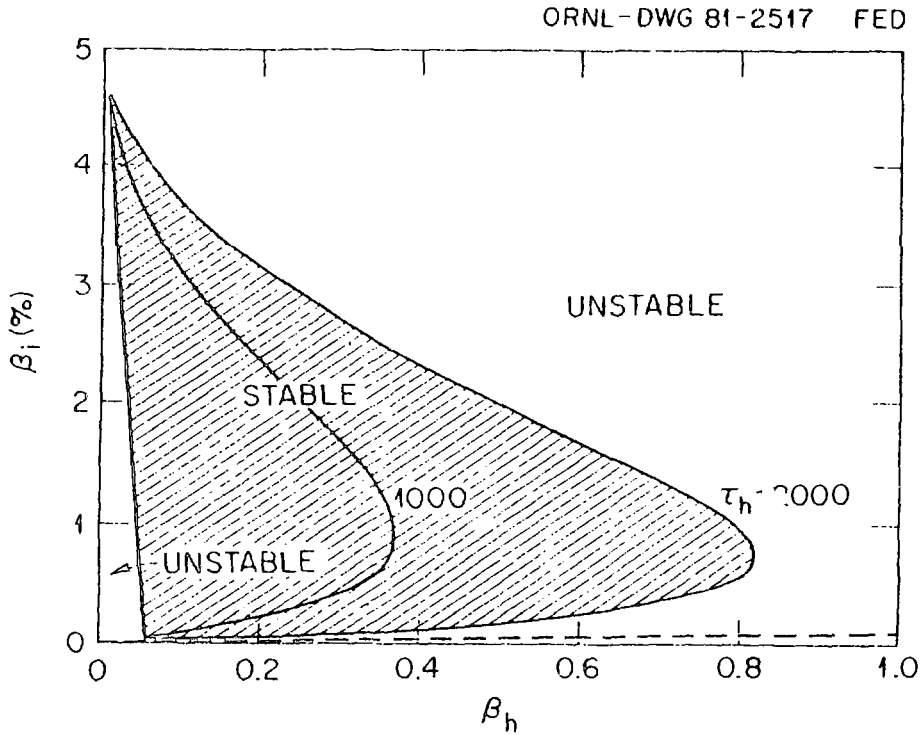


FIG. 2. Stability boundaries for the delta function model in  $\beta_i$ - $\beta_h$  space with  $\tau_h = 1000$  and  $\tau_h = 2000$ . Other parameters are the same as in Fig. 1.

Van Dam and Lee theory,  $\delta$  is kept fixed and  $\tau_h$  changes in the  $\beta_i$ - $\beta_h$  plane. However, this is not exactly the constraint we know from experimental data.

Since  $\delta$  must be less than or equal to one, we have the inequality

$$\beta_i \geq \frac{\beta_h}{\tau_h} \quad (7)$$

An additional boundary in  $\beta_i$ - $\beta_h$  space is then given by  $\beta_i = \beta_h/\tau_h$ , shown in Fig. 2 by the dashed line for  $\tau_h = 1000$ . A similar line for  $\tau_h = 2000$  is even lower and is not shown in Fig. 2. It is clear from Fig. 2 that the additional inequality [Eq. (7)] has no effect on the new stability boundary.

Figure 1 also confirms the low frequency assumption ( $\omega \ll \Omega_i$ ) in the Nelson and Van Dam and Lee theory. The mode involved in the stability discussion is the low frequency flute interchange due to the hot electrons. There is no coupling between the flute-interchange and high frequency ( $\omega \sim \Omega_i$ ) modes although the existence of such modes can be seen from Eq. (1).

Analytically, we can take the limit of no gradients and  $\delta \rightarrow 0$ ; then, Eq. (1) is reduced to

$$\omega^2 = \frac{2b\Omega_i^2}{\beta_i} (1 + \beta_i + \beta_e) \left[ 1 + \left( \frac{v_A}{c} \right)^2 \right]^{-1}$$

which is the dispersion relation of the compressional Alfvén wave. For typical parameters, we have  $\omega \sim \Omega_i$ . In Fig. 3 we show the existence of the compressional Alfvén mode in the dispersion relation given by Eqs (1) and (5). The parameters used in Fig. 3 are the same as those in Fig. 1.

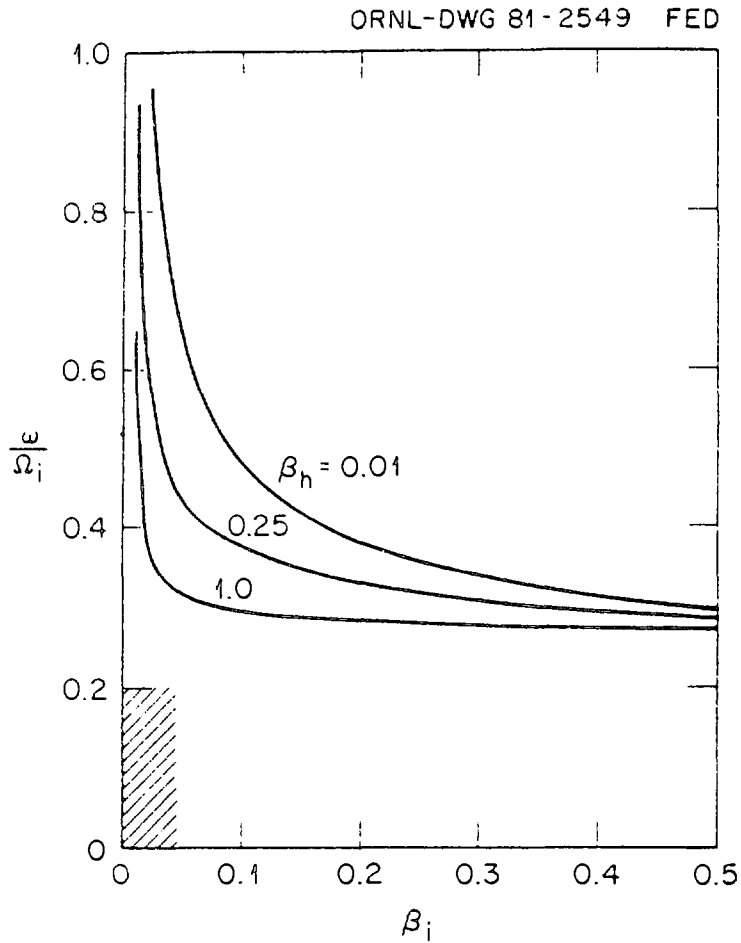


FIG. 3. Compressional Alfvén wave solution of the same dispersion relation used in Fig. 1 and for the same set of parameters. The low frequency solution shown in Fig. 1 occupied the shaded small box in the lower left-hand corner.

It is obvious from Figs 1 and 3 that the Alfvén mode and the interchange mode do not couple to each other.

To test the sensitivity of the stability boundary on the model hot electron distribution function used, we solve the dispersion relation given by Eqs (1) and (4), which is derived from isotropic Maxwellian hot electrons. The constants  $C_1$ ,  $C_2$ , and  $C_3$  are evaluated numerically by first converting the  $y$  integrals to the plasma dispersion function  $Z$  [6] and then performing the  $x$  integration by the Laguerre method. The imaginary part of the  $C$ 's, which is due to the hot electron magnetic drift resonance, is usually very small because  $\omega_{Bh}$  and  $\omega_{ch} \gg \omega$ . Therefore,  $C_1$ ,  $C_2$ , and  $C_3$  again can be regarded as real quantities.

The calculation leading to Fig. 1 is repeated for Eqs (1) and (4), and a surprisingly different result is obtained. Figure 4 shows the result of such a calculation with the same parameters as those in Fig. 1. Unlike the previous delta function model, which shows no coupling between the higher frequency compressional Alfvén mode and the lower frequency flute interchange, the Maxwellian model shows a strong coupling between them when  $\beta_h$  is large enough. As shown in Fig. 4, when  $\beta_h \leq 0.15$  these two modes do not interact with each other. The compressional Alfvén solutions represented by curves on the upper right-hand corner disjoin with the flute-interchange solutions on the lower left corner. When  $\beta_h \cong 0.2$ , these two types of solutions "reconnect" and a new instability region in  $\beta_i$  appears.

To verify that this new coupling is not due to numerical inaccuracy from the two-dimensional integration of the constants  $C_1$ ,  $C_2$ , and  $C_3$ , we replace  $\omega'$  in Eqs (4) by  $\omega - \omega_{dh}$  and perform the integration analytically.

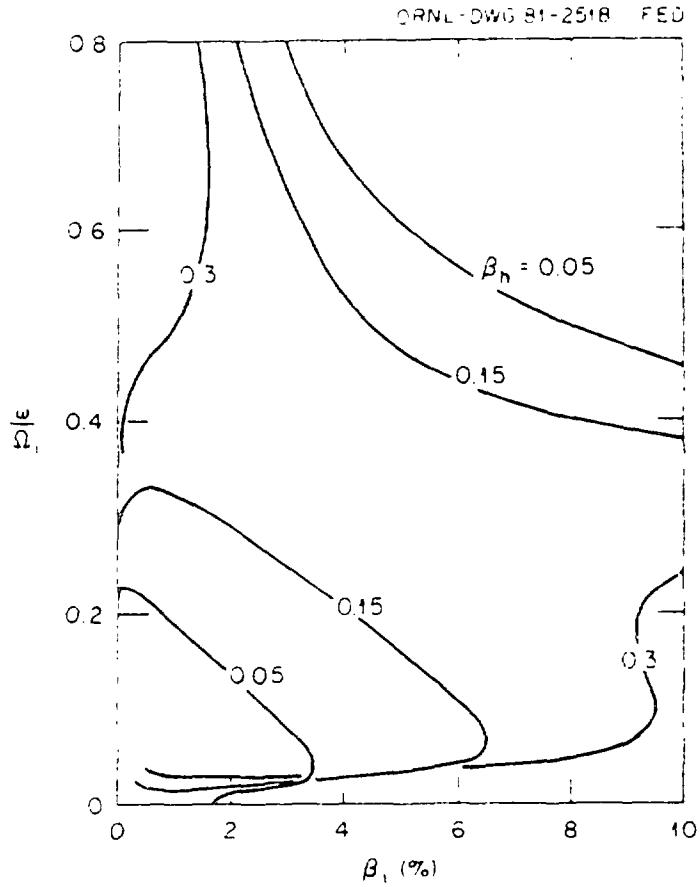


FIG. 4. Solution of the dispersion relation given by Eqs (1) and (4), the Maxwellian model, for the same set of parameters as in Fig. 1.

This approximation is equivalent to evaluating  $\omega'$  at thermal energy and gives

$$C_1 = C_2 = C_3 = \frac{\omega - \omega_{*h}}{\omega - \omega_{dh}} \quad (8)$$

This is the same result as given by Eq. (5) except  $C_2$  is larger by a factor of 2. When Eqs (1) and (8) are solved for the same set of parameters as Figs 1 and 4, similar coupling between the Alfvén and interchange modes is observed. This result is shown in Fig. 5.

The stability boundary implied by Fig. 4 is summarized in Fig. 6. The stable region is vastly different from that in Fig. 2. The dashed line in Fig. 6 is again the line  $\beta_i = \beta_h / \tau_h$  below which we have  $\delta > 1$ , which is impossible. The most important feature of Fig. 6 is that the upper critical  $\beta_i$  increases with  $\beta_h$  until a critical  $\beta_h$  ( $\sim 0.35$ ) is reached. Then, the stability boundary turns around to form a cusp and turns around smoothly to high  $\beta_h$  at a second critical  $\beta_h$  of about 0.2. Between 0.2 and 0.35, for each  $\beta_h$ , there are three critical values of  $\beta_i$  and a channel of stable region. This is due to the coupling of the Alfvén-interchange modes.

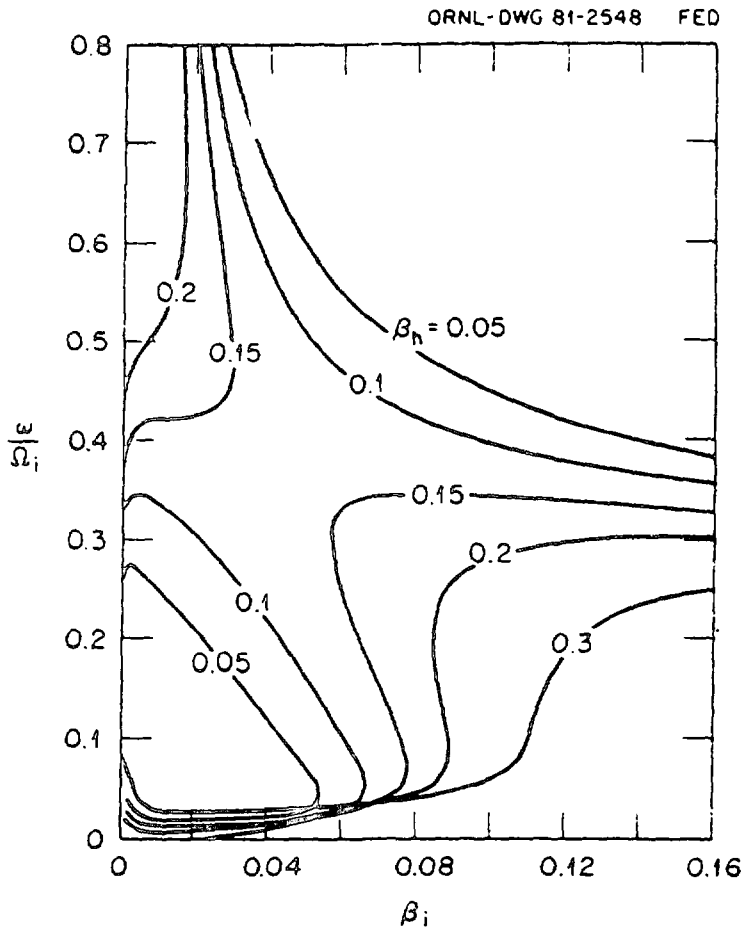


FIG. 5. Solution of the dispersion relation given by Eqs (1) and (8), the quasi-Maxwellian model, for the same set of parameters as in Fig. 1.

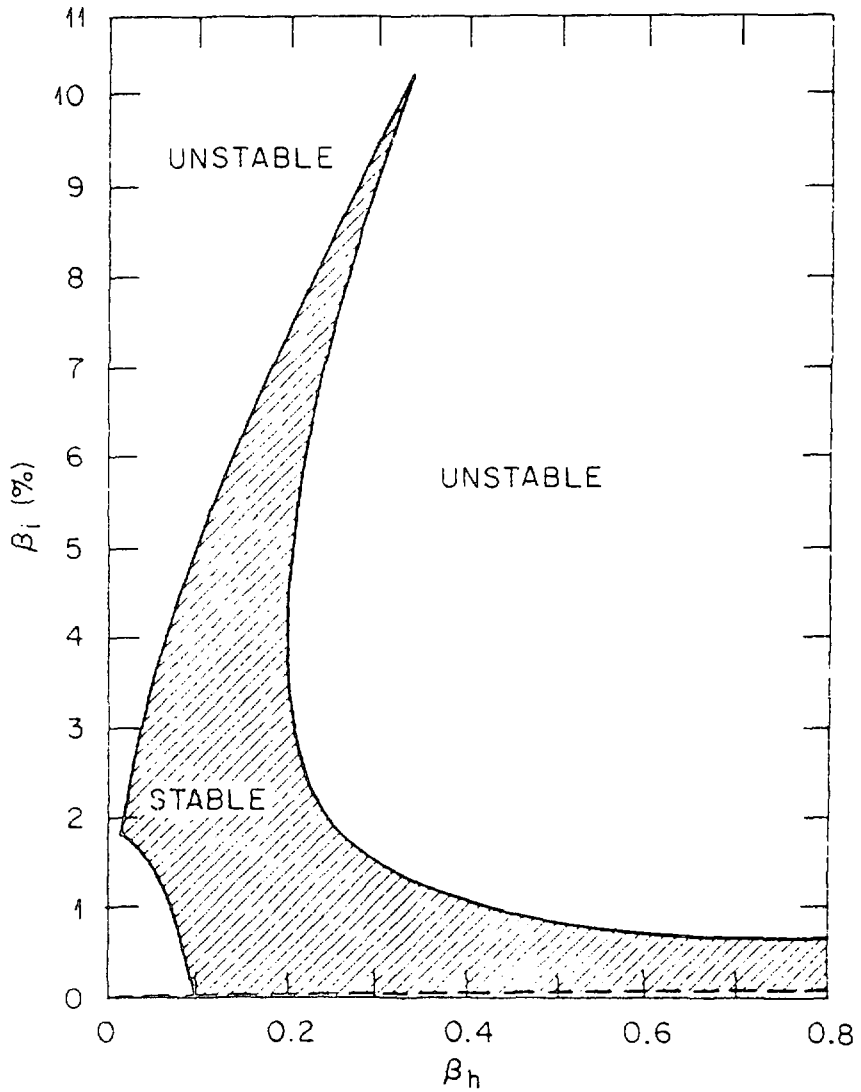


FIG. 6. Stability boundary in  $\beta_i$ - $\beta_h$  space for the Maxwellian model and for the same set of parameters as in Fig. 1.

## 4. DISCUSSION

We have solved numerically the Alfvén-interchange mode dispersion relation for a hot electron plasma in EBT and obtained the stability boundaries for two different models of the hot electron distribution function. In the delta function model, coupling between the Alfvén and interchange modes is not observed, and the stability boundary is similar to that discovered by Nelson and Van Dam and Lee [2-3]. However, a lower critical  $\beta_i$  boundary is missed in their analysis because of the approximation  $\omega \ll \omega_{dh}$  they used. In the Maxwellian model, coupling between the Alfvén and interchange modes is possible, and the stability boundary is significantly different from that of the delta function model. The reason for this difference is that in the Maxwellian model the contribution of  $\beta_h$  to  $D_2$ , which relates the perturbed current to  $A_x$  in Ampère's law, is larger by approximately a factor of 2. Thus, the influence of the hot electron beta to the Alfvén wave is stronger.

Results from the study of these two models suggest that the stable operating region for a hot electron device such as EBT is very sensitive to the model used. Inclusion of the radial structure, anisotropic hot electron temperature, finite ion and hot electron gyroradius effects, and additional coupling to shear Alfvén waves [7] will undoubtedly complicate the already complex stability pictures. Hopefully, the results from these studies will converge to one that is consistent with experiments.

## REFERENCES

1. NELSON, D. B., HEDRICK, C. L., Nucl. Fusion 19 (1979) 283.
2. NELSON, D. B., Phys. Fluids 23 (1980) 1850.
3. VAN DAM, J. W., LEE, Y. C., in Proceedings of the Workshop on EBT Ring Physics, Oak Ridge National Laboratory, 1979, 471.
4. DOMINGUEZ, R. R., BERK H. L., Phys. Fluids 21 (1978) 827.
5. EL-NADI, A. (private communication).
6. FRIED, B. D., CONTE, S. F., Plasma Dispersion Functions, Academic Press, New York (1961).
7. SAMUKI, H., FUJIWARA, M., in Proceedings of the Workshop on EBT Ring Physics, Oak Ridge National Laboratory, 1979, 453.

Analytical Theory of Interchange and  
Compressional Alfvén Instabilities in EBT

by

C. Z. Cheng, Plasma Physics Laboratory  
Princeton University, Princeton, New Jersey 08544

and

K. T. Tsang, Oak Ridge National Laboratory  
P.O. Box Y, Oak Ridge, Tennessee 37830

Abstract

The local stability of the EBT plasma is analyzed for the long wavelength perturbations in the frequency regime,  $\omega \lesssim \Omega_i$  ( $\Omega_i$  is ion cyclotron frequency). In addition to the low frequency interchange instability, the plasma can be unstable to the compressional Alfvén wave. Contrary to the previously obtained quadratic dispersion relation in  $\omega$  for the interchange mode, our dispersion relations for both types of instabilities are cubic in  $\omega$ . New stability boundaries are found, for the hot electron interchange mode, to relate to the enhanced compressibility of the core plasma in the presence of hot electrons. The compressional Alfvén instability is driven due to the coupling of hot electron magnetic drifts and diamagnetic drift with the compressional Alfvén wave. The stability conditions of these two types of instabilities are opposite to each other.

## I. INTRODUCTION

Stability of the plasma in the ELMO Bumpy Torus in the presence of the hot electrons has been studied for the low frequency interchange mode<sup>1-4</sup> driven by the diamagnetic drift and magnetic drifts of the plasma. These earlier works have confirmed that in order to obtain correct stability condition, the hot electrons must be treated by kinetic theory.<sup>2-4</sup> Nelson<sup>2</sup> and Van Dam and Lee<sup>3</sup> have investigated the low frequency interchange mode by retaining only the lowest order hot electron contribution in the electromagnetic part of the dispersion relation,  $D_{em}$ . They find that the hot electrons can enhance the compression of the core plasma and influence the stability analysis. The enhancement of the compressibility of the core plasma is due to a near cancellation in  $D_{em}$ . Therefore, when the next order hot electron contribution in  $D_{em}$  is included, we will expect quite different stability boundary. Since the core plasma compressional Alfvén frequency can be comparable to the hot electron magnetic drift frequency, we also expect the compressional Alfvén wave to be driven unstable by the hot electron magnetic drifts. Therefore, a realistic determination of the stability of EBT plasma should include both the interchange mode and the compressional Alfvén wave.

Because the driving mechanism for these modes is the interaction between the magnetic ( $\nabla B$  and curvature) drifts and diamagnetic drift of the hot electrons and the core plasma, the stability boundary is sensitive to the hot electron distribution function. In this paper we will employ two different models of the hot electron distribution function,  $\delta$ -function and Maxwellian, to analytically study the stability of EBT plasma. The difference between our theory and the previous works<sup>2,3</sup> will be demonstrated.

## II. FORMULATION

Consider a slab model<sup>2,3</sup> with density and magnetic field inhomogenities in the x direction and an equilibrium magnetic field  $\vec{B} = B_z(x)\hat{z} + B_x(x)\hat{x}$  where  $B_x \ll B_z$ . We also assume there are no temperature gradients. The plasma equilibrium is composed of three species - warm ions, warm electrons, and hot electrons. Then the equilibrium condition  $\nabla(p + B^2/8\pi) = \vec{B} \cdot \nabla \vec{B}/4\pi$  can be written locally as

$$1/L_B = 1/L_C - \left(\frac{1}{2}\right)(\beta_h/L_h + \beta_i/L_i + \beta_e/L_e) \quad (1)$$

where  $L_B$ ,  $L_C$ ,  $L_h$ ,  $L_i$ ,  $L_e$  are the magnetic field gradient, magnetic field curvature, hot electron density, warm ion density and warm electron density scale lengths, respectively.  $\beta_s = 8\pi N_s T_s / B^2$  for  $s = i, e, h$ , where  $N$  denotes the density and  $T$  is the temperature. The neutrality condition,  $N_i = N_e + N_h$  relates these equilibrium density scale lengths by

$$1/L_i = (1 - \delta)/L_e + \delta/L_h \quad (2)$$

where  $\delta = N_h/N_i = (\beta_h T_i)/(\beta_i T_h)$ .

We are interested in electromagnetic perturbations with zero parallel wavenumber,  $k_{\parallel} = 0$ , and long perpendicular wavelength  $k_{\perp} \rho_i \ll 1$ , where  $\rho_i$  is the ion gyroradius. We also restrict ourselves to local analysis and set  $k_x = 0$ . Then the perturbations can be specified by the electrostatic potential  $\phi$  and the x-component of the vector potential  $A_x$ . The dispersion relation can be derived from the Vlasov equations and Maxwell's equations. In the limits  $\omega_{pi}/\Omega_i \gg 1$ ,  $\omega/ck \ll 1$  and  $\omega \lesssim \Omega_i$ , where  $\omega_{pi}$ ,  $\Omega_i$  are the ion plasma and

cyclotron frequency respectively,  $c$  is the velocity of light, the dispersion relation can be simplified to the form<sup>5</sup>

$$D_{es} D_{em} + \left(\frac{\beta_i}{2}\right) D_{ct}^2 = 0, \quad (3)$$

where

$$D_{es} = \frac{\omega_{di}(\omega_{*i} - \omega_{di})(1 + \tau_e)}{(\omega - \omega_{di})(\omega - \omega_{de})} - \left(\frac{\omega - \omega_{*i}}{\omega - \omega_{di}}\right) \frac{\Omega_i^2 b_i}{(\omega - \omega_{di})^2 - \Omega_i^2} - \left(\frac{\omega_{*e} - \omega_{de}}{\omega - \omega_{de}}\right) (\delta/\tau_e) + (c_1 - 1)(\delta/\tau_h),$$

$$D_{em} = 1 + \beta_i \left(\frac{\omega - \omega_{*i}}{\omega - \omega_{di}}\right) \left(1 + \frac{(\omega - \omega_{di})^2}{2b_i[(\omega - \omega_{di})^2 - \Omega_i^2]}\right) + \beta_e \left(\frac{\omega - \omega_{*e}}{\omega - \omega_{de}}\right) + \beta_h c_2,$$

$$D_{ct} = \left(\frac{\omega - \omega_{*i}}{\omega - \omega_{di}}\right) \frac{\Omega_i^2}{(\omega - \omega_{di})^2 - \Omega_i^2} + \left(\frac{\omega - \omega_{*e}}{\omega - \omega_{de}}\right) (1 - \delta) + C_3 \delta,$$

$$\omega_{*s} = \lambda_s b_i^{1/2} \tau_s (\rho_i/L_s) \Omega_i, \quad b_i = (k_y \rho_i)^2, \quad \rho_i^2 = T_i/m_i \Omega_i^2,$$

$$\omega_{ds} = \omega_{Bs} + \omega_{cs}, \quad \omega_{Bs} = \lambda_s b_i^{1/2} \tau_s (\rho_i/L_B) \Omega_i,$$

$$\omega_{cs} = \lambda_s b_i^{1/2} \tau_s (\rho_i/L_c) \Omega_i, \quad \tau_s = T_s/T_i, \quad s = h, e, i,$$

and  $\lambda_s = 1$  for ion and  $-1$  for electron. For Maxwellian hot electrons, the constants  $C_1$ ,  $C_2$  and  $C_3$  are given by

$$C_1 = (2/\pi^{1/2})(\omega - \omega_{*h}) \int_0^\infty dx \int_{-\infty}^\infty dy x \exp(-x^2 - y^2)/\omega', \quad (4(a))$$

$$C_2 = (1/\pi^{1/2})(\omega - \omega_{*h}) \int dx dy x^5 \exp(-x^2 - y^2)/\omega' , \quad (4(b))$$

and

$$C_3 = (2/\pi^{1/2})(\omega - \omega_{*h}) \int dx dy x^3 \exp(-x^2 - y^2)/\omega' , \quad (4(c))$$

where

$$\omega' = \omega - (\omega_{Bh} x^2/2 + \omega_{ch} y^2) .$$

If we further make the approximation with  $\omega' = \omega - \omega_{dh}$  in eqs. 4(a) - 4(c) and perform the integrations analytically, then this modified Maxwellian hot electron model gives

$$C_1 = C_2 = C_3 = (\omega - \omega_{*h})/(\omega - \omega_{dh}) . \quad (5)$$

This turns out to be a good approximation when we compare the numerical solutions from both Eqs. (4) and (5).<sup>5</sup> In the following we will employ Eq. (5) for the analytical investigation. If a delta function is used for hot electrons, then

$$C_1 = 2C_2 = C_3 = (\omega - \omega_{*h})/(\omega - \omega_{dh}) . \quad (6)$$

Note that the only difference between Eqs. (5) and (6) is in  $C_2$  and we will write  $C_2 = \hat{C}_2 (\omega - \omega_{*h})/(\omega - \omega_{dh})$  with  $\hat{C}_2 = 1$  for the Maxwellian hot electrons and  $\hat{C}_2 = 1/2$  for the  $\delta$ -function hot electrons.

## III. INTERCHANGE MODE

Let us first consider the low frequency interchange instability with  $\omega_{di}$ ,  $\omega_{*i} < \omega < \omega_{dh}$ ,  $\omega_{*h}$ . In this frequency regime, the three terms in the dispersion relation, Eq. (3), can be simplified to yield

$$\begin{aligned}
 D_{es} &\approx b_i + (\omega_{*i} - \omega_{di})[(1 + \tau_e)\omega_{di}/\omega^2 + \delta/\omega] , \\
 D_{em} &\approx \bar{D}_{em} + \hat{c}_2 \beta_h \left( \frac{\omega_{*h} - \omega_{dh}}{2} \right) \omega , \\
 \bar{D}_{em} &= 1 + \beta_i + \beta_e + \hat{c}_2 \beta_h \omega_{*h}/\omega_{dh} , \tag{7}
 \end{aligned}$$

and

$$D_{ct} \approx \delta\omega_{*h}/\omega_{dh} + (1 + \tau_e)(\omega_{*i} - \omega_{di})/\omega .$$

We note that Eq. (7) will give rise to the usual quadratic dispersion relation if we neglect the second term in  $D_{em}$  which is of  $O(\omega/\omega_{dh})$ . However, the hot electron contribution will give a near cancellation in  $\bar{D}_{em}$  and result in an enhanced compression of the core plasma.<sup>2,3</sup> Therefore, we must treat  $\bar{D}_{em}$  to be the same order as the second term in  $D_{em}$  at marginal stability. From Eq. (7) the dispersion relation can be written as a cubic in  $\omega$ :

$$\omega^3 + A_2 \omega^2 + A_1 \omega + A_0 = 0 , \tag{8}$$

where

$$A_2 = \left[ b_i \bar{D}_{em} + \frac{\beta_i}{2} \left( \delta \frac{\omega_{*h}}{\omega_{dh}} \right)^2 + \hat{C}_2 \beta_h \left( \frac{\omega_{*i} - \omega_{di}}{\omega_{di}} \right)^2 \delta \right] / s \quad ,$$

$$A_1 = \left[ \hat{C}_2 \beta_h \left( \frac{\omega_{*h} - \omega_{dh}}{2} \right) \omega_{di} (1 + \tau_e) + \bar{D}_{em} \delta + \beta_i \delta \left( \frac{\omega_{*h}}{\omega_{dh}} \right) (1 + \tau_e) \right] \left( \frac{\omega_{*i} - \omega_{di}}{s} \right)$$

$$A_0 = \left[ \bar{D}_{em} \omega_{di} + \left( \frac{\beta_i}{2} \right) (1 + \tau_e) (\omega_{*i} - \omega_{di}) \right] \frac{(1 + \tau_e) (\omega_{*i} - \omega_{di})}{s} \quad ,$$

$$s = \hat{C}_2 \beta_h \left( \frac{\omega_{*h} - \omega_{dh}}{2} \right) b_i \quad .$$

Without hot electrons ( $\delta = \beta_h = 0$ ), Eq. (8) reduces to a quadratic in  $\omega$  and describes core plasma interchange instability. With hot electrons the condition for stable interchange mode is that

$$Q^3 + R^2 \leq 0 \quad , \quad (9)$$

where

$Q = (A_1 - A_2^2/3)/3$ ,  $R = (A_1 A_2 - 3A_0)/6 - A_2^3/27$ , and the frequency at marginal stability is  $\omega = -(R^{1/3} + A_2/3)$ . In Fig. 1 we plot the stability boundary from Eq. (9) in the  $\beta_i - \beta_h$  space for the  $\delta$ -function hot electrons with the fixed parameters:  $\rho_i/L_h = \rho_i/L_i = -0.04$ ,  $L_c/L_i = 40$ ,  $\tau_h = 10^3$ ,  $\tau_e = 1$ ,  $\omega_{pi}/\Omega_i = 25$ ,  $m_i/m_e = 1837$ , and  $k_y \rho_i = 0.1$ . Within the closed stability boundary, the interchange mode is stable. The solution from Eq. (3) (denoted by exact) is also shown for comparison and our cubic dispersion relation gives amazingly good results.

We have also plotted in Fig. 1 the stability boundary from the quadratic dispersion relation<sup>2,3</sup> by neglecting the 2nd term in  $D_{em}$  in Eq. (7). The lower stability boundary (core plasma interchange mode) is a good approximation because it is mainly determined by  $D_{es} = 0$ . But the upper

#81T0130

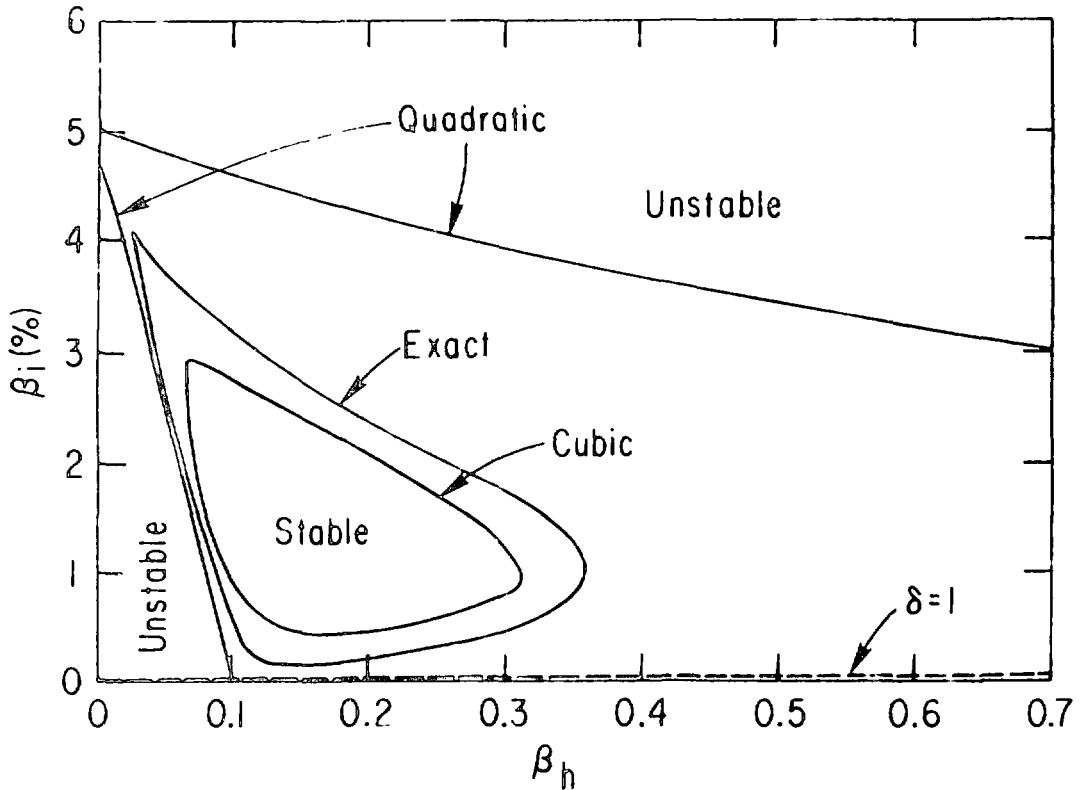


Fig. 1 Marginal interchange stability boundaries in  $\beta_i - \beta_h$  space for the  $\delta$ -function hot electron model. The fixed parameters are  $\rho_i/L_i = \rho_i/L_h = -0.04$ ,  $L_c/L_i = 40$ ,  $k_y \rho_i = 0.1$ ,  $\omega_{pi}/\Omega_i = 25$ ,  $T_h/T_i = 10^3$ ,  $T_e/T_i = 1$ , and  $m_i/m_e = 1837$ . Solutions of the quadratic, cubic, and full dispersion relations are shown for comparison. The compressional Alfvén wave is stable for the set of parameters.

stability boundary (hot electron interchange mode; unstable roughly when  $\bar{D}_{em} \gtrsim 0$ ) does not turn around at small  $\beta_i$  which is due to the absence of the  $O(\omega/\omega_{dh})$  term in  $D_{em}$ . In general, the quadratic dispersion relation predicts more optimistic results than our cubic dispersion relation. Below  $\delta = 1$  line is the forbidden region with  $N_h > N_i$ .

For the Maxwellian hot electrons, the stability boundary in  $\beta_i - \beta_h$  space is shown in Fig. 2 for the same set of parameters as in Fig. 1. Our results are very good in comparison with the solution from Eq. (3). Again stability boundary from the quadratic dispersion relation is also shown for comparison. The lower stability is good, but the upper stability boundary is again over optimistic.

Figure 3 shows that the finite Larmor radius stabilization of the low frequency interchange mode. With the same set of parameters as in Fig. 1, the stability boundaries for two different values of  $k_y \rho_i$  ( $k_y \rho_i = 0.1, 0.05$ ) are plotted in the  $\beta_i - \beta_h$  space. As  $k_y \rho_i$  is reduced the stability boundary moves toward larger  $\beta_h$  and does not intersect with the  $\beta_i$  and  $\beta_h$  axes. Therefore if  $\beta_i$  is small, no matter how large  $\beta_h$  is there is no stability.

#### IV. COMPRESSIONAL ALFVEN WAVE

Now we consider the compressional Alfvén wave with  $\omega \sim k_y v_A \sim \omega_{dh}$ , but  $\omega > \omega_c$ ,  $\omega_d$  for the warm species. Since  $(k_y v_A)^2 = (2b_1/\beta_i) \Omega_i^2$ ,  $k_y v_A$  can be of the same order as  $\Omega_i$ . Therefore, one might expect the compressional Alfvén wave to couple not only with the hot electron magnetic drifts but also with the ion cyclotron waves. In this frequency regime the three terms in the dispersion relation, Eq. (3), can be simplified to yield:

# 81T013

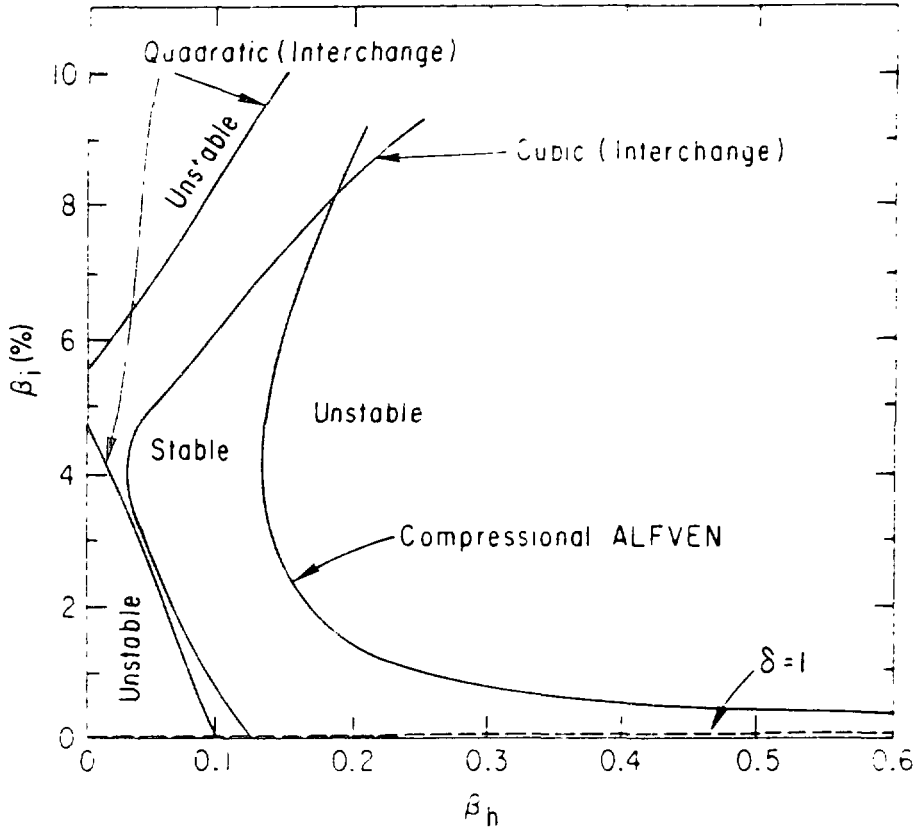


Fig. 2 Marginal stability boundaries in  $\beta_i - \beta_h$  space for the Maxwellian hot electron model. The parameters are the same as in Fig. 1. Solutions of the quadratic and cubic dispersion relations are shown for comparison. The stability window is enclosed by the interchange and the compressional Alfvén stability boundaries.

#81T0132

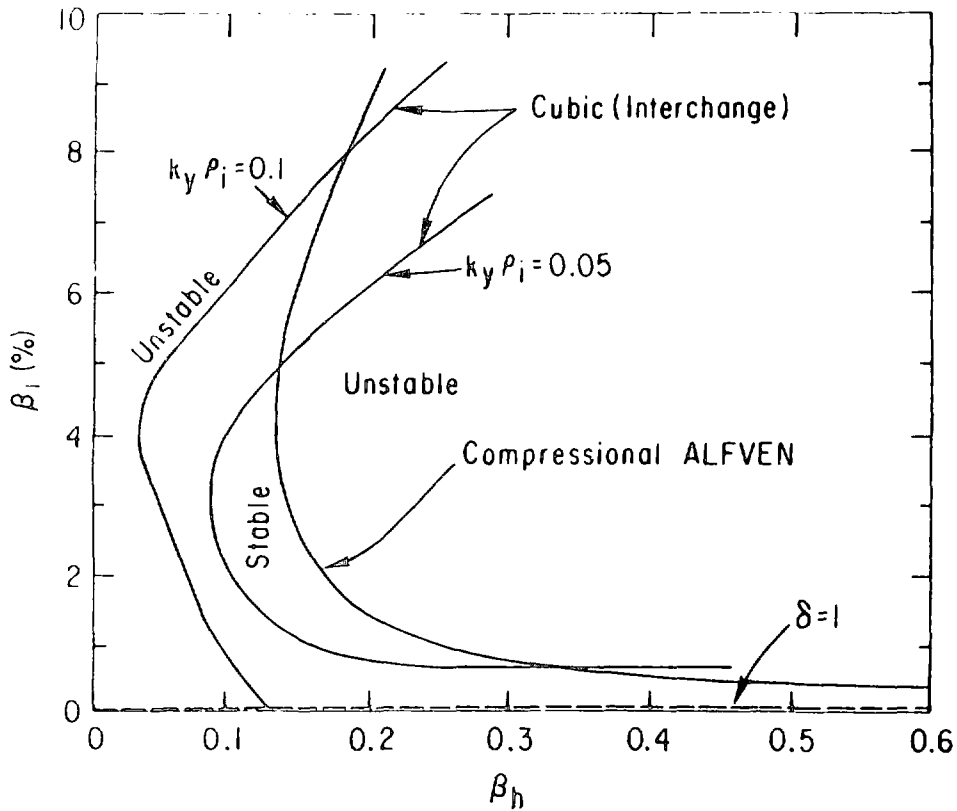


Fig. 3 Finite Larmor radius effects ( $k_y \rho_i = 0.05, 0.1$ ) on the marginal stability boundaries in  $\beta_i - \beta_h$  space for the Maxwellian hot electron model. The compressional Alfvén stability boundary is independent of  $k_y \rho_i$ . The other parameters are the same as in Fig. 1.

$$\begin{aligned}
D_{es} &\approx b_i \frac{\Omega_i^2}{\Omega_i^2 - \omega^2} , \\
D_{em} &\approx 1 + \beta_i + \beta_e + \frac{\beta_i}{2b_i} \frac{\omega^2}{(\omega^2 - \Omega_i^2)} + \hat{C}_2 \beta_h \left( \frac{\omega - \omega_{*h}}{\omega - \omega_{dh}} \right) , \\
D_{ct} &= \frac{\Omega_i^2}{\omega^2 - \Omega_i^2} + (1 - \delta) + \delta \left( \frac{\omega - \omega_{*h}}{\omega - \omega_{dh}} \right) .
\end{aligned} \tag{10}$$

And the dispersion relation becomes

$$\begin{aligned}
&\left\{ \frac{\omega^2}{\Omega_i^2} \left[ 1 + \delta (\omega_{dh} - \omega_{*h}) / (\omega - \omega_{dh}) \right] - \delta^2 \left( \frac{\omega_{dh} - \omega_{*h}}{\omega - \omega_{dh}} \right)^2 \right. \\
&\left. - \frac{2b_i}{\beta_i} \left[ 1 + \beta_i + \beta_e + \hat{C}_2 \beta_h \left( \frac{\omega - \omega_{*h}}{\omega - \omega_{dh}} \right) \right] \right\} / (\omega^2 - \Omega_i^2) = 0 .
\end{aligned} \tag{11}$$

We see that the compressional Alfvén wave decouples from the ion cyclotron waves even in the presence of hot electrons. We further note that in the limits  $\delta = 0$  and  $\beta_h = 0$  (i.e., there are no hot electrons), Eq. (11) recovers the well known compressional Alfvén wave with  $\omega^2 = k_Y^2 v_A^2 (1 + \beta_i + \beta_e)$ . The compressional Alfvén wave mainly couples with and, hence, is destabilized by the hot electron magnetic drifts and diamagnetic drift. If we also assume that

$$\delta^2 \left( \frac{\omega_{dh} - \omega_{*h}}{\omega - \omega_{dh}} \right)^2 < M_{in} \left[ 1, \left( \frac{\omega}{\Omega_i} \right)^2 \right] \tag{12}$$

Then Eq. (11) can be cast into a cubic form in  $\omega$ :

$$Z^3 + A_2 Z^2 + A_1 Z + A_0 = 0, \tag{13}$$

$$Z = (\omega/k_y \rho_i \Omega_i) ,$$

$$A_2 = - (\omega_{dh}/k_y \rho_i \Omega_i) ,$$

$$A_1 = - \frac{2}{\beta_i} (1 + \beta_i + \beta_e + \hat{C}_2 \beta_h) < 0 ,$$

$$A_0 = 2[(1 + \beta_i + \beta_e)\omega_{dh} + \hat{C}_2 \beta_h \omega_{*h}]/(k_y \rho_i \Omega_i) .$$

Since  $A_0$ ,  $A_1$ , and  $A_2$  are independent of  $k_y$ , the stability boundary is also independent of  $k_y$  but the frequency  $\omega$  is linear in  $k_y$ . From Eq. (9), the condition for stable solution is given by

$$\frac{2}{3} (C-A)B^2 + (4C^2 - 3A^2) B + 8C^3 \geq 0 , \quad (14)$$

where

$$A = \hat{C}_2 \beta_h \left(1 - 3 \frac{\omega_{*h}}{\omega_{dh}}\right) - 2(1 + \beta_i + \beta_e) ,$$

$$B = \left(\frac{\omega_{dh}}{k_y \rho_i \Omega_i}\right)^2 \beta_i > 0 ,$$

$$C = 1 + \beta_i + \beta_e + \hat{C}_2 \beta_h > 0 .$$

In general  $\omega_{*h}/\omega_{dh} < 0$  and it is possible to obtain unstable solution only when  $(C-A) = 3(1 + \beta_i + \beta_e + \hat{C}_2 \beta_h \frac{\omega_{*h}}{\omega_{dh}}) = 3 \bar{D}_{em} < 0$ . We note that this is opposite to the instability condition for hot electron interchange mode. On the other hand,  $\bar{D}_{em} > 0$  is sufficient for stable solution. Considering  $L_c/L_B \gg 1$  and  $\delta$ -function hot electrons with  $\hat{C}_2 = 1/2$ , we find

$$(C - A) \approx 3 \left[ 1 + \beta_i + \beta_e - \left( 1 + \frac{\beta_i}{\beta_h} \frac{L_h}{L_i} + \frac{\beta_e}{\beta_h} \frac{L_h}{L_e} \right)^{-1} \right] \quad (16)$$

and the compressional Alfvén wave is always stable for  $\delta$ -function hot electrons when  $L_h/L_i > 0$  and  $L_h/L_e > 0$ . This has been confirmed by numerical solutions. If  $\bar{D}_{em} < 0$ , then in the limit  $\beta_i, \beta_e \ll \beta_h$ , the stability condition, Eq. (14), can be approximately expressed as

$$\left( \frac{\tau_h \rho_i}{2L_h} \right)^2 \beta_i \beta_h^2 \leq \left( \frac{-x + (x^2 - 4y)^{1/2}}{2} \right) \quad , \quad (17)$$

where

$$x \approx \frac{2(1 + \hat{C}_2 \beta_h)^2 - \frac{3}{2} (\hat{C}_2 (\beta_h - 6) - 2)^2}{\left[ 1 + \beta_i + \beta_e - 2\hat{C}_2 \left( 1 + \frac{\beta_i}{\beta_h} \frac{L_h}{L_i} + \frac{\beta_e}{\beta_h} \frac{L_h}{L_e} \right)^{-1} \right]} > 0 \quad ,$$

and

$$y \approx 4 (1 + \hat{C}_2 \beta_h)^3 / \left[ 1 + \beta_i + \beta_e - 2\hat{C}_2 \left( 1 + \frac{\beta_i}{\beta_h} \frac{L_h}{L_i} + \frac{\beta_e}{\beta_h} \frac{L_h}{L_e} \right)^{-1} \right] < 0.$$

Note that for the Maxwellian hot electron model,  $\hat{C}_2 = 1$  and  $x$  and  $y$  are weak functions of  $\beta_i$  and  $\beta_e$  for  $\beta_i, \beta_e < \beta_h \lesssim 1$ . However, for the  $\delta$ -function hot electron model,  $\hat{C}_2 = 1/2$  and  $x$  and  $y$  become inversely proportional to  $\beta_i$  and  $\beta_e$ .

The stability boundary in  $\beta_i - \beta_h$  space for the compressional Alfvén wave from Eq. (14) is shown in Fig. 3 for the Maxwellian hot electron model with the same parameters as in Fig. 1. The approximate solutions are very good in comparison with the exact numerical solutions of the dispersion relation Eq. (3). The behavior of the stability boundary at small  $\beta_i$  can be very well explained by Eq. (17). Now the stability window is enclosed by both the interchange and the compressional Alfvén stability boundaries. As  $k_y \rho_i$

decreases the stable region shrinks mainly due to the shift of the interchange stability boundary. The compressional Alfvén stability boundary is rather insensitive to  $k_y \rho_i$  for  $k_y \rho_i \ll 1$ .

For  $\delta$ -function hot electron model, the compressional Alfvén wave may become unstable only when  $L_h/L_i < 0$  and  $L_h/L_e < 0$  and at somewhat higher  $\beta_i$  and  $\beta_h$  than the Maxwellian hot electron model case. This has been confirmed by the numerical solutions of the full dispersion relation.

## V. CONCLUSION

In this paper we have correctly analyzed the local solutions of the low frequency interchange and the compressional Alfvén instabilities of the EBT plasma in the frequency regime  $\omega \lesssim \Omega_i$ . The analytical solutions are then compared to the numerical solutions of the full dispersion relation with good agreement. These instabilities are mainly determined by the magnetic drifts and diamagnetic drift of the hot electrons. Therefore the stability boundary is very sensitive to the hot electron distribution function. Two different models of hot electron distribution function,  $\delta$ -function and isotropic Maxwellian, are employed in our analysis and yield very different results. Unlike the previously obtained quadratic dispersion relation in  $\omega$ ,<sup>2,3</sup> our simplified dispersion relations are cubic in  $\omega$  for both types of the instabilities. For the low frequency interchange mode, our cubic dispersion relation is due to an extra hot electron term of  $O(\omega/\omega_{dh})$  in the electromagnetic part of the dispersion relation,  $D_{em}$ . This term is ignored in the previous quadratic dispersion relation, but is important because at marginal stability the  $O(1)$  terms in  $D_{em}$  nearly cancel with each other and

become the same order as the  $O(\omega/\omega_{dh})$  term. The stability turns out to be more pessimistic than predicted in the previous theories.

For the compressional Alfvén wave, our cubic dispersion relation is due to the compressional term in  $D_{em}$  and is obtained in the limit  $\delta^2(\omega_{dh} - \omega_{bh})^2/(\omega - \omega_{dh})^2 < M_{in} [1, (\omega/\Omega_i)^2]$ . The stability boundary is independent of  $k_y \rho_i$  and the frequency is linear in  $k_y \rho_i$ . With  $L_h/L_i > 0$  and  $L_h/L_e > 0$ , the compressional Alfvén wave is shown to be stable for  $\delta$ -function hot electrons and can be unstable for Maxwellian hot electrons. With  $L_h/L_i < 0$  and  $L_h/L_e < 0$  the compressional Alfvén wave can be unstable for both models of hot electron distribution function.

Then the stability window of the EBT plasma is determined by both the interchange stability boundary and the compressional Alfvén stability boundary. This somewhat pessimistic result for EBT stability may be improved by a nonlocal calculation in a realistic geometry and with a proper equilibrium including anisotropic hot electron distribution and temperature gradients.

#### Acknowledgments

This work was supported by United States Department of Energy Contract No. DE-AC02-76-CHO3073 and No. W-7405-ENG-26.

## References

1. D. B. Nelson and C. L. Hedrick, *Nucl. Fusion* 19, 283 (1979).
2. D. B. Nelson, *Phys. Fluids* 23, 1850 (1980).
3. J. W. Van Dam and Y. C. Lee, in *Proceedings of the Workshop on EBT Ring Physics* (Oak Ridge National Laboratory, Oak Ridge, Tenn. 1979) Conf. 791228, p. 471.
4. R. R. Dominguez and H. L. Berk, *Phys. Fluids* 21, 827 (1978).
5. K. T. Tsang and C. Z. Cheng, *Proc. of Annual Controlled Fusion Theory Conf.* (Austin, Texas 1981) 3B24.

## 5. HIGH FREQUENCY MODES

*H. L. Berk and D. A. Spong, Session Chairmen*

## MICROSTABILITY OF THE EBT BOUNDARY

N. T. Gladd, N. A. Krall, S. Hamasaki, and J. L. Sperling

JAYCOR, P. O. Box 85154, San Diego, California 92138

We discuss two aspects of the microstability properties of the EBT boundary.

The first aspect is that the relatively sharp gradients in the core plasma of the EBT boundary may excite a variety of drift-type microinstabilities and, through their contribution to transport processes, significantly affect the gross structure of the EBT boundary. In calculating this effect, we take into account that the EBT boundary has several features (e.g., three species of plasma, a diamagnetic well, a separatrix) which may have ameliorating effects on the level of microturbulence. Specifically, we first present an analysis of the microstability properties of the EBT boundary, using local theory to focus on the effects the relativistic electrons have on low and high frequency drift waves. Essentially, we find the ring electrons to have a stabilizing effect, primarily through their contribution to strong magnetic field gradients. Next we use a more detailed nonlocal theory to analyze the effects of the diamagnetic well on the lower-hybrid-drift instability, a particularly virulent high frequency drift instability. We find that the presence of the diamagnetic well reduces this instability's rate of growth but that unstable eigenmodes persist for reasonable values of  $\beta_{\text{ring}}$  and span a significant portion of the boundary layer. We discuss the relative importance of the residual anomalous resistivity when compared to classical resistivity and classical viscosity.

The second aspect of microstability theory deals with modes driven by anisotropy rather than inhomogeneity. We present an analysis of a whistler instability of the ring electrons driven by the temperature anisotropy built up by the ECRH heating process. This kinetic instability, which persists even in the presence of cold plasma, may cause substantial scattering of ring electrons onto unconfined orbits, thus providing a large energy leakage, not previously considered, in the power balance of the ring.

## I. INTRODUCTION

All magnetic confinement geometries, by virtue of their inherent gradients in plasma density and temperature, have diamagnetic currents which may potentially excite drift-like microinstabilities. These instabilities can produce fine scaled turbulence and associated anomalous transport with serious consequences for long time plasma confinement [e.g., drift-tearing (microtearing) and/or drift modes are the likely cause of the anomalous electron thermal transport in tokamaks; the drift-cyclotron-loss-cone mode is responsible for enhanced axial losses in mirrors]. Despite the universality of the driving forces for drift-modes, they are delicate instabilities in their sensitivity to the phase-space distributions of particles and many effects (e.g., finite  $\beta$ , line tying, multiple species, magnetic shear) can either eliminate them or reduce their deleterious effects. In principle, each class of confinement geometries must be closely examined to ascertain the consequences of microinstabilities.

For the purpose of analyzing microinstabilities in the ELMO Bumpy Torus class of confinement geometries, we may divide the plasma into two parts: the central core plasma which has relatively weak gradients ( $\rho_i/L \ll 1$ , where  $\rho_i$  is the ion Larmor radius and  $L$  is a macroscopic gradient scale length) and the plasma edge or boundary layer, with much stronger gradients ( $\rho_i/L \lesssim 1$ ). Our intent here is to discuss some aspects of microinstabilities in the EBT boundary layer.

The boundary layer of EBT is a multispecies plasma consisting mostly of cool ions and electrons ( $T \sim 100$  eV) but with a smaller component ( $\sim 10\%$ ) of relativistic electrons ( $T \sim 100$  keV). Specifically, we shall discuss two

classes of microinstabilities - high frequency drift waves ( $\omega \gtrsim \omega_{ci}$ ) driven by the strong density gradients present in the cool plasma and a whistler instability of the relativistic electrons driven by temperature anisotropy. The drift waves are important because of their potential role in radial transport and because they could affect the relative fraction of cool/hot plasma - a factor crucial to the macroscopic stability of EBT.<sup>1</sup> The relativistic whistler could scatter hot electrons onto unconfined orbits and result in a serious energy drain on the relativistic electron annulus.<sup>2</sup>

## II. PROPERTIES OF THE EBT BOUNDARY LAYER

In Figure 1 we illustrate some generic features of the radial profiles of an EBT boundary layer at the midplane between two adjacent mirror field coils. The magnetic field has a characteristic dip which is the result of the diamagnetic well dug by the annulus of relativistic electrons. There is also a potential well associated with an inwardly directed ambipolar electric field. The core plasma density is relatively flat in the plasma interior but falls rapidly in the boundary layer itself. The density of annulus electrons is much lower than the core plasma density and is concentrated in the boundary layer region. Some of the characteristics of the boundary layer plasma salient to a microinstability analysis are:

- 1) strong plasma gradients ( $\rho_i/L \gtrsim .1$ )
- 2) three plasma components with different temperatures
- 3) a diamagnetic well
- 4) extreme temperature anisotropy of the relativistic electrons
- 5) nonuniformity of the ambipolar field
- 6) a background of microwave radiation
- 7) the presence of a separatrix.

In what follows, we shall use a local theory to address the effects of characteristics 1 and 2 on high frequency drift modes. We shall use a non-local theory to ascertain the consequences of a diamagnetic well, characteristic 3, on the lower hybrid drift instability - a particularly virulent high frequency drift mode. Finally, we shall use a local theory to ascertain the relativistic

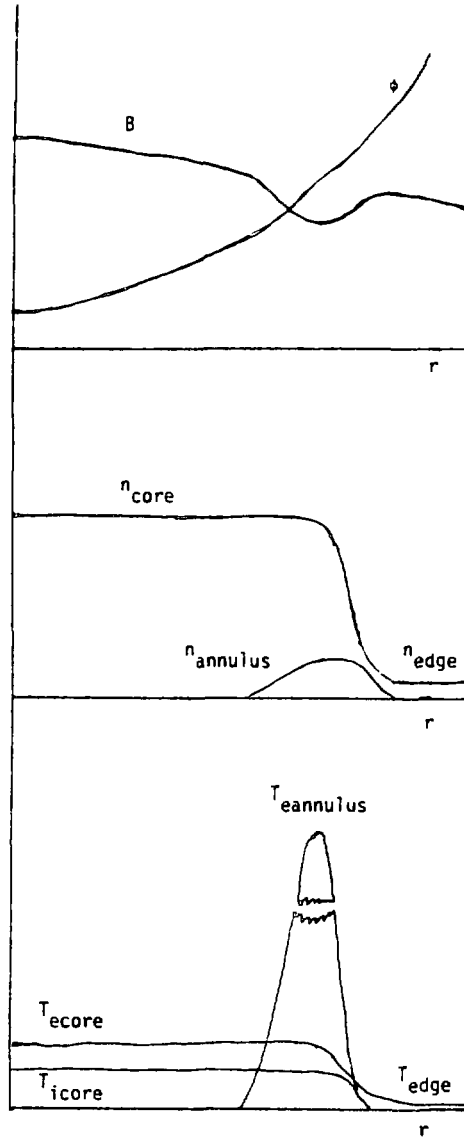


Figure 1. Generic features of radial profiles of an EBT plasma at the midplane of a mirror cell.

corrections to the whistler instability nominally expected to be driven in the temperature anisotropic electron annulus, characteristic 4. The other characteristics, while important, are not as amenable to such straightforward analysis and must await more sophisticated treatments.

### III. MICROSTABILITY OF THE CORE PLASMA

#### A. EQUILIBRIUM

Since the modes we consider are relatively short wavelength and are confined to the boundary layer region, we may neglect cylindrical and toroidal geometry effects and use a slab model as the basis of our analysis. The geometry, fields, and relevant particle drifts are illustrated in Figure 2. The constants of motion are the energy,

$$\epsilon = \frac{1}{2} m v^2 - (mg - qE)x \quad , \quad (1)$$

and the canonical momentum,

$$p_y = m(v_y + x \omega_c) \quad , \quad (2)$$

where  $\omega_c = qB/mc$  and  $g = v_{||}^2/L_c$  is used to model the inertial acceleration due to axial field curvature. We choose a distribution of the form,

$$f_0(x, \underline{v}) \sim \exp\left[-\frac{\epsilon}{T}\right] [1 + \epsilon x] \quad , \quad (3)$$

to represent the cool electrons, which are weakly inhomogeneous ( $\rho_e/L \ll 1$ ) and the form,

$$f_0(x, \underline{v}) \sim \exp\left[\frac{\epsilon - \alpha p_y}{T}\right] \quad , \quad (4)$$

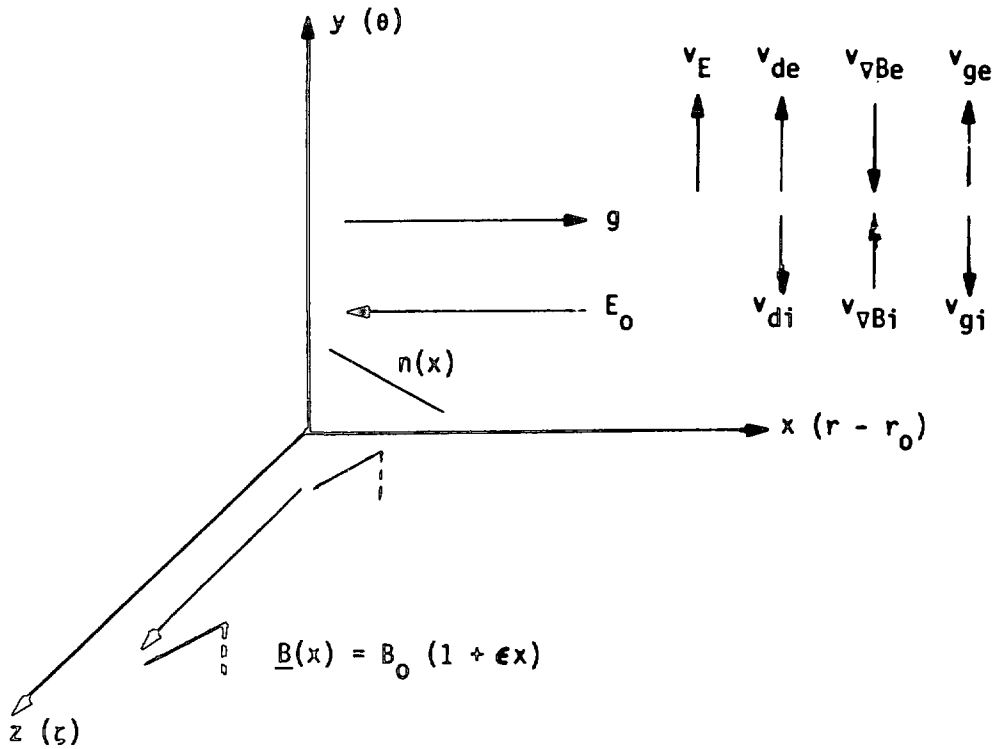


Figure 2. Slab model of boundary layer illustrating particle drifts. Region depicted has  $\nabla n \nabla B < 0$ .

to represent the cool ions and annulus electrons which may be strongly inhomogeneous ( $\rho_i/L \sim \rho_{eA}/L \lesssim 1$ ). The  $v_y$  moments of these distributions yield the diamagnetic drifts,

$$\frac{v_{Dj}}{v_i} = \frac{q_j}{|q|} \frac{T_j}{T_i} \left( \frac{1}{2} \frac{\rho_i}{L_N} - \frac{\rho_i}{L_C} \right) + \frac{v_E}{v_i} , \quad (5)$$

where  $v_i^2 = (2T_i/m_i)$ ,  $v_E = cE_0/B$  and  $\rho_i = v_i/\omega_C$ . Ampere's law yields the consistency requirement,

$$\frac{\rho_i}{L_B} = \frac{\rho_i}{L_{B0}} - \frac{\beta_{eA}}{\Delta} \left( \frac{T_i}{T_{eA}} \right) \left[ \frac{v_{Dj}}{v_i} + (1 - \Delta) \frac{v_{Dec}}{v_i} + \Delta \frac{v_{DeA}}{v_i} \right] , \quad (6)$$

where  $\beta_{eA} = 8\pi nT_{eA}/B_0^2$ ,  $\Delta$  is the relative fraction of annulus to core electrons, and  $L_{B0}$  is the field gradient (due to toroidicity) in the absence of the annulus.

Typical conditions in the EBT boundary layer suggest the scale length ordering

$$L_N \lesssim L_B \ll L_C < L_{B0} , \quad (7)$$

the temperature scaling,

$$T_{eA} \gg T_{ec} \gtrsim T_i , \quad (8)$$

and that the ambipolar field force is small with respect to the diamagnetic force of the annulus,

$$v_E \ll v_{DeA} \quad (9)$$

Under these circumstances the equilibrium is dominated by the annulus electrons and Equation (6) is well approximated by

$$\frac{\rho_i}{L_B} \approx -\frac{\beta_{eA}}{2} \frac{\rho_i}{L_N} \quad (10)$$

#### B. HIGH FREQUENCY DRIFT MODES (LOCAL ANALYSIS)

For perturbations with space-time dependencies,  $e^{-i\omega t + ik_y y}$ , we use local Vlasov analysis to write the electrostatic dispersion equation,

$$\begin{aligned} & 1 + (k_y \lambda_{Dec})^{-2} (1 - \Delta) \left[ 1 + \left( \frac{\omega - k_y v_{Dec}}{\omega} \right) F_{00}(\zeta_{ec}, a_{ec}) \right] \\ & + (k_y \lambda_{DeA})^{-2} \Delta \left[ 1 + \left( \frac{\omega - k_y v_{DeA}}{\omega} \right) F_{00}(\zeta_{eA}, a_{eA}) \right] \\ & + \chi_i(\omega, k_y) = 0 \quad , \end{aligned} \quad (11)$$

where  $\lambda_{Dj}^2 = T_j / 4\pi n q^2$ ,  $\zeta_{ej} = \omega / k_y v_{\nabla B j}$ ,  $v_{\nabla B j} = \frac{1}{2} \frac{v_j^2}{\omega_{cj}} \frac{1}{L_B} \left( \frac{v_{\perp}}{v_j} \right)^2$ ,  $a_{ej} = k_y \rho_{ej}$ , and the integral,

$$F_{00}(a, \zeta) = \int_0^{\infty} dx e^{-x} J_0^2(a \sqrt{x}) \frac{\zeta}{x - \zeta} \quad , \quad (12)$$

allows for the possibility of  $\nabla B$  resonances of the electrons. The form of (11) assumes strongly magnetized electrons in the frequency regime  $\omega \ll \omega_{ce}$ ; its derivation is detailed elsewhere.<sup>3</sup> The choice of a specific form for the

electrostatic ion response depends on the frequency regime of interest. If the density gradient is quite strong  $[(\rho_i/L) > (m_e/m_i)^{\frac{1}{2}}]$ , the ions are unmagnetized and

$$\chi_i(\omega, k_y) = (k_y \lambda_{Di})^{-2} \left[ 1 + \left( \frac{\omega - k_y v_{Di}}{k_y v_i} \right) Z \left( \frac{\omega - k_y v_{Di}}{k_y v_i} \right) \right] . \quad (13)$$

In this regime the mode of interest is the lower hybrid drift mode.<sup>4</sup> If the gradients are slightly weaker  $[(m_e/m_i)^{\frac{1}{2}} < \rho_i/L_N < (m_e/m_i)^{\frac{1}{2}}]$ , then the ions are magnetized and (for  $\omega \approx \omega_{ci}$ )

$$\chi_i(\omega, k_y) = (k_y \lambda_{Di})^{-2} \left[ 1 - \left( \frac{\omega - k_y v_{Di}}{\omega - \omega_{ci}} \right) I_0(b_i) e^{-b_i} \right] , \quad (14)$$

where  $b_i = \frac{1}{2} (k_y \rho_i)^2$ . In this case the mode of interest is the drift-cyclotron mode.<sup>5</sup> Detailed analysis of the transition between these modes has been made.<sup>6</sup>

In the absence of the hot annulus, the modes which we study typically have

$$\omega \sim k_y v_{Di} \quad , \quad k_y \rho_{ec} \sim 1 \quad , \quad (15)$$

in which case

$$\zeta_{ec} \sim 1 \quad , \quad a_{ec} \sim 1 \quad . \quad (16)$$

Therefore, for a small component of annulus electrons, we expect (because  $T_{eA} \gg T_{ec}$ )

$$\zeta_{eA} \ll 1 \quad , \quad a_{eA} \gg 1 \quad , \quad (17)$$

We may use these properties to establish that the contribution of the annulus electrons to the dispersion equation (11) is small by

$$\Delta \left( \frac{T_{ec}}{T_{eA}} \right)^{\frac{1}{2}} \quad (18)$$

with respect to the contribution of the core electrons. Key points in the argument are the highly oscillatory nature of the integrand of  $F_{00}(a, \zeta)$  when  $a \gg 1$  and the fact that the resonant contribution of  $F_{00}(a, \zeta)/\zeta$  is  $O(1)$  for  $\zeta \approx 1$ . This establishes the important result that the annulus electrons make a negligible direct contribution to the dispersion equation of high frequency drift waves. The annulus electrons, however, do make a strong indirect contribution to the growth rates of these modes. This occurs because the equilibrium relation (10) implies that the annulus electrons produce a strong magnetic field gradient. This field gradient results in an  $\nabla B$  drift of the core electrons which may resonate (in regions where  $\nabla n \nabla B < 0$ ) with the drift waves and have a strong damping effect. We now analyze the extent of this stabilizing effect. Since the pressure of the annulus electrons is substantial ( $\beta_{eA} \gtrsim .1$ ), it may reasonably be argued that the electromagnetic response of the annulus electrons must be used to determine the correct dispersion equation for these modes. We present elsewhere a detailed analysis which establishes that this is not the case.<sup>7</sup> In summary, we reiterate that the electrostatic dispersion equation for the core plasma component only is required to describe the dispersive properties of high frequency drift waves - the annulus electrons affect these modes only through their influence on the equilibrium.

### B-1. Lower Hybrid Drift Mode

In the region of a sharply inhomogeneous [ $(\rho_i/L_N > (m_e/m_i)^{\frac{1}{2}})$ ] boundary layer where  $\nabla B \nabla n < 0$ , there will be a resonance of the lower-hybrid-drift mode with core electrons undergoing  $\nabla B$  drifts. We expect this resonance to be stabilizing<sup>3</sup> and calculate here the extent to which this  $\nabla B$  effect suppresses lower-hybrid-drift activity in the boundary layer. In Figure 3 we show the maximum growth rate (with respect to  $k_y$ ) of the lower-hybrid-drift as a function of the annulus pressure,  $\beta_A$ , for different values of the plasma density gradient. The inset in Figure 3 depicts the position within the boundary layer at which the local calculation is performed. Relevant parameters are  $\omega_{pe}/\omega_{ce} = 1$  and  $T_{ec}/T_i = 1$ . From equation (10) we see that  $\beta_A$  is a measure of the magnetic field gradient. For all values of  $\rho_i/L_N$  we see a substantial reduction of the growth rate.

### B-2. Drift-Cyclotron Instability

In a boundary layer with somewhat weaker gradients [ $(m_e/m_i)^{\frac{1}{2}} \lesssim \rho_i/L_N \lesssim (m_e/m_i)^{\frac{1}{2}}$ ], the operative mode is the drift-cyclotron instability. This mode has the same negative energy character as the lower-hybrid-drift instability (although the ion response is quite different) and is also diminished by the  $\nabla B$  resonance of the electrons in regions where  $\nabla B \nabla n < 0$ .<sup>6</sup> In Figure 4 we show the maximum growth rate (with respect to  $k_y$ ) as a function of annulus pressure for different values of density gradient. Relevant parameters are  $\omega_{pe}/\omega_{ce} = 1$  and  $T_{ec}/T_i = 1$ . In the case of the drift-cyclotron mode, different cyclotron harmonics are predominantly excited for different values of density gradients. We consider a first harmonic case ( $\omega \simeq \omega_{ci}$ ,  $\rho_i/L_N = 0.15$ ) and a second harmonic case ( $\omega \simeq 2\omega_{ci}$ ,  $\rho_i/L_N \simeq 0.25$ ). In both cases, however, we again see a substantial reduction of growth rate as the field gradient becomes sharper.

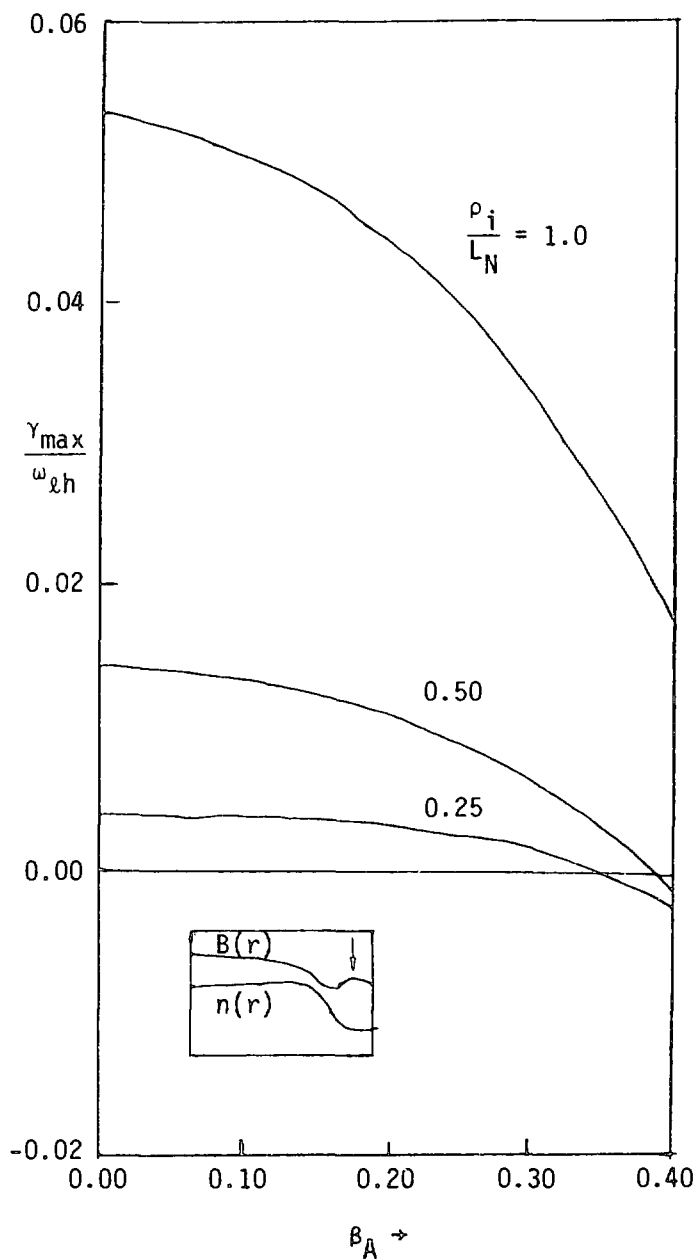


Figure 3. Lower-hybrid-drift maximum growth rates as a function of annulus pressure,  $\beta_A$ , for different density gradients,  $\rho_i/L_N$ . Inset shows the point at which the local analysis was performed.

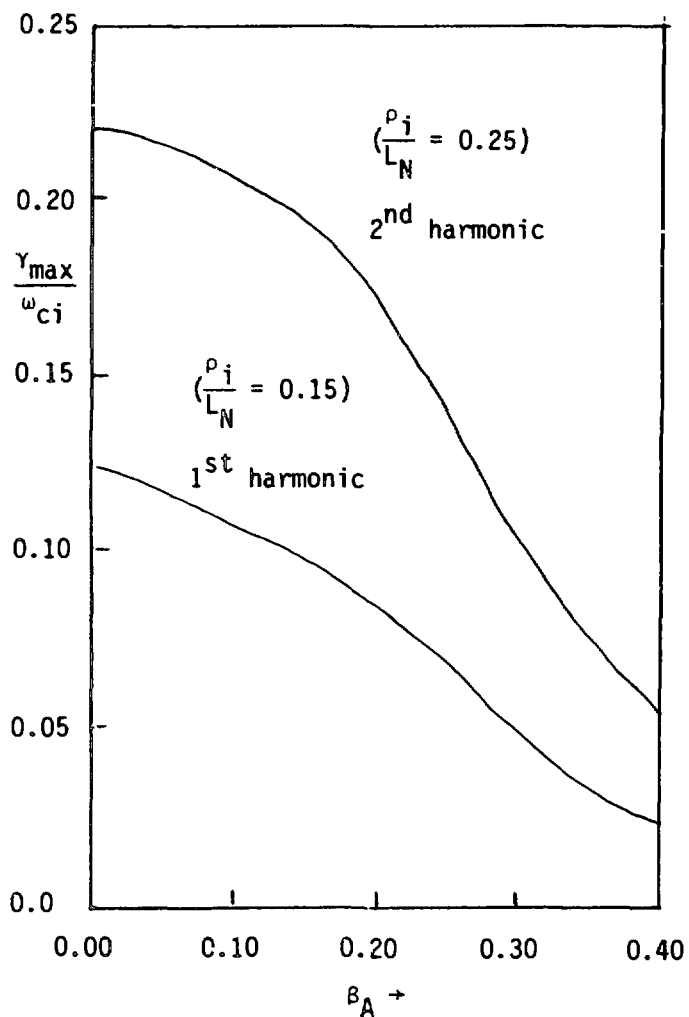


Figure 4. Drift-cyclotron maximum growth rates as a function of annulus pressure,  $\beta_A$ , for different density gradients. Different harmonics dominate in the two cases.

We only preview here some representative cases of the local theory analysis for high-frequency drift modes in EBT boundary layers. A detailed parametric survey of the stability properties of these modes in EBT will be presented elsewhere.<sup>7</sup>

### C. HIGH FREQUENCY DRIFT MODE (NONLOCAL ANALYSIS)

In the local analysis just presented, we have restricted our consideration to the region of the boundary layer where the stabilizing  $\nabla B$  resonance would be greatest, i.e., where  $\nabla B \nabla n$  was most negative. In reality, drift modes have a radial extent in the boundary layer and see different values of  $\nabla B$ . Indeed, they are resident in the diamagnetic well. To obtain a more realistic estimate of the effect of this diamagnetic well in drift modes, we must use nonlocal theory.

By standard methods we derive the nonlocal dispersion equation,

$$\left\{ - (k_y \lambda_{Di})^2 + \frac{\zeta_i}{2} [- 2 \zeta_i + (1 - 2\zeta_i^2) Z(\zeta_i)] \right. \\ \left. - \frac{1}{2} \left( \frac{T_i}{T_{ec}} \right) \left( \frac{\omega - k_y v_{Dec}}{\omega} \right) a_{ec} \frac{\partial F_{oo}}{\partial a_{ec}} \right\} \left( \frac{1}{k_y^2} \frac{\partial^2 \phi}{\partial x^2} \right) \\ + \left\{ (k_y \lambda_{Di})^2 + [1 + \zeta_i Z(\zeta_i)] \right. \\ \left. + \left( \frac{T_i}{T_{ec}} \right) \left[ 1 + \left( \frac{\omega - k_y v_{Dec}}{\omega} \right) F_{oo} \right] \right\} \phi = 0 \quad (19)$$

where  $\zeta_i = (\omega - k_y v_{Dic})/k_y v_i$ . In writing (19) we have taken the ions to be unmagnetized and hence, have restricted our nonlocal analysis to the lower-hybrid drift mode.

To proceed, we choose some representative profiles for the density and field profiles in the EBT boundary layer,

$$n(x) = n_0 \frac{[1 + \delta + \tanh(x/\lambda)]}{(2 + \delta)}, \quad (20)$$

$$B(x) = B_0 \left[ 1 - \beta_A \operatorname{sech}^2 \frac{x - x_M}{\lambda} \right]. \quad (21)$$

These profiles and their logarithmic derivatives are illustrated in Figure 5. The maximum in  $d \ln n / dx$  suggests a preferred localization point for lower-hybrid drift eigenmodes within the boundary layer. In Figure 6 we illustrate a sequence of eigenmodes ("radial") within the boundary layer for a reference case of  $B = \text{constant}$ ,  $\frac{\omega_{pe}}{\omega_{ce}} = 10$ , and  $\frac{T_{ec}}{T_i} = 1$ . The unit of distance is  $x_L = v_i / \omega_{lh} = \rho_{ec} (T_i / T_e)^{1/2}$ . It is clear that the eigenmodes span a significant portion of the boundary layer - typically the mode width is  $\sim 40 x_L \sim \rho_i$ . In addition, the growth rate of the higher order modes is not much different from the fundamental. In Figure 7 we repeat the calculation for a lower density case,  $\omega_{pe} / \omega_{ce} = 1$ , which is more representative of EBT. Interestingly, we see that the density dependence of  $\lambda_D^2$  comes in to play in localizing the modes in this case with the result that the eigenmodes are located to the inside of  $(1/n \, dn/dx)_{\max}$ .

In a nonlocal analysis, many of the effects of interest are coupled by the equilibrium requirements and it is often difficult to focus on a single effect. For example, there are two different effects if we introduce a diamagnetic well into the calculation illustrated in Figure 5. First we increase the growth rate because reducing the magnetic field strength increases the diamagnetic current (if  $1/n \, \partial n / \partial x$  is held constant). Secondly, we introduce

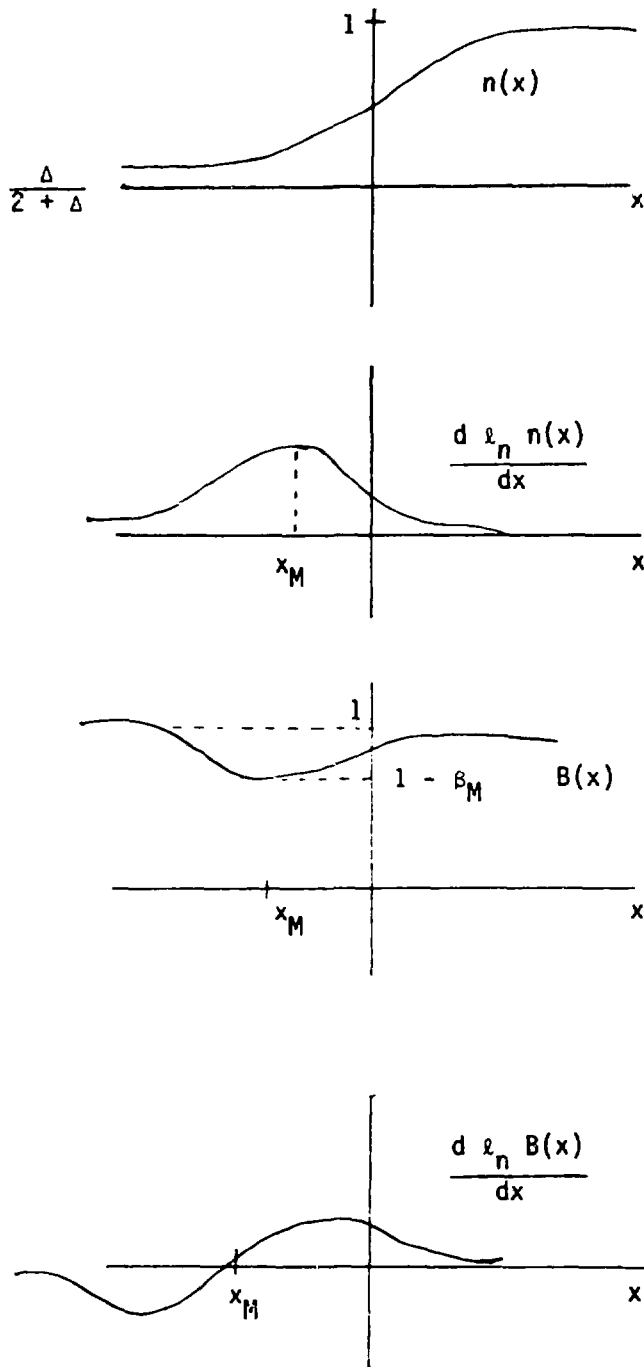


Figure 5. Model profiles of density and magnetic field for the EBT boundary layer.



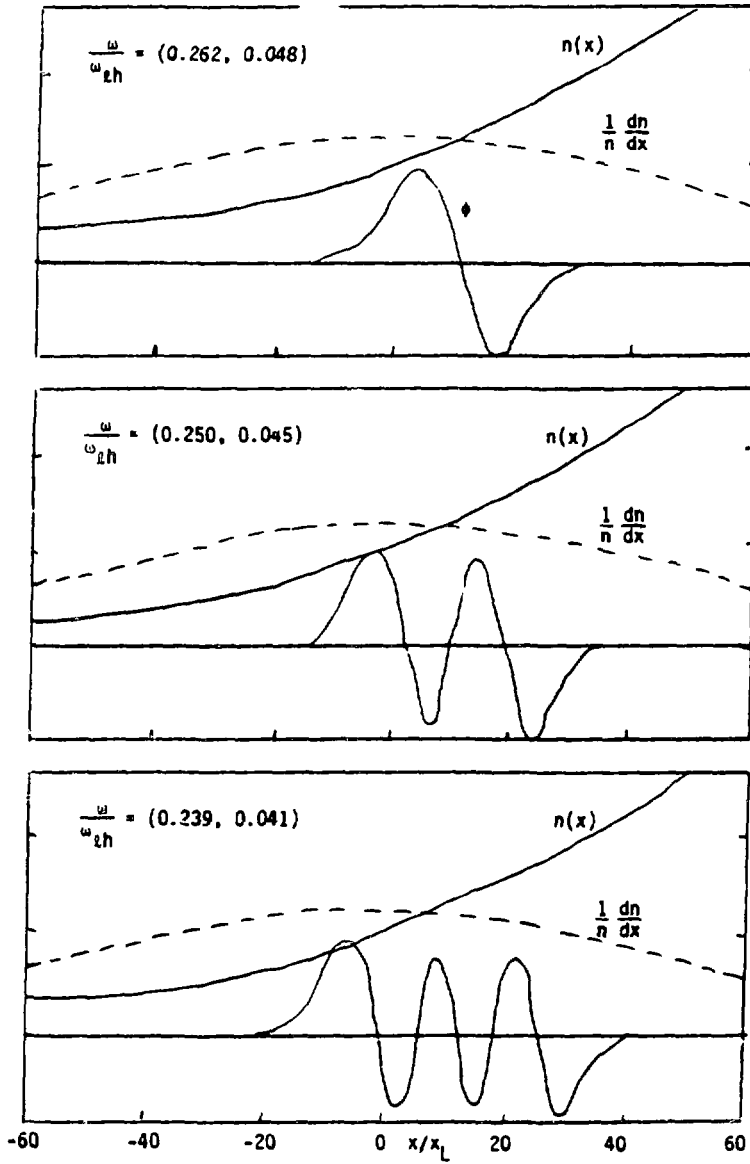


Figure 7. A sequence of lower-hybrid-drift eigenmodes low density case ( $\omega_{pe}/\omega_{ci} = 1$ ).

$\nabla B$ , the stabilizing effects of which being our focus of attention. Therefore, to isolate this second effect we show the effect of a diamagnetic well on the eigenmode illustrated in Figure 5a in two stages. In Figure 8 the well depth is increased but  $\nabla B$  effects are artificially suppressed. We thus see an increase of the growth rate as  $\beta_A$  increases. In Figure 9 we also include the  $\nabla B$  effects and see that the eigenmode is distorted (because  $\nabla B$  effects operate differently depending on the sign of  $\nabla B \nabla n$ ) and that the increase in growth rate is relatively smaller. In Figure 10, we isolate this stabilizing effect by showing the difference between the local theory maximum growth rate (calculated at  $\left. \frac{1}{n} \frac{\partial n}{\partial x} \right|_{\max}$ ) and the nonlocal maximum growth rates for the cases illustrated in Figure 8 and Figure 9.

In essence, the magnetic field gradients associated with the diamagnetic well in the EBT boundary layer are stabilizing on the lower-hybrid-drift mode but (as might be expected) not as much so as a local analysis would indicate. These results represent a first step toward understanding global profile effects on high frequency drift modes in EBT-like boundary layers. Quantitative results, valid for existing or proposed EBT devices, will require careful parametric surveys of stability properties which we defer to later work.<sup>8</sup>

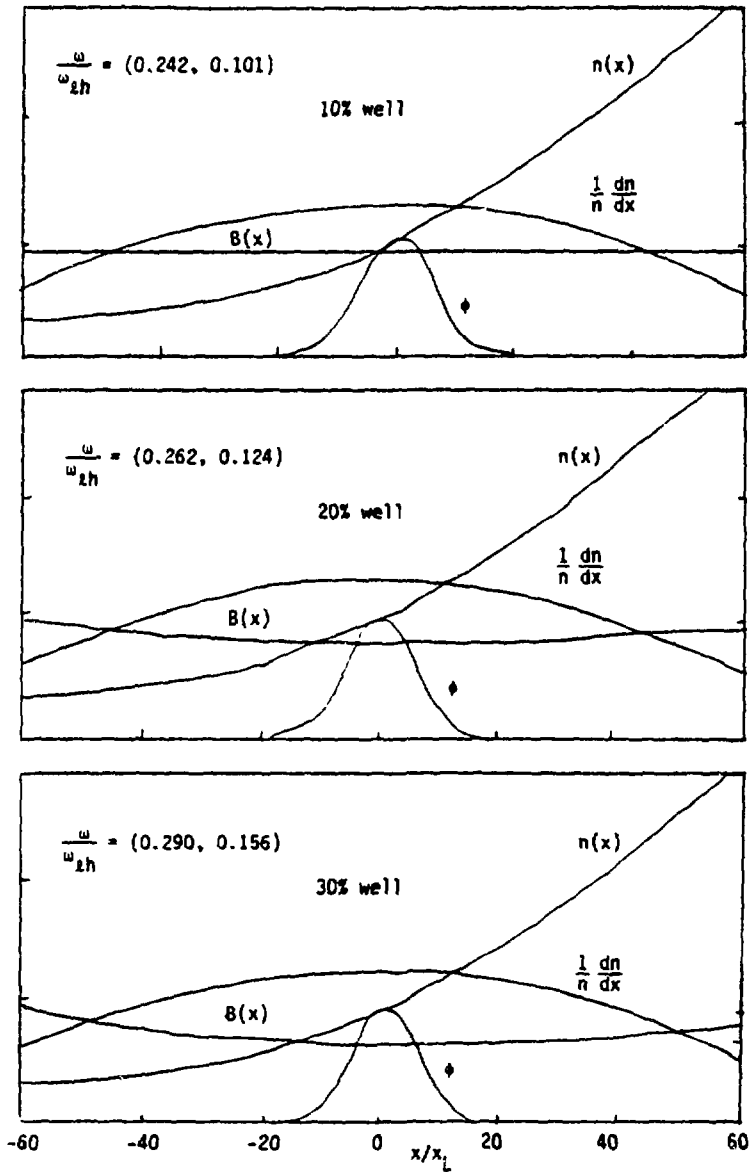


Figure 8. Effect of diamagnetic well on fundamental lower-hybrid-drift eigenmode ( $\nabla B$  effects artificially suppressed).

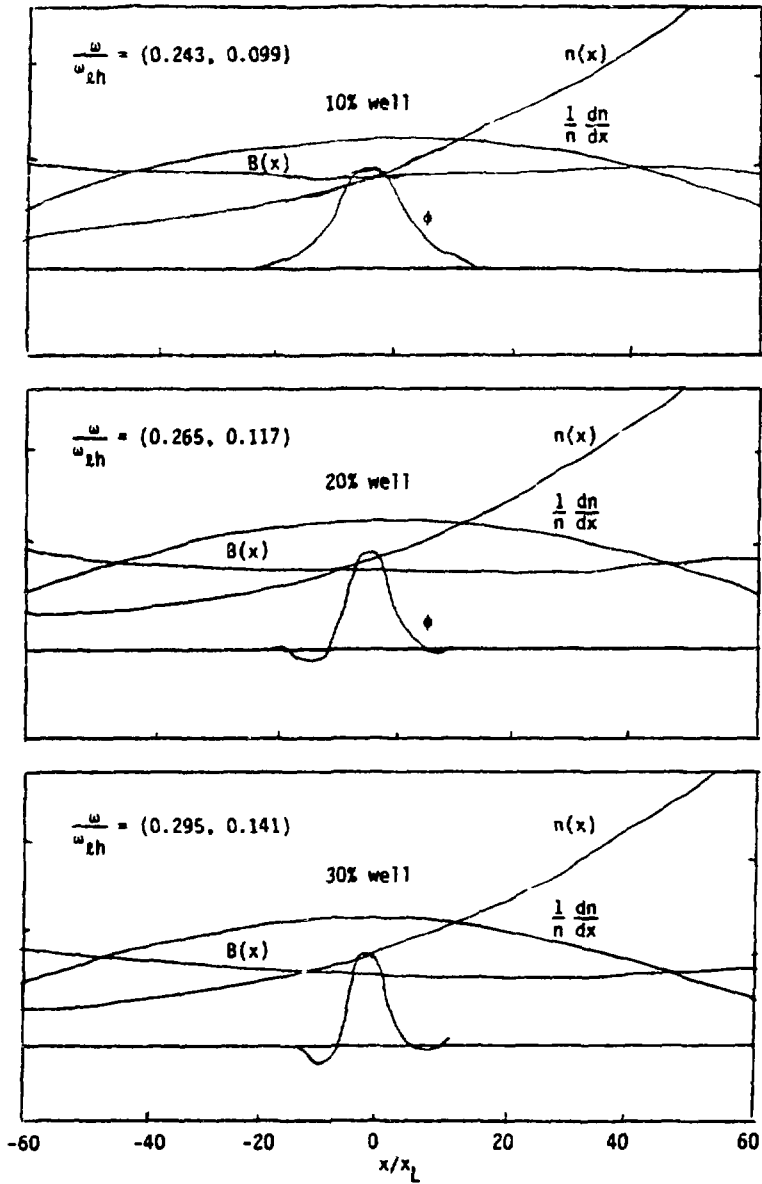


Figure 9. Effect of diamagnetic well on fundamental lower-hybrid-drift eigenmode ( $\nabla B$  effects included).

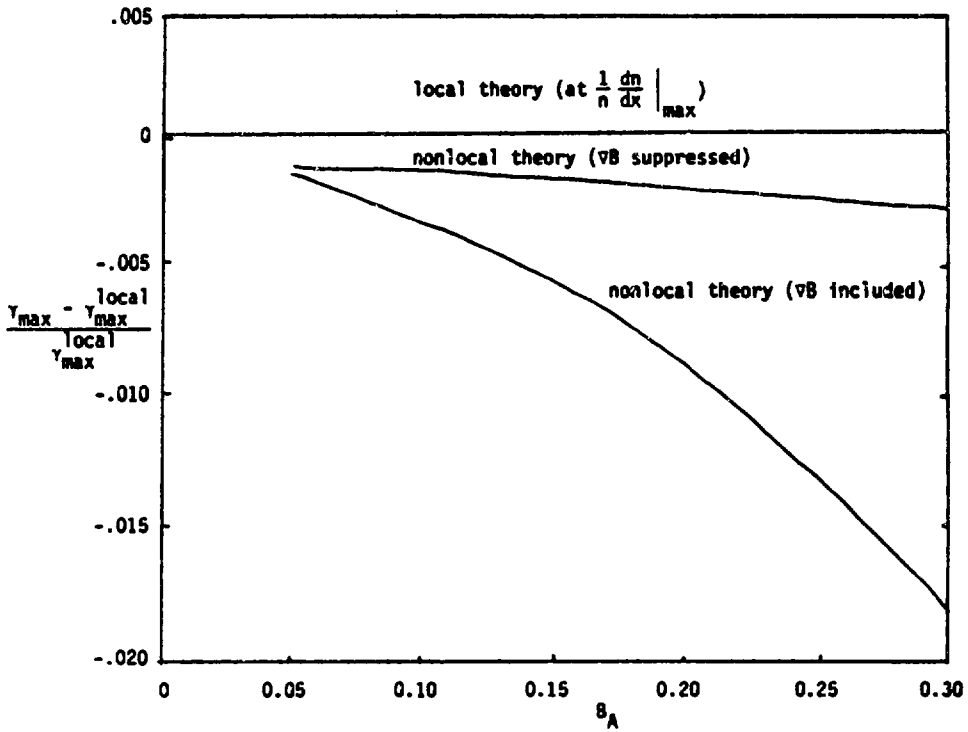


Figure 10. Comparison of local and nonlocal maximum growth rates of lower-hybrid-drift illustrating the stabilizing influence of  $vB$  effects.

#### IV. WHISTLER INSTABILITY OF THE RELATIVISTIC ELECTRON ANNULUS

In the course of a detailed study of energy loss processes from the hot electron annulus in EBT, we have concluded that although the ring temperatures are of the same order as deduced from classical loss processes (Coulomb drag and synchrotron radiation), the scaling of ring energy with magnetic field is not consistent.

Among possible loss processes is the scattering of electrons onto unconfined orbits by the fluctuating fields of various stabilities. In particular, because of the anisotropy of the ring, whistler instabilities must be considered a strong possible loss mechanism.

It has previously been shown that cold plasma background and the effect of a relativistic spread in cyclotron frequency<sup>10</sup> can be influential in suppressing whistlers. We note (nonrelativistically) that in frequency range

$$(k_{\parallel} v_{\parallel})_{\text{cold}} < \omega - \omega_{\text{ce}} < (k_{\parallel} v_{\parallel})_{\text{hot}} \quad , \quad (22)$$

an instability driven by the annulus persists, despite the cold background.

The dispersion equation, modified for relativistic effects is as follows:

$$\omega^2 - k_{\parallel}^2 c_{\parallel}^2 - \frac{\omega_{\text{pi}}^2 \omega_{\text{ci}}}{\omega + \omega_{\text{ci}}} + (1 - \Delta) \frac{\omega_{\text{pe}}^2 \omega_{\text{ce}}}{\omega - \omega_{\text{ce}}}$$

$$- 2\pi\Delta\omega p_e^2 \int_0^\infty P_\perp dP_\perp \int_{-\infty}^\infty dP_\parallel P_\perp^2 \frac{\left[ (\omega\bar{\gamma} - k_\parallel c P_\parallel) \frac{\partial f_0}{\partial P_\perp^2} + (k_\parallel c P_\parallel) \frac{\partial f_0}{\partial P_\parallel^2} \right]}{k_\parallel c P_\parallel - \omega\bar{\gamma} + \omega_{ce}} \quad (23)$$

where  $\bar{\gamma} = [1 + P_\perp^2 + P_\parallel^2]^{\frac{1}{2}}$  and  $\Delta$  is the relative fraction of hot electrons. We examine here the distribution,

$$f_0 = \left[ 4\pi\epsilon \exp(1/\epsilon) K_2(1/\epsilon) \right]^{-1} \left( \frac{T_\perp}{T_\parallel} \right)^{\frac{1}{2}} \exp \left\{ -(1/\epsilon) \left[ 1 + P_\perp^2 + \left( \frac{T_\perp}{T_\parallel} \right) P_\parallel^2 \right]^{\frac{1}{2}} \right\} \quad (24)$$

with  $\epsilon = T_\perp/m_0c^2$ , and  $K_2$  is a Bessel function.

Note that this relativistic distribution function has been chosen to reduce to the relativistic Maxwellian in the isotropic limit  $T_\perp = T_\parallel$ , and to the bi-Maxwellian in the limit  $T_\perp \neq T_\parallel$ ,  $\epsilon \ll m_0c^2$ . This distribution is appealing because of its limiting properties, but is not necessarily characteristic of the EBT ring. The character of the ring distribution is a subject of active research.

We have calculated the whistler growth rates numerically, with results shown in Figures 11 and 12. The instability persists relativistically, and the growth rates become substantial for  $T_\perp > m_0c^2$ .

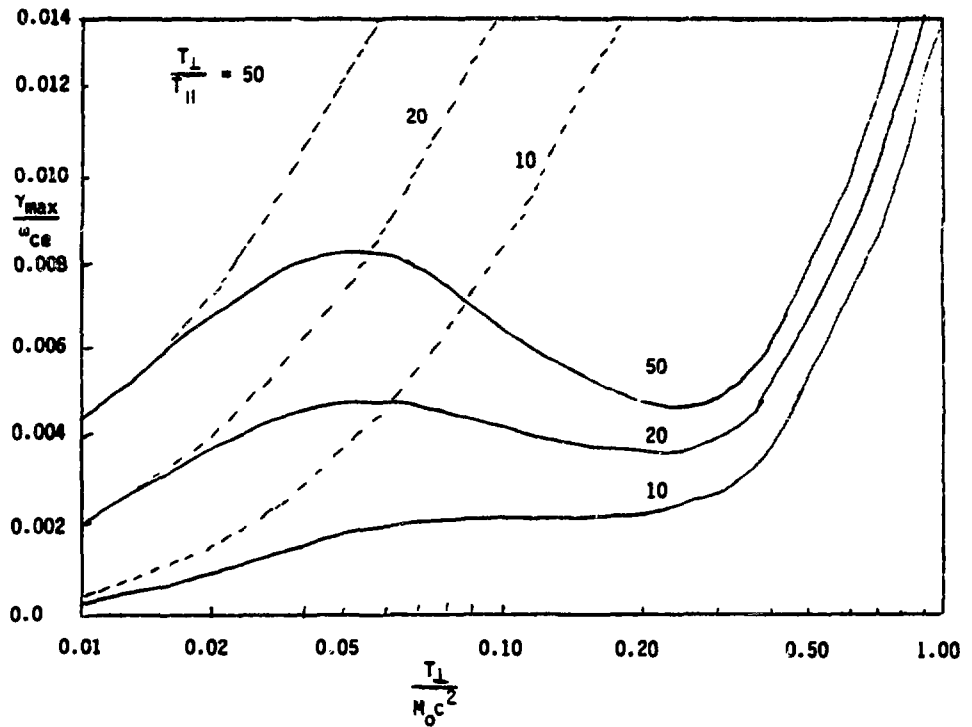


Figure 11. Growth rates for the relativistic whistler versus energy.

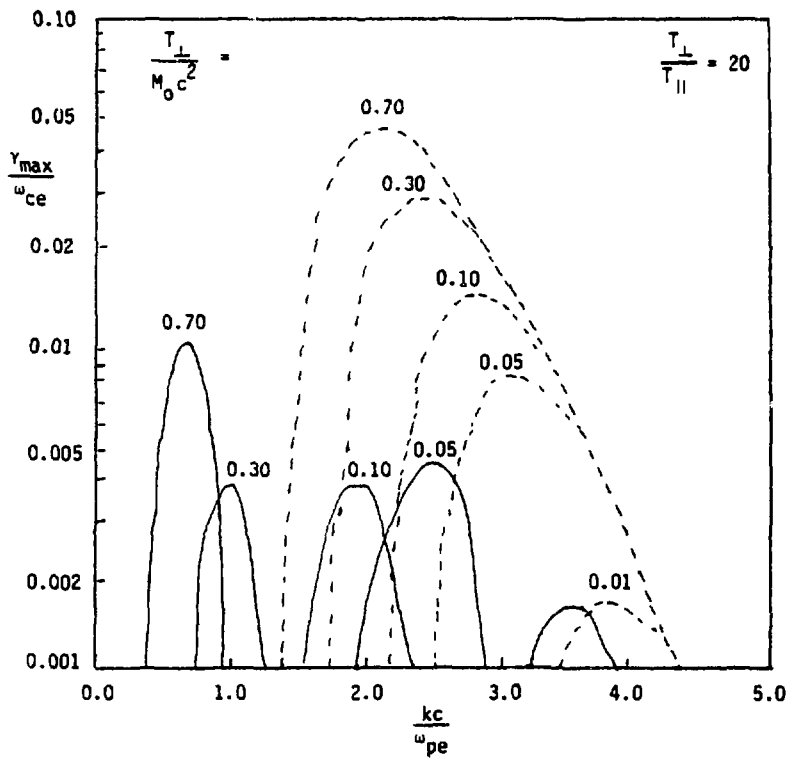


Figure 12. Growth rates for the relativistic whistler (solid lines) versus wavenumber, compared to nonrelativistic rates (dotted lines).

## REFERENCES

1. G. E. Guest, C. L. Hedrick, and D. B. Nelson, *Phys. Fluids* 18, 871 (1975).
2. S. Hamasaki, N. A. Krall, and J. L. Sperling, *Sherwood Theory Meeting*, Austin, Texas (1981).
3. R. C. Davidson, N. T. Gladd, C. S. Wu, and J. D. Huba, *Phys. Fluids* 20, 301 (1977).
4. N. A. Krall and P. C. Liewer, *Phys. Rev. A*, 2094 (1971); N. T. Gladd, *Plasma Physics* 18, 27 (1976); R. C. Davidson and N. T. Gladd, *Phys. Fluids* 18, 1327 (1975).
5. A. B. Mikhailovskii and A. V. Timofeev, *JETP* 17, 626 (1963).
6. N. T. Gladd and J. D. Huba, *Phys. Fluids* 22, 911 (1979) and references sited therein.
7. N. T. Gladd and N. A. Krall (*manuscript in preparation*).
8. N. T. Gladd and N. A. Krall (*manuscript in preparation*).
9. C. L. Hedrick, ORNL-TM-3143 (1970).
10. C. L. Hedrick, (*private communication*) Internal ORNL Report (1971).

dup

Electron-Cyclotron Resonant Heated Electron Distribution Functions\*

Y. Matsuda, W. M. Nevins, and R. H. Cohen

Lawrence Livermore National Laboratory, University of California  
Livermore, California 94550

ABSTRACT

Recent studies at Lawrence Livermore National Laboratory (LLNL) with a bounce-averaged Fokker-Planck code indicate that the energetic electron tail formed by electron-cyclotron resonant heating (ECRH) at the second harmonic is not Maxwellian. We present the results of our bounce-averaged Fokker-Planck code along with some simple analytic models of hot-electron distribution functions.

---

\*Work performed under the auspices of the U.S. Department of Energy by the Lawrence Livermore National Laboratory under Contract Number W-7405-ENG-48.

## I. INTRODUCTION

Populations of energetic, highly anisotropic electrons have been created in many experiments<sup>1-3</sup> by electron-cyclotron resonant heating (ECRH) at the second harmonic. AT LLNL we intend to maintain such a population with ECRH at the second harmonic in the thermal-barrier cell of the Tandem Mirror Experiment-Upgrade (TMX-U)<sup>4</sup> and Mirror Fusion Test Facility-B (MFTF-B) experiments.<sup>5</sup>

The stability of these hot electrons is one of our major concerns. We are particularly interested in high-frequency ( $\omega \gtrsim \Omega_{ce}$ ) electron instabilities. Stability to these modes depends on the form of the electron distribution function. Guest and Sigmar<sup>6</sup> have studied these modes extensively, using various functional forms to model the hot-electron distributions. Hence, any effort to improve upon their previous work requires a more realistic model of the hot-electron distribution function.

In Sec. II we describe a bounce-averaged Fokker-Planck code<sup>7-9</sup> that we have developed to study the evolution of the electron distribution function under the influence of both ECRH and binary collisions. Although we are primarily interested in mirror experiments, we believe that such a code would be a useful tool for studying the hot-electron distribution function in both the Elmo Bumpy Torus (EBT) and Nagoyo Bumpy Torus (NBT) devices.

The steady-state electron distribution function obtained from the bounce-averaged Fokker-Planck code is discussed in Sec. III. We find that this distribution departs significantly from a Maxwellian.

The high-energy tail on the electron distribution function falls off as  $f \sim E^{-5/6}$ , where  $E$  is the kinetic energy. A simple theoretical model that explains this falloff at high energies, and other features of the Fokker-Planck electron distribution is presented in Sec. IV.

## II. THE BOUNCE-AVERAGED FOKKER-PLANCK CODE

A bounce-averaged Fokker-Planck code solves for the distribution function along a single magnetic field line. Bounce-averaged formalism<sup>7-9</sup> assumes that the bounce frequency of a trapped particle  $\omega_T$  is large compared to both the collision frequency  $\nu_C$ , and the heating rate resulting from interaction with the applied microwaves  $\nu_{rf}$ . Within this limit the distribution function depends only on  $\mathcal{E}$  (the particle energy) and  $\mu$  (the magnetic moment).

Our present code assumes that the plasma is confined in a symmetric magnetic mirror. The distribution function can then be written as a function of  $v_0$  and  $\theta_0$ , where  $v_0$  and  $\theta_0$  are the values of a particle's speed and pitch angle when it passes the midplane of the mirror cell. Bernstein and Baxter<sup>9</sup> have presented a comprehensive treatment of the bounce-averaged formalism, including both binary collisions and ECRH. Our code is based on this formalism.

The basic model is shown schematically in Fig. 1. The magnetic field  $B$  has a minimum at  $z = 0$  and a parabolic variation; i.e.,  $B = B_0 (1 + Rz^2/L^2)$ , where  $R$  is the mirror ratio. In general, there can also be an ambipolar potential. In this talk we will only consider runs in which this potential vanishes.

The passing particles only transit the system once in a time  $\omega_T^{-1}$  -- short compared to the time-scale of collisions ( $\nu_C^{-1}$ ) or ECRH ( $\nu_{rf}^{-1}$ ). Hence, the passing-particle distribution function may be specified as a boundary condition. Although the bounce-averaged Fokker-Planck code does not evolve the passing-particle distribution function, collisions between trapped and passing particles are important. These collisions are retained in our code.

We consider the situation in which the microwave frequency  $\omega$  is slightly greater than twice the electron-cyclotron frequency at  $z = 0$ ,  $\Omega_{ce}(0)$ . In this case there is a second harmonic resonance near the bottom of the magnetic well, where  $\omega = 2\Omega_{ce}(z_2)$ , and a first harmonic resonance further up the magnetic well, where  $\omega = \Omega_{ce}(z_1)$  (see Fig. 1).

In this talk we restrict our attention to perpendicular incidence of the microwave heating field (i.e.,  $k_{\parallel} = 0$ ). The trapped particles then experience a jump in their instantaneous perpendicular velocity each time they pass through a resonance on their bounce orbit. When these jumps are small and uncorrelated, the action of ECRH on the trapped particle distribution can be described by a diffusion operator.

Because the bounce orbits of some particles never reach the resonant points  $z_1$  and  $z_2$ , these particles do not strongly interact with the heating field. Figure 2 shows phase space at the magnetic-field minimum. Particles that lie above the line labeled "second harmonic" (region III) turn before they reach the second harmonic resonance point  $z_2$ . Hence, that part of the electron distribution function in region III evolves only due to collisions.

Particles that lie above the fundamental line turn before they reach the fundamental resonance point  $z_1$ , so that particles that lie in region II interact only with the second harmonic resonance. Those particles that lie between the fundamental line and the loss cone boundary (region I) interact with both the fundamental and second harmonic resonances.

It is necessary to provide a boundary condition in solving the Fokker-Planck equation in the trapped region of phase space. The value of the distribution function  $f$  at the loss boundary is determined by the distribution of passing particles. At  $\theta_0 = \pi/2$  we require regularity of the distribution

function. The problem is closed by specifying the behavior of  $f$  at large velocity. We have chosen to set  $f = 0$  along the arc  $v_0 = v_{\max}$ .

Although this boundary condition was originally chosen for convenience, we note that it models an important effect that is not otherwise taken into account by our code: namely, the nonadiabatic scattering of high-energy electrons as they pass the magnetic field minimum.<sup>10</sup> At very high energies electrons will be rapidly scattered in pitch angle. In mirror machines these electrons soon enter the loss cone and are lost out the end, while in EBT's they scatter onto an unconfined drift orbit and are lost to the wall. We find that this loss mechanism is very important in the power balance of the hot electrons.

### III. ECRH DISTRIBUTION FUNCTIONS

Our bounce-averaged code follows the evolution of the electron distribution function in time. Initially, the loss cone is filled by a cold ( $T_e = 17$  eV) plasma stream with a density  $N_e = 10^{10}$  cm<sup>-3</sup> at the mirror throat, while the trapped region is empty. The temperature and density of this cold stream is kept constant throughout the run. This scenario is motivated by the experimental plan in TMX-U, where the hot-electron plasma in the end cells will be built up from a stream of cold plasma that flows from the center cell into the end cells. However, this stream of cold electrons may be viewed as a model for the cold population of electrons created by ionization of neutral gas in EBT<sup>3</sup> and other experiments<sup>1,2</sup> in which hot electron plasmas have been created.

The parameters for the computer runs that we discuss in this section were chosen to model the Symmetric Tandem Mirror (STM) experiment<sup>2</sup> at TRW, Inc. The magnetic field parameters are  $B_0 = 1.75$  kG,  $R = 3$ , and  $L = 35$  cm;

the effects of finite  $\beta$  depression are not included. The microwave frequency is 10 GHz and the electric field of the right-hand, circularly polarized component is taken to be 10 V/cm. Early in these computer runs we saw a buildup of energetic electrons from the cold-electron population in the loss cone. After less than one second, a steady state is reached. We say that a steady state has been attained when  $(1/n) \partial n / \partial t, (1/E) \partial E / \partial t \leq 0.1 \text{ s}^{-1}$ . Figure 3 shows a contour plot of the steady-state electron distribution function obtained when only the diffusion due to the fundamental resonance is retained. The contours are spaced logarithmically; i.e., the value of the distribution function decreases by a factor of 0.58 as you move from one contour to the next.

The fundamental resonance line delimits regions in which the behavior at the distribution function is very different. Below this line in region I, where both ECRH and collisions act on the distribution function, there are strong variations of the distribution function with pitch angle. Above the fundamental resonance line, where the distribution function evolves only due to collisions, the variation of the distribution function with  $\theta_0$  is much weaker.

We can understand the shape of these contours by noting that as particles are heated by the rf component, the perpendicular velocity of their resonant point along the magnetic field increases. This tends to move their turning point in towards the resonant point. In  $(v_{\perp 0}, v_{\parallel 0})$  space the particle is drawn along a hyperbola,

$$v_{\parallel 0}^2 - \left( \frac{\omega}{\Omega_{ce}(0)} - 1 \right) v_{\perp 0}^2 = \text{const} \quad (1)$$

that asymptotes to the fundamental resonance line. As a first approximation, the diffusion due to the ECRH tends to flatten the distribution function along each of the family of hyperbolas defined by Eq. (1). Strong variations in  $f$  occur as you move from one hyperbola to the next. At large  $v_0$ , small variations in pitch angle move you rapidly from one hyperbola to another. Hence, we expect strong gradients of the distribution function in pitch angle below the fundamental resonance line.

Above the fundamental resonance line only binary collisions affect the distribution function. If we were to ignore drag and retain only pitch-angle scattering, then the contours would be segments of arcs centered at  $v_0 = 0$ . For energetic electrons the drag and pitch-angle scattering terms are of the same order. Hence, when drag is included (as it was in our computer runs) we expect the contours to be drawn down somewhat from these arcs like those contours in the region above the fundamental resonance line of Figure 3.

We also considered the combined effect of fundamental and second harmonic heating. Figure 4 shows a contour plot of the electron distribution function when the diffusion from both the first and second harmonic resonances is included. In this run we chose the perpendicular wave number  $k_{\perp} = 4 \text{ cm}^{-1}$ . Three regions of plane phase space are delimited by the fundamental and second harmonic resonance lines. Below the fundamental resonance line (i.e., region I), the distribution function has strong gradients in pitch angle. This behavior is similar to that seen in Fig. 3.

Between the first and second harmonic lines (i.e., region II), the contours of constant phase space density tend to follow the characteristics of the second-harmonic diffusion operation. These characteristics are the hyperbolas

$$v_{\parallel 0}^2 - \left( \frac{\omega}{2\Omega_{ce}(0)} - 1 \right) v_{\perp 0}^2 = \text{const} \quad . \quad (2)$$

In the region above the second-harmonic resonance line, the evolution of the distribution function is due to collision. We would expect the steady-state distribution to vary only weakly with pitch angle in region III. For the parameters of this computer run, the collision frequency is very small for electrons in the tail of the distribution function ( $\tau_c \simeq 1.5$  s at  $v_0 = 10^{10}$  cm/s). Hence, the electron distribution function has not yet reached a steady state in the region above the second-harmonic resonance line.

Figure 4 is instructive because it illustrates the patterns of flow in phase space. The strong gradients of the distribution function in pitch angle near, but slightly above, the second-harmonic resonance line indicate that there is a flux of high-energy electrons into the region above this resonance line. Hence, energetic electrons are first spun up along the diffusion characteristics below the second-harmonic resonance line. Most are lost out the boundary at  $v_0 = v_{\text{max}}$ , i.e., lost due to nonadiabatic scattering.<sup>10</sup> Some energetic electrons pitch-angle scatter into the region above the second-harmonic resonant line where collisions with low-energy electrons slowly drag them down in energy.

Figure 5 shows a plot of the electron distribution vs energy along the second-harmonic resonance line. We have used a log-log scale so that straight lines correspond to power laws. On such log-log scales Maxwellians have downward curvature at all energies.

At low energies ( $E \lesssim 100$  eV) the distribution function is well fit by a Maxwellian with a temperature of about 30 eV. At intermediate energies ( $100 \text{ eV} < E < 5 \text{ keV}$ ) there is a marked departure from a Maxwellian. In this

energy range the distribution function falls off as  $E^{-3/2}$ . Other Fokker-Planck runs indicate that this falloff is characteristic of first harmonic heating. At higher energies ( $E > 5$  keV) we see a tail that falls off as  $E^{-5/6}$ . In the next section we show how much of this behavior can be understood from a relatively simple theoretical model.

#### IV. THEORETICAL CONSIDERATIONS

An important first step in developing a theory to describe the ECRH distribution function is to determine the relative magnitudes of the rf and collisional diffusion in each region of phase space. The collisional diffusion decreases with energy, while the rf diffusion is either approximately independent of energy (at the fundamental), or else is an increasing function of the particle energy (at the second harmonic). Hence, the microwave heating always dominates collisions at high energies.

We can estimate the energy at which microwave heating begins to dominate collisional effects by first equating heating rate  $\nu_{rf}(E)$  to the collision frequency  $\nu_c(E)$  and then solving for  $E$ . The rate at which microwave heating increases a particle's energy can be estimated as

$$\nu_{rf} \simeq \frac{1}{E} \left. \left( \frac{dE}{dt} \right) \right|_{rf} \simeq \frac{1}{v^2} \frac{\langle \Delta v^2 \rangle}{t} \simeq \frac{D_{rf}}{v^2} \quad (3)$$

where  $D_{rf}$  is the rf diffusion coefficient. These coefficients have been calculated, for example, by Bernstein and Baxter.<sup>9</sup>

In region I of phase space fundamental heating is competing with binary collisions. We have found that the fundamental heating will dominate pitch angle scattering out of region I for energies greater than

$$E_1 \simeq 10 \left( \frac{n_{11} B}{\Delta\theta^2 \epsilon^2} \right)^2 \text{ keV} \quad (4)$$

where  $\Delta\theta$  is the angle between the fundamental resonance line and the loss cone,  $\epsilon$  is the amplitude of the heating field in V/cm,  $B$  is the magnitude of the magnetic field in kG, and  $n_{11}$  is the cold electron density in units of  $10^{11}/\text{cm}^3$ . For the parameters of our runs, we find  $E_1 \simeq 0.1$  keV.

At energies greater than  $E_1$ , the electrons should "run away" to form a high-energy tail on the distribution function. In Fig. 5 we see significant departures from a cold Maxwellian at energies above  $E_1$ .

In region II of phase space, only second harmonic heating is competing with collisions. Particles in region II do not see the fundamental resonance so the second harmonic diffusion does not compete with first harmonic diffusion in region II. This is an important point since first harmonic diffusion is much larger (for nonrelativistic particles), and it would mask the effects of second harmonic heating if it were present in region II. We find that second harmonic heating dominates collisional drag for energies greater than

$$E_2 \simeq 70 \left( \frac{n_{11} B}{\epsilon^2} \right)^{2/3} \text{ keV} \quad (5)$$

Inserting parameters appropriate to our computer runs, we find  $E_2 \simeq 10$  keV. Turning back to Fig. 5, we see that there is a pronounced break in the slope of the distribution function in the neighborhood of  $E_2$ . In fact, we find that  $f \sim E^{-3/2}$  for  $E_1 < E \lesssim E_2$  and  $f \sim E^{-5/6}$  for  $E_2 \lesssim E < E_{\text{max}} = 1/2 m v_{\text{max}}^2$ .

At very high energies we can make a good approximation by ignoring collisional effects in calculating the form of the distribution function. The

steady-state distribution functions are then determined by the one-dimensional equation

$$\frac{1}{v_{\perp}} \frac{\partial}{\partial v_{\perp}} v_{\perp} D \frac{\partial}{\partial v_{\perp}} f = 0 \quad , \quad (6)$$

where  $v_{\perp}$  is the perpendicular velocity at the resonant point, and  $D$  is the rf diffusion coefficient. The solution to Eq. (6) that obeys the boundary condition  $f(v_{\max}) = 0$  is

$$f = A \int_{v_{\perp}}^{v_{\max}} \frac{dv_{\perp}}{v_{\perp} D(v_{\perp})} \quad (7)$$

We noted previously that particles that are strongly heated by the microwaves tend to turn near their resonant point. In this region of phase space,  $D(v_{\perp})$  is proportional to  $v_{\perp}^{5/3}$  for second harmonic heating.<sup>9</sup>

Hence, we find

$$f(v_{\perp}) \sim \left( \frac{1}{v_{\perp}^{5/3}} - \frac{1}{v_{\max}^{5/3}} \right) \quad , \quad (8)$$

or

$$f(E) \sim \left( \frac{1}{E^{5/6}} - \frac{1}{E_{\max}^{5/6}} \right) \quad . \quad (9)$$

Note that this theoretical model is in excellent agreement with the result of the Fokker-Planck code in the interval  $E_2 < E < E_{\max}$  (see Fig. 5).

We attempted a similar calculation involving first harmonic heating in an effort to explain the variations of the distribution function with  $E$  in the

interval  $E_1 < E < E_2$ . The agreement between the calculation [which yielded  $f(E) \sim E^{+1/3}$ ] and the Fokker-Planck run was poor. We attribute this to pitch-angle scattering, which is able to compete with first harmonic heating in a narrow boundary layer near the first-harmonic resonance line. When this is the case, it is necessary to solve a two-dimensional problem (in  $v_0$  and  $\theta_0$ ) in order to determine the variation of  $f$  with  $E$  in the range  $E_1 < E < E_2$ . This work is in progress.

## V. SUMMARY

We have found a bounce-averaged Fokker-Planck code to be a useful tool in studying the electron distribution functions produced by ECRH. Although we have focused primarily on mirror-confined electrons in our work, we believe that a bounce-averaged Fokker-Planck code would be very useful in studying the electron distributions in Bumpy Tori as well. Such a code would be useful in analyzing both the stability and the power balance of the hot electron rings.

We have begun a theoretical study of the ECRH distribution function. We now understand many features of the electron distribution functions that have been obtained numerically. More work is needed to understand the variation of the electron distribution function in the intermediate energy range where first harmonic heating dominates. This work is in progress.

In addition, new effects must be added to our model, including relativistic electron dynamics, finite parallel wave numbers, finite  $\beta$ , and variations in the ambipolar potential along the magnetic field. These effects will be included in a new Fokker-Planck code that is currently being developed.

## REFERENCES

1. W. B. Ard et al., in Plasma Phys. and Cont. Nucl. Fusion Res., (Proc. 4th Int. Conf. Madison, 1971), Vol. II, IAEA, Vienna (1971) 619.
2. N. H. Lazar et al., Bull. Am. Phys. 25, 993 (1980); B. H. Quon et al., Bull. Am. Phys. 25, 994, (1980) and R. F. Wuerker et al., Bull. Am. Phys. 25, 994 (1980).
3. R. A. Dandl et al., in Plasma Phys. and Cont. Nucl. Fusion Res. (Proc. 7th Int. Conf. Innsbruck, 1978), Vol. II, IAEA, Vienna (1979) 365.
4. F. H. Coensgen et al., TMX Upgrade Major Project Proposal, Lawrence Livermore National Laboratory, Livermore, CA., LLL-PROP-172 (1980).
5. D. E. Baldwin, B. G. Logan, and T. C. Simonen, Editors, Physics Basis for MFTF-B, Lawrence Livermore National Laboratory, Livermore, CA., UCID-18496 (1980).
6. G. E. Guest and D. J. Sigmar, Nucl. Fusion 11, 151 (1971).
7. K. D. Marx, Phys. Fluids 13, 1355 (1970).
8. T. A. Cutler, L. D. Pearlstein, and M. B. Rensink, "Computation of the Bounce-Average Code," Lawrence Livermore National Laboratory, Livermore, CA., UCRL-52233 (1977).
9. I. B. Bernstein and D. C. Baxter, Phys. Fluids 24, 108 (1980).
10. R. Cohen, in Intrinsic Stochasticity in Plasmas, (Proc. Int. Workshop on Intrinsic Stochasticity in Plasmas, Corse, France, 1979) edited by G. Laval and D. Gresillon, Editions de Physique, Orsay (1979), 181.

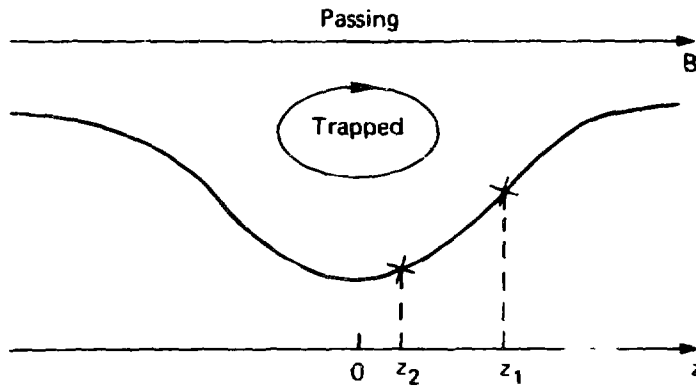


Fig. 1. Sketch of passing and trapped particle orbits, and magnetic-field strength  $B$ . The fundamental and second harmonic resonance points are labeled as  $z_1$  and  $z_2$ , respectively.

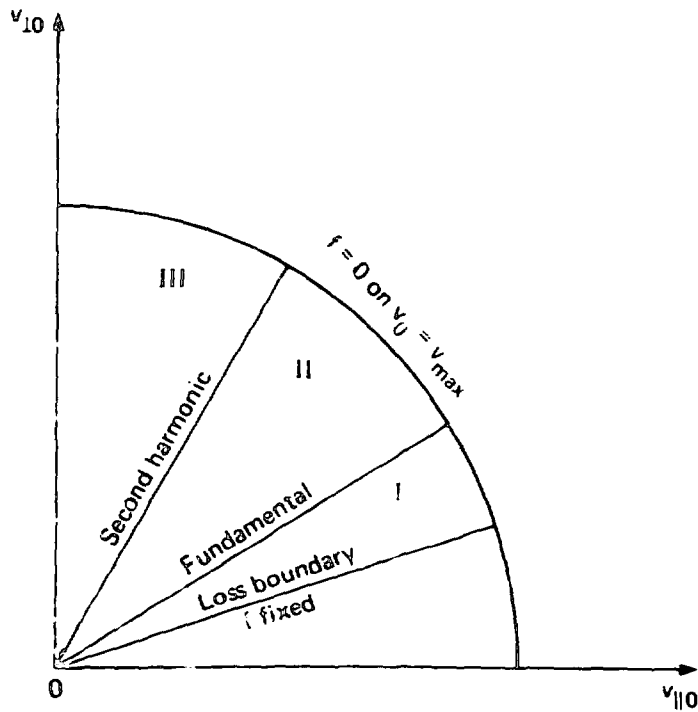


Fig. 2. Phase space at magnetic-field minimum.

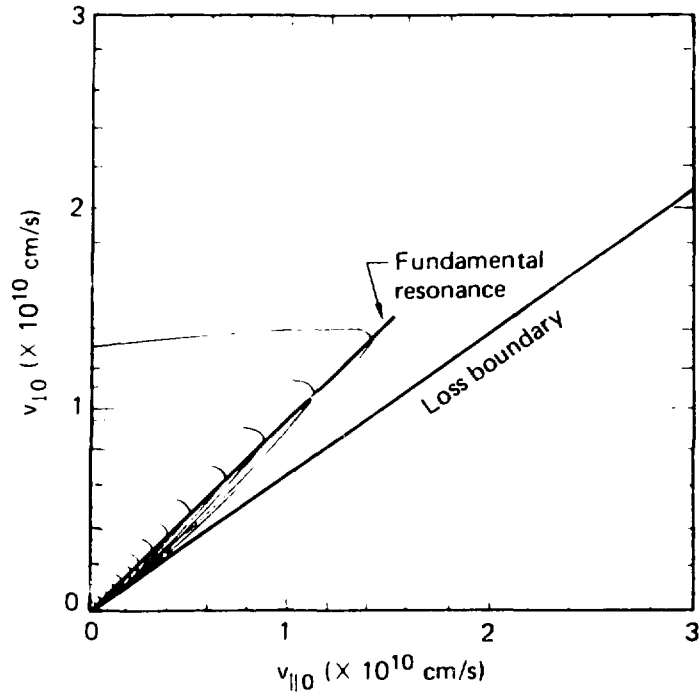


Fig. 3. Steady-state distribution function (fundamental heating only).

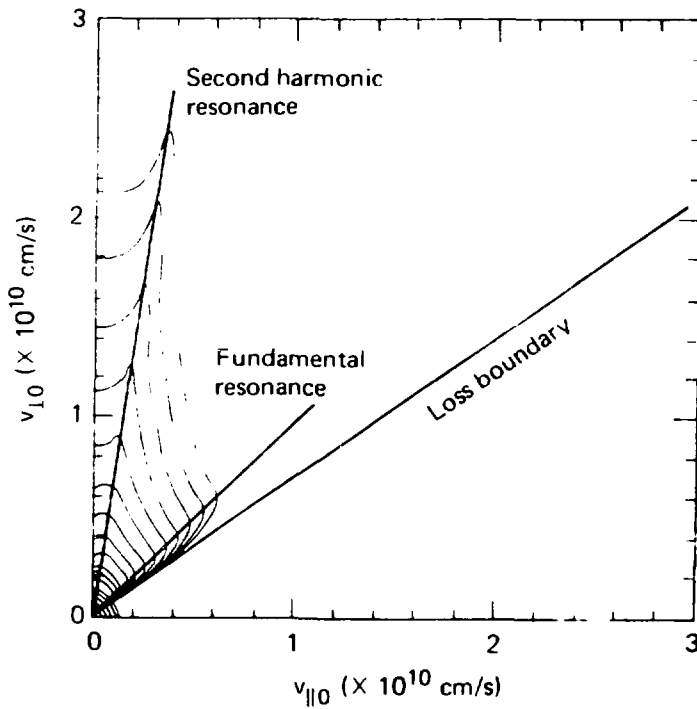


Fig. 4. Steady-state distribution function (fundamental and second harmonic heating).

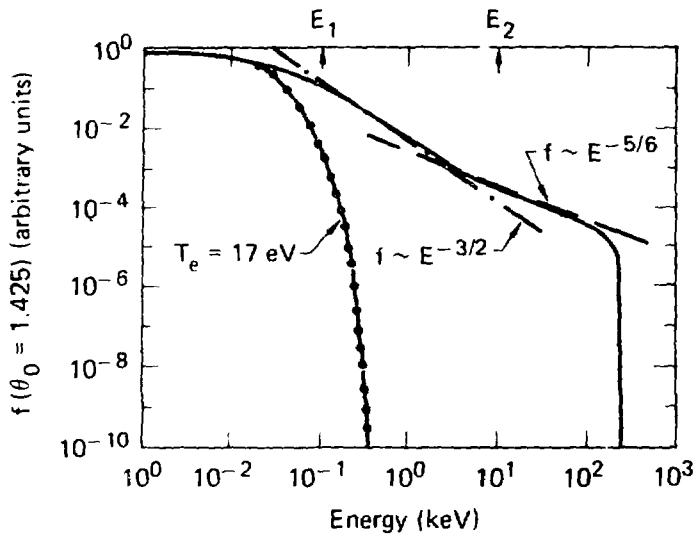


Fig. 5. Variation of distribution function with energy.  $\theta_0 = 1.425$  is the second harmonic resonance line (see Fig. 4).

**Numerical Analysis of Equilibrium and Stability in Bumpy Cylinder**

H. Sanuki, T. Ogino<sup>\*</sup>, S. Ishiguro and T. Kamimura

Institute of Plasma Physics, Nagoya University

Nagoya 464, Japan

\* Research Institute of Atmosphericics,

Nagoya University, Toyokawa, Japan

Abstract

The dynamical tensor pressure equilibria of a bumpy cylinder are investigated numerically by using the two-dimensional magnetohydrodynamic (MHD) equation. An isotropic bulk plasma pressure and an anisotropic hot electron pressure are assumed. The nonlinear evolution of two-dimensional MHD equation are studied, revealing that the hot electron annuli play an important role in the equilibria of bumpy cylinder. Using the numerical equilibrium solutions, several stability criteria are also studied for a class of MHD instabilities. The attainable beta value of the bulk plasma that is derived from the equilibrium point of view seems to be somewhat smaller than that predicted by the stability analysis of the rigid annulus model.

Considerable attention has been paid recently to the bumpy torus confinement system. While a closed-line torus with isotropic pressure and monotonically increasing  $\int dl/B$  is always unstable to interchange modes<sup>1</sup>, the diamagnetic current associated with hot electron annuli transforms the bumpy torus into a local average minimum-B configurations, in which these modes are stabilized. The anisotropic nature of the hot electron annulus, the localized high- $\beta$  region, the closed magnetic field lines, and the mirror symmetry should all be incorporated into a realistic model of the bumpy torus equilibrium.

Since the bumpy torus is not toroidally symmetric, the equilibria are, in general, three-dimensional. For large aspect ratio, however, the configuration may be approximated by its infinite aspect-ratio limit, namely, the straight bumpy cylinder. Many sufficient conditions for general mirror equilibria have been discussed first by Grad<sup>2</sup> and several authors<sup>3,4,5</sup>. Numerical studies of typical 2-D bumpy cylinder<sup>6,7</sup> and typical 3-D bumpy torus<sup>8</sup> equilibria have been done in the guiding-center formulation including the anisotropic hot electron population in the equilibrium force balance. Recently, analytic toroidal equilibria of bumpy torus configurations have been calculated by Freidberg<sup>9</sup> based on an asymptotic expansion in the amplitude of the bumpiness.

In the present study, we consider the dynamical effects of hot electron annulus on the bumpy torus equilibria using MHD equations with isotropic bulk plasma and anisotropic hot electron pressures. Two-dimensional equilibria are obtained that are applied to study the stability criteria against the MHD instabilities discussed in Refs. 4 and 5.

The basic MHD equation relevant to the present problem is discussed in Figure 1, where an artificial viscosity term  $\vec{\phi}$ , artificial damping term  $v\vec{v}$ , and also diffusion term  $D\nabla^2\rho$  are introduced to control the behavior of the numerical scheme employed. Here, all quantities are normalized. The model equations are solved numerically in cylindrical coordinates. Here we restrict ourselves to the  $\theta$ -symmetric system, which allows one to study a reduced domain as shown in Figure 2. The geometry characterizes the EBT and NBT experiments with the  $z$ -dimension equal to  $b_0$  and the  $r$ -dimension equal to  $a$ . The hot electron annulus is approximately  $\Delta r$  wide and  $\Delta z$  long located at the position  $(r_1, z=0)$ . The present boundary conditions are shown in Figure 3. We assume the periodicity in  $z$  and impose periodic boundary conditions at  $z = -b_0/2$  and  $z = b_0/2$ . On the radial boundaries,  $r = 0$  and  $r = 1$ , we impose fixed boundary conditions, i.e. at  $r = 1$ , and at  $r = 0$  we impose a mirror boundary condition.

The pressure components are shown in Figure 4. The first term in these expressions describes the bulk plasma, and the second one describes the hot electrons. For the scalar pressure term, we can change the pressure profile for the bulk plasma by changing the factor  $\alpha$ . To simulate the annular hot electron plasma, we use the initial pressure distribution for hot electron annulus model, which has been discussed in Refs. 3-5. The MHD equations (see, Figure 1) are solved as an initial value problem by a modified two step Lax-Wendroff method under the boundary conditions (Figure 3). An initial solution of MHD equations as an initial value for numerical calculations is discussed in Figure 5. For numerical purposes, we decompose the flux function into  $\psi = \psi_e + \psi_{in}$ , where  $\psi_e$  is

### Normalized MHD Equation

$$\frac{\partial \rho}{\partial t} = -\vec{\nabla} \cdot (\vec{\nabla} \rho) + D \vec{\nabla}^2 \rho$$

$$\frac{\partial \vec{v}}{\partial t} = -(\vec{\nabla} \cdot \vec{\nabla}) \vec{v} - \frac{1}{\rho} \vec{\nabla} \cdot \vec{p} + \frac{1}{\rho} \vec{J} \times \vec{B} + \frac{1}{\rho} \vec{\phi} - \nu \vec{\nabla}^2 \vec{v}$$

$$\frac{\partial p_{\parallel}}{\partial t} = -(\vec{\nabla} \cdot \vec{\nabla}) p_{\parallel} - p_{\parallel} \vec{\nabla} \cdot \vec{\nabla} - 2p_{\parallel} \vec{b} \cdot (\vec{b} \cdot \vec{\nabla}) \vec{\nabla}$$

$$\frac{\partial p_{\perp}}{\partial t} = -(\vec{\nabla} \cdot \vec{\nabla}) p_{\perp} - 2p_{\perp} \vec{\nabla} \cdot \vec{\nabla} + p_{\perp} \vec{b} \cdot (\vec{b} \cdot \vec{\nabla}) \vec{\nabla}$$

$$\frac{\partial \vec{B}}{\partial t} = \vec{\nabla} \times (\vec{\nabla} \times \vec{B} - n \vec{J})$$

where

$$\vec{b} = \vec{B} / |\vec{B}| \quad ; \quad n = 0$$

$$\vec{J} = \vec{\nabla} \times \vec{B} \quad , \quad \vec{p} = p_{\perp} \vec{I} + (p_{\parallel} - p_{\perp}) \vec{b} \vec{b}$$

$\vec{\phi} = \mu \vec{\nabla}^2 \vec{v}$  : Artificial Viscosity Term

$\nu \vec{\nabla}^2 \vec{v}$  : Artificial Damping Term

$$\rho / \rho_0 \quad \rightarrow \quad \rho$$

$$\vec{v} / v_{A_2} \quad \rightarrow \quad \vec{v}$$

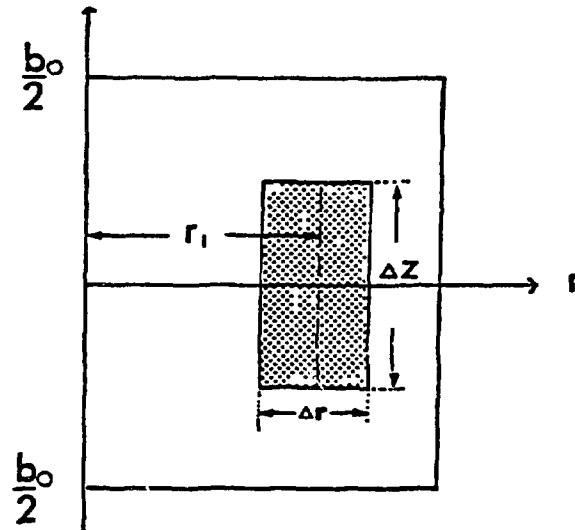
$$\rho / (B_0^2 / 2\mu_0) \rightarrow \rho$$

$$\vec{J} / (\frac{\mu_0 B_0}{d}) \rightarrow \vec{J}$$

$$\vec{B} / B_0 \quad \rightarrow \quad \vec{B}$$

Figure 1. Normalized MHD equation

Configuration



- Cylindrical Coordinate  $(r, \theta, z)$
- $\theta$ -Symmetry
- Domain :  $0 \leq r \leq a=1$   
 $-\frac{b_0}{2} \leq z \leq \frac{b_0}{2}$
- Hot Electron Ring :  $\Delta r$  Wide and  $\Delta z$  Long

Figure 2. Configuration and coordinate

Boundary ConditionsZ-direction : Periodic Boundary

$$\phi(r, -\frac{b}{2}) = \phi(r, \frac{b}{2})$$

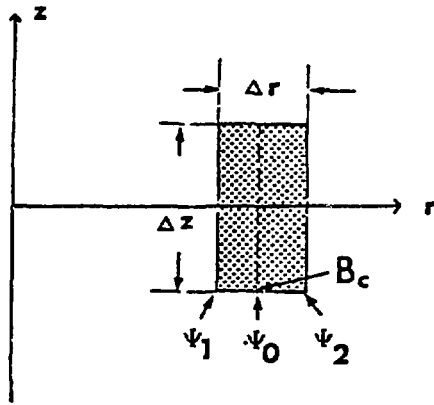
R-directionAt R=a : Fixed Boundary $\phi(a, z)$  independent of timeAt R=0 : Mirror Type Boundary

$$\begin{aligned} V_r(0, z) = V_\theta(0, z) = B_r(0, z) = B_\theta(0, z) \\ = J_r(0, z) = J_\theta(0, z) = 0 \end{aligned}$$

$$\begin{aligned} \left. \frac{\partial \rho}{\partial r} \right|_{r=0} = \left. \frac{\partial V_\theta}{\partial r} \right|_{r=0} = \left. \frac{\partial P_{||}}{\partial r} \right|_{r=0} = \left. \frac{\partial P_\perp}{\partial r} \right|_{r=0} \\ \left. \frac{\partial B_z}{\partial r} \right|_{r=0} = \left. \frac{\partial J_z}{\partial r} \right|_{r=0} = 0 \end{aligned}$$

Figure 3. Boundary conditions

## Pressure Distribution



$$\psi_1 = \psi(r_1 - \frac{\Delta r}{2}, 0)$$

$$\psi_2 = \psi(r_1 + \frac{\Delta r}{2}, 0)$$

$$\psi_0 = \frac{1}{2}(\psi_1 + \psi_2)$$

$$B_c = |B(r_1, -\frac{\Delta z}{2})|$$

$$P_{\parallel} = P + \Delta P_{\parallel}$$

$$P_{\perp} = P + \Delta P_{\perp}$$

where for given  $P_0$  and  $S$

$$P = P_0 \left[ \frac{(\psi_2 - \psi)}{\psi_2} \right]^{\Gamma} \quad (\psi < \psi_2)$$

$$\Delta P_{\parallel} = \frac{1}{2} S (B_c - B)^2 \frac{(\psi - \psi_1)^2 (\psi_2 - \psi)^2}{(\psi_0 - \psi_1)^2 (\psi_2 - \psi_0)^2}$$

$$-\frac{\Delta z}{2} < z < \frac{\Delta z}{2}$$

{

$$\Delta P_{\perp} = \frac{1}{2} S (B_c^2 - B^2) \frac{(\psi - \psi_1)^2 (\psi_2 - \psi)^2}{(\psi_0 - \psi_1)^2 (\psi_2 - \psi_0)^2}$$

$$-\frac{\Delta r}{2} < r < \frac{\Delta r}{2}$$

}

Figure 4. Pressure model for bulk and hot electron plasmas

Flux Function  $\psi$ 

$$\vec{B} = \frac{1}{r} \vec{\nabla} \psi \times \vec{\theta} = \left( -\frac{1}{r} \frac{\partial \psi}{\partial z}, 0, \frac{1}{r} \frac{\partial \psi}{\partial r} \right)$$

$$\vec{J} = \left( 0, -\frac{\partial}{\partial r} \left( \frac{1}{r} \frac{\partial \psi}{\partial r} \right) - \frac{1}{r} \frac{\partial^2 \psi}{\partial z^2}, 0 \right)$$

 $\psi_e$  produced by external coils

$$\Delta^* \psi_e = 0 \quad \longrightarrow$$

$$\psi_e = \frac{1}{2} r^2 + a_1 \{ r I_1(k_1 r) \cos(k_1 z) + a_2 r I_1(k_2 r) \cos(k_2 z) \}$$

 $\psi_{in}$  due to hot electron current

$$\Delta^* \psi_{in} = -r J_h$$

$$\psi_{in} = b_1 (r_1 r)^{1/2} \cos(k_{r1} \tilde{r}) \{ \sin(k_{r2} \tilde{r}) + b_2 \cos(k_{r1} \tilde{r}) \} \cos(k_z z)$$

where

$$k_1 = 2\pi/b_0, \quad k_2 = 4\pi/b_0, \quad k_{r1} = \pi/\Delta r, \quad k_{r2} = 2\pi/\Delta r.$$

$$k_z = \pi/\Delta z, \quad \tilde{r} = r - r_1$$

Figure 5. Initial solutions

related to external fields and  $\psi_{in}$  is due to hot electron currents.

Then, we can determine a magnetic geometry relevant to EBT/NBT machines by adjusting coefficients  $a_1$ ,  $a_2$ ,  $b_1$  and  $b_2$  in  $\psi_e$  and  $\psi_{in}$ . How to determine these coefficients is discussed in Figure 6. Now we have four typical parameters, namely, the mirror ratio  $R_m$ , the current ratio  $R_c$  between the negative and positive values of the dipole current in the hot annulus region, the parameter  $(B_z^{in})^{min}$  characterizing the minimum-B configuration created due to hot electrons, and the parameter  $a_2$  representing the magnitude of the magnetic field. For given those parameters, we can determine the coefficients  $a_1$ ,  $a_2$ ,  $b_1$  and  $b_2$ . The equilibrium solution is defined on an r-z mesh. The number of spatial mesh coordinate units are  $(r,z) = (34,34)$  or  $(66,66)$  including the fixed boundaries.

The parameters used in the calculations are shown in Figure 7. We study several cases in which we change the maximum value of bulk plasma pressure  $p_0$  over the range of 0.01 ( $\beta_p \approx 2\%$ ) - 0.1 ( $\beta_p \approx 20\%$ ), and the parameter  $S$  in Figure 4 over the range of 0.5 ~ 2.0, where we defined  $\beta_p = 2\mu p/B_0^2$  and  $\beta_h = 2\mu p_h/B_0^2$ . For the case of  $a = 20$  cm and  $B_0 = 1$  T under the present parameters, we obtain  $a_1 = -0.138$ ,  $a_2 = 0.0$ ,  $b_1 = -0.144$ , and  $b_2 = 0.279$ . The domain and magnetic geometry are also illustrated in Figure 7.

An example of the calculation is shown in Figures 8 and 9. Here, the initial beta values of the bulk plasma and the hot electron annulus are about 1% and 25% at the center, respectively. An equilibrium state in this case is defined after the time step  $t = 10.24$ , namely, about ten times the Alfvén transit time. Figure 8 gives contour levels of the flux  $\psi$  and indicates clearly the local minimum in  $B$  created by

How to determine Coefficients  $a_1$ ,  $a_2$ ,  $b_1$  and  $b_2$

$$B_r^{\text{ext}} = -\frac{1}{r} \frac{\partial \psi}{\partial z} e, \quad B_z^{\text{ext}} = \frac{1}{r} \frac{\partial \psi}{\partial r} e$$

$$B_r^{\text{in}} = -\frac{1}{r} \frac{\partial \psi}{\partial z} i_n, \quad B_z^{\text{in}} = \frac{1}{r} \frac{\partial \psi}{\partial r} i_n$$

$$J_\theta = -\frac{\partial}{\partial r} \left( \frac{1}{r} \frac{\partial \psi}{\partial r} \right) - \frac{1}{r} \frac{\partial^2 \psi}{\partial z^2}$$

$$\text{Mirror Ratio : } R_m = \frac{B_z^{\text{ext}}(0, \frac{b}{2})}{B_z^{\text{ext}}(0, 0)}$$

$$\rightarrow a_1 = \frac{1 - R_m}{(k_1 + a_2 k_2)(1 + R_m)}$$

$$B_z^{\text{in}}(r_1, 0) = (B_z^{\text{in}})^{\text{min}}$$

$$\rightarrow b_1 = (B_z^{\text{in}})^{\text{min}} / k_{r2}$$

Current Ratio :

$$R_c = \frac{J_\theta(k_{r2} \tilde{r} = \frac{\pi}{2})}{J_\theta(k_{r2} \tilde{r} = \frac{\pi}{2})}$$

$$\rightarrow b_2 = \frac{R_c C_3 - C_1}{C_2 - C_4 R_c}$$

$C_1 - C_4$  : given

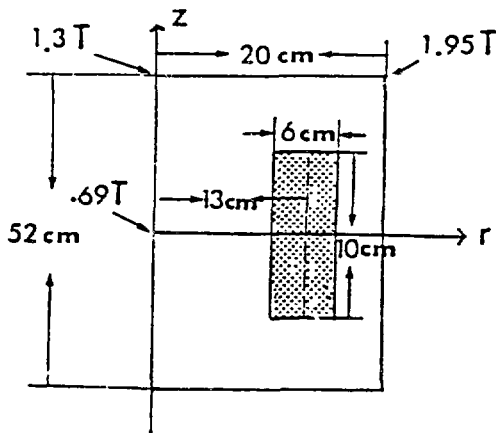
$R_m$ ,  $(B_z^{\text{in}})^{\text{min}}$ ,  $R_c$  and  $a_2 \rightarrow a_1, a_2, b_1$  and  $b_2$

Figure 6. Determination of coefficients  $a_1$ ,  $a_2$ ,  $b_1$  and  $b_2$ .

### Parameters

$r_1$	$\Delta r$	$\Delta z$	$b_0$	$R_m$	$a_2$	$(B_z^{in})_{min}$
0.65	0.3	0.5	2.6	1.9	0.0	-0.2 ~ -0.3
$R_c$	$P_0$	$S$	$D$	$\mu$	$\nu$	$\eta$
-0.9	0.01 ~.1 (2%) ~(20%)	0.1- 2.0	0.003	0.1	0.10	0.0

For  $A_0=20\text{cm}$        $B_0=1\text{T}$



$$a_1 = -0.138$$

$$b_1 = 0.048 \quad p_z^{min} = -0.144$$

$$a_2 = 0.0$$

$$b_2 = 0.279$$

Figure 7. Parameters used in the numerical calculation. The domain and magnetic geometry are also shown.

## Mod-B &amp; Flux

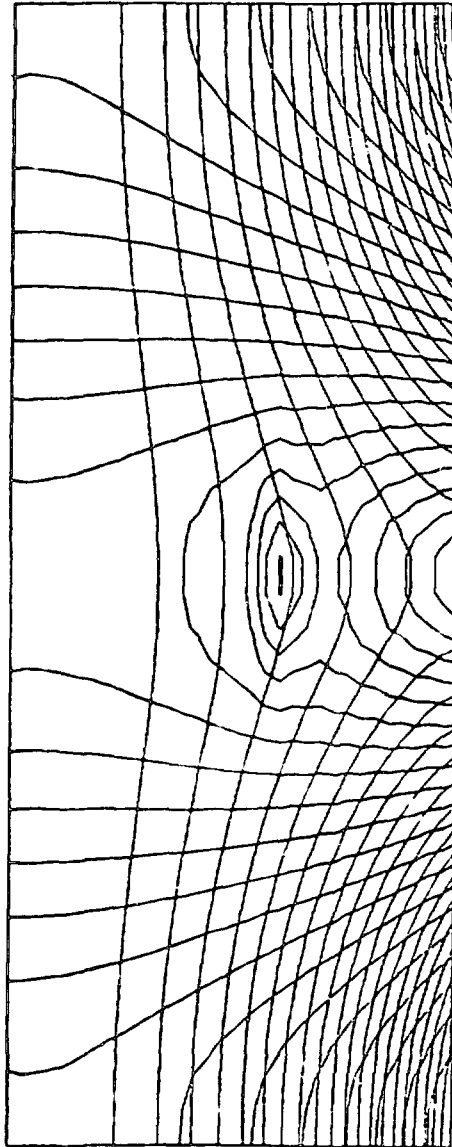


Figure 8. Mod-B and level contours of flux  $\psi$  are shown, which indicate the local minimum in B created by the diamagnetic current of the annulus.  $\beta_h = 25\%$  and  $\beta_p = 1\%$ .

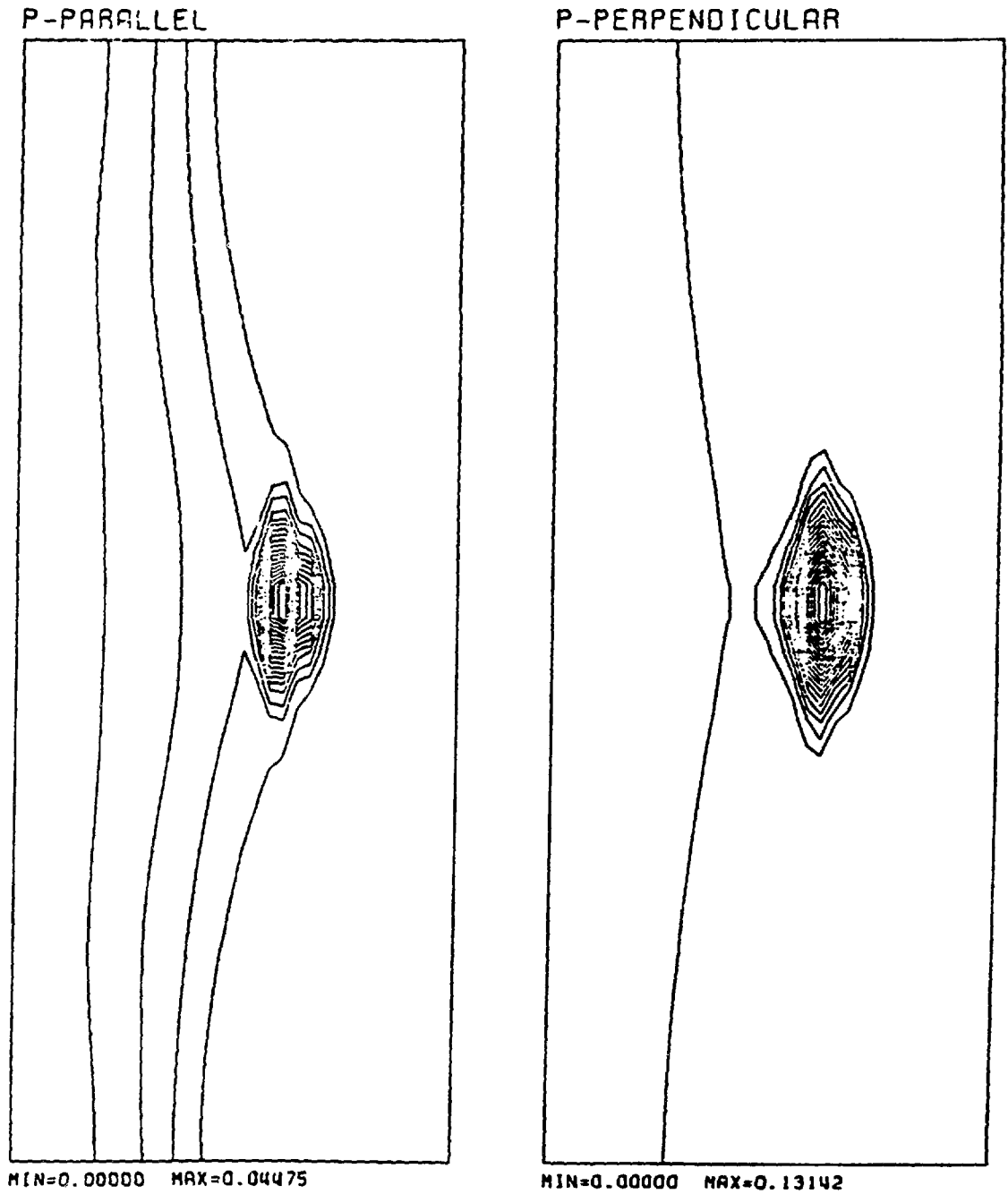


Figure 9. Parallel and perpendicular pressure contours in  $r$ - $z$  plane at equilibrium.  $\beta_h = 25\%$  and  $\beta_p \approx 1\%$ .

the diamagnetic current of the hot electrons. The magnetic gradients are increased in the vicinity of the hot electron annulus, but the curvature is hardly changed. Figure 9 shows the parallel and perpendicular pressure contours. Both the parallel and perpendicular pressures are shifted a little inward from the initial position and the axial length and the radial width of the perpendicular pressure distribution are larger than those of the parallel pressure distribution. The radial profiles of mod-B, current, parallel and perpendicular pressures at the midplane are shown in Figure 10 for several values of hot electron annulus beta  $\beta_h$ , namely, 15.6%, 20.0%, and 29.0%, which are defined at the equilibrium state. The local magnetic wells at the annulus region become deeper and broader as the annulus beta  $\beta_h$  is increased. Next we studied the equilibria for high bulk plasma beta. Consequently, it turns out that the hot electron annulus may be shifted inside or outside depending on the pressure profiles and value of  $\beta_p/\beta_h$ . Here we used the factor characterizing the bulk plasma pressure profile  $\alpha = 1.2$ . However, we will use  $\alpha = 0.2$  when we investigate the stability criterion later. The relationship between beta values of the bulk and the hot electron annulus are plotted in Figure 11 for several equilibria in which the hot electron annulus are located at  $r = 0.600, 0.625, \text{ and } 0.65$ . We obtain an equilibrium at  $r = 0.65$ , resulting in  $\beta_p/\beta_h \approx 0.3$  at this position.

We next consider the influence of the hot electron annulus on the bulk plasma stability. Studies of bulk stability limitations are developed in two approaches: rigid ring models<sup>6,10</sup> and interacting ring models<sup>11,12</sup>. The rigid ring models show that the linear improve-

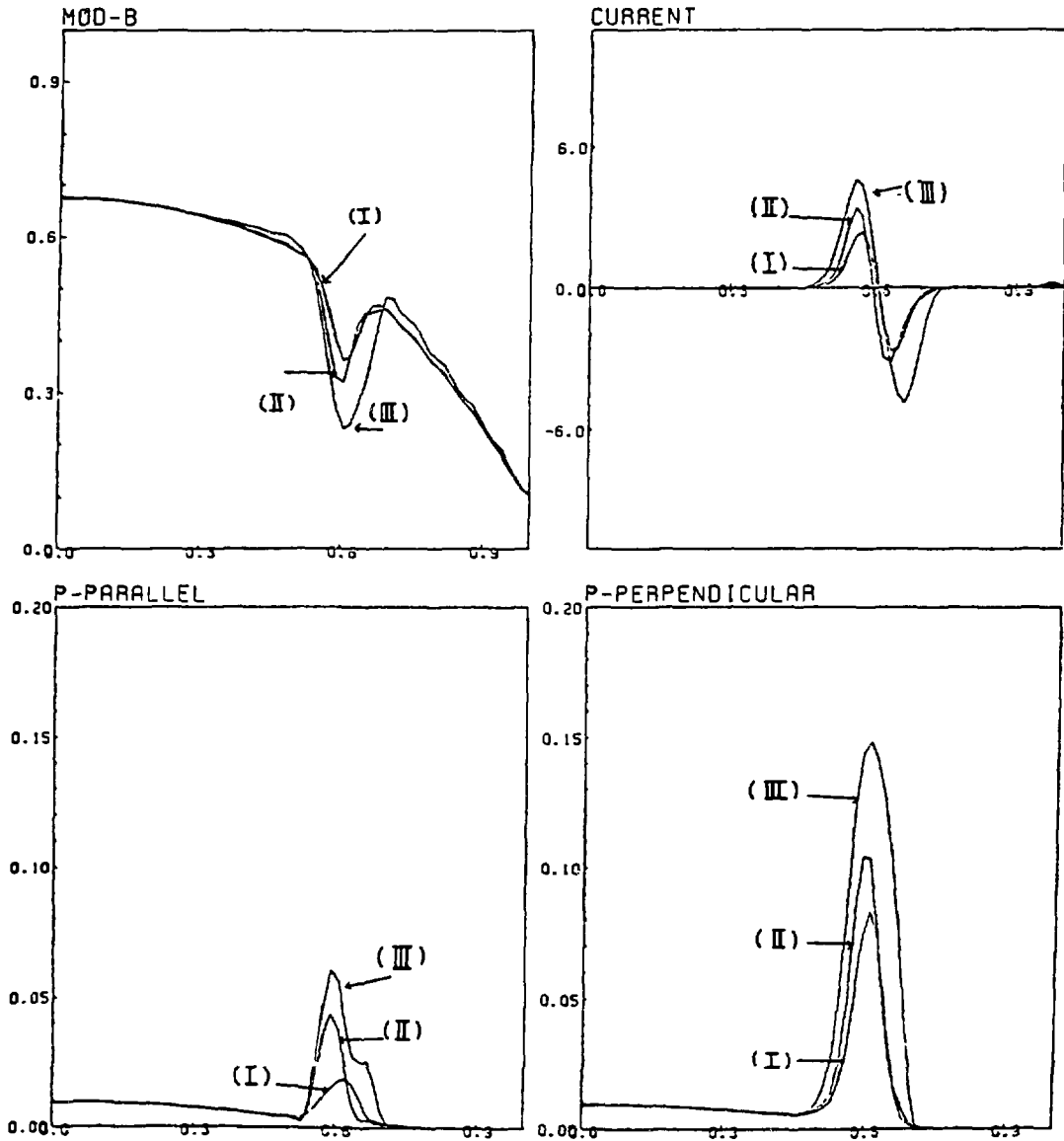


Figure 10. Radial profiles of mod-B, current, parallel and perpendicular pressures in midplane at equilibrium are shown for several values of the annulus beta,  $\beta_h \approx 15.6\%$  (I),  $20.0\%$  (II), and  $29.0\%$  (III) at the equilibrium.

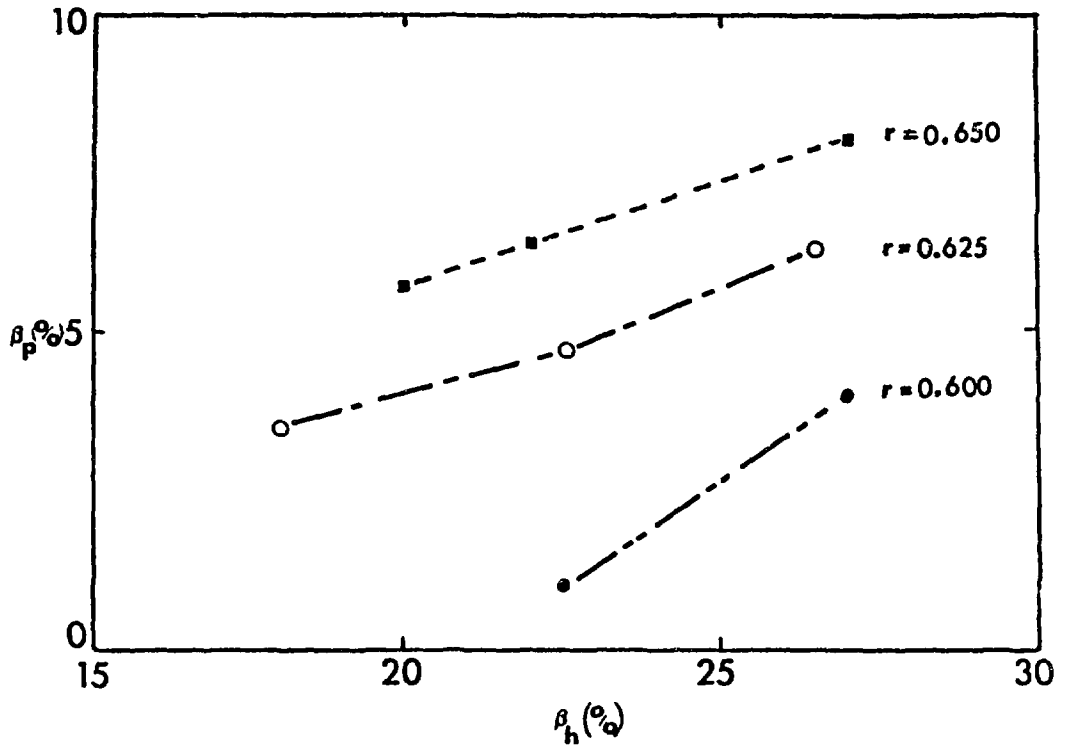


Figure 11. Relationship between the bulk and the annulus beta values are plotted for several equilibria in which the annuli at equilibrium are located at  $r = 0.600$ ,  $0.625$ , and  $0.650$ .

ment in attainable  $\beta_p$  values with  $\beta_h$ . However, the interacting ring models predict that this tendency is not present at higher values of  $\beta_h$ .

We study the role of high- $\beta$  hot electron annulus in maintaining the stability of the bulk plasma against a class of MHD instabilities using the stability criteria (see, Figure 12), which have been discussed in Refs. 3-5). D. Spong has summarized these criteria for flute modes and pressure driven ballooning modes in Ref. 13. The self-dug well of the annulus could stabilize over interchanges most of the ring region, however, at the outer edge, some of line-tying would be necessary if the plasma pressure extended beyond the edge of the magnetic well. In contrast to this type of mode, pressure-driven ballooning modes distort and stretch the magnetic field lines. Then, the stability criterion for this mode involves only curvature, which is not effectively modified by finite beta. Consequently, it is more difficult to satisfy than the criterion for flute modes.

Some results on the stability criteria for flute and ballooning modes are shown in Figure 13. We chose  $\alpha = 0.2$  in the bulk plasma pressure model (see, Figure 4). In this case, the bulk plasma pressure profile is flat more than that for  $\alpha = 1.2$ . We used the numerical equilibrium solutions when we carry out the field line integration in the stability criteria. The results, which are stable against flute and ballooning modes (O), stable for flute modes but unstable for ballooning modes ( $\Delta$ ), and unstable against both flute and ballooning modes (\*), are plotted in this figure. The results by Van Dan and Lee (Ref. 12) is also illustrated for comparison. These results indicate the situation of stability of bumpy torus mentioned above, but the results presented

## STABILITY CRITERIA

### 1. Rosenbluth - Longmire

$$\left\langle \frac{\kappa}{rB} \frac{\partial p_{\perp}}{\partial \psi} + \frac{\partial \ln B}{\partial \psi} \frac{\partial p_{\perp}}{\partial \psi} \right\rangle \leq 0$$

### 2. Generalized Interchange

$$\left\langle \frac{\kappa}{rB} \frac{\partial p_{\perp}}{\partial \psi} + \frac{\partial \ln B}{\partial \psi} \frac{\partial p_{\perp}}{\partial \psi} \right\rangle + \frac{\left\langle \frac{\partial p_{\perp}}{\partial \psi} \right\rangle^2}{\langle \tau B^2 \rangle} \leq 0$$

### 3. Localized Perturbations

$$\left\langle \frac{\kappa}{rB} \frac{\partial p_{\perp}}{\partial \psi} + \frac{\partial \ln B}{\partial \psi} \frac{\partial p_{\perp}}{\partial \psi} \right\rangle + \left\langle \frac{\left( \frac{\partial p_{\perp}}{\partial \psi} \right)^2}{\tau B^2} \right\rangle \leq 0$$

where

$$\langle f \rangle = \oint \frac{1}{B} f \, dl$$

Figure 12. Stability criteria against a class of MHD instabilities such as flute and ballooning modes.

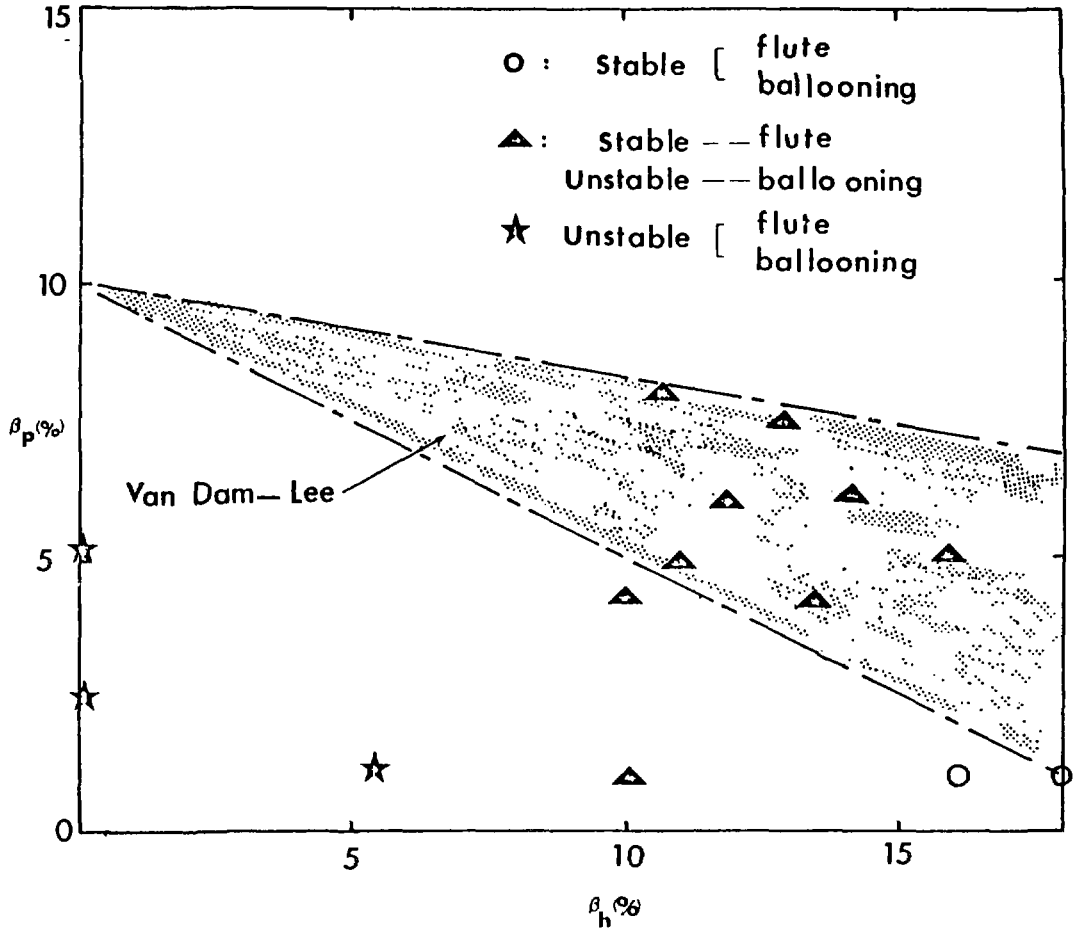


Figure 13. Results on stability criteria for flute and ballooning modes. Stable against flute and ballooning modes (○), stable for flute mode but unstable for ballooning mode (Δ), and unstable against flute and ballooning modes (★). For comparison, the result by Van Dam and Lee is also plotted.

here would be altered a little by more improved numerical calculations, the geometry and profile effects such as the variations on the length and width of the hot electron annulus, different pressure profiles, etc.

## KINETIC STABILITY ANALYSES IN A BUMPY CYLINDER\*

R. R. Dominguez  
General Atomic Company,  
San Diego, California 92138

and

H. L. Berk  
Institute for Fusion Studies,  
Austin, Texas 78712

## ABSTRACT

Recent interest in the ELMO Bumpy Torus (EBT) has prompted a number of stability analyses of both the hot electron rings<sup>1,2</sup> and the toroidal plasma.<sup>3,4</sup> Typically these works employ the local approximation, neglecting radial eigenmode structure and ballooning effects to perform the stability analysis. In the present work we develop a fully kinetic formalism for performing nonlocal stability analyses in a bumpy cylinder. We show that the Vlasov-Maxwell integral equations (with one ignorable coordinate) are self-adjoint and hence amenable to analysis using numerical techniques developed for self-adjoint systems of equations. The representation we obtain for the kernel of the Vlasov-Maxwell equations is a differential operator of arbitrarily high order. This form leads to a manifestly self-adjoint system of differential equations for long wavelength modes.

\*Work supported by Department of Energy,  
Contract DE-AT03-76ET51011.

## 1. INTRODUCTION

Recent kinetic stability analyses of EBT have typically neglected radial structure and finite length effects. Several methods have been proposed during the workshop to study nonlocal effects, including the generalized  $\delta W$  formulation and the "bumpiless" EBT Z-pinch model.

A different method for analyzing linear stability, including nonlocal effects increasingly used in plasma physics, is a variational formulation of Maxwell's equations.

The variational method obtains second order accuracy in the eigenvalues with only first order accuracy in the trial eigenvectors.

The ingredients necessary for a variational formulation satisfying these conditions are:

- (i) self-adjoint kernel, and
- (ii) prescription for choosing trial adjoint eigenvector.

Recent applications of the variational technique in the literature do not always satisfy these criteria--the quadratic form is not stationary and eigenvalues not guaranteed to be second order accurate.

Here we consider self-adjoint structure and the variational formulation of the Vlasov-Maxwell equations in the case of equilibria with one and two nonignorable coordinates. The principle results are:

- (i) definition of generalized self-adjointness and relation between eigenvectors and adjoint eigenvectors, and
- (ii) construction of integral operator kernel (including full kinetic effects) in the form of a manifestly self-adjoint differential operator of arbitrarily high order.

The kinetic Vlasov-Maxwell equations in a bumpy cylinder follow from (i) and (ii).

## 2. SELF-ADJOINTNESS AND THE VARIATIONAL METHOD

We consider equilibria  $N(\underline{x})$ ,  $T(\underline{x})$ , and  $B(\underline{x})$ , where  $\underline{x}$  is a one- or two-dimensional vector. The linearized Vlasov-Maxwell equations are of the form

$$\sum_{\beta} \int d\underline{x}' L_{\alpha\beta}(\underline{x}, \underline{x}', \omega) \phi_{\beta}(\underline{x}') = 0 \quad , \quad (1a)$$

with the adjoint system of equations

$$\sum_{\beta} \int d\underline{x}' \phi_{\beta}^{+}(\underline{x}') L_{\beta\alpha}(\underline{x}', \underline{x}, \omega) = 0 \quad . \quad (1b)$$

These results follow from the functional

$$\langle \phi | L | \phi \rangle = \sum_{\alpha, \beta} \int d\underline{x} d\underline{x}' \phi_{\alpha}^{+}(\underline{x}) L_{\alpha\beta}(\underline{x}, \underline{x}', \omega) \phi_{\beta}(\underline{x}') \equiv 0 \quad , \quad (2)$$

when variations of Eq. (2) are performed with respect to  $\underline{\phi}^{+}$  and  $\underline{\phi}$ , respectively.

The variational method seeks to minimize the functional  $\langle \phi | L | \phi \rangle$ . We choose trial functions

$$\underline{\phi} = \underline{\phi}_0 + \epsilon \delta \underline{\phi} \quad , \quad \underline{\phi}^{+} = \underline{\phi}_0^{+} + \epsilon \delta \underline{\phi}^{+} \quad , \quad (3)$$

which determine the trial eigenvalue  $\omega_0$  by  $\langle \phi_0 | L(\omega_0) | \phi_0 \rangle = 0$ . For self-adjoint  $L$ , i.e.,  $\langle \phi | L | \psi \rangle = \langle \psi | L | \phi \rangle$ , the frequency shift is second order

$$\delta\omega = \omega - \omega_0 = -\epsilon^2 \frac{\langle \delta\phi | L | \delta\phi \rangle}{\langle \phi_0 | \partial L / \partial \omega | \phi_0 \rangle} + O(\epsilon^3) \quad (4)$$

The condition  $\langle \phi | L | \psi \rangle = \langle \psi | L | \phi \rangle$  translates into the definition of generalized self-adjointness

$$L_{\alpha\beta}(\underline{x}, \underline{x}', \omega) = \sigma_\alpha \sigma_\beta L_{\beta\alpha}(\underline{x}', \underline{x}, \omega) \quad , \quad (5)$$

where

$$\sigma_\alpha = \begin{cases} +1 & \text{ignorable coordinate} \\ -1 & \text{nonignorable coordinate} \end{cases}$$

Microscopic symmetry under simultaneous time-reversal/parity transformation is sufficient (although perhaps not necessary) to insure the generalized self-adjointness of the Vlasov-Maxwell equations.

## 3. CONJUGATE TRAJECTORIES

Generalized self-adjointness follows from important symmetry of particle orbits. Consider the single particle Lagrangian:

$$L = \frac{1}{2} m v^2 + \frac{q}{c} \underline{v} \cdot \underline{A}_0 - q \phi_0 \quad (6)$$

Transformation which leaves  $L$  invariant  $\rightarrow$  same equations of motion in new coordinates.

Simultaneous time-reversal/parity transformations which leave  $L$  invariant define equivalent orbits--known as conjugate trajectories.

Examples of conjugate trajectories:

(i) One-dimensional field:  $\underline{B}_0 = B_\theta(r) \hat{\theta} + B_z(r) \hat{z}$ .

Conjugate trajectories:  $(\underline{r}_0^+ + \delta \underline{r}^+(t), \underline{v}^+(t))$  and  
 $[\underline{r}_0^- + \delta \underline{r}^-(-t), \underline{v}^-(-t)]$ .

$$\delta r^-(-t) = \delta r^+(t), \quad \delta \theta^-(-t) = -\delta \theta^+(t), \quad \delta z^-(-t) = -\delta z^+(t).$$

$$v_r^-(-t) = -v_r^+(t), \quad v_\theta^-(-t) = v_\theta^+(t), \quad v_z^-(-t) = v_z^+(t).$$

(ii) Two-dimensional field (bumpy cylinder):  $\underline{B}_0 = B_r(r, z) \hat{r} + B_z(r, z) \hat{z}$ .

Conjugate trajectories:  $(\underline{r}_0^+ + \delta \underline{r}^+(t), \underline{v}^+(t))$  and  
 $[\underline{r}_0^- + \delta \underline{r}^-(-t), \underline{v}^-(-t)]$ .

$$\delta r^-(-t) = \delta r^+(t), \quad \delta \theta^-(-t) = -\delta \theta^+(t), \quad \delta z^-(-t) = \delta z^+(t)$$

$$v_r^-(-t) = -v_r^+(t), \quad v_\theta^-(-t) = v_\theta^+(t), \quad v_z^-(-t) = -v_z^+(t) .$$

The equivalence of conjugate trajectories is used to "symmetrize" the kernel of the Vlasov-Maxwell equations and obtain the self-adjointness property.

## 4. ELECTROSTATIC KERNEL

First we illustrate results using the simpler Poisson equation for the two-dimensional perturbed potential

$$\phi(\underline{x}, t) = \phi(r, z) \exp i(\ell\theta - \omega t) \quad . \quad (7)$$

The Poisson integral equation is

$$\int d\underline{\rho}' [L_V(\underline{\rho}, \underline{\rho}') + L_P(\underline{\rho}, \underline{\rho}', \omega)] \phi(\underline{\rho}') = 0 \quad , \quad (8)$$

$\underline{\rho} = (r, z)$  and

$$L_V = \left[ \frac{\ell^2}{(rr')^{1/2}} + \left( \frac{\partial}{\partial z} \frac{\partial}{\partial z'} + \frac{\partial}{\partial r} \frac{\partial}{\partial r'} \right) (rr')^{1/2} \right] \\ \times \delta(r - r') \delta(z - z') \quad , \quad (9)$$

and

$$L_V(\underline{\rho}, \underline{\rho}') = L_V(\underline{\rho}', \underline{\rho}) \quad . \quad (10)$$

The plasma response is

$$L_P(\underline{\rho}, \underline{\rho}', \omega) = \sum_{\mathbf{s}} 4\pi q_{\mathbf{s}}^2 \int d\underline{v}_0 \int r_0 dr_0 dz_0 \sum_{\mathbf{n}} (\omega - \omega_{\mathbf{n}})^{-1} \\ \times \left( \omega_{\mathbf{n}} \frac{\partial}{\partial \epsilon} + \ell \frac{\partial}{\partial p_{\theta}} F_0^{(\mathbf{s})} \right) I_{\mathbf{n}}(\underline{\rho}, \underline{\rho}') \quad , \quad (11)$$

with  $I_n(\underline{\rho}, \underline{\rho}') = [\rho_n^+(\underline{\rho})]^* \rho_n^+(\underline{\rho}')$ ,  $\omega_n = n\langle\omega_c\rangle + \ell\langle\dot{\theta}\rangle$ , and  $\langle\omega_c\rangle =$  average gyrofrequency

$$\rho_n^+(\underline{\rho}) = \frac{1}{\tau} \int d\tau' \delta[\underline{\rho} - \underline{\rho}_0 - \underline{\delta\rho}(\tau')] \exp[i\Omega_n^+(\tau')] \quad ;$$

$$\tau = \frac{2\pi}{\langle\omega_c\rangle} \quad , \quad (12)$$

and  $\Omega_n^+(\tau) = \omega_n\tau + \ell\delta\theta(\tau)$ .  $L_p$  is not manifestly self-adjoint. Self-adjointness follows when we note that conjugate particles have the same constants of motion  $\epsilon, p_\theta$ .

Grouping the response of conjugate particles,

$$I_n(\underline{\rho}, \underline{\rho}') + \frac{1}{2} \{ [\rho_n^+(\underline{\rho})]^* \rho_n(\underline{\rho}') + [\rho_n^-(\underline{\rho})]^* \rho_n^-(\underline{\rho}') \} \quad ,$$

and using the relation between conjugate trajectories

$$\rho_n^-(\underline{\rho}) = [\rho_n^+(\underline{\rho})] \quad . \quad (13)$$

Hence,

$$I_n(\underline{\rho}, \underline{\rho}') = \frac{1}{2} \{ [\rho_n^+(\underline{\rho})]^* \rho_n^+(\underline{\rho}') + \rho_n^+(\underline{\rho}) [\rho_n^+(\underline{\rho}')]^* \} \quad , \quad (14)$$

and we have the result

$$L_p(\underline{\rho}, \underline{\rho}', \omega) = L_p(\underline{\rho}', \underline{\rho}, \omega) \quad . \quad (15)$$

## 5. ELECTROMAGNETIC KERNEL

We choose a gauge where  $\phi = 0$ ,

$$\underline{A}(\underline{x}, t) = [A_1(\underline{\rho})\hat{r} + A_2(\underline{\rho})\hat{\theta} + A_3(\underline{\rho})\hat{z}] \exp i(\ell\theta - \omega t) \quad , \quad (16)$$

with  $\underline{\rho} = (r, z)$ . The Vlasov-Maxwell equations are of the form

$$\sum_{\beta} \int d\underline{\rho}' [L_{\nu\alpha\beta}(\underline{\rho}, \underline{\rho}', \omega) + L_{\rho\alpha\beta}(\underline{\rho}, \underline{\rho}', \omega)] A_{\beta}(\underline{\rho}') = 0 \quad . \quad (17)$$

The kernel is now more complicated, e.g.,

$$L_{\underline{z}\nu} = \{L_1 \quad L_2 \quad L_3\} \delta(r-r')\delta(-z-z') \quad (18)$$

where

$$L_1 = \left[ \begin{array}{l} \frac{\ell^2}{(rr')^{1/2}} + \left( \frac{\partial}{\partial z} \frac{\partial}{\partial z} - \frac{\omega^2}{c^2} + \sum_s \frac{\omega^2}{s c^2} \right) (rr')^{1/2} \\ i\ell \frac{r}{r'} \frac{\partial}{\partial r} \\ r' \frac{\partial}{\partial r} \frac{\partial}{\partial z} \end{array} \right]$$

$$L_2 = \left[ \begin{array}{c} -i\ell \frac{r'}{r} \frac{\partial}{\partial r'} \\ \left( \frac{\partial}{\partial z} \frac{\partial}{\partial z'} - \frac{\omega^2}{c^2} + \Sigma \frac{\omega^2}{s c^2} \right) (rr')^{1/2} + rr' \frac{\partial}{\partial r} \frac{\partial}{\partial r'} (rr')^{-1/2} \\ i\ell \frac{\partial}{\partial z} \end{array} \right]$$

$$L_3 = \left[ \begin{array}{c} r \frac{\partial}{\partial r'} \frac{\partial}{\partial z'} \\ -i\ell \frac{\partial}{\partial z'} \\ \frac{\ell^2}{(rr')^{1/2}} + \left( \Sigma \frac{\omega^2}{s c^2} - \frac{\omega^2}{c^2} \right) (rr')^{1/2} + \frac{\partial}{\partial r} \frac{\partial}{\partial r'} (rr')^{1/2} \end{array} \right]$$

with  $\omega_{ps}^2 = 4\pi q_s^2 N_s / m_s$ .

The plasma response is

$$\underline{\underline{L}}_{\underline{\underline{p}}} = - \sum_{\underline{\underline{s}}} \frac{4\pi q_s^2}{c^2} \int d\underline{\underline{v}}_0 \int r_0 dr_0 dz_0 \sum_{\underline{\underline{n}}} (\omega - \omega_n)^{-1} \\ \times \left( \omega_n \frac{\partial}{\partial \varepsilon} + \underline{\underline{z}} \frac{\partial}{\partial \underline{\underline{p}}_0} \right) F_0^{(s)} \underline{\underline{M}}_{\underline{\underline{n}}}(\underline{\underline{\rho}}, \underline{\underline{\rho}}') \quad , \quad (19)$$

where conjugate trajectories are used to obtain  $\underline{\underline{M}}_{\underline{\underline{n}}}$ ,

$$\underline{\underline{M}}_{\underline{\underline{n}}\alpha\beta}(\underline{\underline{\rho}}, \underline{\underline{\rho}}') = [\underline{\underline{m}}_{\alpha}(\underline{\underline{\rho}}|n)]^* \underline{\underline{m}}_{\beta}(\underline{\underline{\rho}}'|n) + \sigma_{\alpha} \underline{\underline{m}}_{\alpha}(\underline{\underline{\rho}}|n) [\underline{\underline{m}}_{\beta}(\underline{\underline{\rho}}'|n)]^* \sigma_{\beta} \quad , \quad (20)$$

with  $\sigma_{\alpha} = +1$  ( $\alpha = 2$ ),  $-1$  ( $\alpha = 1, 3$ ), and

$$\underline{\underline{m}}(\underline{\underline{\rho}}|n) = \frac{1}{\tau} \int d\tau' \underline{\underline{v}}(\tau') \delta[\underline{\underline{\rho}} - \underline{\underline{\rho}}_0 - \delta\underline{\underline{\rho}}(\tau')] \exp[i\Omega_n(\tau')] \quad . \quad (21)$$

## 6. SUMMARY OF THE RESULTS IN THE BUMPY CYLINDER

Vlasov-Maxwell equations

$$\int d\rho' \underline{\underline{L}}(\underline{\rho}, \underline{\rho}', \omega) \cdot \underline{A}(\underline{\rho}') = 0 \quad .$$

$\underline{\underline{L}}$  is self-adjoint

$$L_{\alpha\beta}(\underline{\rho}, \underline{\rho}', \omega) = \sigma_{\alpha}\sigma_{\beta}L_{\beta\alpha}(\underline{\rho}', \underline{\rho}, \omega) \quad .$$

Adjoint eigenvector:

$$A_{\alpha}^{+}(\underline{\rho}) = \sigma_{\alpha}A_{\alpha}(\underline{\rho}) \quad .$$

The generalized self-adjoint structure in two dimensions (with full kinetic effects) is different from the two-dimensional tokamak response (see Tsang<sup>5</sup> or Frieman et al.<sup>6</sup>) which is not self-adjoint.

## 7. APPLICATIONS OF THE FORMALISM

(i) Minimize the functional

$$\int d\underline{x} d\underline{x}' \underline{A}^+(\underline{x}) \cdot \underline{L}(\underline{x}, \underline{x}', \omega) \cdot \underline{A}(\underline{x}') \quad ,$$

using the trial function  $\underline{A}$  and prescription for  $\underline{A}^+$ .

(ii) Express  $\underline{L}$  as a differential operator, converting from integral to differential equations of arbitrary order. This is useful only if natural truncation of the order is available.

## 8. DIFFERENTIAL OPERATOR FORM

Transformation of  $\underline{\underline{L}}$  to a differential form proceeds as follows: we use identities

$$\exp\left(a \frac{\partial}{\partial \rho}\right) f(\rho) = f(\rho + a) \quad , \quad (22)$$

$$\int d\underline{\underline{\rho}} g(\rho) \exp\left(a \frac{\partial}{\partial \rho}\right) f(\rho) = \int d\rho f(\rho) \exp\left(-\frac{\partial}{\partial \rho} a\right) g(\rho) \quad ,$$

and apply to the vector functions  $\underline{\underline{m}}(\rho|n)$  [Eq. (21)]. After partial integrations, integration over the  $\delta$  function is trivial and, schematically,

$$\begin{aligned} \int d\underline{\underline{x}} \underline{\underline{L}}_{\underline{\underline{p}}} \cdot \underline{\underline{A}} &\rightarrow \int d\underline{\underline{y}}_0 \sum_{n,s} \langle \exp\left(-\frac{\partial}{\partial \rho} \cdot \delta \underline{\underline{\rho}}\right) \underline{\underline{y}} \exp(i\underline{\underline{\Omega}}_n) \rangle G(F_0^{(s)}) \\ &\times \langle \exp(-i\underline{\underline{\Omega}}_n) \underline{\underline{y}} \exp\left(\delta \underline{\underline{\rho}} \cdot \frac{\partial}{\partial \rho}\right) \rangle \underline{\underline{A}}(\underline{\underline{\rho}}) \quad , \end{aligned} \quad (23)$$

with  $\underline{\underline{\rho}} = (r, z)$ .

The factors  $\langle \exp\left[-\left(\partial/\partial \rho\right) \cdot \delta \underline{\underline{\rho}}\right] \underline{\underline{y}} \exp(i\underline{\underline{\Omega}}_n) \rangle$  must be expandable for this form to be useful. Two cases:

- (i)  $\frac{\partial}{\partial \rho} \cdot \delta \underline{\underline{\rho}} \approx \Omega_n \ll 1 \quad ,$
- (ii)  $\frac{\partial}{\partial \rho} \cdot \delta \underline{\underline{\rho}} \ll 1$  but  $\Omega_n$  is finite .

In these cases, differential equations for long wavelength modes may be obtained. Examples of interest include:

- (i) "bumpless" one-dimensional mode of EBT (VanDam et al.), and
- (ii) a two-dimensional bumpy cylinder.

#### REFERENCES

1. H. L. Berk, Phys. Fluids 19, 1255 (1976).
2. R. R. Dominguez and H. L. Berk, Phys. Fluids 21, 827 (1978).
3. D. B. Nelson, Phys. Fluids 23, 1850 (1980).
4. J. W. VanDam and Y. C. Lee, in Proceedings of the EBT Ring Physics Workshop (Oak Ridge, TN), Conf. 791228, p. 471.
5. K. T. Tsang, "Finite Larmor Radius Stabilization of Ballooning Modes in Tokamaks," Oak Ridge National Laboratory Report ORNL/TM-7324 (1980).
6. E. A. Frieman, G. Rewoldt, W. M. Tang, and A. H. Glasser, "General Theory of Kinetic Ballooning Modes," Princeton Plasma Physics Laboratory Report PPPL-1560 (1979).

## BALLOONING STABILITY IN TOROIDAL DEVICES

Shoichi Yoshikawa

Princeton Plasma Physics Laboratory  
Princeton, New Jersey 08544

and

Institute for Fusion Studies  
University of Texas at Austin  
Austin, Texas 78712ABSTRACT

The marginal stability condition of ballooning instabilities for toroidal confinement devices is derived for low critical stability  $\beta$  ( $\beta \leq 10\%$ ). The stability condition derived here should be applicable to EBT and multipoles as well as tokamaks and stellarators. For EBT and multipoles a more compact expression for the stability condition is possible and is given here in the appendix.

The MHD, finite  $\beta$  ballooning instability is expected to limit the maximum  $\beta$  in toroidal devices (tokamaks, stellarators, and EBT) as well as tandem mirrors. Thus it may behoove us to refine the critical  $\beta$  criterion which was first pointed out in the 1960's by a number of authors.<sup>1-3</sup> The usual way to determine the critical value is taking advantage of the fact that the growth rate,  $s$ , squared, is real in the MHD approximation. Hence the problem is reduced to solving for marginal stability condition,

$$v_A^2 \frac{d^2 \phi}{d\ell^2} + w_O^2(\ell) \phi = 0 \quad (1)$$

where  $w_O^2(\ell)$  is the local interchange growth rate,  $v_A$  is the Alfvén wave speed and  $\ell$  is taken parallel to  $B$ . In actual experimental situations, this simplification is somewhat modified as the magnetic field strength,  $B$ , is usually a function of  $\ell$ . But what will be described here presumably improves the usual assumption that  $w_O^2(\ell)$  is expanded in Fourier series and retained to the first term, thus transforming Eq. (1) into Mathieu's equation.

We shall impose periodic boundary condition such that  $\phi(\ell+L) = \phi(\ell)$ . And introduce a new variable

$$\theta = 2\pi \frac{\ell}{L} . \quad (2)$$

Then Eq. (1) may be rewritten as

$$\frac{d^2\phi}{d\theta^2} - \gamma[h + f(\theta)]\phi = 0 \quad (3)$$

$$\gamma \equiv \frac{\bar{R}_c a}{(L/2\pi)^2} \beta \quad (4)$$

$$0 = \int_0^{2\pi} d\theta f(\theta) \quad (5)$$

$$\bar{R}_c^2 \int \left( \frac{1}{R(\theta)} - h \frac{1}{\bar{R}_c} \right)^2 d\theta \equiv \int f^2(\theta) d\theta \quad (6)$$

$$\frac{h}{\bar{R}_c} \equiv \frac{1}{2\pi} \int \frac{d\theta}{R(\theta)} > 0 \quad (7)$$

Here  $R$  is defined as

$$\frac{1}{R} = \frac{d \ln B^2}{2 d \vec{n}} \cdot \frac{d\psi/d\vec{n}}{|d\psi/d\vec{n}|} \quad (8)$$

where  $\vec{n}$  is the normal component to constant pressure surface and often (but not necessarily always) coincides with the (quasi) magnetic surface. The difficulty which arises in many devices is that we cannot keep  $1/R$  such that  $d(\ln p)/d\vec{n} \cdot R$  is negative everywhere.

The function  $f$  is nondimensional and  $\langle f^2 \rangle$  is taken usually between  $0.5 \sim 2$ . It is not too difficult to impose one particular value for  $\langle f^2 \rangle$  but sometimes it is advantageous to define  $\langle f^2 \rangle$  at our discretion.

(i) Method of low  $\beta$  approximation.

The equation (3) can be solved rather easily by numerical methods. But often it is convenient to have an analytical solution available. Here we try that. We order coefficients of Eq. (3) as  $\gamma f(\theta) \sim 0(\epsilon)$ ,  $\gamma h \sim 0(\epsilon^2)$ . Usually  $h$  is  $\sim 1/10$  whereas  $f(\theta) \sim 1$ , so this ordering is not inconsistent. Finally,  $\gamma \sim \beta^2/h$  as we see later, so if  $\beta \leq 0.1$ ,  $\gamma$  is considered to be small.

Then to the zeroth order we obtain

$$\phi_0 = 1 . \quad (9)$$

To the next order

$$\frac{d^2 \phi_1}{d\theta^2} = \gamma f \phi_0 = \gamma f . \quad (10)$$

This is integrated once to yield

$$\frac{d\phi_1}{d\theta} = \gamma \int_0^\theta f(\theta) d\theta + C \equiv \gamma F(\theta) + C \quad (11)$$

$d\phi_1/d\theta$  satisfies the boundary condition in view of Eq. (5).

Integrating once more

$$\phi_1 = \gamma \int_0^\theta d\theta F(\theta) + C\theta + C_1 \quad . \quad (12)$$

The constant  $C_1$  may be absorbed by  $\phi_0$ . The constant  $C$  must be chosen to satisfy the boundary condition that is

$$C = -\frac{\gamma}{2\pi} \int_0^{2\pi} d\theta F(\theta) \equiv -\frac{\gamma}{2\pi} G(2\pi) \quad . \quad (13)$$

We defined

$$F(\theta) = \int_0^\theta f(\theta) d\theta, \quad F(2\pi) = 0 \quad (14)$$

$$G(\theta) = \int_0^\theta F(\theta) d\theta \quad (15)$$

Thus

$$\phi_1 = \gamma \left( G(\theta) - \frac{\theta}{2\pi} G(2\pi) \right) \quad (16)$$

To the next order

$$\frac{d^2\phi_2}{d\theta^2} = \gamma h + \gamma^2 f\phi_1 \quad . \quad (17)$$

Integrating once

$$\frac{d\phi_2}{d\theta} = \gamma h\theta + \gamma^2 \left[ \int_0^\theta d\theta fG(\theta) - \frac{G(2\pi)}{2\pi} \int_0^\theta f(\theta)\theta d\theta \right] + C_2. \quad (18)$$

$C_2$  is necessary to satisfy the boundary condition for  $\phi_2$ , but the necessity of satisfying the boundary condition for Eq. (18) brings out the  $\beta_c$ . Since at  $\theta=0$ ,  $d\phi_2/d\theta = C_2$ , it follows that

$$2\pi h + \gamma \left[ \int_0^{2\pi} d\theta fG(\theta) - \frac{G(2\pi)}{2\pi} \int_0^{2\pi} f(\theta)\theta d\theta \right] = 0. \quad (19)$$

The first term in the bracket gives [note  $F(2\pi) = 0$ ]

$$\int_0^{2\pi} d\theta fG = FG \Big|_0^{2\pi} - \int_0^{2\pi} G'F d\theta = - \int_0^{2\pi} F^2 d\theta. \quad (20)$$

Also

$$\int_0^{2\pi} f(\theta)\theta d\theta = F \cdot \theta \Big|_0^{2\pi} - \int_0^{2\pi} F d\theta = -G(2\pi). \quad (21)$$

Hence

$$\gamma = \frac{2\pi h}{\int_0^{2\pi} F^2 d\theta - \frac{1}{2\pi} [G(2\pi)]^2} \quad (22)$$

Schwartz's inequality assures the positiveness of the divisor except for the trivial case ( $f \equiv 0$ ).

Thus

$$\beta = \frac{2a\bar{R}_c}{(L/2\pi)^2} h \frac{\pi}{\int_0^{2\pi} F^2 d\theta - \frac{1}{2\pi}(G(2\pi))^2} \equiv \beta_{co} \cdot I . \quad (23)$$

$\beta_{co}$  is the critical  $\beta$  for  $f = \cos \theta$  and  $I$  is the correction factor for other functional forms of  $f(\theta)$ .

(ii) Some Examples

Let us calculate some simple examples. Assuming  $h$  is small from Eq. (6) and letting  $1/R(\theta) = (1/R_p)\cos\theta$  where  $R_p$  is the minimum field curvature radius, we get  $\bar{R}_c = R_p$ . Also  $I = 1$  because  $G(2\pi) = 0$ . So we get

$$\beta = \frac{2a^3 R_p}{(L/2\pi)^2} h = \beta_{co} \quad (24)$$

as is expected.

Take

$$\begin{aligned} f(\theta) &= 1, & 0 \leq \theta \leq \pi, \\ f(\theta) &= -1, & \pi \leq \theta \leq 2\pi. \end{aligned} \quad (25)$$

Again,  $\bar{R}_c = |R_p|$ . The calculation yields

$$\int_0^{2\pi} F^2 d\theta = \frac{2}{3} \pi^3 \quad (26)$$

$$G(2\pi) = \int_0^{\pi} d\theta \cdot \theta + \int_{\pi}^{2\pi} (2\pi - \theta) d\theta = \pi^2 . \quad (27)$$

Thus,

$$I = \frac{6}{\pi^2} \quad \text{or} \quad \beta = \frac{6}{\pi^2} \beta_{CO}. \quad (28)$$

If

$$f = \alpha, \quad 0 < \theta < \theta_1, \quad (29)$$

$$f = -\delta, \quad \theta_1 < \theta < 2\pi, \quad (30)$$

such that

$$\alpha\theta_1 = (2\pi - \theta_1)\delta. \quad (31)$$

Then after rather tedious, but straightforward calculations we get (by equating  $\delta = 1$ , thus  $R_C = R_{bad}$ )

$$I = \frac{6}{(2\pi - \theta_1)^2}, \quad (32)$$

$$\beta_C = \frac{2a|R_b|}{(L/2\pi)^2} h \frac{6}{(2\pi - \theta_1)^2}. \quad (33)$$

Thus,  $\beta_C$  could be smaller than the ordinary eigenvalue of Mathieu's equation.

If  $f = f(\theta) = \cos N\theta$  where  $N$  is an integer, we get

$$F = \frac{1}{N} \sin\theta. \quad (34)$$

Thus, we arrive at  $I = N^2$ . In other words,

$$\beta_C = \frac{2a|R_p|h}{(L/2\pi N)^2}. \quad (35)$$

That is even in systems such as Octupole or EBT, the connection length is determined by one period of bad-good curvature.

(iii) Comparison with wave mechanical solution.

The usual method to solve eigenvalues could, of course, be used. Let us take the case of Eq. (25) slightly modified so that

$$\begin{aligned} f(\theta) &= 1, & 0 \leq \theta \leq \frac{\pi}{2}, & \frac{3\pi}{2} \leq \theta \leq 2\pi \\ f(\theta) &= -1, & \frac{\pi}{2} \leq \theta \leq \frac{3\pi}{2}. \end{aligned} \quad (36)$$

The starting point is Eq. (32). We define

$$\begin{aligned} \gamma_1 &= (1 + h)\gamma, \\ \gamma_2 &= (1 - h)\gamma. \end{aligned} \quad (37)$$

Then in the domain I where  $f(\theta) = 1$ , we have

$$\phi = C_1 \cos h \gamma_1^{1/2} \theta. \quad (38)$$

In domain II where  $f(\theta) = -1$ , we have

$$\phi = C_2 \cos \gamma_2^{1/2} (\pi - \theta). \quad (39)$$

The connection at  $\theta = \frac{\pi}{2}$  and  $\frac{3\pi}{2}$  requires

$$\gamma_1^{1/2} \tan h \gamma_1^{1/2} \frac{\pi}{2} = \gamma_2^{1/2} \tan \gamma_2^{1/2} \frac{\pi}{2}. \quad (40)$$

The above equation can be solved for arbitrary  $\gamma$  numerically.

In the small  $\gamma$  limit we obtain

$$\frac{\pi}{2} \gamma_1 - \frac{\pi^3}{24} \gamma_1^2 = \frac{\pi}{2} \gamma_2 + \frac{\pi^3}{24} \gamma_2^2 \quad (41)$$

or

$$h\pi = \gamma \frac{\pi^3}{12} (1 + h^2) . \quad (42)$$

Thus we get

$$\beta_c = \frac{a\bar{R}_c}{(L/2\pi)^2} \cdot 2h \cdot \frac{6}{\pi^2} \frac{1}{(1 + h^2)} . \quad (43)$$

This is to be compared with Eq. (28) ( $h^2 \ll 1$ ).

We conclude that Eq. (23) is probably accurate enough for estimating critical  $\beta$  in normal situations.

### Acknowledgments

Discussions with Professor Marshall Rosenbluth are gratefully acknowledged.

This work was supported by United States Department of Energy Contract No. DE-AC02-76-CHO3073.

### References

<sup>1</sup>H. P. Furth, J. Killeen, M. N. Rosenbluth, and B. Coppi, in Plasma Physics and Controlled Nuclear Fusion Research (Proc. 2nd Int. Conf., Culham, 1965) Vol. I, IAEA, Vienna, 1966, p. 103.

<sup>2</sup>R. M. Kulsrud, in Plasma Physics and Controlled Nuclear Fusion Research (Proc. 2nd Int. Conf., Culham, 1965) Vol. I, IAEA, Vienna, 1966, p. 127.

<sup>3</sup>B. Coppi, M. N. Rosenbluth, and S. Yoshikawa, Physical Review Letters 20, 190 (1968).

APPENDIX  
CLOSED FIELD LINE DEVICES

In the case of floating multipoles or EBT, the geometry is very simple, so that a more formal set of equations can be utilized. In these devices, closed field lines  $\oint \frac{d\ell}{B} = \text{const}$  form the magnetic surfaces,  $\psi$ . And we can choose another orthogonal coordinate,  $\chi$  as  $\int B d\ell$  and the third coordinate  $\vec{\nabla}\psi \times \vec{\nabla}\chi$  is an ignorable coordinate.

Starting with a two fluid theory, using the usual assumptions among which  $|k_{\perp} \rho_i| \ll 1$  where  $k_{\perp}$  is the wave vector perpendicular to  $\vec{B}$ , and  $\rho_i$  is the ion Larmor radius, we arrive at

$$\frac{d\psi}{dn_0} \frac{1}{\mu_0} \nabla_{\parallel}^2 n + \left( \vec{\nabla} \frac{1}{B^2} \right)_n (nkTB) - \frac{MS^2 n}{B\kappa} = 0 \quad (1A)$$

where  $n_0$  is the unperturbed density,  $n$  is perturbed density, subscript  $n$  in  $\vec{\nabla} \frac{1}{B^2}$  means  $\vec{\nabla} \frac{1}{B^2} \cdot \vec{\nabla}\psi / |\vec{\nabla}\psi|$ ,  $kT = kT_e + kT_i$  is assumed constant,  $B$  is the magnitude of  $\vec{B}$ ,  $\kappa$  is the density gradient as defined  $(\nabla \ln n)_n$  with subscript  $n$  having the same meaning as  $(\vec{\nabla} \frac{1}{B^2})_n$ ,  $M$  is the mass of ions and  $S^2$  is the growth rate in the limit of  $|k_{\perp} \rho_i| \ll 1$ .

Since only  $S^2$  appears,  $S^2$  is real in Eq. (1A). Thus at marginal state the last term of Eq. (1A) can be made 0. Since  $B$  is a function of  $\ell$ ,  $\psi$ , where  $\ell$  is the coordinate in the direction of  $B$ , Eq. (1A) will be written as

$$B \frac{\partial}{\partial \ell} \frac{1}{B} \frac{\partial n}{\partial \ell} + \frac{dP_0}{d\psi} B^2 \mu_0 \frac{\partial}{\partial \psi} \frac{1}{B^2} = 0 \quad (2A)$$

or

$$\frac{\partial^2 n}{\partial \chi^2} + \frac{dP_0}{d\psi} \mu_0 \left( \frac{\partial}{\partial \psi} \frac{1}{B^2} \right) n = 0. \quad (3A)$$

Since the field lines are closed, it follows that

$$\oint d\chi = \chi_0 \propto \Sigma I_i, \quad (4A)$$

where  $\Sigma I_i$  is the total net current (in coils) enclosed by the closed field lines.

We define  $\left( \frac{\partial}{\partial \psi} \frac{1}{B^2} \right)_A$  as

$$\frac{\partial}{\partial \psi} \frac{1}{B^2} = \frac{d}{d\psi} \left\{ \frac{d\chi/B^2}{\chi_0} + \left( \frac{\partial}{\partial \psi} \frac{1}{B^2} \right)_A \right\}. \quad (5A)$$

Since  $\psi$  and  $\chi$  are orthogonal, the change of the order of operations involving  $\chi$  and  $\psi$  is permitted. Then Eq. (5A) implies

$$\left\{ \left( \frac{\partial}{\partial \psi} \frac{1}{B^2} \right)_A d\chi = \left( \frac{\partial}{\partial \psi} \left\{ \frac{d\ell}{B} \right\}_A \right) = 0. \quad (6A)$$

Thus, Eq. (3A) is reduced to

$$\frac{\partial^2 n}{\partial \chi^2} + \frac{dP_0}{d\psi} \mu_0 n \left( \frac{d}{d\psi} \left\{ \frac{d\chi}{B^2} \right\}_{\chi_0} \right) + \frac{dP_0}{d\psi} n \mu_0 \left( \frac{\partial}{\partial \psi} \frac{1}{B^2} \right)_A = 0. \quad (7A)$$

Again, ordering three terms of Eq. (7A) as  $1, \epsilon^2, \epsilon$ , we arrive at the critical  $dP_0/d\psi$  as

$$\frac{dP_0}{d\psi} = \frac{\frac{1}{\mu_0} \frac{d}{d\psi} \int \frac{d\ell}{B}}{\int H^2(\chi) d\chi - \frac{J^2(\chi_0)}{\chi_0}} \equiv L(\psi) \quad (8A)$$

where

$$H(\chi) \equiv \left( \frac{d}{d\psi} \int_0^\chi \frac{d\chi}{B^2} \right)_A = \left( \frac{d}{d\psi} \int_0^\chi \frac{d\ell}{B} \right)_A \quad (9A)$$

$$J(\chi) = \int_0^\chi H(\chi) d\chi. \quad (10A)$$

If  $|dP_0/d\chi|$  is larger than given in (8A), the plasma is unstable. Thus, in marginal stability cases

$$P = \int_{\psi_0}^{\psi} L(\psi) d\psi \quad (11A)$$

with  $P(\psi_0) = 0$  at  $\psi = \psi_0$ . Note in a  $\int d\ell/B$  stable plasma

$$\frac{dP_0}{d\psi} \frac{d}{d\psi} \int \frac{d\ell}{B} > 0. \quad (12A)$$

## EFFECT OF BETA LIMITS ON REACTOR PERFORMANCE IN EBT

N. A. Uckan and D. A. Spong  
Oak Ridge National Laboratory

and

D. B. Nelson  
Office of Fusion Energy  
Department of Energy  
Washington, D.C.

ABSTRACT

Theoretical models indicate limits on core beta ranging from a few percent to 10-20% depending on the models and/or assumptions. Some of the parameters that enter into these beta limits are: the ratio of the ring radial scale length to the average radius of curvature,  $\epsilon = \Delta/R_c$ ; the ratio of the cold to the hot plasma density,  $f_R = n_{\text{cold}}/n_{\text{hot}}$ ; the ratios of the hot electron drift frequency to the ion cyclotron frequency,  $\omega_{\text{dh}}/\omega_{\text{ci}}$ , and to the drift Alfvén frequency  $\omega_{\text{dh}}/kV_A$ ; the ratio of the ring electron temperature to the core ion temperature,  $T_R/T_i$ ; the ring beta  $\beta_R$ ; etc.

Because of uncertainties in extrapolating results of simplified models to a reactor plasma, the above parameters that influence the beta limits cannot be determined accurately at the present time. Also, reasonable changes within the models and/or assumptions are seen to affect the core beta limits by almost an order of magnitude. Hence, at the present, these limits cannot be used as a rigid (and reliable) requirement for ELMO Bumpy Torus (EBT) reactor engineering considerations. However, sensitivity studies can be carried out to determine the boundaries of the operating regime and to demonstrate the effects of various modes, assumptions, and models on reactor performance (Q value). First the modes believed to limit the core  $\beta$  and ring plasma performance are discussed, and the simplifications and/or assumptions involved in deriving these limits are highlighted. Then, the implications of these limits for a reactor are given.

## 1. INTRODUCTION

In the ELMO Bumpy Torus (EBT), there are two principal plasma components: toroidal core plasma, where the fusion reactions occur, and hot electron rings, which are essential to the stability of the overall configuration. The stability requirements of ring and core plasmas are closely coupled, and their interaction defines stable operating regimes of both plasmas and determines core  $\beta$  limits [1-3]. The economic viability of an EBT reactor improves significantly if the average core beta  $\langle \beta_{\text{core}} \rangle$  exceeds  $\sim 10\%$  and an average "minimum-B" stabilization requires  $\beta_{\text{ring}} \geq 10-15\%$  [1,4].

The role of high  $\beta$ , hot electron rings in maintaining the stability of the toroidal plasma against flute and interchange modes may be seen from Fig. 1 and the simple stability criterion given below [1]:

$$(p' + \gamma p U'/U)(U' - p' \oint dl/B^3) > 0 \quad , \quad (1)$$

where  $U = \oint dl/B$  and  $' = d/d\psi$ . For stability, Eq. (1) must be satisfied on each flux surface  $\psi$ . In Fig. 1, typical profiles of  $\oint dl/B$ , the magnetic field  $B$ , and the pressures (core and ring) are given as a function of the radius at the midplane. Equation (1) indicates that in the central plasma region, stability is attained if either  $p' = 0$  or  $p'U > -\gamma p U'$ ; i.e., pressure gradients may be stably supported up to some critical slope. At the inside of the plasma edge, where  $p' < 0$  and  $U' > 0$  and increasing, somewhat larger pressure gradients can be tolerated because (see Fig. 1)  $U'$  (inside edge)  $> U'$  (central region). Finally, at the outer edge where  $p \rightarrow 0$ ,  $p' < 0$ , and  $U' < 0$ , stability is possible if  $|p'| < |U'|/\oint dl/B^3$ . Thus, the electron ring modifies the  $B$  field and  $\oint dl/B$  in such a way as to stably support plasma pressure gradients in the regions in which they are largest. The stability threshold is then related to the critical value of ring beta required to make  $U' < 0$ , where  $U'$  may be written as

$$U' = - \oint dl (\kappa/r + \partial B/\partial \psi) / B^2 < 0 \quad (2)$$

ORNL-DWG 81-2904 FED

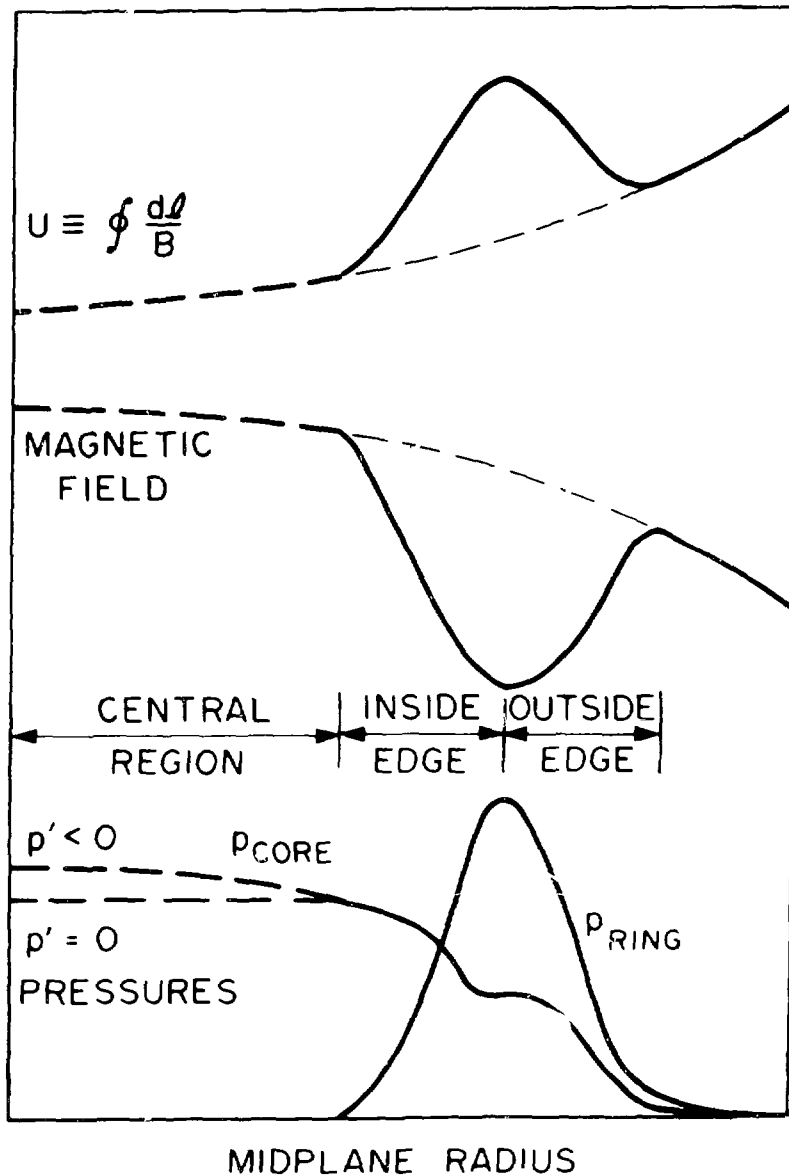


Fig. 1 Typical profiles of  $U \equiv \int dl/B$ , the magnetic field  $B$ , and the pressures (core and rings) are given as a function of radius at the midplane. Rings modify  $\int dl/B$  and  $B$  to support pressure gradients in regions where they are largest.

for stability. Considering the regions of positive and negative curvature  $\kappa$  for field lines and using the appropriate scale lengths, one then finds the necessary value of ring beta to reverse the gradients is to be given as follows [1]:

$$(\beta_{\text{ring}})_{\text{crit}} \approx 2\Delta/R_c, \quad (3)$$

where  $\Delta$  = ring scale length and  $R_c \cong$  magnetic radius of curvature (mid-plane). This ring beta ( $\beta_{\text{ring}} \sim 5\text{-}15\%$ ) agrees with the experimental observation of the transition to the quiescent mode of operation (C-T transition [5]).

Both magnetohydrodynamic (MHD) models [1] (derived from modified energy principle) and kinetic models in slab geometry [2-3] show that the core plasma is stabilized only if the ring beta exceeds the critical value given by Eq. (3) that is required to produce a distinct local minimum in B. At higher values of ring beta, the earlier decoupled MHD calculations [1] indicated stable core betas to be as high as the ring beta ( $\beta_{\text{core}} \sim 30\text{-}40\%$ ). Coupled kinetic calculations [2-3], on the other hand, indicate a saturation in core beta to values near  $0(\beta_{\text{crit}})$ . The various aspects of the EBT stability were treated at this workshop, and readers should refer to other papers for details [6].

In the present experiments, the core  $\beta$  is limited to  $\beta_{\text{core}} \leq 0.5\%$  because of transport and heating considerations (small size as well) rather than stability, whereas  $\beta_{\text{ring}} \sim 10\text{-}40\%$  is routinely attained and the stabilization of a low  $\beta_{\text{core}}$  plasma by the hot electron rings has been amply demonstrated [5]. Experimental confirmation of high  $\beta_{\text{core}}$  predictions is not possible at the present time. However, the next planned device, the EBT Proof-of-Principle (EBT-P) experiment, is expected to have  $\beta_{\text{core}}$  values on the order of a few percent that could be able to test some of the predictions.

In this paper, we will briefly discuss the results of coupled core-ring stability calculations, the stability of the hot electron rings, and the implications of these stability limits for a reactor.

## 2. COUPLED CORE-RING STABILITY LIMITS

Stability problems often fall into two categories, macrostability and microstability. In EBT, these distinctions are somewhat complicated by the requirement of a kinetic treatment for traditional macroscopic modes (interchange, for example) because the requirements for MHD are not satisfied for the hot electron rings. This also results in a given class of modes being called different names by different authors in the literature.

At present, EBT stability calculations have indicated the existence of three modes which can limit the core  $\beta$ , core density, and ring density; these are the core interchange, the compressional Alfvén wave stability, and the hot electron interchange [6-8]. For simplicity, these are often treated as separate modes and will be considered as such in the following. However, calculations in slab geometry which take all three modes into account indicate that [9-10] in certain parameter ranges two of these modes can become coupled, resulting in lower stability boundaries than would be found by considering each mode separately [8]. Such coupling requires further examination in the reactor case.

### 2.1 Core interchange and MHD ballooning modes

These are low frequency modes and are identified as the modes responsible for the quiescent mode of operation (C-T transition [5]). These modes are driven by curvature in the magnetic field and by the core pressure gradients. The stability boundary of these modes is sensitive to the hot electron distribution function. They are stable if [2-3]

$$\beta_{\text{ring}} \equiv \beta_R > 4\Delta/\langle R_c \rangle, \quad (4a)$$

$$\beta_{\text{core}} \equiv \beta_* \lesssim \alpha\epsilon/(1 + \beta_{\perp}) \quad , \quad (4b)$$

where  $\alpha \sim 2-4$ , depending on the hot electron distribution function,  $\epsilon = \Delta/R_c$  is the ring radial scale length divided by the radius of curvature within the ring length, and  $\beta_{\perp}$  is the perpendicular component of the hot

electron pressure (beta). The first inequality [Eq. (4a), which is the same as Eq. (3)] is the requirement that the hot electrons form a magnetic well, and the second inequality is the fundamental  $\beta_{\text{core}}$  limitation in that well, which is normally in the 5-15% level for a reactor.

The estimate given by Eq. (4b) is based on a slab model that neglects variations along the field lines. Such variations have been taken into account in a generalized energy principle [11] derived for low frequency modes ( $\omega \ll \omega_{\text{dh}}, \omega_{*h}$ ). Preliminary estimates of the beta limit from the energy principle indicate values in the same range as Eq. (4b). However, by taking into account details of the equilibrium fields and modifications introduced in  $R_c$  by supplementary field shaping [i.e., aspect ratio enhancement (ARE) and symmetrizing (SYM)] coils [12], it may be possible to optimize the  $\beta_*$  limit to higher values than would be predicted by the simplified local slab theory.

## 2.2 Compressional Alfvén mode

The compressional Alfvén mode places a limitation on the core plasma density [8-10]. This does not appear to be a severe problem for either present-day or reactor-like devices provided the mode is sufficiently localized to the ring region. For radial wavelengths on the same order as the ring thickness ( $k_r \Delta \gtrsim 1$ ), a local slab model predicts [8] for stability

$$k_{\perp}^2 V_A^2 > 4(\Delta_B/R_c)\omega_B^2 \quad (5)$$

where  $k_{\perp}^2 = k_r^2 + k_{\theta}^2$ ;  $k_r = 2n/\Delta$  with  $n = 1, 2, \dots$ ;  $k_{\theta} = m/a_p$  with  $m = 1, 2, \dots$  and  $a_p$  the plasma radius;  $V_A$  is the Alfvén velocity;  $\Delta_B \approx 2\Delta/\beta_R$  is the finite  $\beta$  ring  $\nabla B$  scale length; and  $\omega_B = k_{\theta} V_B (= \omega_{\text{dh}})$  is the  $\nabla B$  hot electron drift frequency.

## 2.3 Hot electron interchange mode

The hot electron interchange mode results in a lower limit on the ratio  $n_{\text{cold}}/n_{\text{hot}}$  ( $\equiv n_{\text{core}}/n_{\text{ring}}$ ). This mode is stable in the local slab model [8] if

$$\omega_B^2 (\Delta_B / R_c)^2 > (4V_A^2 / \Delta_B R_c) (k_\theta / k_\perp)^2 \quad . \quad (6)$$

It is conjectured in Refs. [8-10] that this mode could exist near the T-M transition in EBT [5], especially, when its coupling with the compressional Alfvén mode is taken into account. For a reactor, this mode will result in an upper limit on the hot electron beta ( $\beta_R$ ), but this should be in excess of what is required to reverse the magnetic field gradient and create a well.

#### 2.4 Coupling of various modes

The importance of core-ring interaction has led to slab models which take into account nonadiabatic terms ( $\sim \omega / \omega_{dh}$ ) and ion cyclotron harmonics ( $\omega_{dh} \sim \omega_{ci}$ ) in order to treat the coupling of various modes discussed earlier [9-10]. The inclusion of  $O(\omega / \omega_{dh})$  terms shows results with dependence on  $T_{ring} / T_{core}$  ( $= T_R / T_*$ ) and a slightly lower  $\beta_*$  limit. The inclusion of ion cyclotron terms results in coupling of compressional Alfvén waves to interchange modes with higher permissible core  $\beta_*$  and core density limits [10].

### 3. STABILITY OF HOT ELECTRON RINGS

As has been observed in earlier electron cyclotron heating (ECH) experiments in simple mirrors [13], the rings themselves may be subject to various macroscopic and microscopic instabilities.

One of the more fundamental electron ring stability limits is the mirror instability, which may be related to a loss of equilibrium. Conditions for the stabilization of this mode (driven by pressure anisotropy  $p_{\perp} \gg p_{\parallel}$ ) relate to properties of the ECH process, particularly the effective (mirror) ratio at the resonant magnetic field. In both theory and experiment [13], if  $B_{\text{res}}/B_{\text{min}} \geq 1.2$ , then  $T_{\perp}/T_{\parallel} [\cong (B_{\text{res}}/B_{\text{min}} - 1)^{-1}]$  can be kept below a certain threshold and the plasma is relatively free of the instability. In addition, a class of MHD instabilities occurs; these are flute interchanges at fairly low values of ring beta and finite beta ballooning modes. Interchange modes have been examined using both guiding center theory [14] and Vlasov-Maxwell kinetic models [15]. These show that the modes could be stabilized by the self-dug well, provided  $\beta_R \geq 15\%$  [14], and by the presence of sufficient cold plasma density [15]. At sufficiently high ring beta, ballooning modes are also energetically possible, but kinetic treatments of these instabilities have indicated that they may be significantly stabilized by the large drift frequency of the hot electrons relative to the ion cyclotron frequency [4] and by the presence of cold plasma [16].

Most of the possible ring microinstabilities are driven by the anisotropic nature of the ring distribution function. Such modes could potentially have an adverse effect on ring power balance. However, it has been experimentally observed that nearly classical ring energy losses are obtained if off-resonant heating is applied [17]. An example is the Whistler instability, which is an electromagnetic mode. A relativistic analysis [18] of this instability indicates that sufficient relativistic spread in the electron cyclotron frequency results in resonant particles in the high energy tail contributing damping rather than growth. Such instabilities could be suppressed by building up the tail density of hot electrons to some critical level. A recent study [19] indicates a similar

damping effect; however, the instability persists if  $T_{\perp}/T_{\parallel}$  is large enough. A second type of microinstability is the Timofeev half-harmonic modes. These are electrostatic modes and are commonly seen in ELMO but not in EBT. The modes are stabilized if  $T_{\parallel}/T_{\perp}$  is sufficiently large (i.e., if  $T_{\parallel}/T_{\perp} \geq 1/6$ ) [20]. In the experiments this is attained by added off-resonant heating [17].

#### 4. DISCUSSION OF THE RESULTS AND THEIR IMPLICATIONS FOR A REACTOR

As discussed in the previous sections, the theoretical models have indicated the existence of several modes that can limit the performance of the ring and core plasmas. All of these analyses predict a stable finite beta operating regime with reasonable and self-consistent parameters. However, predicted limits on core beta range from  $\beta_* \sim$  few percent to  $\beta_* > 10\text{-}20\%$  for reasonable but different parameters and/or assumptions within the same model. Some of the parameters that enter into these beta limits are  $\alpha$ ,  $\epsilon = \Delta/R_c$ ,  $\Delta_B/R_c$ ,  $f_R = n_{\text{cold}}/n_{\text{hot}}$ ,  $\omega_{\text{dh}}/\omega_{\text{ci}}$ ,  $\omega_{\text{dh}}/kV_A$ ,  $T_R/T_i$ ,  $\beta_R$ , etc. Some of these parameters change significantly in going from present-day experiments to reactor-like devices. Because of uncertainties in extrapolating results of simplified models to a reactor plasma, dependence of stability limits on the above parameters cannot be determined accurately at the present time. In the following, we will show the sensitivity of the reactor Q value to some of these uncertainties. It should be pointed out that it is not clear what the non-linear consequences of the various instabilities will be and it is not clear that the system has to be stable against all of the possible modes.

The core interchange is one of the most serious modes that will limit the core  $\beta$ , with two key parameters  $\alpha$  and  $\epsilon$  determining this limit; core plasma is stable if  $\beta_* \leq \alpha\epsilon$  [see Eq. (4b)]. Depending on the hot electron distribution function and details of the equilibrium fields,  $\alpha$  varies from 2 to 6. An accurate determination of  $\epsilon = \Delta/R_c$  in a reactor requires knowledge of the ring thickness  $\Delta$  and the radius of curvature  $R_c$ , both of which are difficult to extrapolate at the present time. Using scaling data from the present experiments,  $\epsilon \approx 10^{-2} - 5 \times 10^{-2}$  is likely in a reactor. In the experiments, the hot electron rings form at the location of the second harmonic ( $\omega \sim 2\omega_{\text{ce}}$ ) resonance with a radial half-width  $\Delta$  of a few hot electron gyroradii  $\rho_{\text{eR}}$  [13]. For ring temperatures characteristic of past, present, and near-term ECH experiments ( $T_R \lesssim 1.5$  MeV), drag losses dominate [13] and ring energies are limited by non-adiabatic particle behavior, obeying  $\rho_{\text{eR}}/\Delta_B \sim 5\text{-}6 \times 10^{-2}$  scaling [21]. In a reactor, the ring temperature ( $T_R \geq 2$  MeV) is expected to be in a radiation dominated regime, and ring energies will be limited by radiation cooling.

Defining a reactor Q value that is roughly the ratio of the fusion power produced ( $P_{th} \sim \beta^2 B^4$ ) to the ring sustaining power ( $P_{\mu R} \sim \beta_R B_R^4 \sim f_R^{-1} \beta_*^2 B_*^4$ ) and taking into account the appropriate conversion efficiencies, the overall  $Q_E$  ( $Q_{electric}$ ) value can be given as [13,22]

$$Q_E \approx 7.7 \times 10^{18} f_R (V_P/V_R) \langle \sigma v \rangle_{DT} (T_*/T)^2 (\beta^2 B^4 / \beta_*^2 B_*^4) G(\gamma, \beta_*)$$

$$\approx 4 \times 10^{18} \cdot f_R \cdot \epsilon^{-1} \cdot \langle \sigma v \rangle_{DT} \cdot k^2 \cdot G(\gamma, \beta_*) \quad , \quad (7)$$

where  $V_P$  and  $V_R$  are the toroidal and ring plasma volumes ( $V_P/V_R \approx 1.3/\epsilon$  for a system with a mirror ratio of  $\sim 2-2.3$ ),  $\beta_* \sim n_* T_*/B_R^2$  is the toroidal core plasma beta near the vicinity of the ring (which enters in the stability calculations),  $k = \bar{n}/n_* \approx \bar{T}/T_*$  is the profile factor,  $\beta \sim \bar{n} \bar{T}/B^2 \sim \beta_* k^2/2$  is the volume average core beta,  $\gamma$  is the relativistic factor, and  $G(\gamma, \beta_*)$  is given by

$$G(\gamma, \beta_*) = [\gamma / \sqrt{\gamma^2 - 1} + 1.3 \times 10^{-4} (\gamma^2 - 1) T_*/\beta_*]^{-1} \quad . \quad (8)$$

Figure 2 shows the variation of  $Q_E/f_R$  with the ring temperature for the possible range of uncertainty levels involved in  $\epsilon$  and  $\alpha$ . As pointed out earlier, the stability of hot electron rings requires an appreciable cold electron density component near the vicinity of the rings and the value of  $f_R$  in a reactor is  $O(10^1-10^2)$ . This leads to  $Q_E$  values ranging from as low as few ( $\sim 2-5$ ) to  $\sim 50$  depending on the uncertainties in ring scale lengths (Fig. 2a) and  $\beta_*$  limits (Fig. 2b). It can be seen from Fig. 2 that at low temperatures ( $T_R < 1.5$  MeV), where drag losses dominate,  $Q_E$  indicates an almost inverse linear dependence to ring scale lengths for fixed  $\alpha$  (basically dependence on ring volume and not on core beta  $\beta_*$ ). At high ring temperatures ( $T_R \gg 1$  MeV), there is an almost linear dependence of  $Q_E$  on  $\beta_*$  for fixed scale lengths.

As pointed out, the compressional Alfvén mode does not appear to be a severe problem for a reactor and imposed core density limitations are in excess of what is needed in a reactor. However, the hot electron drift mode, which is stable (see Refs [4,16]) if

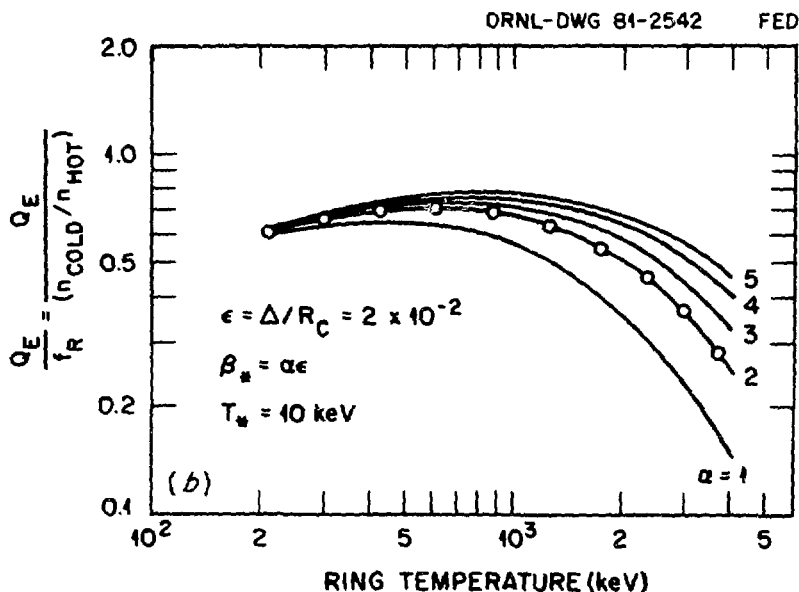
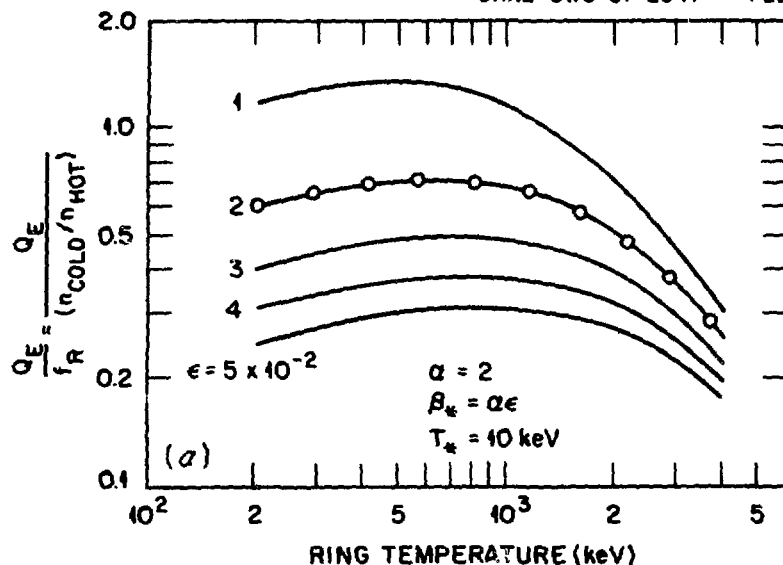


Fig. 2 Variation of overall reactor  $Q_E$  value (for given  $f_R = n_{\text{COLD}}/n_{\text{HOT}}$ ) with ring temperature indicates (a) an almost inverse linear dependence to ring scale lengths for fixed  $\alpha$  at low ring temperatures ( $T_R < 1.5 \text{ MeV}$ ,  $Q_E \sim 1/\epsilon \sim 1/\text{ring volume}$ ) that is basically due to change in ring volume and (b) an almost linear dependence on  $\alpha$  or  $\beta_*$  ( $= \alpha\epsilon$ ) for fixed scale lengths at high ring temperatures. The value of  $f_R$  in a reactor is  $0(10^1-10^2)$ .

$$\omega_{dh} \geq \omega_{ci} \quad \text{and} \quad n_{cold}/n_{hot} > 1 \quad , \quad (9)$$

or the hot electron interchange, which is stable (see Ref. [8]) if Eq. (6) is satisfied or, alternatively,

$$\omega_{dh}^2/\omega_{ci}^2 > f(\Delta_B/R_c, k_\theta/k_l, \omega_{pi}, \dots) \quad , \quad (10)$$

requires careful analysis and trade-off. In a reactor, achieving the first inequality in Eq. (9) will require either very energetic ( $>10$  MeV) electrons or very small  $\Delta$ , i.e., very small  $\epsilon$ . Similar conclusions can be drawn from Eq. (10); however, the picture is somewhat complicated because of the involvement of various mode numbers ( $k_\theta/k_l$ ). In both cases there is a trade-off between the hotter electrons, which cause severe radiation losses, and smaller  $\epsilon$  (smaller  $\Delta$ ), which lowers the  $\beta_*$  limit. This trade-off can be seen from Fig. 2.

#### ACKNOWLEDGMENTS

The authors would like to thank J. W. Van Dam, C. L. Hedrick, and H. L. Berk for many helpful discussions.

## REFERENCES

1. D. B. Nelson, C. L. Hedrick, Nucl. Fusion 19 (1979) 283.
2. J. W. Van Dam, Y. C. Lee, Stability Analysis of a Hot Electron EBT Plasma, *EBT Ring Physics: Proc. of the Workshop* (N. A. Uckan, Ed.), Oak Ridge National Laboratory CONF-791228 (1980) 471-489.
3. D. B. Nelson, Phys. Fluids 23 (1980) 1850.
4. G. E. Guest, C. L. Hedrick, and D. B. Nelson, Phys. Fluids 18 (1975) 871.
5. R. A. Dandl, et al., *Plasma Physics and Controlled Nuclear Fusion Research 1978*, Vol. 2 (1979) 365; R. A. Dandl, et al., *Plasma Physics and Controlled Nuclear Fusion Research 1974*, Vol. 2 (1975) 141.
6. See papers in this proceedings.
7. D. A. Spong, Review of Recent EBT Coupled Ring Core Stability Theory, in this proceedings.
8. J. W. Van Dam, et al., Radially-Dependent Stability Theory for EBT; D. A. Spong, et al., Numerical Solutions of the EBT Radial Eigenmode Problem, in this proceedings.
9. D. A. Spong, A. M. El-Nadi, The Interchange Mode in Three-Species Bumpy Torus Plasmas, Bull. Am. Phys. Soc. 25 (1980) 964.
10. K. T. Tsang, C. Z. Cheng, Stability of Hot Electron Plasma in the ELMO Bumpy Torus; C. Z. Cheng, K. T. Tsang, Analytical Theory of Interchange and Compressional Alfvén Instabilities in EBT in this proceedings.
11. J. W. Van Dam, M. N. Rosenbluth, Y. C. Lee, A Generalized Kinetic Energy Principle, IFS Report #12 (1981).
12. L. W. Owen, N. A. Uckan, EBT Reactor Magnetics and Particle Confinement, J. Fusion Energy (to be published).
13. N. A. Uckan, Ed., *EBT Ring Physics: Proc. of the Workshop*, Oak Ridge National Laboratory CONF-791228 (1980).
14. G. E. Guest, C. L. Hedrick, D. B. Nelson, Oak Ridge National Laboratory Rep. ORNL-TM-4077 (1972).
15. H. L. Berk, Phys. Fluids 19 (1976) 1255.

16. R. R. Dominguez, H. L. Berk, *Phys. Fluids* 21 (1978) 827;  
R. R. Dominguez, Flute Interchange Stability in a Hot Electron Plasma, in Ref. [13], pp. 383-407.
17. R. A. Dandl, et al., in *Plasma Physics and Controlled Nuclear Fusion Research*, Vol. 2 (1969) 435; *Plasma Physics and Controlled Nuclear Fusion Research*, Vol. 2 (1972) 607; R. A. Dandl, Review of Ring Experiments, in Ref. [13], pp. 31-57.
18. C. L. Hedrick, Suppression of the Whistler Instability by Relativistic Effects, Oak Ridge National Laboratory Rep. ORNL-4688 (1971) 6-9.
19. N. T. Gladd, et al., Microstability of EBT Boundary, in this proceedings.
20. G. E. Guest, D. J. Sigmar, *Nucl. Fusion* 11 (1971) 151.
21. N. A. Uckan, Adiabatic Energy Limit in ECH Hot Electron Plasmas (unpublished).
22. N. A. Uckan, Physics Issues of an EBT Reactor, *IAEA Proc. Symposium on Physics Problems of Fusion Reactors* (to be published).

## AUTHOR INDEX

- I. Alexeff, 83  
D. E. Baldwin, 1  
L. Bighel, 75  
H. L. Berk, 1, 97, 115, 249  
C. Z. Cheng, 141, 161  
R. H. Cohen, 211  
R. R. Dominguez, 249  
N. T. Gladd, 181  
H. Grad, 1  
G. E. Guest, 15  
S. Hamasaki, 181  
G. R. Haste, 63, 75  
C. L. Hedrick, 1  
S. Ishiguro, 229  
T. Kamimura, 229  
A. Komori, 75  
N. A. Krall, 1, 181  
Y. Matsuda, 211  
D. B. Nelson, 281  
W. M. Nevins, 211  
T. Onigo, 229  
M. N. Rosenbluth, 97, 115  
H. Sanuki, 229  
M. Saylor, 83  
J. L. Sperling, 181  
D. A. Spong, 1, 33, 97, 115, 281  
K. T. Tsang, 141, 161  
N. A. Uckan, 1, 63, 281  
J. W. Van Dam, 97, 115  
S. Yoshikawa, 265

## ATTENDANCE LIST

## EBT STABILITY THEORY WORKSHOP

May 13-14, 1981

Oak Ridge, Tennessee

I. Alexeff Dept. of Electrical Engineering University of Tennessee Knoxville, TN 37916	J. D. Callen University of Wisconsin Nuclear Engineering Department Madison, WI 53706
W. B. Ard, Bldg. 107 McDonnell Douglas Astronautics Co. P. O. Box 516 St. Louis, MO 63166	R. B. Campbell TRW, Incorporated One Space Park, Bldg. #1 Redondo Beach, CA 90278
F. W. Eaity Oak Ridge National Laboratory P. O. Box Y Oak Ridge, TN 37830	B. A. Carreras Oak Ridge National Laboratory P. O. Box Y Oak Ridge, TN 37830
D. E. Baldwin, L-630 Lawrence Livermore National Lab. P. O. Box 5511 Livermore, CA 94550	C. Z. Cheng Princeton Plasma Physics Lab. P. O. Box 451 Princeton, NJ 08544
D. B. Batchelor Oak Ridge National Laboratory P. O. Box Y Oak Ridge, TN 37830	M. Clark, Jr. Combustion Engineering, Inc. 1000 Prospect Hill Road Windsor, CT 06095
H. L. Berk Institute of Fusion Studies University of Texas at Austin Austin, TX 78712	J. A. Cobble Oak Ridge National Laboratory P. O. Box Y Oak Ridge, TN 37830
L. A. Berry Oak Ridge National Laboratory P. O. Box Y Oak Ridge, TN 37830	R. J. Colchin Oak Ridge National Laboratory P. O. Box Y Oak Ridge, TN 37830
L. Bighel Oak Ridge National Laboratory P. O. Box Y Oak Ridge, TN 37830	K. A. Connor Rensselaer Polytechnic Institute ECSE Department Troy, NY 12181
S. K. Borowski The University of Michigan Dept. of Nuclear Engineering Cooley Bldg., North Campus Ann Arbor, MI 48105	W. A. Cooper Oak Ridge National Laboratory P. O. Box Y Oak Ridge, TN 37830

R. L. Copeland  
Oak Ridge National Laboratory  
P. O. Box Y  
Oak Ridge, TN 37830

E. C. Crume, Jr.  
Oak Ridge National Laboratory  
P. O. Box Y  
Oak Ridge, TN 37830

W. A. Davis  
Oak Ridge National Laboratory  
P. O. Box Y  
Oak Ridge, TN 37830

R. R. Dominguez  
General Atomic  
P. O. Box 81608  
San Diego, CA 92138

R. A. Dory  
Oak Ridge National Laboratory  
P. O. Box Y  
Oak Ridge, TN 37830

J. L. Dunlap  
Oak Ridge National Laboratory  
P. O. Box Y  
Oak Ridge, TN 37830

H. O. Eason  
Oak Ridge National Laboratory  
P. O. Box Y  
Oak Ridge, TN 37830

W. R. Ellis  
Office of Fusion Energy  
Department of Energy  
MS-256  
Washington, DC 20545

M. E. Fenstermacher  
University of Michigan  
Dept. of Nuclear Engineering  
Ann Arbor, MI 48105

H. H. Fleischmann  
Cornell University  
Department of Applied Physics  
Ithaca, NY 14853

N. T. Gladd  
JAYCOR  
11011 Torreyana Road  
San Diego, CA 92138

J. C. Glowienka  
Oak Ridge National Laboratory  
P. O. Box Y  
Oak Ridge, TN 37830

R. C. Goldfinger  
Oak Ridge National Laboratory  
P. O. Box Y  
Oak Ridge, TN 37830

M. R. Gordinier  
McDonnell Douglas Astronautics Co.  
P. O. Box 516  
St. Louis, MO 63166

M. J. Gouge  
Department of Energy  
Oak Ridge Operations  
Oak Ridge, TN 37830

H. Grad  
Courant Institute  
New York University  
251 Mercer Street  
New York, NY 10012

W. Grossmann  
Courant Institute  
New York University  
251 Mercer Street  
New York, NY 10012

G. E. Guest  
Applied Microwave Plasma Concepts  
2210 Encinitas Bldg., Suite F  
Encinitas, CA 92024

G. A. Hallock  
RPI/ORNL  
P. O. Box Y  
Oak Ridge, TN 37830

G. R. Haste  
Oak Ridge National Laboratory  
P. O. Box Y  
Oak Ridge, TN 37830

C. L. Hedrick  
Oak Ridge National Laboratory  
P. O. Box Y  
Oak Ridge, TN 37830

D. L. Hillis  
Oak Ridge National Laboratory  
P. O. Box Y  
Oak Ridge, TN 37830

J. T. Hogan  
Oak Ridge National Laboratory  
P. O. Box Y  
Oak Ridge, TN 37830

E. B. Hooper, Jr.  
Lawrence Livermore National Lab.  
P. O. Box 5511  
Livermore, CA 94550

W. A. Houlberg  
Oak Ridge National Laboratory  
P. O. Box Y  
Oak Ridge, TN 37830

H. Iguchi  
Institute of Plasma Physics  
Nagoya University  
Nagoya 464, Japan

H. Ikegami  
Institute of Plasma Physics  
Nagoya University  
Nagoya 464, Japan

E. F. Jaeger  
Oak Ridge National Laboratory  
P. O. Box Y  
Oak Ridge, TN 37830

R. E. Juhala  
McDonnell Douglas Astronautics Co.  
P. O. Box 516  
St. Louis, MO 63166

T. Kammash  
University of Michigan  
Dept. of Nuclear Engineering  
Ann Arbor, MI 48105

R. J. Kashuba  
McDonnell Douglas Astronautics Co.  
P. O. Box 516  
St. Louis, MO 63166

N. A. Krall  
JAYCOR  
11011 Torreyana Road  
San Diego, CA 92138

L. L. Lao  
TRW, Incorporated  
One Space Park  
Redondo Beach, CA 90278

B. J. Leikind  
UCLA  
Physics Department  
Los Angeles, CA 90024

J. B. McBride  
Science Applications, Inc.  
1200 Prospect St.  
La Jolla, CA 92037

W. H. Miner  
Science Applications, Inc.  
1710 Goodridge Dr.  
McLean, VA 22102

M. Mond  
New York University  
251 Mercer Street  
New York, NY 10012

M. Murakami  
Oak Ridge National Laboratory  
P. O. Box Y  
Oak Ridge, TN 37830

D. B. Nelson  
Office of Fusion Energy  
Department of Energy  
MS-256  
Washington, DC 20545

W. M. Nevins  
Lawrence Livermore National Lab.  
P. O. Box 5511  
Livermore, CA 94550

L. W. Owen  
Oak Ridge National Laboratory  
P. O. Box Y  
Oak Ridge, TN 37830

Y. Pao  
New York University  
251 Mercer Street  
New York, NY 10012

R. E. Price  
Office of Fusion Energy  
Department of Energy  
Washington, DC 20545

R. K. Richards  
Oak Ridge National Laboratory  
P. O. Box Y  
Oak Ridge, TN 37830

J. R. Roth  
University of Tennessee  
Dept. of Electrical Engineering  
Knoxville, TN 37916

M. J. Saltmarsh  
Oak Ridge National Laboratory  
P. O. Box Y  
Oak Ridge, TN 37830

H. Sanuki  
Institute of Plasma Physics  
Nagoya University  
Nagoya 464, Japan

T. Shoji  
Institute of Plasma Physics  
Nagoya University  
Nagoya 464, Japan

G. W. Shuy  
UCLA  
6291 Boelter Hall  
Los Angeles, CA 90024

A. Simon  
University of Rochester  
MAS Department  
Rochester, NY 14627

T. C. Simonen, L-441  
Lawrence Livermore National Lab.  
P. O. Box 5511  
Livermore, CA 94550

L. Solensten  
RPI/ORNL  
P. O. Box Y  
Oak Ridge, TN 37830

D. A. Spang  
Oak Ridge National Laboratory  
P. O. Box Y  
Oak Ridge, TN 37830

D. W. Swain  
Oak Ridge National Laboratory  
P. O. Box Y  
Oak Ridge, TN 37830

J. S. Tolliver  
Oak Ridge National Laboratory  
P. O. Box Y  
Oak Ridge, TN 37830

K. T. Tsang  
Science Applications, Inc.  
934 Pearl Street, Suite A  
Boulder, CO 80302

J. M. Turner  
Office of Fusion Energy, ER-56  
Department of Energy  
Washington, DC 20545

N. A. Uckan  
Oak Ridge National Laboratory  
P. O. Box Y  
Oak Ridge, TN 37830

T. Uckan  
Oak Ridge National Laboratory  
P. O. Box Y  
Oak Ridge, TN 37830

C. M. Van Atta  
Lawrence Livermore National Lab.  
P. O. Box 5511  
Livermore, CA 94550

J. W. Van Dam  
Institute of Fusion Studies  
University of Texas  
Austin, TX 78712

H. Weitzner  
New York University  
251 Mercer Street  
New York, NY 10012

J. B. Wilgen  
Oak Ridge National Laboratory  
P. O. Box Y  
Oak Ridge, TN 37830

J. T. Woo  
Rensselaer Polytechnic Inst.  
Troy, NY 12181

S. Yoshikawa  
Princeton Plasma Physics Lab.  
P. O. Box 451  
Princeton, NJ 08544

## EBT STABILITY THEORY WORKSHOP

May 13-14, 1981  
 Holiday Inn, Oak Ridge, Tennessee

Sponsored By

OAK RIDGE NATIONAL LABORATORY  
 Oak Ridge, Tennessee

## AGENDA

Wednesday, May 13, 1981

- 9:00 L. A. Berry: Welcome
- 9:15 Session A: Overview  
 N. A. Krall and N. A. Uckan, Chairmen
- A.1 G. E. Guest, "Rudimentary Theories of the Stability of Microwave Heated Plasmas"
- A.2 D. A. Spong, "Review of Recent EBT Coupled Ring-Core Stability Theory"
- A.3 N. A. Uckan and G. R. Haste, "Brief Survey of Experimental Investigation of Instabilities in Microwave Heated Plasmas"
- 11:00 Session B: Experimental Observations  
 W. B. Ard and H. Grad, Chairmen
- B.1 L. Bighel, G. Haste, and A. Komori, "Fluctuation Measurements in EBT"
- B.2 I. Alexeff and M. Saylor, "Hot-Electron Ring Stability at The University of Tennessee"
- 12:00 LUNCH
- 1:00 Session C: Ring-Core Coupling, Low Frequency Modes  
 D. E. Baldwin and C. L. Hedrick, Chairmen
- C.1 J. W. Van Dam, H. L. Berk, M. N. Rosenbluth, and D. A. Spong, "Eigenmode Stability Analysis for a Bumpy Torus"
- C.2 D. A. Spong, J. W. Van Dam, H. L. Berk, and M. N. Rosenbluth, "Numerical Solutions of the EBT Radial Eigenmode Problem"
- C.3 K. T. Tsang and C. Z. Cheng, "Stability of Hot Electron Plasma in the ELMO Bumpy Torus"
- C.4 C. Z. Cheng and K. T. Tsang, "Analytical Theory of Interchange and Compressional Alfvén Stabilities in EBT"
- 2:45 BREAK

## EBT STABILITY THEORY WORKSHOP AGENDA CONT'D.

Wednesday, May 13, 1981

- 3:00            Session D: High Frequency Modes  
                  H. L. Berk and D. A. Spong, Chairmen
- D.1        N. T. Gladd, N. A. Krall, S. Hamasaki, and J. L. Sperling, "Microstability of the EBT Boundary"
- D.2        W. M. Nevins, R. H. Cohen, and Y. Matsuda, "ECRH Electron Distribution Functions"
- 4:00            Session E: Equilibria and Computational Formalism of Stability  
                  H. Grad and N. A. Krall, Chairmen
- E.1        H. Sanuki, T. Ogino, S. Ishiguro, and T. Kamimura, "Numerical Analysis of Equilibrium and Stability in Bumpy Cylinder"
- E.2        R. R. Dominguez and H. L. Berk, "Kinetic Stability Analyses in A Bumpy Cylinder"
- E.3        Shoichi Yoshikawa, "Generalized Ballooning  $\beta$  Criterion for Closed Machines"
- 6:00-9:00      COOKOUT, CARBIDE PARK

Thursday, May 14, 1981

- 9:00            Session F: Reactor Implications  
                  C. L. Hedrick, Chairman
- F.1        N. A. Uckan, D. A. Spong, and D. B. Nelson, "Effect of Beta Limits on Reactor Performance in EBT"
- 9:30            Session O: Open Forum  
                  Panel: D. E. Baldwin, H. L. Berk, C. L. Hedrick, H. Grad, N. A. Krall, D. A. Spong, and N. A. Uckan
- 11:30          Session S: Summaries by Chairmen
- 12:15          CLOSING